NOTICE

The quality of this microform is heavily dependent upon the quality of the original thesis submitted for microfilming. Every effort has been made to ensure the highest quality of reproduction possible.

If pages are missing, contact the university which granted the degree.

Some pages may have indistinct print especially if the original pages were typed with a poor typewriter ribbon or if the university sent us an inferior photocopy.

Reproduction in full or in part of this microform is governed by the Canadian Copyright Act, R.S.C. 1970, c. C-30, and subsequent amendments.

AVIS

La qualité de cette microforme dépend grandement de la qualité de la thèse soumise au microfilmage. Nous avons tout fait pour assurer une qualité supérieure de reproduction.

S'il manque des pages, veuillez communiquer avec l'université qui a conféré le grade.

La qualité d'impression de certaines pages peut laisser à désirer, surtout si les pages originales ont été dactylographiées à l'aide d'un ruban usé ou si l'université nous a fait parvenir une photocopie de qualité inférieure.

La reproduction, même partielle, de cette microforme est soumise à la Loi canadienne sur le droit d'auteur, SRC 1970, c. C-30, et ses amendements subséquents.

Infrared Studies of Silica Surfaces

by

Andrew J. McFarlan

A thesis submitted in partial fulfillment

of the requirements for the degree of

Doctor of Philosophy

in

Chemistry

Department of Chemistry

University of Ottawa

Ottawa, Ontario.

Canada

B. A. Morrow

Professor of Chemistry

Research Supervisor

Andrew J. McFarlan

Ph. D. Candidate

ISBN 0-315-70485-3

UNIVERSITÉ D'OTTAWA
UNIVERSITY OF OTTAWA

TABLE OF CONTENTS

ABSTRACT

The silanol distributions on "as received" aerosil and precipitated silica have been studied (1) by using time-resolved infrared spectroscopy in order to follow a reaction with $AlMe_3$, $TiCl_4$, or BCl_3, (2) by spectroscopically comparing the accessibility of probe molecules having different steric dimensions, that react with surface silanols (SiOH) either by chemisorption or H/D exchange, and (3) by gravimetrically measuring surface silanol densities using vacuum microbalance techniques. The results have been used to compare and characterize these non-porous silicas of similar surface area.

Initially, H-bonded silanols are relatively more reactive than isolated silanols in the order of reagents, $BCl_3 > TiCl_4 > AlMe_3$. In the fully hydroxylated "as received" state, the number of silanol groups on either silica which react with various hydrogen sequestering (HS) agents decreases as the size of the agent increases ($ZnMe_2$, BCl_3, $TiCl_4$, $AlMe_3$ and $Me_3SiNHSiMe_3$ (HMDS) in increasing size). The number of silanols that undergo H/D exchange also decreases as the size of the probe molecule increases (D_2O, ND_3, and deuterated methanol, i-propanol and t-butanol). The total number of silanol groups on the precipitated silica is 6.8/nm^2 of which 5.6 can exchange with the smallest H/D exchange molecule (D_2O or ND_3), and on aerosil it is 3.1/nm^2 of which 2.5 will exchange. The number of SiOH/nm^2 which react with a given HS agent is about the same on either silica, and this is substantially smaller than the number which will undergo exchange. The difference between the extent of chemisorption versus exchange has been attributed to the steric blocking effect of the immobile chemisorbed product.

HMDS can only react monofunctionally with surface SiOH, and the number of trimethylsilyl (TMS) groups which can be attached to either silica is about the same, *i.e.* 1.4-1.5/nm^2. Both hydroxylated silicas contain about 1.1 isolated SiOH/nm^2, all of which

react with HMDS. However, the number of TMS species derived from silanols which were originally H-bonded is 0.3 to 0.4/nm^2. The reaction between HMDS and H-bonded silanols occurs preferentially with the terminal silanols of a chain, and we propose that these silanols occupy sites which are inherently more accessible to this bulky reactant.

Infrared spectroscopy has been used to study the isolated SiOH surface modes in the 500-5000 cm^{-1} spectral region of aerosil and precipitated silicas. Experiments have been carried out using samples of either silica which had been activated under vacuum between 150 and 1000°C, and spectra of the SiO—H stretching bands (3700-3800 cm^{-1}), the Si—O—H deformation bands (500-1000 cm^{-1}), and the combination bands (4300-4700 cm^{-1}) have been recorded at room temperature and at 82 K.

The combination band at about 4550 cm^{-1} in the room-temperature spectrum of either silica splits into a doublet having components at 4580 and 4510 cm^{-1} when the sample is cooled to 82 K. The low-temperature spectrum of the sharp SiO—H stretching band at 3750 cm^{-1} reveals a low-wavenumber component at about 3740 cm^{-1} which accounts for the peak position and asymmetry to low wavenumber in the room temperature spectrum of either silica. In the spectral region of the bulk SiO_2 modes, two fundamental SiOH vibrations at 840 and 760 cm^{-1} are observed. This spectral region has been probed using thin self-supporting disks and spectral subtraction following, CO adsorption at 82 K, deuterium exchange, or reaction with BCl_3. When the isolated SiOH groups on either silica are exchanged with D_2O or ND_3, the isolated SiO—H stretching bands shift from 3750, 3740 cm^{-1} to 2760, 2756 cm^{-1}, respectively, however, only a single band is observed for the SiOD deformation mode (610 cm^{-1}) and combination mode (3370 cm^{-1}).

By following the evolution of the SiOH bands on both silicas in all three spectral regions for 450, 600, and 800°C activation, we have assigned bands to two types of isolated silanols. The type I silanols are preferentially eliminated between 450 and 800 °C activation and are more abundant on precipitated silica than on aerosil. Type II silanols (isolated single silanols) dominate the surface of highly activated aerosil or precipitated silica, as is evident

from their nearly identical infrared spectra following activation at 800 °C. Combinations of the fundamental SiOH stretching and bending vibrations are observed at, 840 + 3740 = 4580 cm^{-1} for type I silanols, and 760 + 3750 = 4510 cm^{-1} for type II silanols. The combination band due to type II SiOD is observed at 610 + 2760 = 3370 cm^{-1}. We propose that mixing of the pure SiOH bending mode with a nearly degenerate local SiO mode can account for the observed frequencies and extinction coefficients of the 840 and 760 cm^{-1} bands in the spectra of the H-silicas.

The physical adsorption of CO, N_2, and CH_4 at 82 K on 800°C activated aerosil silica has been studied by infrared spectroscopy in order to assess the utility of these molecules as low-temperature surface probes. Specific interaction at low coverage perturbs the "free" SiOH vibrational modes giving rise to new infrared bands between 500 and 5000 cm^{-1} due to the pnysically adsorbed complexes, SiOH...X (X = CO, N_2, and CH_4). The vibrational spectra between 500 and 5000 cm^{-1} are reported for these adsorbed species, and the nature of their specific interaction with surface SiOH is discussed.

Infrared spectroscopy and phosphorus-31 magic angle spinning nuclear magnetic resonance spectroscopy have been used to study the adsorption of trimethyl phosphite (TMP) on silica. At 23°C, TMP reacts rapidly with surface silanol groups to give $SiOCH_3$ as a chemisorbed product and adsorbed dimethyl phosphite (DMP). The formation of DMP ceases when about half of the SiOH groups have been consumed because DMP strongly hydrogen bonds to the remaining silanols, thereby inhibiting further reaction between TMP and SiOH. TMP also isomerizes to dimethyl methylphosphonate (DMMP), and this surface reaction is catalyzed by SiOH. As the number of silanol groups initially present on the surface is decreased (by increasing the activation temperature of the silica), the quantity of DMP produced decreases whereas that of DMMP increases. Mechanisms are proposed for the room-temperature reaction between SiOH and TMP to produce DMP, and the SiOH-catalyzed isomerization of TMP to DMMP.

At 100°C, isomerization does not occur, all SiOH groups are consumed and the major

products are DMP and surface $SiOCH_3$, accompanied by a small quantity of a chemisorbed phosphorus-containing species having the proposed structure, $(SiO)_2(H)P{=}O$. This surface species is stable up to 400°C. IR and NMR results show that, when TMP is heated with silica from 100 to 400°C, chemisorbed $(SiO)_2(CH_3)P{=}O$ and $SiOCH_3$ are formed on the surface. The advantages of a combined IR-NMR approach are discussed.

The reaction of dimethylzinc ($ZnMe_2$) with aerosil silica has been studied by infrared spectroscopy. On 150°C activated aerosil, $ZnMe_2$ reacts with isolated and H-bonded silanols producing gas-phase CH_4 and two chemisorbed CH_3-containing species. On 450 and 800°C activated aerosil, the reaction with H-bonded silanols is less significant, as these silanols are mostly eliminated between 150 and 450°C activation. However, in addition to the product of the reaction with isolated silanols on 450 and 800°C activated silica, other CH_3-containing chemisorbed species are observed, one of which is probably $SiCH_3$ produced during a reaction with a small number of siloxane sites. Thin film experiments have been carried out in order to identify the low-frequency infrared bands (below 1300 cm^{-1}) due to the various surface species present on $ZnMe_2$-treated silica. Additionally, changes in the silica spectrum due to surface silica modes between 1000 and 1300 cm^{-1} have been studied for aerosil silica activated at 23, 150, and 450°C, followed by deuterium exchange and/or reaction with $ZnMe_2$. We suggest that dimethylzinc's ability to coordinate to the surface through one or two oxygen atoms may account for its unexpected reactivity and the rather complex infrared spectra in the CH_3-stretching region.

ACKNOWLEDGEMENTS

To my research supervisor, Professor Barry A. Morrow,

Thank you for your encouragement and guidance along the way, and for sharing your expertise in surface chemistry so willingly. I have learned much from you.

To my fellow graduate students, Wang, Steve, Lynn, and Bruce,

Thank you for your companionship and helpful discussions throughout my graduate studies. It has been a pleasure working with you.

To the Staff of the Department of Chemistry,

I am indebted to all of you for your help along the way. Thank you everyone.

To my loving wife and dear friend, JoAnne,

Thank you for your selfless patience and support.

CHAPTER 1

General Introduction

An Outline of the Thesis and Its Objectives

Synthetic silicas are important materials commercially and are used in a variety of applications. Silicas are used as adsorbents in gas separation and waste gas purification processes. They are used as a supporting material for metal catalysts (Pd, Pt, Ni, and Fe for example) and their surfaces can also be chemically modified by reaction with metal halides or alkyl metals to enhance their catalytic activity [1,2]. Silicas which have been chemically modified by attaching alkyl substituents to the surface play a paramount role as the stationary phase in chromatographic separation technology. In addition, many products contain silicas as additives, *e.g.* to improve the ink-jet-printing quality of paper, as fillers in polymers, as bonding agents in composite materials and ceramics, and as flow-improvement agents. The development of new technologies, and improvements in existing technologies and applications, rely on an understanding of the surface chemistry of silica [1-5].

Advances in the relatively young field of surface science include the development of a diverse selection of surface-sensitive instrumental techniques for studying the structure and reactivity of surfaces. The suitability of a particular technique depends on the nature of the material (*e.g.* metal single crystals, oxide films on metal substrates, supported metals) and the interface being studied (*i.e.* vacuum-solid, gas-solid, liquid-solid and solid-solid). High-surface-area amorphous silica can be easily studied using Fourier Transform Infrared (FTIR) spectroscopy or Raman spectroscopy. Although transmission infrared spectroscopy is not inherently surface-sensitive, this is compensated for by the very high surface-area-to-mass ratio which is typical of manufactured silicas. Solid-State Magic-Angle-Spinning Nuclear

Magnetic Resonance Spectroscopy (MAS/NMR) is another effective spectroscopic tool for studying silica and, for ^{29}Si solid-state NMR studies of hydroxylated silica, surface sensitivity may be enhanced using Cross Polarization (CPMAS).

A primary objective of this thesis has been to obtain new information regarding the structure and reactivity of the silica surface and to compare the surface properties of silicas that differ in origin. Experimental methods have been developed which permit thermal activation of the silica under vacuum while simultaneously carrying out in situ FTIR investigations of the silica surface at the vacuum-solid or gas-solid interface over a wide temperature range. Gravimetric studies have been carried out to compare quantitatively the surface densities of silanols, SiOH, that mainly determine the surface chemistry of silica. The surface silanol sites can be characterized qualitatively by FTIR on the "as received" silicas, and after thermal activation under vacuum between room temperature and 1000°C. Several methods for spectroscopically probing these silanol sites, at room temperature and at low temperature, have been used to compare the silanol distribution on two different silicas.

Two of the chapters in this thesis are devoted to comparative studies of the surfaces of an aerosil and a precipitated silica; the distribution and reactivity of surface silanols on the "as received" materials are compared in Chapter 3, and a spectroscopic investigation of their silanol distributions as a function of activation temperature is presented in Chapter 4. The background material that follows serves as a general introduction to the silicas being studied, and to Chapters 3 and 4. By the end of Chapter 4, the majority of the experimental techniques employed will have been discussed, as will the infrared spectrum of silica, over a wide spectral range and under numerous experimental conditions.

A second objective has been to determine the utility of several small molecules as "probe" molecules by studying their adsorption on aerosil silica. The physical adsorption of CO, N_2 and CH_4 on aerosil silica at low temperature is investigated in Chapter 5, and chemical modification of aerosil silica surface by reaction with dimethylzinc is presented in Chapter 7.

A third objective in this work has been to assess the utility of a combined IR/NMR approach to studying the adsorption and reactivity of trimethyl phosphite on silica. Chapter 6 describes a collaborative study of aerosil silica (with Professor Ian Gay at Simon Fraser University) which combines solid-state ^{31}P NMR spectroscopy and FTIR spectroscopy.

The remainder of Chapter 1 will present an overview of the nature of synthetic silicas according to their origin, and will briefly describe how infrared spectroscopy can be used to study the chemical structure at silica surfaces. Some recent findings from ^{29}Si solid-state NMR studies of silicas (including silica gels) will also be discussed in this chapter. By the end of Chapter 1, some of the known similarities and differences between aerosil and precipitated silicas will have been explained, and some questions which remain to be answered regarding the nature of their surfaces will have been put forth.

This introduction discusses only manufactured silicas and does not include the various crystalline forms of silica which occur in nature. It is limited further to silicas "as received" from the manufacturer, prior to any custom modification. Finally, aerosil and precipitated silicas are the subjects of research in this thesis, however, many contributions to the general understanding of the surface chemistry of silica have been based on silica gel, a close relative to precipitated silica, and some relevant studies of this material are included here.

Morphology of Silicas

In geography, morphology refers to studies of the external structure of rock formations in relation to the development of their topographical features and their geological origin. The morphology of silica, by analogy, is a study of structure in relation to origin which takes place on a scale that is smaller by 10-12 orders of magnitude and describes their surface topography at a microscopic or even molecular level. The surface topography of silica varies depending on its origin, thermal treatment, or chemical modification, and an understanding of this miniature landscape is basic to understanding its surface chemistry.

1. Synthetic Methods

The properties of an "as received" silica are largely determined by the manufacturing process used, and there are currently several different commercial methods for synthesizing high-surface-area silicas. The different synthetic methods have evolved with the demand for high-purity silicas whose surface area, particle size, and porosity may be varied over a wide range, but under strictly controlled conditions. Manufactured silicas may be classified into three general types depending on the method of synthesis, *i.e.* pyrogenic (fumed, aerosil) silica, precipitated silica, and silica gel [1,2].

Pyrogenic, fumed, or aerosil silicas (we will use the term, aerosil, to refer to this type) are produced by flame hydrolysis. The pyrolysis of $SiCl_4$ in a hydrogen flame at about 1000 to 1100°C (reaction 1) results in the formation of minute silica particles ranging between 5 and 25 nm in diameter. SiF_4, SiH_4 or other halogenated silanes may also be used as starting materials.

$$SiCl_4 + 2\,H_2 + O_2 \longrightarrow SiO_2 + 4\,HCl \qquad (1)$$

The primary particles are essentially spherical and non porous, and the particle size can be controlled by varying the proportions of the reactants in (1). Chains of the smooth spherical primary particles form larger particles (like a string of beads), as revealed by electron microscopy [6].

Precipitated silicas and silica gels are synthesized in the liquid phase, from the acidification of alkaline, aqueous silicate solutions (reaction 2) or solutions of alkoxysilanes in aqueous alcohol (reaction 3).

$$Na_2SiO_3 + H_2SO_4 \longrightarrow SiO_2 + H_2O + Na_2SO_4 \qquad (2)$$

$$Si(OR)_4 + 2\,H_2O \longrightarrow SiO_2 + 4\,ROH \qquad (3)$$

In aqueous alkaline solutions, silica dissolves readily producing a mixture of monomeric silicate anions of silicic acid, $(SiO_4)^{4-}$, in equilibrium with oligomeric silicate anions. Upon lowering the pH, the reverse process occurs and this might be described as the polymerization and condensation of silicic acid. ^{29}Si NMR has been used to study the structure of the oligomeric silicate anions [7], and to follow the polymerization reaction in aqueous methanol [8].

In reactions 2 and 3 above, a highly dispersed colloidal phase of silica particles is formed initially. The eventual conversion of this phase to precipitated silica, or silica gel, depends on the careful control of the **coalescence** and **flocculation** of the primary particles of silica [9]. Coalescence refers to the process whereby primary particles nucleate to form larger particles, with a resultant decrease in the total surface area of the particles. Flocculation, also referred to as aggregation or coagulation, describes the process whereby small particles link together forming a floc. The shape of the individual particles is still recognizable in a floc, and there is little decrease in the total surface area.

When coalescence of the particles is encouraged, precipitated silicas are formed. At a pH > 7, a significant concentration of oligomeric silicate anions is present, and electrostatic repulsion between these negatively charged silica grains tends to prevent flocculation and favour coalescence. This effect may be counteracted by the addition of a salt; by increasing the ionic strength of the aqueous medium, aggregation of the silica grains is encouraged and silica gel is formed. Alternatively, the addition of ammonia at pH > 7, or the addition of acid until pH < 7, also favours the formation of silica gel. Unlike aerosil, the silicas obtained in aqueous or alcoholic media must be carefully dried as a final step in order to ensure that their texture is retained in the powder form.

2. Surface Area, Porosity

The chemical structure of bulk aerosil silicas, precipitated silicas and silica gels is essentially the same, *i.e.* they all consist of amorphous particles of silicon dioxide, SiO_2.

However, these materials may vary greatly in specific surface area and porosity and, consequently, the chemical structure and reactivity at the surface of the "as received" silicas varies accordingly.

Specific surface area (of silica and other high-surface-area powders) is defined as the area per unit mass, usually expressed in m^2/g, and is most often calculated using the monolayer coverage of N_2 or Ar determined from the B.E.T. adsorption isotherm [10]. Although this method is approximate and, as such, has a limited accuracy (± 10%, see for example, [16]), it is widely accepted as a reliable method for reporting surface areas of highly dispersed solids when calibrations are made using surface area standards [5]. Considerable quantitative significance is placed on the specific surface area of silicas, given that other surface properties (*e.g.* surface silanol densities) are expressed in terms of the specific surface area and thus rely on the accuracy of this measurement.

Porosity may be described as the extent to which internal surfaces contribute to the specific surface area. Internal surfaces may arise where surfaces of solid spherical particles are in close contact as a result of flocculation (as an analogy, consider the hidden surfaces of grapes in a bunch), in deep crevices which partly split solid particles, and in particles which are not solid, but which have a sponge-like or honeycomb structure. Although the size and shapes of internal cavities will vary depending on the material, traditional porosimetry methods characterize materials according to the distribution of their pore widths (*e.g.* diameters of cylindrical pores), and are based on studies of hysteresis in adsorption isotherms or mercury intrusion. Three classifications of porous materials according to the average width, w, of their pores have been adopted by the International Union of Pure and Applied Chemistry: **macroporous**, $w > 50$ nm; **mesoporous**, 2 nm $< w <$ 50 nm; **microporous**, $w <$ 2 nm.

Aerosil silicas are typically non porous or macroporous at most. The extent to which porosity occurs in precipitated silicas and silica gels is generally greater than for aerosil and can vary over a wider range; precipitated silicas range from being non porous to mesoporous,

whereas silica gels are often microporous. The maximum specific surface area of these silicas depends on the degree of porosity; aerosil and precipitated silicas are limited to specific surface areas less than about 400 m^2/g, whereas silica gels can have specific surface areas approaching 800 m^2/g. In the latter case, the internal surface may exceed the external surface by an order of magnitude or more [5].

3. Fractal Dimension

Fractal analysis has been established as a useful technique for describing irregular surfaces, *i.e.* the departure from an ideal 2-dimensional surface that arises naturally in landforms [11], as well as at the surface of highly dispersed solids on a molecular scale. Many of the techniques currently used to study the fractal nature of powder surfaces originate from the pioneering work by Avnir *et al.* [12-14].

An apparent surface area can be determined from the number of "yardstick" molecules, n, having surface area, σ, which just form a monolayer coverage on the surface. On an irregular surface, the apparent surface area obtained in this manner will depend on the size of the yardstick chosen, *i.e.*

$$n(\sigma) \propto \sigma^{-D/2} \tag{4}$$

The non-integer **fractal dimension, D**, describes the surface roughness and is bound by the Euclidean dimensions, $\mathbf{d} = 2$, and $\mathbf{d} = 3$, for 2- and 3-dimensional space, respectively. The degree of irregularity on a surface is given singularly by the value of **D**, where $2 \leq \mathbf{D} < 3$, and is a geometric representation of the surface morphology.

Avnir *et al.* have studied the irregularity of an aerosil silica by applying fractal analysis to a series of commercially available silicas (Degussa Aerosils) having specific surface areas between 50 and 300 m^2/g [13]. The average particle diameters of these silicas, determined by electron microscopy, ranged from 40 nm for the Aerosil-50 silica to 7 nm for

the Aerosil-300 silica. The "yardstick" used to measure the surface area remained constant (in this case, $\sigma(N_2) = 0.162$ nm^2), and $D = 1.98 \pm 0.06$ was determined from the variation in surface area with the average particle diameter. This result led the authors to conclude that aerosil silica has a smooth surface at the molecular level.

At the other extreme, adsorption studies have shown that silica gels can have a fractal dimension near 3 ($D = 2.94$ from surface area determinations using an homologous series of adsorbate molecules having known σ values). This suggests that a high degree of irregularity and self-similarity occurs over a certain range of scale in silica gel, and is characteristic of a microporous material [14].

More recently, adsorption studies, small-angle X-ray, and neutron scattering techniques have been used to determine the fractal surface dimension of four grades of aerosil silica (CAB-O-SIL, Cabot Corp.) having specific surface areas ranging from 90-380 m^2/g [15,16]. Specific surface area measurements obtained from adsorption of nitrogen, pentane, and heptane were limited to low relative pressures of adsorbate in order to minimize the effects of interparticle condensation. Under these conditions, the fractal surface dimension varied between 2.1 and 2.5 ($D = 2.3$ for CAB-O-SIL HS5, the aerosil silica used here), and further, D was found to increase with the specific surface area of the silica. These results were consistent with those obtained from the scattering experiments. The authors have suggested that aerosil silicas may be better described as self-affine (*i.e.* surface roughness is limited to a finite layer) rather than self-similar and that information about surface roughness may be lost in the multiple layer adsorption region.

4. Summary: A Comparison of the Physical Properties of Silicas, A, P, G and S

The general physical properties of four "as received" silicas of different origin have been compared in an extensive, collaborative study of their surface chemistry, recently undertaken by Legrand *et al.* [2]. An aerosil silica (A), a precipitated silica (P), a silica gel derived from sodium silicate (G), and an alkoxide silica (S), were chosen as representative

samples from a wide variety of manufactured silicas. Their comparative study is based on a comprehensive examination of these silicas using the identical experimental techniques. In Table 1.1 we present the results of their studies of the surface morphology of silicas A, P, G, and S. Table 1.1 serves to summarize the general physical properties of silica which have been discussed here.

Physical Characteristic	Silica A	P	G	S
1. Synthesis	$SiCl_4$, H_2, O_2, 1000°C	Na_2SiO_3, H_2O, pH > 7	Na_2SiO_3, H_2O, pH > 7	$Si(OR)_4$, H_2O, NH_3
2. B.E.T. Specific Surface Area (m^2/g)	215	200	390	3.8
3. average particle diameter (μm)	0.012 [a]	8	7	0.8
4. porosity (average w)	nonporous	mesoporous (42 nm)	mesoporous (22 nm)	nonporous
5. Fractal Dimension				
(i) B.E.T.	2.4	2.4-2.6	2.4-2.7	- - - -
(ii) SAXS [b]	2.1 ± 0.05	2.4 ± 0.05	2.5 ± 0.05	- - - -

Table 1.1. Physical Properties of Aerosil, Precipitated Silica and Silica Gels
(a) primary particle diameter [12].
(b) Small Angle X-ray Scattering

Comparing of the physical properties of silicas A and P we see that, whereas an aerosil silica is generally nonporous, a precipitated silica having the same specific surface

area may exhibit mesoporosity. An increased fractal dimension (2.4 *vs.* 2.1 by method (ii)) also indicates a higher degree of surface irregularity in silica P which may be associated with mesoporosity. Silica G has a specific surface area almost double that of silica A or P, and porosity measurements for silica G revealed that both the average pore width and the distribution of pore widths was significantly narrower. It is not unreasonable to suggest that a greater portion of the surface is internal for silica G. A fractal dimension, D = 2.5, for silica G reflects a narrow distribution of mesopores and an absence of micropores.

It is clear that there are no sharp boundaries within which the physical properties of a particular type of silica will lie. To the contrary, the variation is continuous and widespread. Although specific properties in a series of silicas may correlate well (*e.g.* surface area and particle size in aerosils), generally trends are observed at best.

The background material presented to this point has focused on the nature of silica surfaces based only on measurements of their macroscopic properties, however, these studies allow us to visualize how silica surfaces might appear at the molecular level. Having created an image of this miniature landscape, we can imagine how the surface topography might influence the local chemical structure and/or the surface chemistry of silica. We now turn our attention to those studies specifically directed at characterizing the local chemical structure of silica surfaces.

Chemical Structures at Silica Surfaces

The surface structure of silica (external and internal) consists of silanol groups, SiOH, and surface siloxane bridge sites, SiOSi [1-4]. Both sites incorporate silicon atoms located at the gas-solid interface of the amorphous SiO_2 network, and surface hydroxyls reside at those silicons which would otherwise have one or more unfilled valences. In most cases, the surface chemistry of silica is dictated by the reactivity of the surface silanols; siloxane bridge sites are relatively unreactive with most molecules unless extreme temperatures of activation have been employed. In terms of its chemical reactivity, it follows that one of the most

important characteristics of a silica surface is the surface silanol density.

1. Silanol Densities

The surface silanol density (the number of hydroxyls per unit surface area, usually expressed as OH/nm^2 or $\mu mols(OH)/m^2$) for an "as received" silica varies significantly, depending on its origin. Aerosil silicas are generally sparsely populated with silanols, having surface silanol densities between 2.5 - 3.5 OH/nm^2 [17,18] whereas fully hydroxylated precipitated silicas and silica gels may contain as many as 12 - 14 OH/nm^2, where there is a large internal surface and/or many Si bonded to more than one hydroxyl [2].

In their comparative study of silicas A, P, and G, Legrand *et al.* report total silanol densities to be 3.8, 13.4, and 10.8 OH/nm^2, respectively [2,19]. The silicas had been equilibrated in a humid atmosphere prior to evacuation at 25°C, and following this, total silanol densities were calculated from the mass of H_2O liberated in vacuum between 25 and 800°C. This decrease in mass is generally attributed to a surface reaction whereby neighbouring pairs of silanols condense, liberating water, to form a surface siloxane bridge site according to reaction 5.

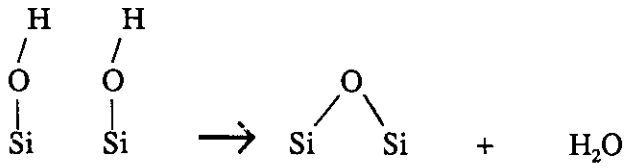

(5)

Zhuravlev has determined the silanol densities of 100 different samples of amorphous silicas of different origins, and having specific surface areas ranging between 10 and 950 m^2/g [20]. These silicas were fully hydroxylated (in aqueous slurries) then dried in vacuum at 180-200°C prior to analysis by deuterium-exchange/mass spectrometry. Silanol densities ranged between 4 and 6 OH/nm^2 with an average of 4.9 OH/nm^2, and Zhuravlev concluded that a value of 5 OH/nm^2 may be considered to be a physical chemical constant of silicas, independent of their origin or morphology.

An explanation for the apparent discrepancy between their own results and those of Zhuravlev has been put forward by Burneau *et al.* [19]. They have attributed the very large surface silanol densities to the presence of "internal" silanols in ultramicropores in silicas P and G. These silanols are inaccessible to the exchange molecule, D_2O, and cannot be measured by isotopic exchange. These inaccessible silanols can, however, be detected as molecular water liberated at high temperatures during the thermogravimetric analysis (reaction 5). Further, they propose that, because the internal silanols fill the internal volume of the ultramicropores in silicas P and G, the specific surface area measured by nitrogen adsorption may be lowered, leading to apparently large values for the surface silanol densities.

The above measurements of silanol densities illustrate that the local environment of surface silanols on silica affects their ability to react and, furthermore, that a certain fraction of the total silanol density is due to silanols which are inaccessible to reactant molecules. The silanol density data also indicate that the origin of the silica and the pretreatment conditions may affect the overall silanol distribution. Lastly, the surface silanol density may depend on the method used to obtain the measurement as well as the distribution of silanols on the surface. These issues are addressed in the comparative study of aerosil and precipitated silica in Chapter 3.

2. Characterization of the Silica Surface by Infrared Spectroscopy

The present understanding of the nature of the silica surface at the molecular level is largely due to spectroscopic studies of this material. The vast majority of spectroscopic work related to the surface modification of silica has been accomplished using infrared vibrational spectroscopy [3,4], and this technique has continued to flourish in recent years as a result of the revolutionary advances in Fourier Transform (FTIR) instrumentation [21]. A significant portion of this thesis specifically addresses FTIR studies of the surface silanol distribution on silicas, and detailed discussions of the nature of these studies is reserved for later chapters. At this point, we will introduce the transmission infrared technique and present a generally-

accepted model of the silanol distribution on silica that is based on the results of many previous infrared studies.

Figure 1.1, A-C shows the transmission infrared spectrum of an aerosil silica, evacuated at 150°C for 1 hr, for silica disks containing 10, 2.5 or 0.1 mg of silica per cm^2, respectively. A similar series of spectra for precipitated silica is shown in Figure 1.2. For a fixed cross-sectional area (*i.e.* the area illuminated at the focus of the infrared beam), the thickness of the transparent silica disk determines the quantity of silica being sampled, and this is usually expressed in units of mg/cm^2. The minimum quantity of silica which will still produce a self-supporting disk is about 2 mg/cm^2 (Figures 1.1 and 1.2, B), but this thickness can be further reduced by an order of magnitude if the silica is supported by a transparent window or a fine Ni mesh (Figures 1 and 2, C) [22].

The 4000-3000 cm^{-1} region exhibits the characteristic features due to SiO—H stretching vibrations of surface silanols, and these are the only features present between about 4400 and 2000 cm^{-1} in the silica spectrum. The strong absorption features near 1100, 800, and 475 cm^{-1} are due to bulk SiOSi modes, however, several fundamental vibrational modes of surface silanols are also buried in these intense absorption bands. The broad, weak features at about 1600 and 1850 cm^{-1} are overtones or combinations of the bulk silica modes [1-4,23].

Infrared vibrational spectroscopy can distinguish various types of surface silanols by the frequencies of their normal vibrational modes. The frequency of the SiO—H stretching vibration is particularly sensitive to the local environment and to hydrogen-bonding interactions with neighbouring silanols. There are numerous possible configurations of silanols on a silica surface where H-bonding interactions and weaker perturbations of the SiO—H stretching vibrations could occur, and some of these are shown in Figure 1.3.

The sharp band at 3747 cm^{-1} in the infrared spectrum of "as received" aerosil silica (Figure 1.1A) is due to isolated SiOH which do not interact with other sites. In the spectrum of "as received" precipitated silica (Figure 1.2A), the band assigned to isolated SiOH appears at 3738 cm^{-1} and is slightly broader and weaker than in the spectrum of aerosil. Thus, it

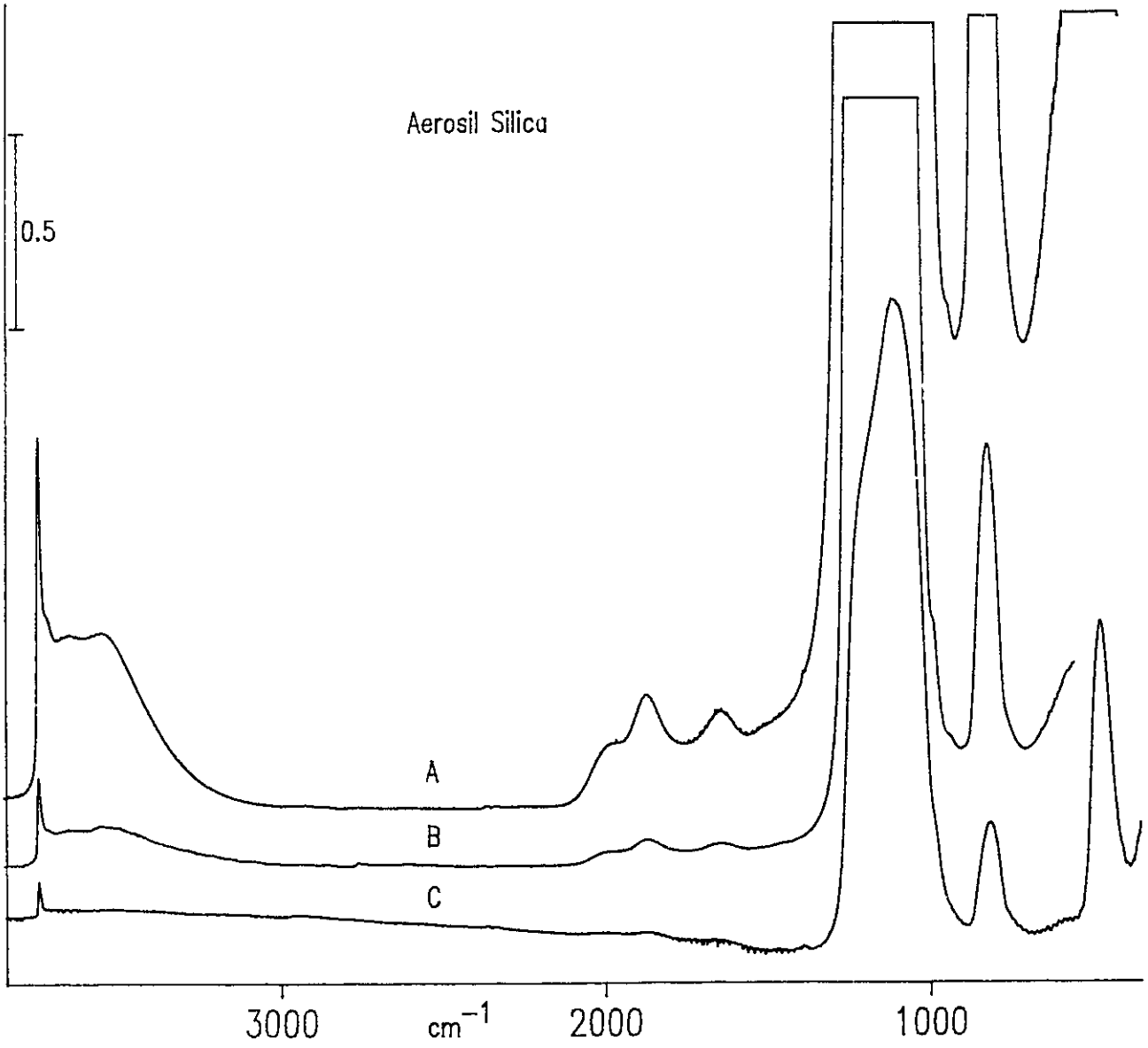

Figure 1.1. Transmission infrared spectrum in absorbance of "as received" aerosil silica obtained using samples containing (A) 10 mg/cm^2, (B) 2.5 mg/cm^2, and (C) 0.1 mg/cm^2 silica.

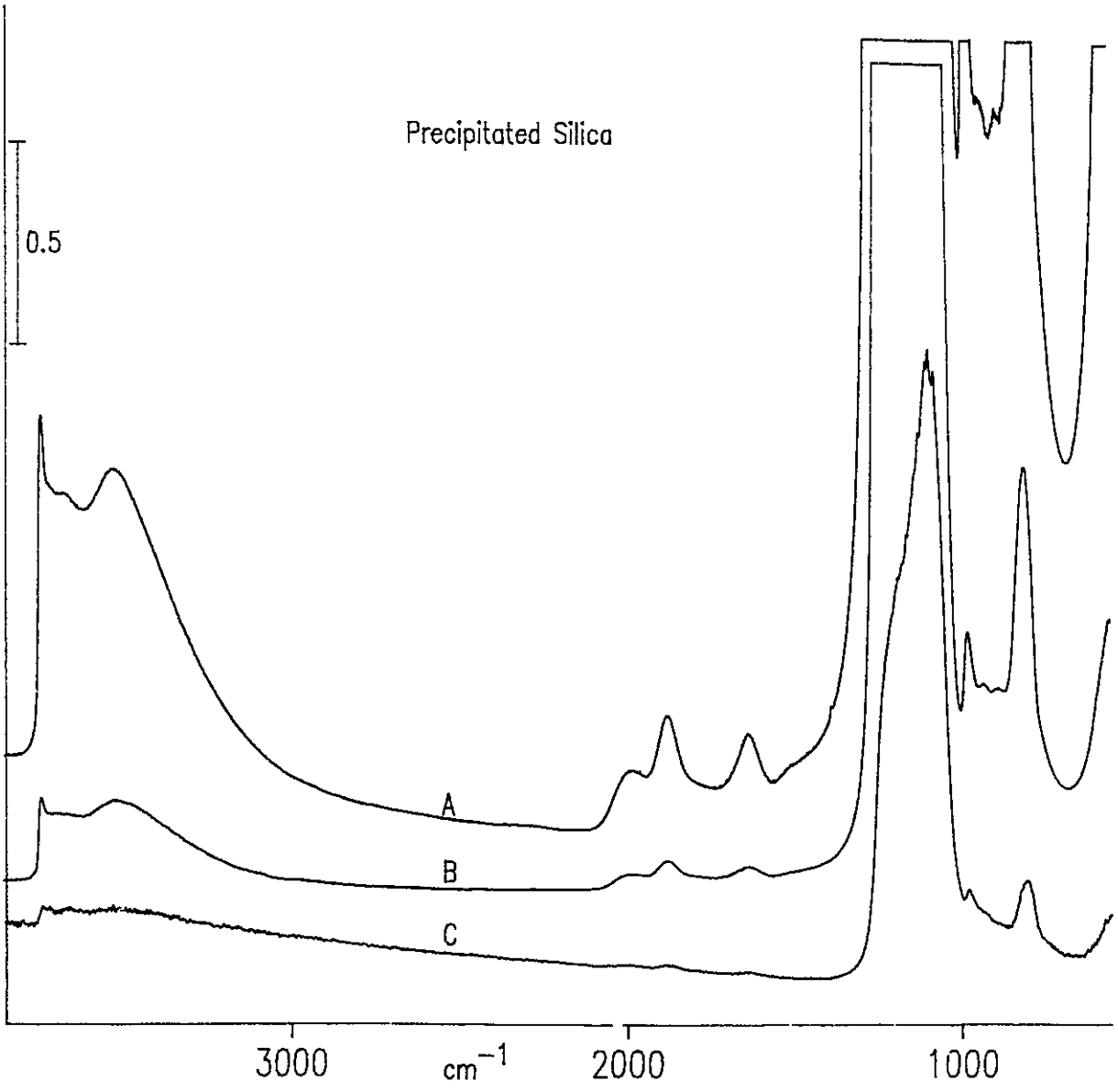

Figure 1.2. Transmission infrared spectrum in absorbance of "as received" precipitated silica obtained using samples containing (A) 10 mg/cm^2, (B) 2.5 mg/cm^2, and (C) 0.1 mg/cm^2 silica.

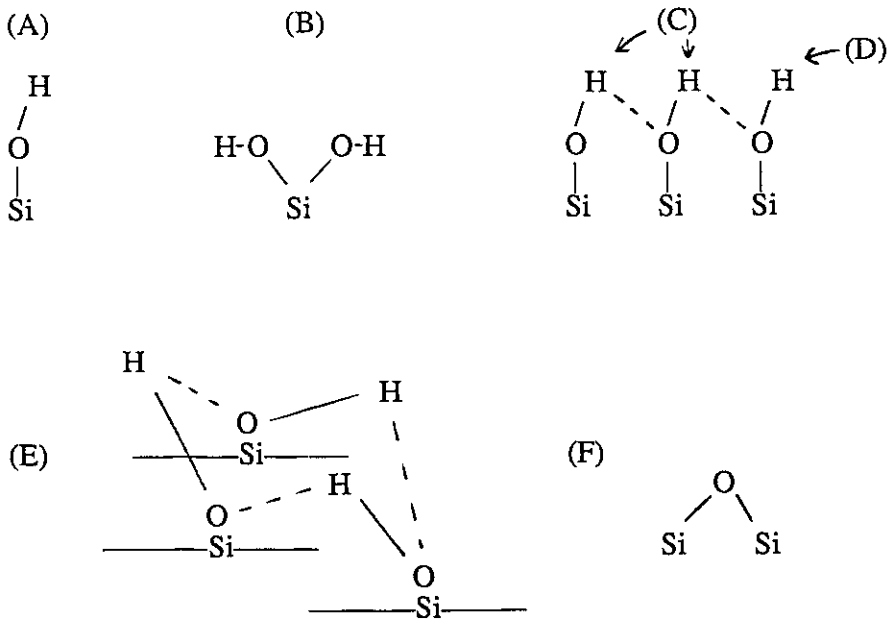

Figure 1.3. Infrared band assignments to surface silanol structures on silica. (A) single isolated silanols (3748-3738 cm^{-1}). (B) geminal silanols (3748-3738 cm^{-1}). (C) vicinal H-bonded silanols in pairs and triplets (3600-3400 cm^{-1}). (D) terminal silanol in pairs and triplets of H-bonded silanols (3720-3715 cm^{-1}). (E) vicinal H-bonded silanols in cyclic 3- or 4-membered rings (3600-3400 cm^{-1}). (F) surface siloxane bridge sites (<1300 cm^{-1}).

would appear that the isolated silanols on precipitated silica differ from those on aerosil. The 10 cm^{-1} difference in frequency could arise from two isolated silanols species which differ in structure, *e.g.* single and geminal isolated SiOH (Figure 1.3, A and B). Alternatively, the small downward shift in frequency could be due to isolated silanols which have a slightly more (or less) strained local SiO_4 structure. As will be discussed in Chapter 4, the isolated

SiOH profiles of aerosil and precipitated silica are noticeably different after vacuum activation at 450°C but converge by about 800°C activation. This observation has prompted us to compare infrared bands associated with isolated SiOH in several spectral regions in order to learn more about their isolated silanol distributions.

In addition to isolated silanols, Figure 1.3 shows H-bonded silanol structures on the surface of hydroxylated silicas [2,24]. The broad band at about 3520 cm^{-1} in the spectra of the "as received" silicas is associated with hydrogen-bonded silanols and these may occur as chains (Figure 1.3C) or in cyclic structures (Figure 1.3E). The strength of the H-bonding interactions varies considerably, as is evident from the width of the band due to H-bonded silanols, but as a result, its lack of structure prevents us from directly determining the exact nature of these interactions from the infrared spectrum. Further, Figure 1.3 cannot account for every possible silanol structure because, in principle, single and geminal silanols may participate in H bonding, the number of silanols in a chain or ring may vary, and many different orientations of silanols may arise because the silica surface is irregular (its fractal dimension is greater than 2). All of these H-bonded silanols are expected to absorb in the 3400-3600 cm^{-1} region. Finally, Figure 1.3 does not include a structure for "internal" or "inaccessible" silanols. These silanols may be present in the silica bulk, or in regions where silica particles are in close contact. In any case, they do not react and are only clearly observed as a residual, broad absorption feature at about 3660 cm^{-1}. Hockey's group has shown that, as the pressure used to form a silica disk is increased, the number of silanols which are unable to undergo D_2O exchange also increases [25,26].

In order to compare the silanol distribution on different silicas, surface chemists rely on infrared spectroscopic methods which employ probe molecules to react with (or interact with) the surface silanols. These spectroscopic techniques make it possible to observe differences in reactivity for various silanol types which may be attributed to their structure or local environment. Chemical modification using reactive molecules and deuterium exchange [18], or esterification [27] of the surface silanols may be used to monitor differences in the

chemical reactivity of various silanol types on aerosil and precipitated silica. Burneau *et al.* have studied how water molecules interact with silanols on aerosil and precipitated silica using infrared spectroscopy, and have assigned bands between 3730 and 3750 cm^{-1} to "free silanols" located on outer and inner surfaces of silica [19]. They have also probed the silanols by using deuterium exchange with D_2O and t-BuOD and they observed that fewer "internal silanols" are capable of exchanging with the larger t-BuOD molecule [28]. In Chapter 3, we compare the silanol distributions on aerosil and precipitated silica by using chemical and H/D exchange probes of varying size, time-resolved spectroscopy, and gravimetric determinations of their silanol densities.

As a final comment, the ability to distinguish single and geminal silanols by their infrared vibrational frequencies has been, for the most part, unsuccessful. Several attempts have been made at assigning a frequency between 3735 and 3750 cm^{-1} to the SiO–H stretching vibration of a free geminal silanol, however, the controversy over their assignment remains unresolved [29]. On the other hand, solid-state ^{29}Si NMR spectroscopy has confirmed the existence of geminal silanols on silica and this technique is discussed further in the section to follow.

3. Characterization of Silica Surfaces by NMR

Solid state nuclear magnetic resonance (NMR) spectroscopy has proven to be a useful technique for characterizing solids. In particular, ^{29}Si solid-state NMR has been used extensively to study the surface properties of silica [2,29-33]. A high degree of structural resolution may be achieved using magic angle spinning (MAS) which reduces line-broadening due to chemical shift anisotropy and dipolar interactions. Cross polarization combined with magic angle spinning (CPMAS) transfers magnetization from a more abundant spin reservoir to a less abundant spin. For silica, surface sensitivity is increased using solid-state ^{29}Si CPMAS NMR; surface ^{29}Si nuclei are selectively polarized over the bulk ^{29}Si nuclei because of their proximity to the more abundant ^{1}H spin reservoir.

Concerning the geminal silanol controversy, strong evidence that single SiOH and geminal ($Si(OH)_2$) silanols populate the surface of an "as received" silica gel was first reported as recently as 1980 by Maciel using solid state CPMAS ^{29}Si NMR [30]. Peaks at about -90, -100, and -110 ppm relative to tetramethylsilane were assigned to the silicon resonance of geminal silanols, single silanols, and siloxane sites, respectively, thereby demonstrating the powerful structure-determining capability of this surface-sensitive technique.

Morrow and Gay have shown by ^{29}Si MAS NMR that geminal silanols and single silanols are present on aerosil silica which has been activated in vacuum between 160 and 800°C [29]. Similar studies using silica gels have also found that the fraction of silanol silicon sites which contain geminal hydroxyls, $\mathbf{f_g}$ does not vary appreciably with increasing activation temperature [31,32]. Legrand *et al.* report $\mathbf{f_g}$ to be 17%, 18%, and 21% for their silicas G, P, and A, respectively [2].

A comparison of the surface morphology of aerosil and precipitated silicas has been made by Tuel *et al.*, based on evidence obtained from ^{29}Si CPMAS NMR studies of the fully hydrated silicas [33]. From measurements of the relative abundances of the geminal, single, and siloxane ^{29}Si signals in the CPMAS spectrum, the authors were able to estimate an average effective distance, **L**, between an hydroxyl group and a $*Si(O\text{-})_4$ silicon site, beyond which cross polarization is no longer effective. According to their model, a larger value of **L** indicates a greater degree of surface roughness. On a rough surface, some $*Si(O\text{-})_4$ sites are very close to surface hydroxyls and are polarized by the ^1H spin reservoir, and this has the effect of increasing the average value of **L**. They observed that **L** was greater for precipitated silica than for aerosil on the hydrated, "as received" samples, suggesting a greater degree of surface roughness, or a greater fractal dimension. On the other hand, both silicas exhibited similar values of **L** after activation at 600°C, suggesting that their surface textures become more similar when extreme thermal treatments are employed.

The NMR results of Tuel *et al.* are consistent with fractal measurements of the

surfaces of "as received" aerosil and precipitated silica (see Table 1.1). Further, our studies of the isolated silanol distribution on activated silicas, to be presented in Chapter 4, also suggest that the surfaces of these silicas are more similar for higher activation temperatures than for the "as received" materials.

CHAPTER 2

EXPERIMENTAL SECTION

The Silicas

This work was carried out using a pyrogenic or aerosil type silica, Cab-O-Sil HS5, and a high-purity (Na 60 ppm, Al < 100 ppm, Fe 20 ppm, Ti < 20 ppm) non-porous precipitated silica. The pyrogenic silica (referred to for convenience as aerosil hereafter) is commercially available from Cabot Inc., U.S.A., and the precipitated silica was supplied by Rhône-Poulenc, France.

The B.E.T. specific surface areas of the two silicas were determined from adsorption isotherms obtained between 20 and 200 Torr N_2 (corresponding to relative pressures between 0.02 and 0.2) using a vacuum microbalance apparatus, and are reported in Table 2.1 for silica samples which had been vacuum activated for 1 hr at temperatures between 25 and 800°C. The specific surface area of the aerosil silica did not vary significantly with activation temperature, however, the precipitated silica exhibited an increase in surface area between 25 and 450°C activation, followed by a significant decrease between 450 and 800°C. As will be discussed in Chapter 3, the number of H-bonded silanols on precipitated silica which are eliminated as water upon heating from 150 to 450°C is about three times greater than the number which are eliminated from aerosil. The increase in B.E.T. surface area between 25 and 450°C activation is probably due to the removal of this H-bonded network of silanols, thus permitting increased adsorption of N_2. The precipitated silica exhibited a larger decrease in surface area than the aerosil silica between 450 and 800°C activation. This is likely due to sintering of the silica particles, which occurs to a greater extent in this temperature range for the precipitated silica by nature of its origin.

Silica Type	Activation Temp. (°C)	Specific Surface (m^2/g)
Precipitated Silica	25	265 ± 5
(Rhône-Poulenc)	150	265
	450	287
	800	242
Cabosil HS-5	25	320
(Cabot Inc.)	150	320
	450	325
	800	316

Table 2.1. B.E.T. Specific Surface Areas for Aerosil and Precipitated Silica

For the purpose of calculating silanol densities, we believe that an area of 285 m^2/g is more representative of the real area of the precipitated silica for vacuum activation between 25 and 450°C, and this value has been used to calculate the silanol density data discussed in Chapter 3.

Sample Preparation

Silica samples for transmission infrared studies were prepared in the following way. The silica powder was weighed in air using an analytical balance, then compacted at 10^7 Pa into a thin self-supporting disk using 1.9 cm or 2.5 cm diameter cylindrical dies. Silica disks containing between 2 and 80 mg/cm^2 in air were obtained using this procedure. Silica thin films containing between 0.1 and 0.2 mg/cm^2 were prepared by spreading and compacting the powder evenly over the surface of a slightly roughened transparent window (ZnSe, KBr) using a smooth stainless steel spatula. Disks containing 100 mg silica for vacuum microbalance studies were pressed in a 1.3 cm diameter cylindrical die.

Vacuum Activation

All silica samples were activated in vacuum for one hour at a predetermined temperature, then cooled to room temperature under dynamic vacuum before recording the initial infrared spectrum. When presenting the results in later chapters, the aerosil and precipitated silicas will be designated by the terms A-**x** and P-**x** respectively, where **x** is the temperature of activation in degrees Celsius.

The Infrared Spectrometers

Fourier transform infrared (FTIR) spectra were recorded using a Bomem DA3.02 instrument or a Bomem Michelson MB100 instrument. The DA3.02 instrument is capable of a maximum resolution of 0.02 cm^{-1} and is equipped with two separate sample compartments, one having a mercury cadmium telluride (MCT) detector, and the other having a deuterium tryglycine sulphate (DTGS) detector. This instrument also offers a selection of two light sources, a glowbar source which emits in the infrared, and a quartz halogen lamp which emits in the visible region of the spectrum and in the infrared to about 2200 cm^{-1}. The MB100 instrument is capable of a maximum resolution of 1 cm^{-1} and has a single DTGS detector. Both instruments are equipped with KBr beamsplitters and windows for use in the mid-infrared region, 5000-400 cm^{-1}.

Spectra were acquired on the DA3.02 and processed using Bomem software running on a Digital Electronics Corporation PDP11-compatible computer. Spectra were acquired on the MB100 and processed using Spectra-Calc software running on a IBM-compatible, 286-12 MHz, or 386-25 MHz computer. All spectra shown here are plotted in units of absorbance ($-\log_{10}(I/I_0)$) *vs.* wavenumber (cm^{-1}) unless indicated otherwise.

The Infrared Cells

Two infrared cell designs have been used in this study. The infrared cell design shown in Figure 2.1, and previously described by Morrow and Ramamurthy, consists of three

main parts [34]. The quartz sample holder sandwiches a 2.5 cm diameter disk between two rings which are fused to each of the two fingers at one end. The opposite end of the holder has two sealed guides, one of which is filled with iron bars. When assembled, the sample holder may be moved by pulling the iron bar with a magnet along the outside of the pyrex top assembly. This permits the silica sample to be moved to and from the furnace region and the window region of the quartz bottom assembly. The furnace is wrapped with nichrome wire and insulated with a glass wool matting. Temperatures inside the cell are measured using a thermocouple on the exterior side of the bottom assembly, between the nichrome wire and the insulating mat. Calibrations of the thermocouple have been performed by replacing the top assembly with a special assembly containing a thermometer well which protrudes into the furnace region. The large ground glass taper, joining the top and bottom assemblies, is lubricated with Apiezon H grease, and the vacuum stopcock and ground glass swivel joint are lubricated with Apiezon N grease. The total internal volume of this infrared cell is about 300 ml.

The infrared cell shown in Figure 2.2 has been developed here for carrying out *in situ* experiments over a wide range of sample temperatures. The IR cell body is constructed from a quartz tube, 25 mm O.D. and 22 mm I.D., which has a 50 mm flat, ground quartz flange fused to one end. The other end is ground perpendicular to serve as a flange for fastening a 25 mm ZnSe infrared window with epoxy (Figure 2.2A). A removable 50 mm infrared window forms a vacuum seal on the large flange, lightly greased with Apiezon H. The quartz sample holder consists of a slotted ring which has quartz rods fused to either end to prevent the sample holder assembly from sliding back and forth in the IR cell (Figure 2.2B). The pyrex vacuum stopcock is attached via a 5 mm I.D tube with a quartz-pyrex graded seal about 2 cm from the 50 mm flange. The stopcock must extend sufficiently so that it can be operated outside of a purged sample compartment in the infrared spectrometer. The cell is connected to a portable vacuum line at the ground pyrex swivel joint. The internal volume of this IR cell is about 80 ml.

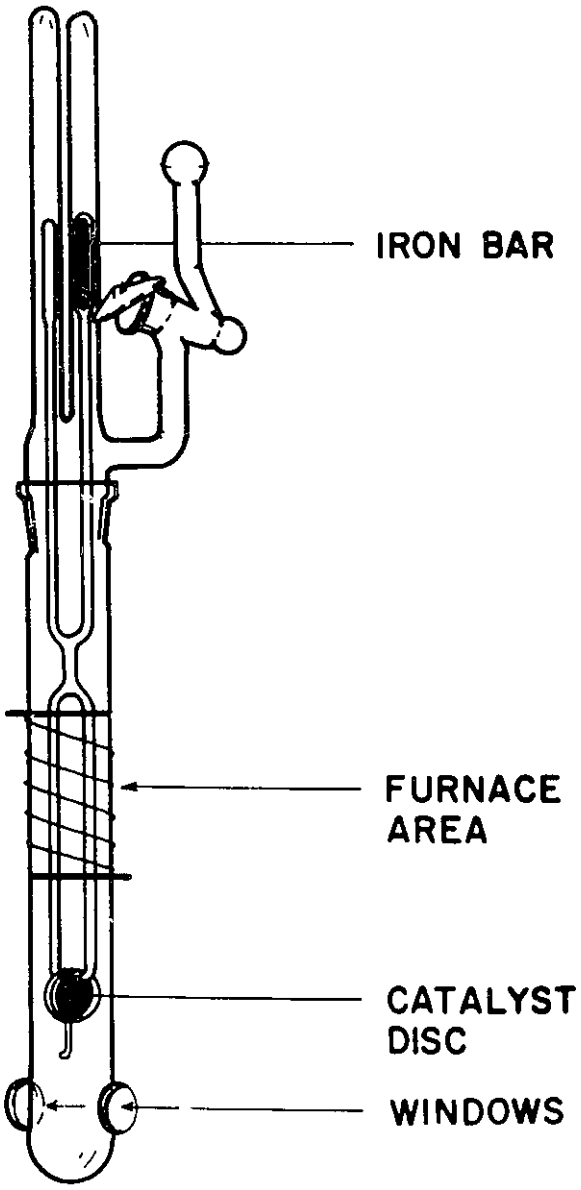

Figure 2.1 Conventional Infrared Vacuum Cell

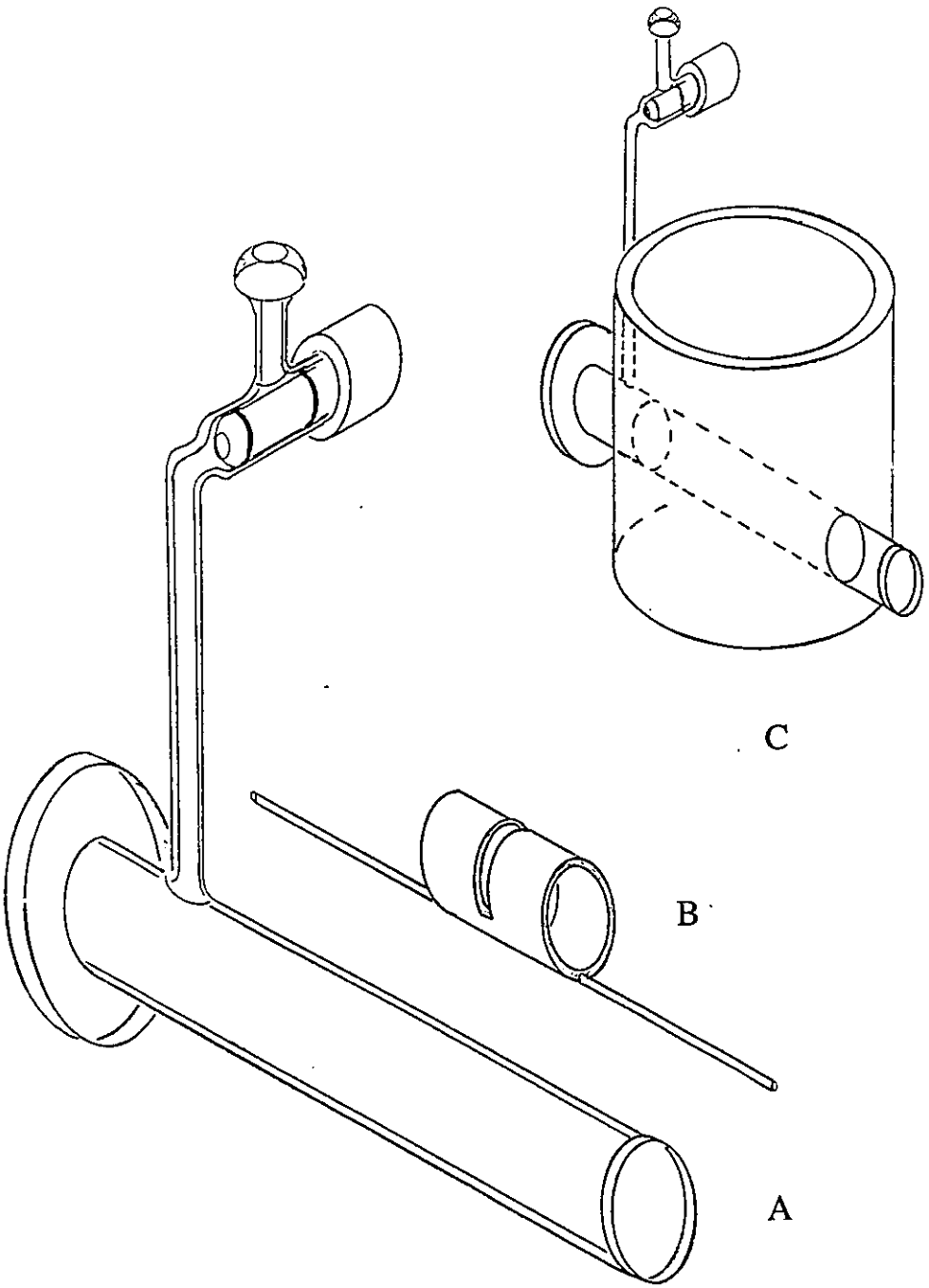

Figure 2.2 Variable-Temperature, *In Situ* Infrared Vacuum Cell. (A) Infrared cell body. (B) Quartz sample holder. (C) Infrared cell and polystyrene dewar assembly for recording low-temperature spectra.

Thermal activation of the silica sample is accomplished by sliding a short quartz tube furnace, slightly larger than 25 mm I.D., over the IR cell. The tube furnace can also be used for recording *in situ* spectra at elevated temperatures. External air-cooling of both windows is required when the sample is heated to 450°C or higher.

The silica sample can be cooled to temperatures near 77 K by immersing the sample region of the IR cell in liquid nitrogen. The infrared cell slides through a rigid polystyrene cup (commercially available as a beverage cooler), which has 25 mm diameter holes bored transversely through it about 1 cm above the inside bottom surface, forming a dewar flask around the middle region of the IR cell (Figure 2.2C). When spectra are being recorded with the IR cell bathed in liquid nitrogen, the cell assembly must be contained in a purged dry N_2 atmosphere to prevent frosting of the infrared windows.

Sample temperatures can be measured externally at the furnace using a thermocouple, as described above for the conventional cell. Alternatively, temperatures can be measured inside the cell, near the sample in the infrared beam, using a very fine thermocouple probe sealed in a flexible stainless steel jacket. A small ground glass vacuum joint near the large flanged end of the cell (not shown) provides access for the thermocouple probe, which is positioned near the sample surface after placing the sample holder in the cell, and before assembling the large IR window. Activation temperatures measured inside the cell and at the furnace do not differ by more than 2 degrees between room temperature and 450°C.

The jacketed thermocouple arrangement allows careful measurement of temperatures near the sample during either thermal activation or cooling. The sample temperature is 82 ± 1 K when the cell is bathed in liquid nitrogen with 0.5 to 2.0 Torr of a conducting gas in the cell. The heating effect of the infrared beam begins to raise the sample temperature when the pressure of the conducting gas falls below 0.1 Torr. The temperature increases by 5 K at 0.02 Torr and is likely greater (about 10 K increase) for an evacuated cell, but it is difficult to obtain this measurement accurately in an evacuated system.

The Vacuum Microbalance

Vacuum microbalance experiments were carried out using an electronic Sartorius model 4433 instrument. This balance is a symmetrical two-arm balance which can be operated in three mass ranges, *i.e.* ± 140 mg load with a sensitivity of 10 μg, ± 14 mg load with a sensitivity of 1 μg, and ± 1.4 mg load with a sensitivity of 0.1 μg.

The range chosen for a given experiment was selected based on an estimate of the change in mass. For example, when measuring B.E.T. specific surface areas, silica samples containing 100 mg (weighed in air) were tared on the balance, *i.e.* "zero" mg reading. These samples typically lost between 3 to 5 mg of adsorbed water when evacuated at ambient temperatures, and the mass of adsorbed nitrogen at liquid nitrogen temperatures and 200 Torr on 100 mg samples of aerosil or precipated silica was about 12 to 14 mg. Therefore, the ± 14 mg sensitivity range best suited this experimental setup.

The vacuum microbalance is equipped with pyrex envelopes which may be immersed in liquid nitrogen for B.E.T. experiments. These envelopes also permit silica samples to be vacuum activated at temperatures up to 450°C using a removable tube furnace. For higher temperatures of activation, a quartz envelope must be used on the sample side. The tapered glass/stainless steel vacuum joint must be air cooled externally for activation temperatures above 300°C.

The Vacuum Manifold

Silica samples were vacuum activated, and reagents were added to, and evacuated from the samples using a pyrex vacuum manifold. The standard portable design is a 300 ml-volume manifold equipped with six inlets (connections are made using 14/23 ground glass taper joints) and isolation at each inlet is provided by 8 mm I.D. pyrex/teflon stopcocks. A 15 mm I.D. pyrex/teflon stopcock can isolate the manifold from the vacuum pumps at the outlet. The manifold is pumped by an oil vapor diffusion pump through a liquid nitrogen trap, and a two-stage rotary vane roughing pump is connected to the outlet of the diffusion

pump. A minimum base pressure between 10^{-6} and 10^{-7} Torr can be achieved under ideal conditions, but a base pressure of 10^{-5} Torr can usually be reached in about 30 min when evacuating an IR cell from atmospheric pressure.

Absolute pressures of gaseous reagents in the manifold were measured using digital readout capacitance manometers. Three pressure ranges of manometers were used depending on the experiment, *i.e.* 10^{-3} to 10, 10^{-2} to 100, and 10^{-1} to 1000 Torr. These manometers could be mounted on the vacuum manifold at any of the six inlets.

Chemicals

Dimethylzinc was synthesized on a 5 g scale in a reaction between methyl iodide (Baker) and a mixture of zinc and copper metal powders (Aldrich) [35]. The metal powders were added to a 500 ml-volume stainless steel autoclave which had been reduced to about 50 ml capacity by adding glass beads. The autoclave was evacuated at room temperature and methyl iodide was distilled into the autoclave under vacuum. The reaction was allowed to proceed in the sealed vessel in an oven at 115°C for 12 hrs. The product was distilled from the reaction vessel under vacuum and purified by distillation under vacuum at -78°C. The infrared spectrum of the gas-phase product and the ^{1}H NMR spectrum of the liquid were compared to those previously reported [36]. No unreacted methyl iodide was detected when at least a two-fold excess of the copper/zinc powder mixture was used, and the ^{13}C NMR spectrum of the dimethylzinc product indicated less than 1 % C-containing impurities.

Hexamethyldisilazane was purchased from Pierce Chemical, titanium tetrachloride from Fisher Scientific, trimethylaluminum (electronic grade) from Alpha Ventron, and boron trichloride from Matheson. D_2O, ND_3, CD_3OD, i-PrOD, and t-BuOD were purchased from MSD Isotopes and had a deuterium isotopic abundance greater than 99.4%. Methanol (spectroscopic grade), trimethyl phosphite (NMR grade) and dimethyl phosphite (99%) were purchased from Aldrich. Carbon monoxide, nitrogen, helium, and methane were purchased from Matheson.

All reagents were transferred under vacuum to storage bulbs equipped with glass/teflon, or greased vacuum stopcocks. The reagents were degassed by repeatedly freezing the liquid or gas in a liquid nitrogen bath and evacuating the dead space. Carbon monoxide was purified by passing the gas slowly through a liquid nitrogen trap to remove iron carbonyls which form in the steel cylinder. Nitrogen, methane, and helium were dried by passing them through a column containing P_2O_5. Purity checks were routinely performed via infrared and/or mass spectrometric analysis.

Methods Used to Improve Signal to Noise Ratio in Transmission Infrared Spectra

The signal to noise ratio (S/N) of a single beam spectrum is proportional to the **throughput** (the light intensity arriving at the detector) and the **specific detectivity**, D^*, of the detector, which is a measure of its sensitivity. S/N also increases as the square root of the **observation time** (*i.e.* the number of scans which are signal-averaged) [21]. These three factors largely determine the background noise level in a spectrum obtained in transmission or absorbance, however, S/N also depends on the number of absorbing species being sampled. Detector characteristics are usually matched to the application at the time of purchase, and in most cases D^* will have been optimized by the manufacturer [37]. Throughput may be varied, depending on the interferometer optics, the detector's sensitivity ($D^* > 10^{10}$), and its area. The Bomem DA3.02 spectrometer, equipped with a 1 mm^2 MCT detector, allows such optimization, although the same flexibility is not available using the DTGS detector which has a much lower D^* value.

Many of the infrared studies carried out here concentrated on specific regions of the silica spectrum. Experimental procedures for optimizing the S/N ratio in two spectral regions, between 500 and 1000 cm^{-1}, and above 3000 cm^{-1}, are discussed below.

The spectrum of silica below about 1300 cm^{-1} is dominated by the strong absorptions of bulk SiO_2 modes to the extent that samples containing greater than about 20 mg/cm^2 silica become totally opaque between 400 and 1300 cm^{-1}. Figures 1.1 and 1.2 show that silica disks

containing 10 mg/cm^2 have two partly-transmitting "windows", between 600 and 750 cm^{-1}, and between 850 and 1000 cm^{-1}, whereas samples containing less than 3 mg/cm^2 are mostly transmitting above 500 cm^{-1}, except for the 1000 to 1300 cm^{-1} region. Because the lower limit for a self-supporting disk of either aerosil or precipitated silica is about 2 mg/cm^2, a thin film technique must be employed in order to access the total spectral region of silica below 1300 cm^{-1}.

Generally, for transmission infrared studies of the window region of silica (between 500 and 1000 cm^{-1}), there is little to be gained in terms of S/N from the thin film technique over the use of self-supported disks. Transmission of infrared radiation in this region is increased for a thin silica film, but at the expense of greatly reducing the number of surface species being observed, so that the net result is little improvement in S/N of the absorbance spectrum. The effect that reducing the quantity of silica from 2.5 to 0.1 mg/cm^2 has on the number of surface species being sampled in the IR beam can be seen clearly by comparing the intensities of the SiO–H stretching profiles in Figures 1.1 and 1.2, B and C.

Although they are rather fragile, the use of self-supporting disks may have other advantages over a silica thin film on a supporting window. For instance, the disks may be subjected to thermal activation treatments well beyond the upper limit imposed by the supporting window material. (This temperature is about 500°C for ZnSe, and about 400°C for KBr). Further, the use of self-supporting disks eliminates any problems associated with the chemical reactivity and resiliance to thermal shock of the supporting window.

The maximum absorbance at 800 cm^{-1}, for self-supporting disks containing between 2 and 2.5 mg/cm^2, is in the range of 1.2 to 1.8, and a reasonably low level of background noise can be achieved when signal averaging is employed. Signal averaging is a very effective means of enhancing S/N ratio, however, this technique requires long acquisition times when greater than about 90 percent of the incident light intensity is either absorbed or scattered by the sample. The former situation is encountered in the silica window region using thin disks while the latter is encountered in the spectral region above 3000 cm^{-1} using thick silica disks.

In both cases, further improvement in S/N may be achieved by reducing the overall bandwidth, while increasing the throughput in the desired spectral region.

The DA3.02 spectrometer, equipped with a 1 mm^2 MCT detector, uses a variable aperture stop to limit the throughput at the detector during high-resolution scanning. When using a broadband source (glowbar) at low resolution (2 or 4 cm^{-1}) in an open beam configuration, the MCT detector still requires that throughput be limited in order to prevent detector saturation [21,38,39], and this is accomplished with the variable aperture. High-pass and/or low-pass filters optical filters may be used to reduce the bandwidth of the infrared source radiation, while throughput may be controlled using the variable aperture stop. Their combined effect on the spectral energy distribution, for the purpose of improving S/N in the window region, and above 3000 cm^{-1}, is illustrated in Figure 2.3.

The single beam energy spectrum in an open beam configuration using, an MCT detector, a glowbar source, and no optical filters is shown in Figure 2.3A. The single beam spectra have been normalized to the energy maximum (at about 1000 cm^{-1}) in Figure 2.3A, allowing us to compare the relative energy for several experimental setups.

When a low-pass filter is employed (Figure 2.3B), the bandpass is limited to frequencies below about 1600 cm^{-1}, thereby allowing the throughput at the detector to be increased without saturation, by increasing the diameter of the aperture stop. This results in an increase by about a factor of two in the incident energy between 1500 and 500 cm^{-1} using the glowbar source.

The same approach may be used to improve S/N in the spectral region above 3000 cm^{-1}. In this region, the energy reaching the detector begins to fall off appreciably due to reduced beamsplitter performance and detector response, and this can be seen as a tail to higher wavenumber in Figure 2.3A. Light-scattering losses in thick silica disks may also contribute to a poor S/N ratio in this spectral region. Optical quartz functions as a high-pass filter, effectively reducing the bandpass to the spectral region above 2200 cm^{-1} (Figure 2.3C), so that the MCT detector may be fully illuminated without saturation using a wide aperture.

A further increase in the incident intensity (by about a factor of two at 4000 cm^{-1}) can be achieved by switching from the infrared glowbar source to a visible quartz-halogen source while using the high-pass filter (compare Figure 2.3, A and C at 4000 cm^{-1}). This visible source option may be software-selected on the DA3.02 instrument.

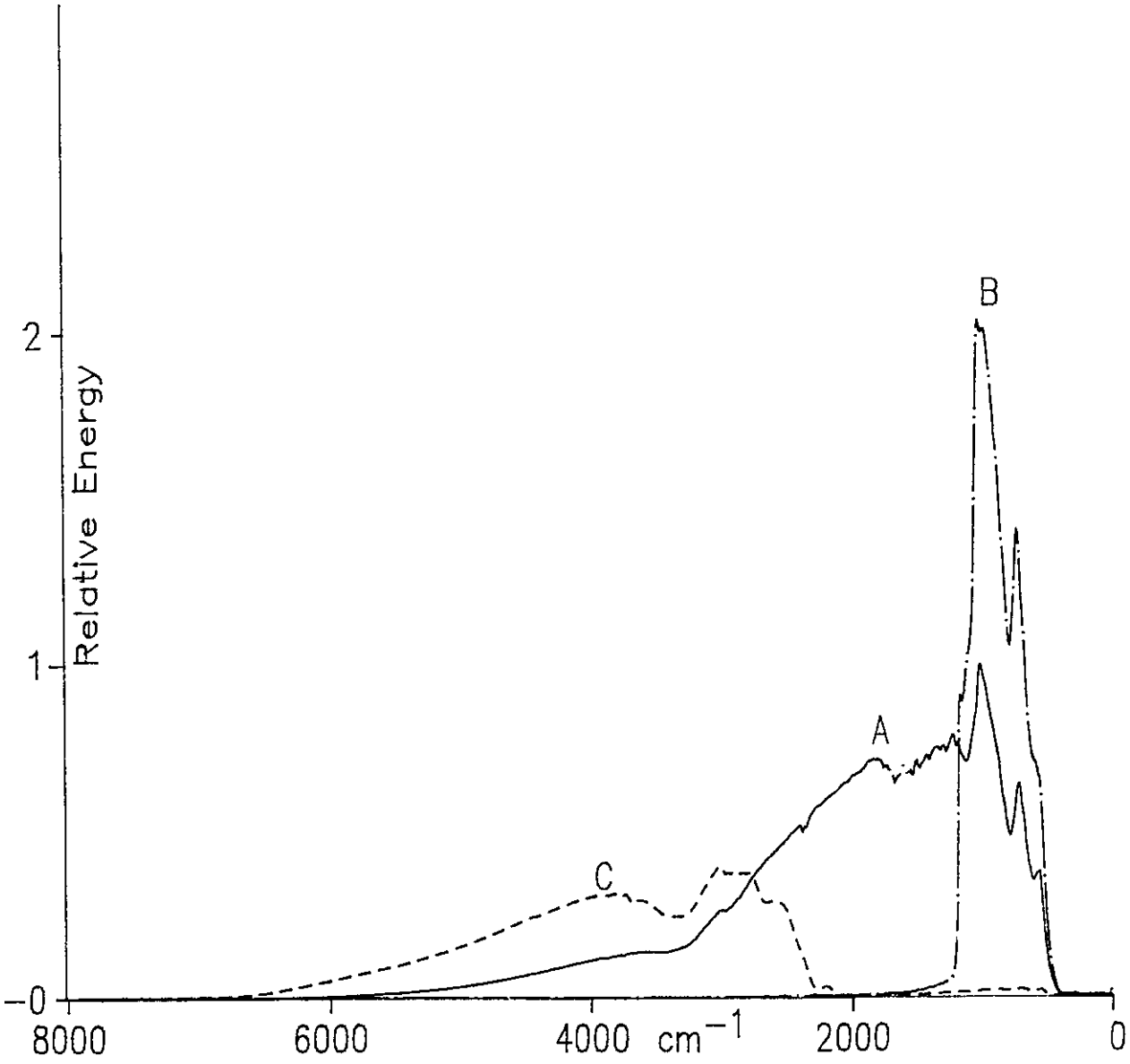

Figure 2.3. Single beam infrared spectra showing relative energy versus wavenumber for various optical configurations. A) no filters, glowbar source. B) low-pass filter, glowbar source. C) high-pass filter, quartz halogen source.

CHAPTER 3

An Infrared and Gravimetric Study of Aerosil and Precipitated Silica Using Chemical and H/D Exchange Probes

Introduction

The density of surface silanol groups on "as received" aerosil and precipitated silicas can vary considerably according to the method of preparation [2,40]. The silanol groups on either silica can strongly interact via hydrogen bonding with proton donor or acceptor molecules and this property largely determines the interfacial chemistry [1-4]. A normally hydrophillic hydroxylated surface can be chemically modified by replacing the SiOH groups by other functionalities. For example, the SiOH groups can react with a variety of hydrogen-sequestering (HS) agents, MX_n, via reaction (1) thereby altering the structure and adsorption characteristics of the surface [18,41].

$$SiOH + MX_n \longrightarrow SiOMX_{n-1} + HX \qquad (1)$$

When the HS agent contains a trialkylsilyl group, SiOH is converted into $SiOSiR_3$, and a relatively inert hydrophobic material can be produced which might be more suitable for chromatographic or other purposes [42]. Whatever the HS agent used, the extent to which the silanols react depends on the silanol density and/or the size of the HS agent used, and these steric factors ultimately influence the number of silanols which react.

In this work we have compared the properties of surface silanols on an aerosil and a precipitated silica. We have used chemical modification and H/D exchange in order to assess

the relative reactivity of isolated and H-bonded silanols, compare the accessibility of the silanols to reactants of various size, and measure the silanol densities of isolated and H-bonded silanols on these "as received" materials. Chemical modification has been carried out using HS agents of different size [$ZnMe_2$, BCl_3, $TiCl_4$, $AlMe_3$ and $Me_3SiNHSiMe_3$ (HMDS)] and exchange has been carried out using D_2O, ND_3, and deuterated methanol, i-propanol and t-butanol. The results are used to develop a quasi-quantitative model of the silanol structure on these silicas.

Experimental Section

The silica samples, used to obtain the transmission infrared spectra shown here, contained 10 mg/cm^2 in a 2.5 cm dia self-supporting disk. The silica disks were activated in vacuum for one hour at 150°C or 450°C. All spectra were recorded at 2 or 4 cm^{-1} resolution and are shown in absorbance.

The aerosil and precipitated silica are described in Chapter 2 and their B.E.T. (N_2) surface areas for 150 and 450°C activation are listed in Table 2.1. A specific surface area of 285 m^2/g has been used to calculate the silanol densities for P-150 and P-450, as explained in Chapter 2.

Chemical reactions were carried out in the 300 ml conventional IR vacuum cell using an excess of reactant compared to the number of SiOH groups (see later for this parameter). The reactions went to completion after a few minutes at 22°C for $AlMe_3$, BCl_3, and $TiCl_4$, after about 20 min at 22°C for $ZnMe_2$, and after about 1 h at 150°C for HMDS. A "complete reaction" was said to have occurred when there was insignificant further spectral change over an additional period of about 20 min]. The exchange reactions were all carried out at 22°C and the procedure will be described later.

Results

(a) Untreated Silica

The surface silanol groups on silica exhibit characteristic OH stretching vibrations in the spectral region from 3800 to 3200 cm^{-1}. The infrared spectrum of aerosil after vacuum activation at 150°C for 1 hour (A-150) is shown in Figure 3.1A and that of the precipitated silica (P-150) is shown in Figure 3.1A'. Both spectra show a sharp peak near 3747-3737 cm^{-1} characteristic of isolated non-interacting surface silanols and a broad feature with a maximum near 3520 cm^{-1} which has been attributed to hydrogen-bonded silanols [1-4]. For aerosil, a shoulder near 3720 cm^{-1} can just be discerned and the 3720, 3520 cm^{-1} pair of bands have been assigned to the H-bonded and free silanol groups, respectively, of a pair or chain of silanols (see Figure 1.3 also).

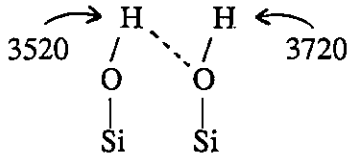

A slight inflection near 3660 cm^{-1} in Figure 3.1A is attributed to internal silanols which are perturbed due to interparticle contact. These silanols are largely inaccessible to many reactants [25,26,43,44] and we will refer to them in later discussions as either "perturbed" or "inaccessible" silanols. The 3720 and 3660 cm^{-1} features are not resolved in the spectrum of the precipitated silica (Figure 3.1A') which, instead, exhibits a broad feature near 3695 cm^{-1}.

The above spectrum of aerosil is identical to that which can be observed after evacuation for 1 h at 22°C. Ghiotti *et al.* first reported that evacuation at room temperature removes all physically adsorbed water on aerosil silica [45], and our vacuum microbalance experiments have confirmed that there is no mass loss upon going from 1 h evacuation at 22°C to further evacuation at 150°C for 1 h. Therefore, the spectrum shown in Figure 3.1A can be considered to be that of an "as received" hydroxylated aerosil which contains no

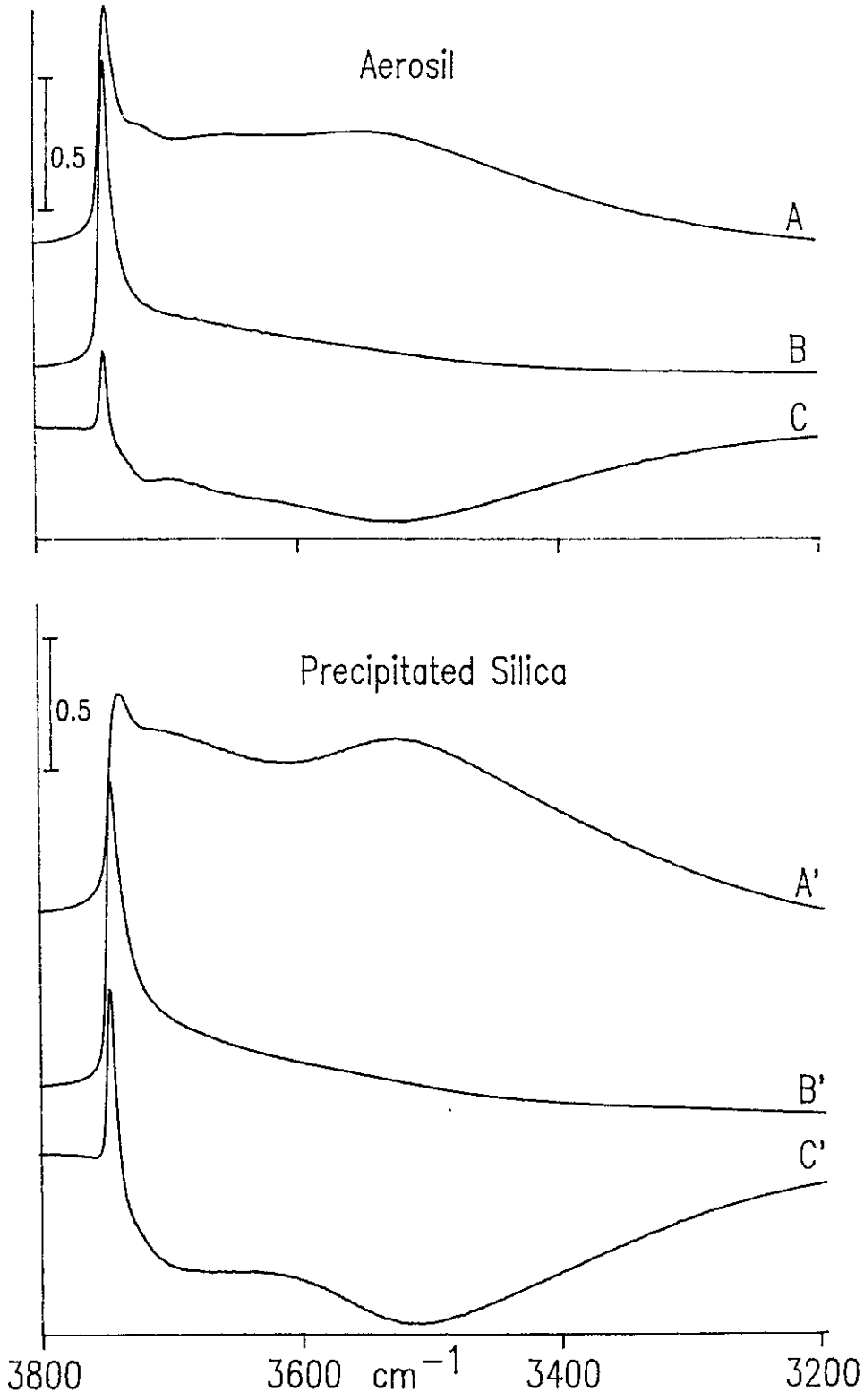

Figure 3.1. Infrared spectra of A-150 (A) and A-450 (B) in the SiO–H stretching region. Curve C is the difference spectrum, B-A. Curves A', B' and C' are the corresponding spectra for the precipitated silica.

adsorbed water.

The infrared spectrum of the precipitated silica is almost identical to that which can be observed after evacuation at ambient temperature for 1 h except that there was about a 5% decrease in the intensity of the broad 3520 cm^{-1} feature upon going to 150°C. Microbalance experiments indicated that there was a small decrease in mass of the sample upon going from evacuation at 22°C to activation at 150°C. After evacuation of either silica for 1 h at 22°C there was no indication of an infrared band at 1620 cm^{-1}, characteristic of the bending mode of physically adsorbed H_2O [19,45]. This demonstrated that the ambient temperature vacuum treatment was sufficient to remove all adsorbed water. Therefore, the loss of mass of the precipitated silica upon going from 22°C to 150°C can probably be attributed to the slow condensation of pairs of H-bonded silanols resulting in the desorption of water (Chapter 1, reaction 5). Further, this mass loss continued with prolonged evacuation of P-150 at 150°C (but not with A-150), suggesting that the condensation reaction is a continuous slow process even at 150°C. This poses difficulties in specifying the number of SiOH groups which are present on P-150. Because most of the data described later relative to both silicas were obtained after a standard 1 h activation at 150°C, we have measured the initial SiOH density under these conditions only, accepting that these numbers would be slightly lower for the precipitated silica if longer activation times were used. These results will be presented in the next section.

A visual comparison of the spectra of A-150 and P-150 after 150°C activation (Figure 3.1, A and A' respectively) shows that the integrated intensity of the precipitated silica is apparently greater than that of aerosil. In a series of spectra recorded with identical 2 cm^{-1} resolution, the mean integrated intensities were 150 and 292 cm^{-1} for the same quantity (10 mg/cm^2) of aerosil or precipitated silica (for convenience the unit cm^{-1} will be omitted in future discussions of integrated intensities). These integrated intensities have limited quantitative meaning because the extinction coefficient of an H-bonded OH oscillator varies with wavenumber [46], but they do suggest that there are more silanol groups on the

precipitated silica under these conditions. Our silanol density measurements, which will be presented in more detail in part d, show that there are about 3.1 and 6.8 silanols per nm^2, on A-150 and P-150, respectively.

Activation of both silicas at 450°C resulted in the loss of virtually all of the intensity at 3520 cm^{-1} (Figure 3.1, B and B') and an increase in the intensity of the peak due to isolated silanol groups. The changes between the 150 and 450°C activation are more clearly seen in the difference spectra shown in Figure 3.1, C and C'. These spectra correspond to spectrum B or B' minus spectrum A or A', and peaks going upward show bands which have increased in intensity upon going from 150 to 450°C while those going downward show bands which have decreased in intensity.

In both cases, there was a loss in intensity associated with H-bonded silanols which can be attributed to condensation processes like reaction 5, Chapter 1. The increase in the isolated SiOH band intensity with increasing temperature might be attributed to a similar condensation process whereby a group containing an odd number of H-bonded silanols (a chain of three in the example below) condense to liberate water, thereby creating a siloxane bridge site and an isolated silanol:

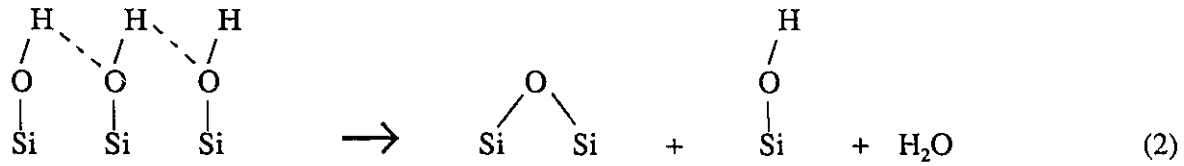

(2)

Such effects have been observed previously for other silicas [19,23], and in this case the changes were more pronounced for the precipitated silica.

(b) Relative Rates of Reaction of Various Silanol Types

Time-resolved studies of the reactions of A-150 and P-150 silicas with $AlMe_3$, BCl_3, and $TiCl_4$ have been carried out in order to determine if there is a difference in reactivity at

22°C between the accessible H-bonded silanols (3520 cm^{-1}) and free isolated silanols (3748-3738 cm^{-1}). The procedure involves adding excess reactant and following the spectral changes as a function of time as the reaction proceeds. Spectra have been acquired using the DA3.02 spectrometer and MCT detector which enables us to acquire a single 4 cm^{-1} resolution spectrum in 0.25 sec. Using this technique, we have observed that the reactions of $AlMe_3$, BCl_3, and $TiCl_4$ are essentially complete after 12, 24 and 60 s, respectively, for an exposure of 4 to 8 mmol of reactant per gram of silica (this exposure corresponds to about a 3 or 4-fold excess of reactant when compared with the number of SiOH groups which react).

The reaction between $TiCl_4$ and a single, isolated, geminal or H-bonded SiOH might yield a surface $SiOTiCl_3$ species (the general case is shown in reaction 1). In addition, geminal silanols or vicinal silanols might yield the bridged species SiO_2TiCl_2 or $(SiO)_2TiCl_2$ respectively, via a bifunctional reaction [47]. In principle, a bifunctional reaction is also possible with $AlMe_3$ or BCl_3, although $GaMe_3$ and BEt_3 appear <u>not</u> to react bifunctionally [48,49]. Therefore, it is conceivable that size of the reactant, and/or its ability to react bifunctionally, could influence the rate at which isolated and H-bonded silanols react.

The rapid scan capability of the FTIR spectrometer is illustrated with reference to the reactions of A-150 and P-150 silicas with $TiCl_4$. Figure 3.2 shows a series of spectra observed every 4 sec after $TiCl_4$ was admitted at room temperature to 10 mg/cm^2 samples of A-150 and P-150 (two different experiments). Four scans were signal-averaged for each spectrum. As such, these spectra are not particularly diagnostic because there is always a certain number of SiOH species which remain inaccessible to a given reactant. The broad peak at about 3660 cm^{-1}, after the reaction had ceased, is a measure of the inaccessible silanols and these will be discussed later when we consider the static reactions.

In order to compare the reactivity of free isolated and H-bonded silanols, the results of the time-resolved experiments are presented as difference spectra in Figure 3.3. These spectra show the <u>changes</u> which occurred in a given time interval. The number of scans acquired and the interval between spectra are listed in Table 3.1. Only the first three intervals are shown

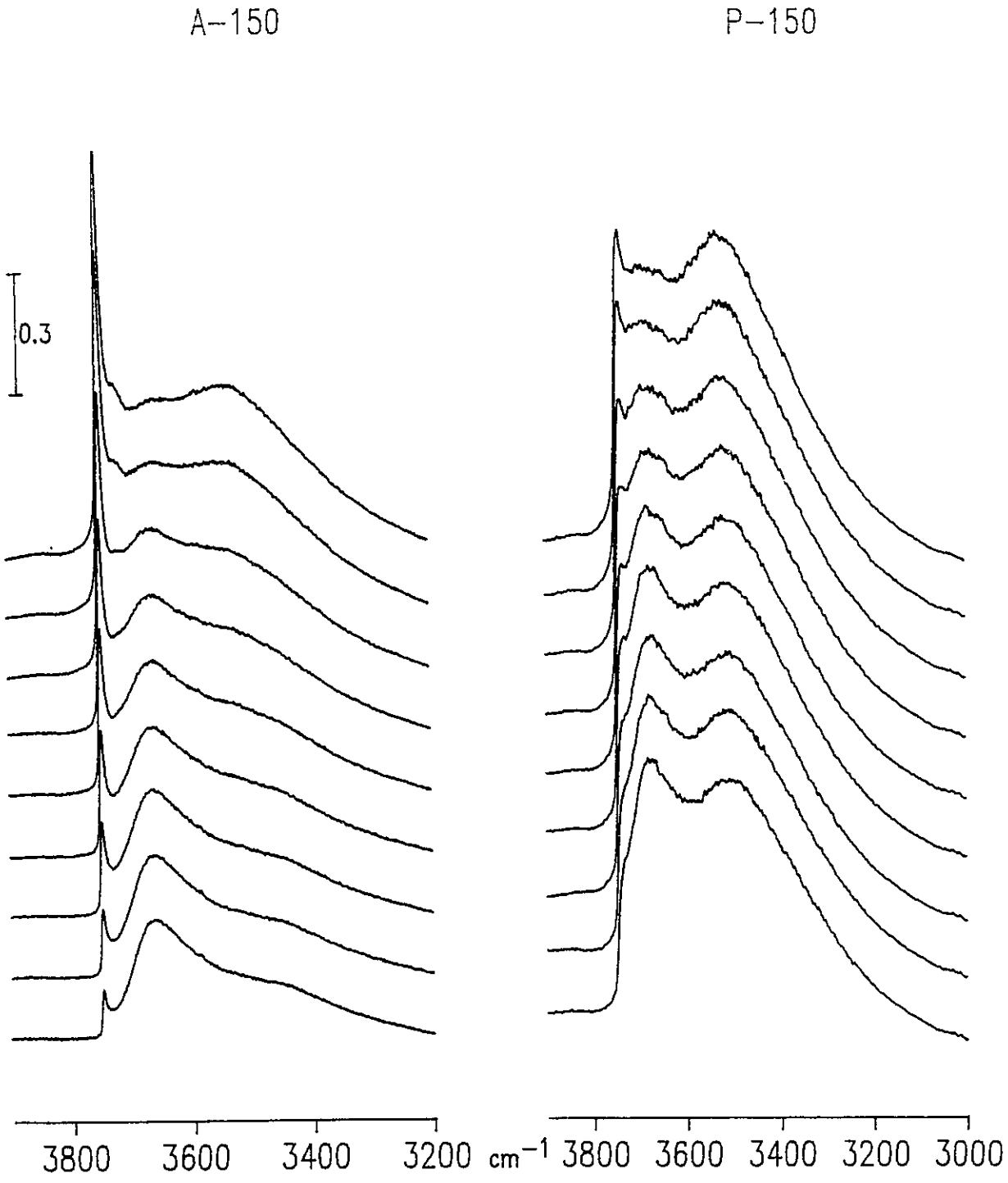

Figure 3.2. Time-resolved spectra showing the evolution of the SiOH band during the reaction of $TiCl_4$ at 22°C with A-150 and P-150 silicas.

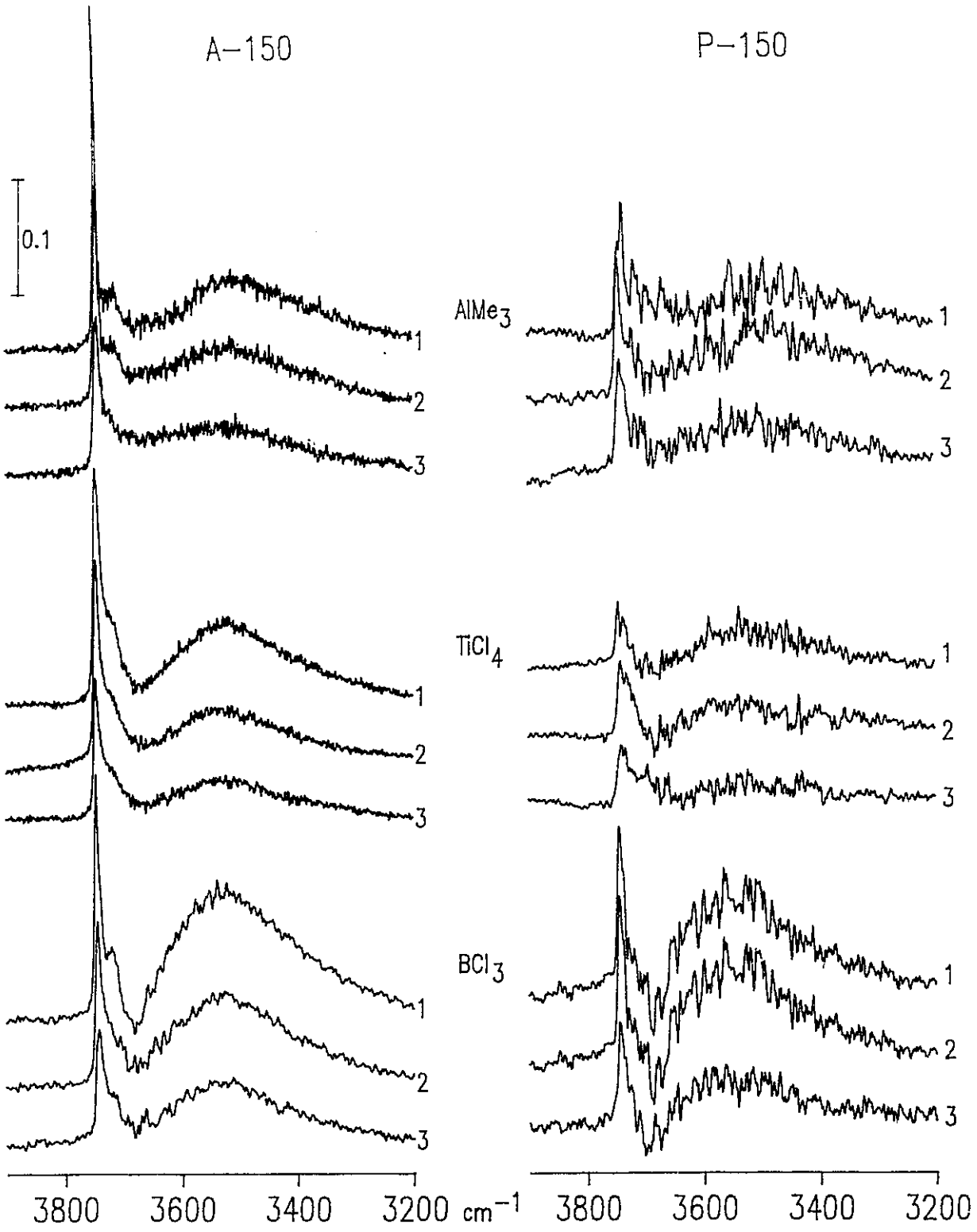

Figure 3.3. Difference spectra showing what has reacted in the first 3 intervals during the reactions of $AlMe_3$, $TiCl_4$, and BCl_3 with A-150 and P-150. The duration of an interval (seconds between spectra) is shown in Table 3.1.

because 50 to 70% of the silanols had reacted at the end of the third interval, and the duration of each interval was chosen so as to represent about the same degree of reaction for each reactant.

Reactant	A-150 Interval (sec)	A-150 number of scans[(a)]	P-150 Interval (sec)	P-150 number of scans[(a)]
$AlMe_3$	1	1	2	1
BCl_3	2	1	2	1
$TiCl_4$	4	4	4	4

Table 3.1. Time and Scan Data for Fast Scan Spectra.

(a) A single scan requires 0.25 sec. For multiple scans, one 0.25 sec scan can be acquired every 0.5 sec.

The signal-to-noise level in these spectra is poor, especially for BCl_3 and $AlMe_3$ where a single scan was used. A greater degree of background scattering reduces the transmitted intensity, thereby decreasing the S/N even further for the series of spectra showing what has reacted with P-150. However, particularly in the first interval for the A-150 series, a visual inspection shows that the broad 3520 cm^{-1} band due to H-bonded silanols has a greater intensity in the order $BCl_3 > TiCl_4 > AlMe_3$. This trend continues for the other intervals.

We also determined a parameter, **R**, which is the ratio of the peak height of the isolated SiOH peak (≈3745 cm^{-1}) to that at 3520 cm^{-1}. From the spectra shown, and other sets of experimental data, the **R** values are estimated to be 5.0 ± 0.3 for $AlMe_3$, 2.7 ± 0.2 for $TiCl_4$ and 1.9 ± 0.1 for BCl_3. A low value of **R** indicates that the H-bonded silanols are initially relatively more reactive than the isolated silanols, this being in the order $BCl_3 > TiCl_4 > AlMe_3$.

For the P-150 series, there is not a such a clear difference in the rate of disappearance of the 3520 cm^{-1} band relative to the 3745 cm^{-1} band with any reactant. Qualitatively, the trend follows the same order as for A-150, but we have not attempted to characterize this via the **R** factor in view of the very poor signal-to-noise level.

Although not shown in Figure 3.3, from about the 5th interval on for any reactant and for either silica, there was very little change in intensity due to H-bonded silanols, whereas the sharp peak at 3745 cm^{-1} continued to "disappear", albeit to a lesser extent than in the earlier intervals. This shows that the reaction with H-bonded silanols ceases before that with isolated silanols. As will be discussed below, this is consistent with the results obtained for the static reactions with chemical and H/D exchange probes.

(c) Chemical and H/D Exchange Probes of 150°C Activated Silica

In the preceding section, time-resolved studies using $AlMe_3$, BCl_3, and $TiCl_4$ examined how fast the isolated silanols on A-150 or P-150 reacted relative to the H-bonded silanols (as indicated by the **R** value), and whether or not the relative rate of reaction remained constant as the reaction proceeded. We have also examined spectroscopically how many silanols react on A-150 and P-150 silicas for a series of chemically reactive HS agents of differing steric dimensions; this provides us with a measure of the accessibility of surface silanols towards these chemical probes.

Figure 3.4 shows infrared spectra of A-150 and P-150 before (curves A and A', respectively) and after complete reaction (B and B') with excess $TiCl_4$. Curves C and C' show the difference spectra (A-B and A'-B') illustrating the spectral change as a result of the reaction. Not all of the silanols are capable of reacting with this reactant, as is evident by the residual intensity near 3660 cm^{-1} in curves B and B' due to inaccessible silanols.

Figure 3.5 shows a series of spectra observed after the complete reaction of A-150 with HS agents decreasing in size in the order, HMDS, $TiCl_4$, $AlMe_3$, BCl_3, $ZnMe_2$. Figure 3.6 shows the corresponding spectra for P-150. For comparison, the SiOH exchange reaction

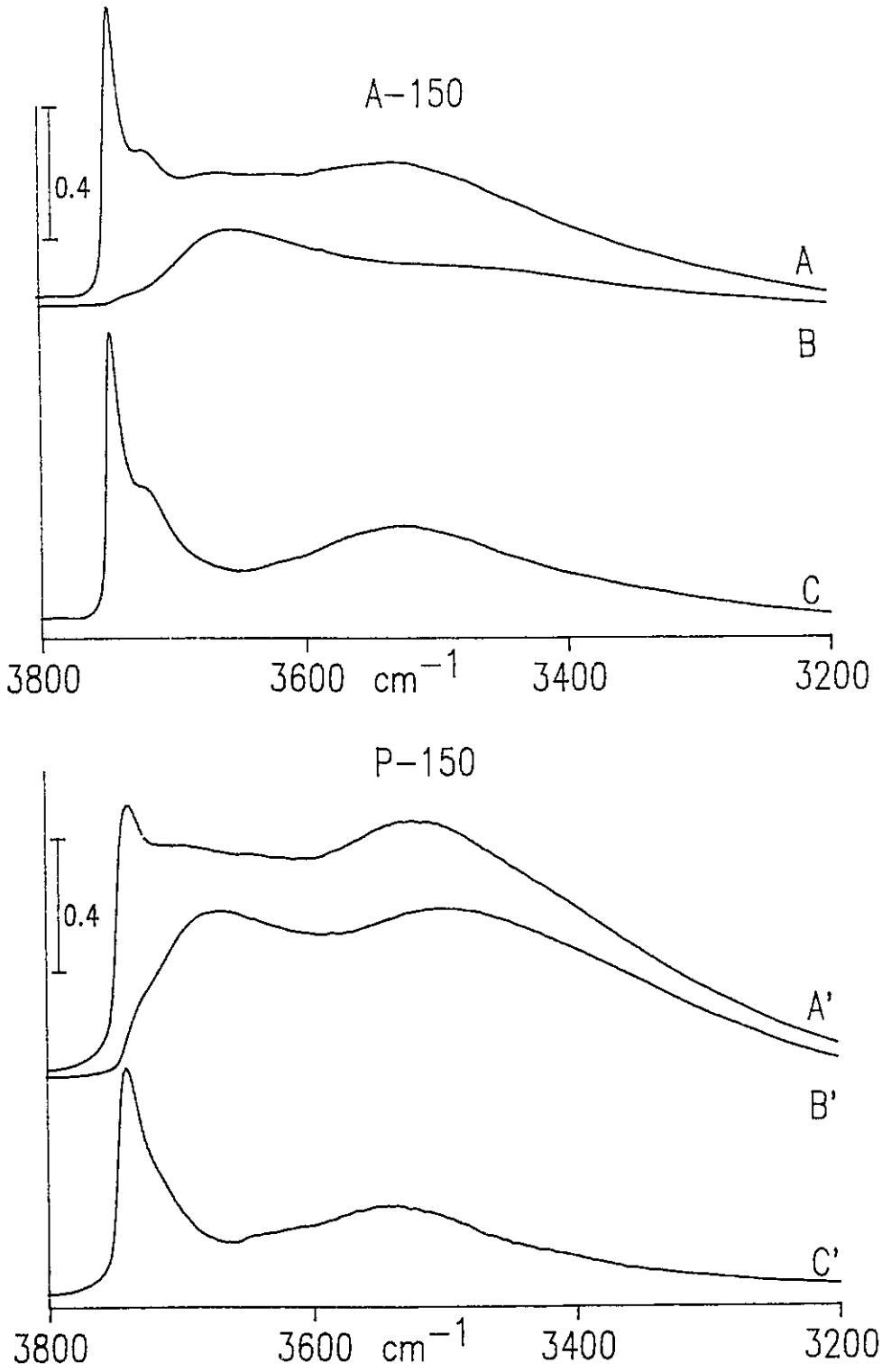

Figure 3.4. Infrared spectra of A-150 and P-150 before (A and A' respectively) and after (B and B') complete reaction at 22°C with $TiCl_4$. Curves C and C' are the difference spectra A-B and A'-B' respectively.

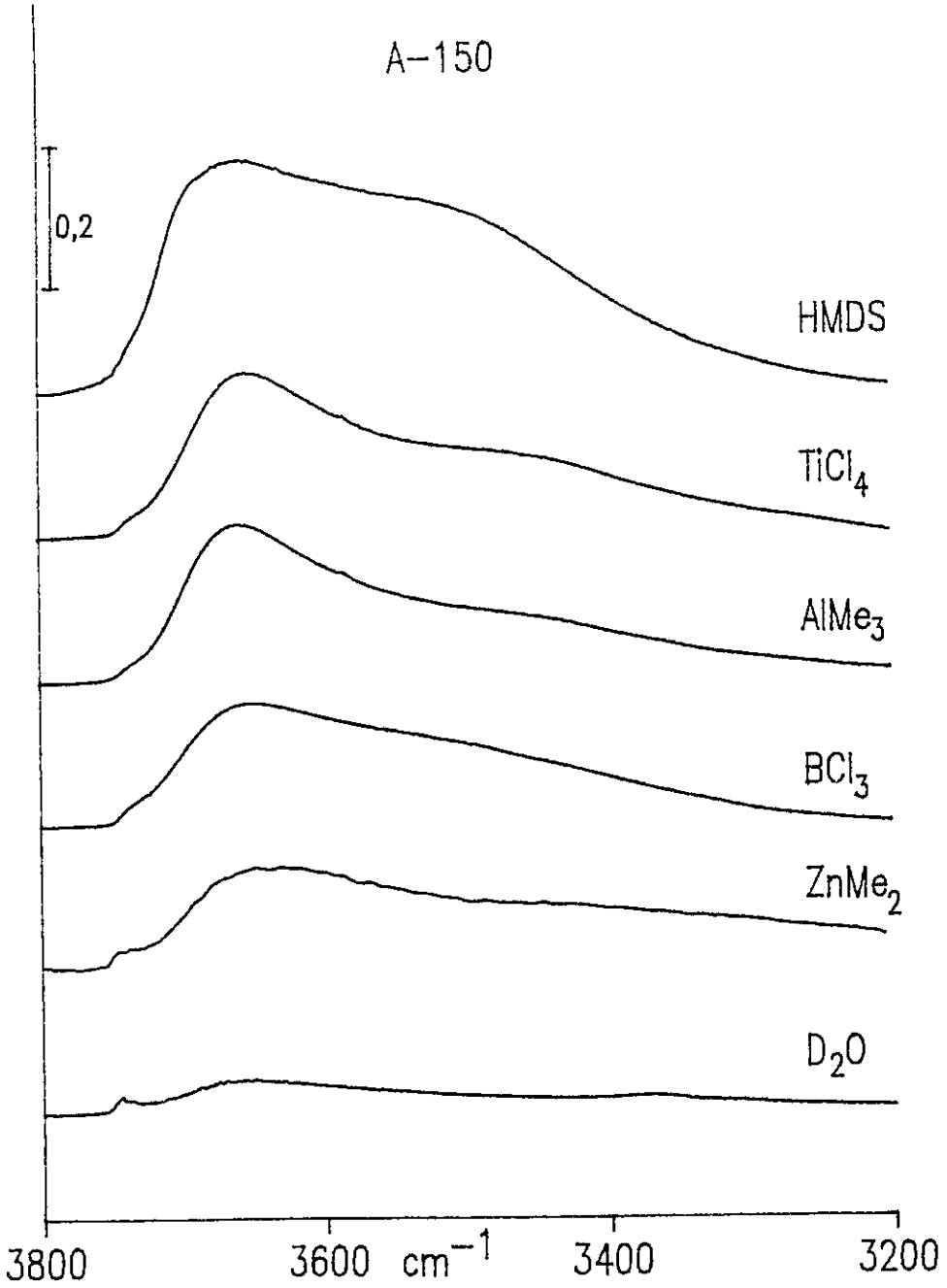

Figure 3.5. Infrared spectra of aerosil silica, A-150, after complete reaction at 22°C with the indicated hydrogen sequestering agent, or after H/D exchange with D_2O. The integrated intensities are shown in Table 3.2.

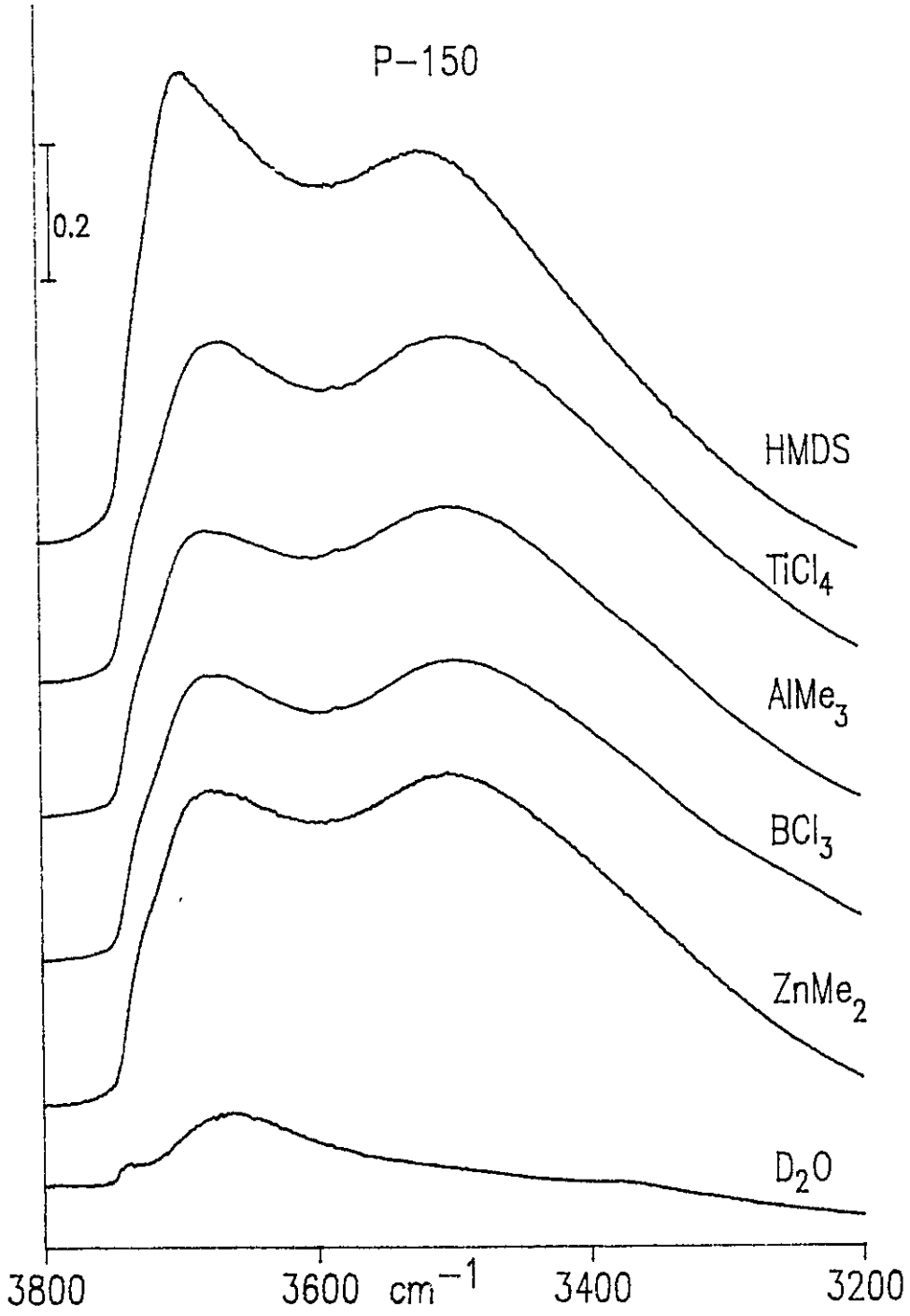

Figure 3.6. Infrared spectra of precipitated silica, P-150, after complete reaction at 22°C with the indicated hydrogen sequestering agent, or after H/D exchange with D_2O. The integrated intensities are shown in Table 3.2.

of A-150 and P-150 with D_2O has been included in Figures 3.5 and 3.6, respectively. A visual inspection shows that there is a considerable difference in the residual intensity in the 3700 to 3500 cm^{-1} region, depending on the nature of the reactant.

Figure 3.7 shows the difference spectra for each HS agent on A-150 and P-150 (*i.e.*, each spectrum is like curves C and C' for $TiCl_4$ in Figure 3.4.) In spite of large obvious differences in the "after reaction" curves in Figures 3.5 and 3.6 for each silica, the difference spectra in Figure 3.7 are remarkably similar for the same HS agent on these two silicas.

We have attempted to quantify the effect of the size of the chemically reactive probe molecule on the number of silanols which react with a given probe. Table 3.2 shows the cross sectional area of each HS probe, the normalized integrated intensity of the residual silanol band profile after reaction with each HS probe (and D_2O), and the percentage decrease of the initial SiOH band intensity.

		A-150		P-150	
Reactant	Reactant area ($Å^2$)	Intensity[a] I_A	% SiOH change[c]	Intensity[b] I_P	%SiOH change[c]
HMDS[d]	54.2	100	33	248	15
$TiCl_4$	35.2	54	64	200	32
$AlMe_3$	32.1	45	70	189	35
BCl_3	30.3	47	69	196	33
$ZnMe_2$	25.7	36	76	188	36
D_2O	10.5	12	92	22	92

Table 3.2. Chemisorption Data for Reactions on A-150 and P-150

(a) Normalized integrated intensity I_A after reaction. Initial normalized intensity $I_{oA} = 150$.

(b) Normalized integrated intensity I_P after reaction. Initial normalized intensity $I_{oP} = 292$.

(c) Percent decrease in the SiOH intensity after reaction, I/I_o for A-150 and P-150.

(d) Hexamethyldisilazane.

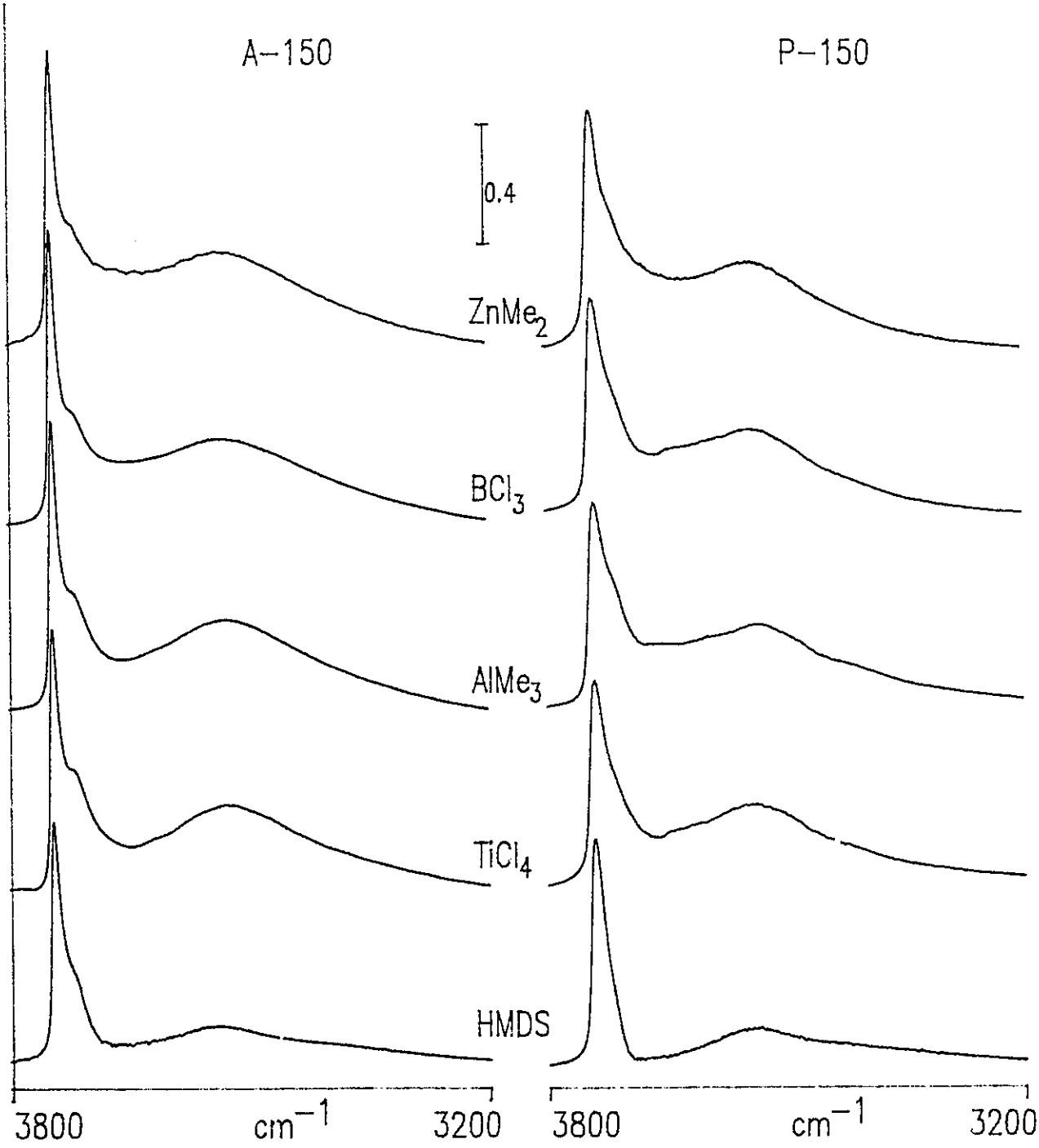

Figure 3.7. Infrared spectra of A-150 and P-150 showing the spectral changes after a complete reaction with the indicated HS agent. These spectra show the silanol groups which have reacted with the indicated HS agent (see text).

The integrated intensities shown in Table 3.2 were determined from the spectra of A-150 or P-150 silica discs which were pressed under identical conditions and which contained about the same quantity of silica, 10 mg/cm^2. Measurements of the integrated intensities before reaction did not vary by more than 5% between samples and average values of, I_{oA} = 150, and I_{oP} = 292 were chosen for aerosil and precipitated silica, respectively. Subsequently, all of the spectra in Figures 3.5 and 3.6, and the intensity data in Table 3.2 have been normalized to these values of I_{oA} and I_{oP}. The reactant areas (σ) were calculated according to

$$\sigma = 1.091\ (M / N_0\ \rho)^{2/3}$$

where M is the molecular weight (g/mol), N_0 is Avogadro's number, and ρ is the density (g/ml) of the liquid at room temperature. This method approximates the molecules to be spherical and arranged in hexagonal close-packing, and is the same method used to calculate B.E.T. cross sectional areas [10]. As such, these areas are at best approximate, *e.g.* a molecule like $ZnMe_2$ having a linear C-Zn-C configuration is probably far from spherical in its reactive cross-section.

In spite of their limited quantitative significance, the data in Table 3.2 clearly show that the integrated intensity of the residual band after reaction with A-150 or P-150 increases as the size of the reactant increases, indicating that the number of accessible silanols decreases with increasing reactant size. The data also show slight differences between the two silicas: whereas there is a gradual increase in the % SiOH reacting for A-150 for the series of HS probes (and D_2O), the percentage of SiOH reacting with P-150 hardly changes in going from $TiCl_4$ to $ZnMe_2$, then changes drastically upon going from $ZnMe_2$ to exchange with D_2O. Finally, the integrated intensity of P-150 before reaction is about twice that of A-150 (292 *vs.* 150) suggesting that there is a greater number of silanols initially on P-150, however, the percentage of silanols which react with a given HS probe on P-150 is consistently about one-half of the percentage reacting on A-150, according to Table 3.2.

Before considering the implication of the above results, we will first show how H/D exchange of A-150 and P-150 depends on the area of the exchange reagent used. This has been carried out using exchange molecules of differing steric dimension (D_2O, ND_3 and OD-containing methanol, i-propanol and t-butanol). For recording IR spectra, the activated samples were exposed at 22°C to 10 Torr of a given molecule for 10 min, followed by evacuation for 10 min. This was repeated a total of five times, and after the last exposure, the sample temperature was raised to 150°C while evacuating the sample, held at 150°C for 10 min, and cooled to 22°C before recording of the spectra. There was very little change between the 4th and 5th exposure and final spectra for both silicas are shown in Figure 3.8. Table 3.3 shows the area of each exchange molecule, the normalized integrated intensity after exchange and the percent change in the integrated intensity as a result of the exchange. The same normalization procedure was used here, as for the HS probes.

		A-150		P-150	
Reactant	Reactant area (Å^2)	Intensity[a] I_A	% SiOH change[c]	Intensity[b] I_P	% SiOH change[c]
t-BuOD	31.7	36	76	74	75
i-PrOD	27.6	23	85	54	81
CD_3OD	18.0	17	89	36	88
ND_3	12.9	13	92	21	93
D_2O	10.5	12	92	22	92

Table 3.3. Exchange Data for Reactions on A-150 and P-150

(a) Normalized integrated intensity I_A after exchange. Initial intensity $I_{oA} = 150$.
(b) Normalized integrated intensity I_P after exchange. Initial intensity $I_{oP} = 292$.
(c) Percent decrease in SiOH intensity after exchange, I/I_o for A-150 and P-150.

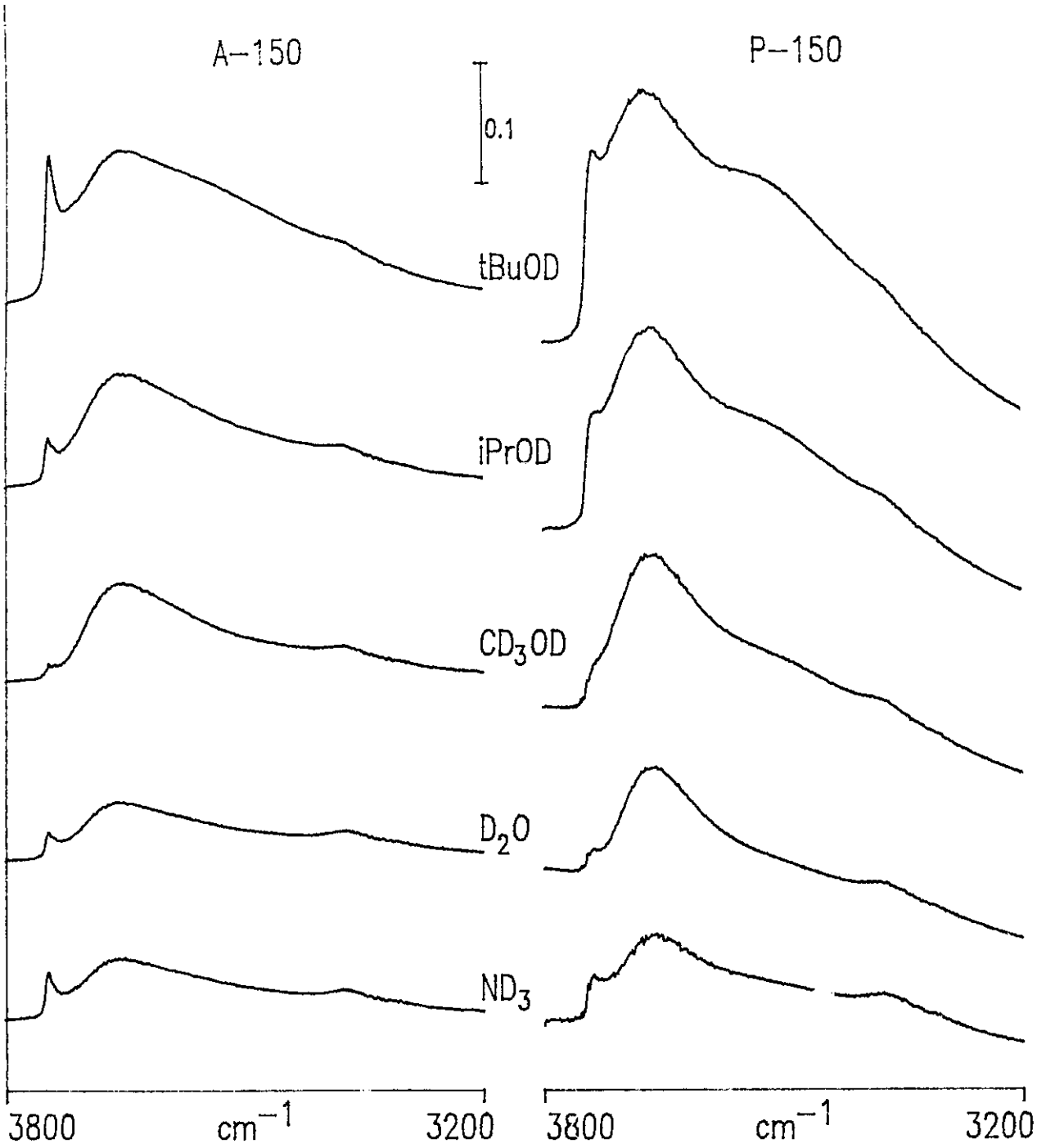

Figure 3.8. Infrared spectra of A-150 and P-150 after H/D exchange at 22°C with the indicated molecule. The integrated intensities are shown in Table 3.3.

Not surprisingly, the percent exchange for each reactant also increases as the size of the reactant decreases. However, for a given exchange molecule, the percent exchange is virtually identical for each silica. Equally important, upon comparing the data in Tables 3.2 and 3.3, one can see that for molecules of comparable size, those that exchange are accessible to many more silanol groups than those that chemisorb. For example, compare i-PrOD or t-BuOD with the series $ZnMe_3$, BCl_3, $AlMe_3$ and $TiCl_4$. The contrast is particularly dramatic for P-150; only about 33% of the silanols are accessible to the molecules which chemisorb on silica, whereas 80% undergo exchange with i-PrOD or t-BuOD.

(d) Gravimetric Determinations of Silanol Densities

In part (c) above, we have used integrated intensity data to measure the relative total silanol densities on A-150 and P-150 and their relative accessibility to chemical and H/D exchange probes having different steric dimensions. We have already pointed out that these measurements alone lack any quantitative significance because the extinction coefficients of the various silanol types cannot be measured accurately. On the other hand, the infrared data show that the number of silanols which react or undergo exchange depends on the size of the reactant molecule. Therefore, any quantitative measurement of the silanol density on silica, based on a method which uses a chemical or H/D exchange reaction, will certainly depend on the size of the probe molecule employed. Here, we present the results of gravimetric determinations of the silanol densities on aerosil and precipitated silica. We also present the results of a combined, spectroscopic and gravimetric measurement of the isolated silanol densities on these silicas.

We have attempted to measure the silanol density ($SiOH/nm^2$) for both silicas after 1 h activation. This poses the problem of whether one wants to measure the accessible silanol density or the total silanol density, knowing that in the former case, the size of the reactant will obviously influence the results. We have used three gravimetric procedures in order to

measure silanol densities. Using the microbalance, we have measured accessible silanol densities for (i) exchange with either D_2O or ND_3, and (ii) after complete reaction with HMDS (hexamethyldisilazane). In order to obtain the total silanol densities on these silicas, method (iii), we have measured the water loss upon heating the silicas from 150 to 800°C (this eliminates all of the H-bonded and perturbed inaccessible silanols) and the mass change after complete reaction of A-800 or P-800 with HMDS. The mass changes associated with these gravimetric experiments, and the results are summarized in Tables 3.4, and 3.5, respectively. Table 3.5 also includes data from method (ii) for A-450 and P-450 which will be used to calculate the isolated silanol densities.

Method		Mass Change (g/mol SiOH)
(i) H/D Exchange:	$SiOH \xrightarrow{D_2O} SiOD$	+ 1.00
(ii) HMDS reaction:	$SiOH \xrightarrow{HMDS} SiOSiMe_3$	+ 72.18
(iii) Total[a] SiOH:	$2SiOH \xrightarrow{-H_2O} SiOSi$	− 18.02

Table 3.4. Gravimetric Methods for Determining Silanol Densities

(a) Method (iii) uses reaction with HMDS to react away isolated hydroxyls on A-800 or P-800 to give total silanol density.

Methods (i) and (ii) measure the accessible silanol densities using the smallest (D_2O, ND_3) and largest (HMDS) probe molecules. Further, these molecules react monofunctionally with surface silanols; methods (i) and (ii) are limited to reagents which cannot react bifunctionally with vicinal or geminal silanols (see Table 3.4 and reaction 1). Finally, the relative errors associated with the HMDS measurements in Table 3.5 are much less than those

for H/D exchange. This is due to the large difference in mass between a trimethylsilyl substituent and deuterium; this can only be partly compensated for experimentally by increasing the sample size in the exchange reaction.

Silica	Method[a]	SiOH/nm^2
A-150	(i) H/D exchange	2.5 ± 0.1
	(ii) HMDS reaction	1.42 ± 0.02
	(iii) Total SiOH	3.1 ± 0.1
	(iv) isolated SiOH	1.1 ± 0.1
P-150	(i) H/D exchange	5.6 ± 0.3
	(ii) HMDS reaction	1.48 ± 0.02
	(iii) Total SiOH	6.8 ± 0.3
	(iv) isolated SiOH	1.1 ± 0.1
A-450	(ii) HMDS reaction	1.41 ± 0.02
P-450	(ii) HMDS reaction	1.63 ± 0.02

Table 3.5. Silanol Density (SiOH/nm^2) on A-x and P-x via Different Methods
(a) see text

The most important result of the data in Table 3.5 is that the total silanol density of P-150 is about 2.2 times greater than that on A-150, and this factor is also reflected in the number accessible to D_2O or ND_3 for exchange. However, nearly equal numbers of silanols on both A-150 and P-150 are capable of reacting with HMDS. This idea is also supported by the IR difference spectra in Figure 3.7 and it is qualitatively applicable to all of the HS agents used. That is, the spectral changes for complete reaction with a given HS agent are virtually identical for the two silicas.

Although the gravimetric results are quantitative, these experiments cannot distinguish types of silanols which react with a given probe molecule. On the other hand, the infrared spectroscopic results show qualitatively how the relative number of isolated to H-bonded silanols depends on the size of the probe molecule. By combining the two techniques, method (iv), we have been able to obtain a measurement of the surface densities of isolated silanols on A-150 and P-150 silicas. These results are presented below and in Table 3.5.

The peak due to isolated silanols at 3747 cm^{-1} on aerosil increases in intensity upon heating the sample from 150 to 450°C (Figure 3.1C). Because of the superimposed decrease in intensity of the 3720 and broad 3660 cm^{-1} peaks, it is impossible to accurately determine by how much this peak intensity increases in 3.1C. We have measured this change in intensity in the following way. Figure 3.9A shows the change in intensity due to the reaction of HMDS with isolated silanols on A-450. Figure 3.9B shows the change in intensity when A-150 similarly reacts. For A-150, all isolated silanols react with HMDS, but the terminal silanols (3720 cm^{-1}) and a small number of H-bonded silanols (3520 cm^{-1}) also react. For A-450, only isolated silanols react.

The number of silanols which react with HMDS is essentially the same for A-150 and A-450 (Table 3.5). Therefore, because some H-bonded and terminal H-bonded silanols react on A-150, it follows that the isolated silanol density on A-150 is less than 1.42 $SiOH/nm^2$. In Figure 3.9A and 3.9B, the peak intensity ratio at 3747 cm^{-1} is 0.75 for the spectra A-150/A-450. If there are 1.41 isolated $SiOH/nm^2$ on A-450, then the isolated silanol density on A-150 will be 0.75 x 1.41 = 1.06 $SiOH/nm^2$. This calculation assumes that the extinction coefficient at 3747 cm^{-1} is the same in Figures 3.9A and 3.9B, and although it cannot be proven, there is not likely to be a large difference between the extinction coefficients of isolated silanols on A-150 and A-450. Further, we have verified that the 3720 cm^{-1} component does not contribute to the 3747 cm^{-1} peak in Figure 3.9B. Given these uncertainties, we conclude that A-150 silica contains about 1.1 isolated silanols out of a total of 2.5 which are accessible to D_2O, and therefore, about 1.4 which are H-bonded or perturbed.

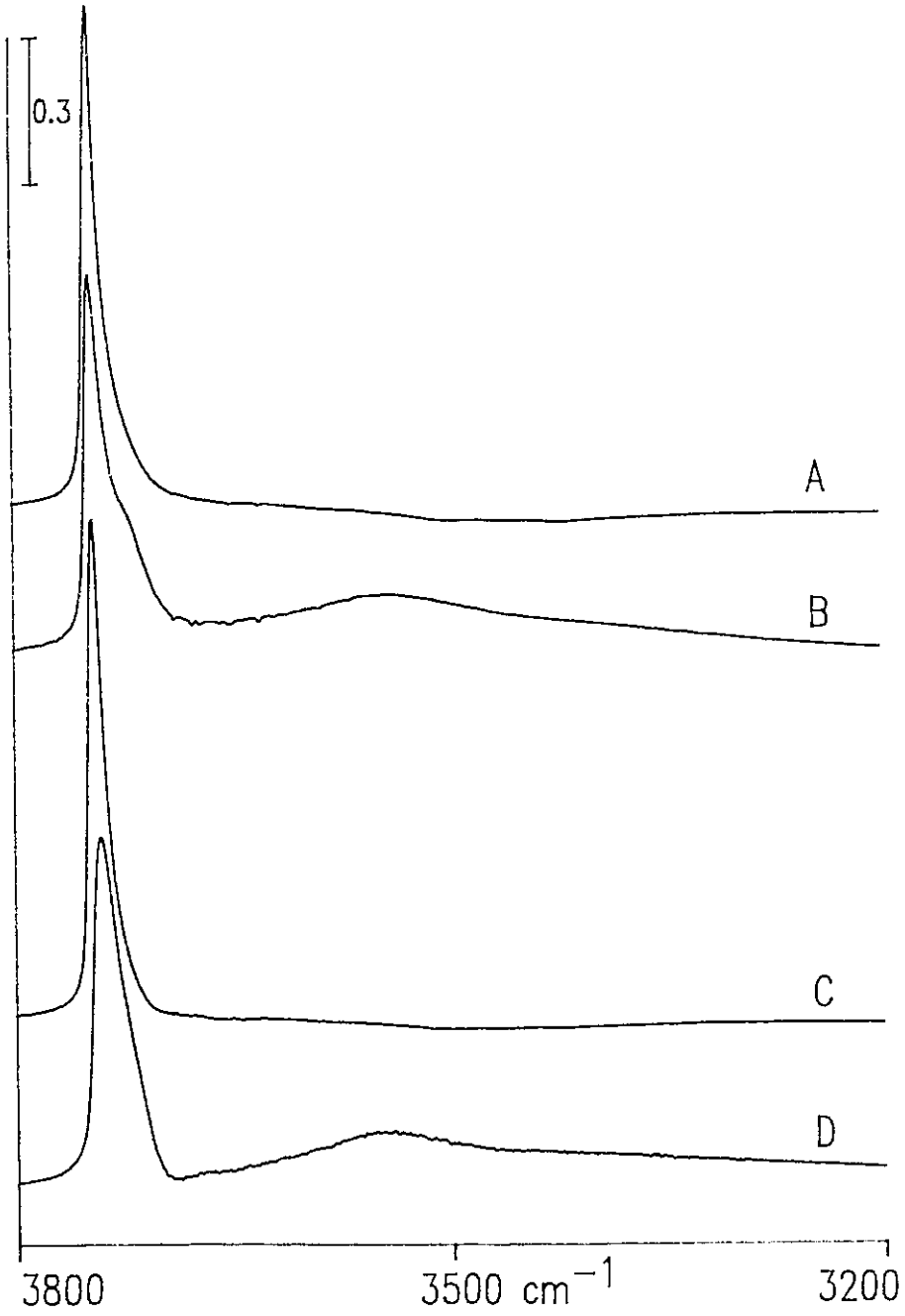

Figure 3.9. Infrared difference spectra showing spectral changes for a complete reaction with HMDS on, (A) A-450, (B) A-150, (C) P-450, (D) P-150. These spectra show the silanol groups which have reacted with HMDS.

The precipitated silica P-150 contains a far greater number of D_2O accessible silanols, 5.6 SiOH/nm^2, of which 1.48 are accessible to HMDS (Table 3.5). Using similar arguments, the ratio of the intensities of the isolated silanol bands for P-150/P-450 is 0.70 (compare Figure 3.9C and 3.9D) and, because there are 1.63 isolated SiOH/nm^2 on P-450 (Table 3.5), the isolated silanol density on P-150 is 0.70 x 1.63 = 1.14 SiOH/nm^2 (or about 1.1). Therefore, the total number of H-bonded and perturbed SiOH/nm^2 accessible to D_2O is 5.6 - 1.1 = 4.5.

Discussion

The objective of this work has been to compare the surface density, reactivity and accessibility of silanols on two "as received", non porous silicas having similar surface areas, but which differ in origin. We have used time-resolved spectroscopy to compare the relative rate of reaction of isolated to hydrogen-bonded hydroxyls for several very reactive HS probes. We have shown how steric factors influence the degree of chemical modification and H/D exchange of surface silanols. Finally, we have obtained quantitative measures of the surface silanol density from gravimetric studies. With this information we can compare the silanol distribution on the surfaces of A-150 and P-150 silicas.

The total SiOH density on P-150 is about two times greater than on A-150 (Table 3.5, 6.8/3.1 = 2.2). The number of SiOH/nm^2 accessible to exchange with D_2O/ND_3 also differs by about a factor of two (Table 3.5, 5.6/2.5 = 2.2). The infrared results show that for a given exchange reagent listed in Table 3.3, about the same percentage of the total number of silanols exchange on each silica, implying that the number of silanols on P-150 which are inaccessible to each exchange reagent is greater by about a factor of two.

The number of SiOH/nm^2 which react with HMDS (Table 3.5) is about equal for both silicas, and the infrared difference spectra for reaction with the various HS agents (Figure 3.7) show that about the same number of silanols on each silica react with a given HS agent. Given that the total silanol density is two times greater on P-150, it follows that the "percent

SiOH change" for A-150 would be about twice that observed for P-150, and this is borne out in Table 3.2 (compare columns 4 and 6).

Approximately the same fraction of silanols on each silica are accessible to a given exchange reagent. This suggests that the surface characteristics of the precipitated silica are similar to those of the aerosil type. The number of SiOH/nm^2 which react with a given HS agent is the same on both silicas. That is, when a similar density of chemisorbed product is formed, then further reaction is essentially inhibited. This point of inhibition presumably occurs when a shroud of chemisorbed product covers the accessible external surface, thereby preventing diffusion of the reactant to other silanols which are normally accessible to the exchange probes used. Because both silicas have similar surface areas, this shroud is formed when the same number of silanols have reacted. That the degree of exchange is much larger than the degree of chemisorption for molecules of comparable size presumably arises because the exchange molecule is not fixed to the surface and diffusion permits access to those silanols which would have been inaccessible during the chemisorption reaction.

The time-resolved studies showed that there is a difference in the reactivity of H-bonded and isolated silanols. The chlorine-containing HS agents initially reacted more rapidly with H-bonded silanols and this may be related to their ability to react bifunctionally with vicinal pairs of silanols. The observed differences in the initial relative rates of reaction (R values) may also reflect differences in the HS agents' ability to diffuse along the surface or to achieve a particular orientation on the surface which is suitable for reaction with a surface silanol. In this respect, the B.E.T. "areas" are probably a more realistic measure of the steric cross-sectional areas of these molecules than their reactive cross-sectional areas. For these reasons, and given the poor S/N ratio observed in these studies, we do not wish to speculate on the significance of the measured R values during the first few seconds of reaction. Nevertheless, in the later stages of reaction on either silica, the H-bonded silanols ceased to react well before the isolated silanols, for all three HS agents studied. We attribute this to the blocking effect of adjacent derivatized silanols, *i.e.* the time-resolved studies

illustrate that the shroud of chemisorbed product effectively prevents further reaction, whatever the size of the reactant.

With regard to the total silanol densities (Table 3.5), a value of about 4.5 - 5.0 $SiOH/nm^2$ is generally accepted for "fully hydroxylated" silicas, although there is considerable scatter in the data [1,4,40]. Our values are well within the ranges expected for both types of silica considered as "as received" materials. Where the hydroxylated states of these silicas differ most strikingly is in the number of H-bonded silanols present on the surface. Both silicas contain nearly the same number of isolated silanols, but the precipitated silica contains 4.5/1.4 = 3.2 times the number of H-bonded silanols which are accessible to a small molecule such as water or ammonia.

We previously suggested that the increase in the intensity of the isolated SiOH peak upon heating from 150 to 450°C might be due to a condensation process of the type shown in reaction (3). The increase in intensity might also be due to the migration of water to the external surface as a result of the condensation of inaccessible silanols, thereby reforming isolated silanols. (Such a migration would initially create a vicinal pair of silanols which, if the protons were sufficiently mobile at 450°C, could conceivably yield isolated silanols). We have investigated the nature of the process whereby isolated silanols are created upon heating either silica in vacuum from 150 to 450°C in the following experiments.

Figure 3.10, A and A' show the spectra of A-450 and P-450 respectively, and curves B and B' are the spectra after complete reaction with HMDS. C and C' show the spectra of A-150 and P-150, respectively, which had been completely reacted with HMDS and subsequently heated in vacuum for 1 h at 450°C. These spectra reveal several important and unexpected results.

The IR spectra after reacting A-150 or P-150 with HMDS followed by heating to 450°C (Figure 3.10, C and C') are almost identical to those which are observed after direct activation at 450°C followed by reaction with HMDS (Figure 3.10, B and B'). Upon heating HMDS-treated A-150 or P-150 to 450°C, there is virtually no increase in intensity at 3747

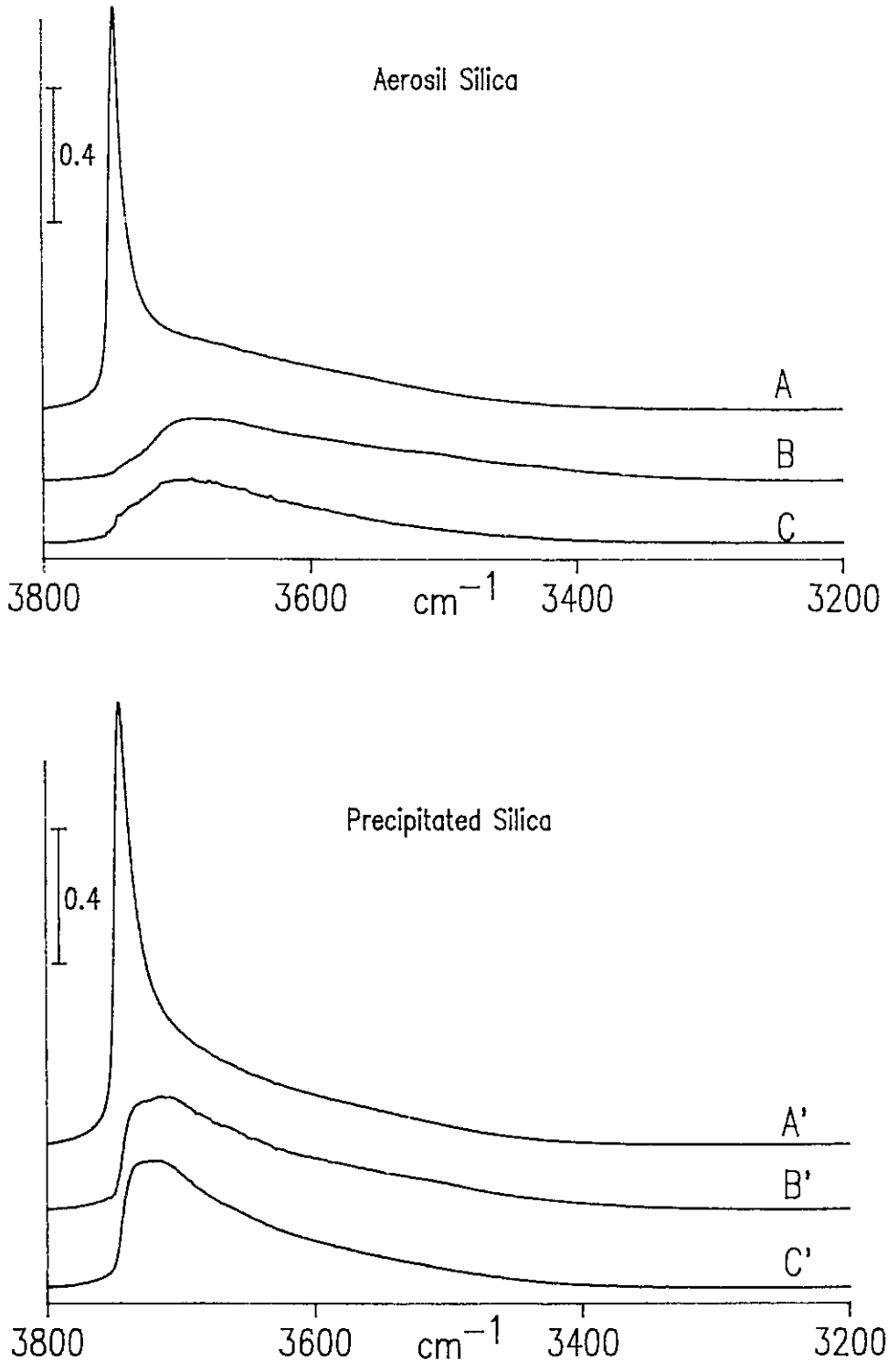

Figure 3.10. A and A', infrared spectra of A-450 and P-450, respectively, and B and B', after complete reaction with HMDS. C and C', A-150 and P-150 respectively, after complete reaction with HMDS followed by vacuum activation to 450°C for 1 h.

cm^{-1}, indicating that no isolated silanols are created on either silica. This confirms that water migrating from the bulk does not subsequently rehydrate the surface.

It is apparent that, following HMDS treatment of A-150 or P-150, all of the remaining H-bonded silanols (3520 cm^{-1}) and inaccessible silanols (3660 cm^{-1}) are in a suitable environment for condensation and liberation of water upon heating to 450°C. Only for untreated, 150°C activated samples are there some H-bonded silanols which are not in a suitable environment to condense, and we observe the isolated silanol band increasing in intensity upon heating to 450°C (Figure 3.1). Therefore, it is probable that the small number of H-bonded and/or some terminal silanols which react with HMDS on the 150°C activated silicas are the same ones that become transformed into isolated silanols after heating to 450°C in the absence of the HMDS treatment. The terminal SiOH band (3720 cm^{-1}) almost entirely disappears following reaction with HMDS (and with the other HS agents) and this probably indicates that these groups more readily react with these agents than do the H-bonded silanols. The terminal silanols appear to be inherently more accessible than the H-bonded silanols, however, the spectroscopic data do not permit us to say more about the nature of these sites.

As a final comment, Sindorf and Maciel [50], and Snyder and Ward [51] have studied the reaction of HMDS with several silica gels having different surface areas and found that the coverage by trimethylsilyl (TMS) groups was limited. Based on steric models, Sindorf and Maciel calculated that the maximum coverage of TMS groups could range from 2.2 to 2.8 per nm^2, depending on the model used. Using a chromatographic injection method, both groups found that there was an initial fast uptake of TMS, followed by a much slower process. Snyder and Ward determined the uptake in the "fast" process for a silica gel having a surface area comparable to ours, (sample II, 319 m^2/g) to be 1.64 TMS/nm^2. Sindorf and Maciel found that the "fast" uptake corresponded to about 1.5 TMS/nm^2 (their method 3 at 200°C). Although we have not attempted to reproduce their experimental conditions, our reaction for 1 h at 150°C probably closely duplicates the injection method and our values for

the TMS surface density are similar.

Conclusions

Chemisorption and H/D exchange have been used to study the surface properties of non-porous aerosil and precipitated silicas having comparable surface areas but very different silanol densities. Our findings can be summarized as follows:

(1) The number of silanols on the hydroxylated surfaces which undergo H/D exchange decreases as the size of the exchange molecule increases, but the fraction which exchange with a given molecule on both silicas is about the same.

(2) The number of silanols which react with a given HS agent is about the same on both silicas and this number decreases as the size of the reactant increases. The number which react is considerably smaller than the number which undergo H/D exchange.

(3) Both silicas contain about the same density of isolated silanols (1.1 $SiOH/nm^2$) in the hydroxylated state, but the number of H-bonded silanols which will subsequently exchange with D_2O is about 1.4 $SiOH/nm^2$ on aerosil and about 4.5 $SiOH/nm^2$ on the precipitated silica.

(4) On both silicas, about 18% of the silanols are inaccessible to the small probe molecules D_2O or ND_3.

(5) The number of silanols which can become trimethylsilated with HMDS at 150°C is about 1.5 $SiOH/nm^2$ on both silicas, a value which is comparable to those which have previously been found for other high-surface-area silica gels.

(6) The terminal silanols of H-bonded chains of silanols are inherently more accessible than H-bonded silanols since they react readily with all HS agents. Some terminal silanols probably become isolated silanols when either silica is activated in vacuum from 150 to 450°C whereas the majority of the H-bonded silanols condense to liberate water.

Finally, this work has demonstrated the utility of probing the silanol groups on silica

using both chemisorption and H/D exchange. We could not have reached these conclusions without this combined approach using probes of differing steric dimensions. It seems that the chemisorption probes inhibit reaction by blocking access to other silanols whereas this does not occur with the H/D exchange probes. It would be interesting to extend this study to include meso- or microporous silicas in order to assess the possible role of proton migration in the exhange reaction.

CHAPTER 4

Vibrational Modes of Isolated Silanol Groups on Aerosil and Precipitated Silica

Summary

Infrared vibrational spectroscopy is particularly useful for characterizing the surface silanol groups on high-surface-area silicas. This investigation has been undertaken to study the nature of the infrared bands due to the isolated surface silanols (SiOH) on aerosil and precipitated silica. The approach has been to probe several regions of the infrared spectrum of both silicas where stretching vibrations, bending vibrations, and combinations of these vibrations appear. The two silicas have been studied for temperatures of activation ranging between 150 and 1000°C, and spectra of both silicas have been obtained at room temperature and at 82 K in the three spectral regions. This comparative study has uncovered new infrared spectroscopic evidence for two distinct types of isolated silanols on aerosil and precipitated silica.

In order to optimize experimental conditions for a particular spectral region, it was necessary to carry out separate experiments in each of the three spectral regions of interest. Likewise, the background material and results have been organized according to the spectral region being studied, with relevant discussions at various points in order to provide continuity. Part 1 concentrates on the spectral region between 4000 and 5000 cm^{-1} and studies the effects of activation temperature and deuterium exchange on the low-temperature spectra of the combination bands of aerosil and precipitated silica. Part 2 extends the study to the 3000-4000 cm^{-1} region to show how the SiO–H stretching profile is affected in similar experiments. Part 3 demonstrates how physical adsorption of CO at low temperature,

deuterium exchange, and chemical modification by BCl_3 may be used to probe the fundamental vibrational modes of SiOH in the 500-1000 cm^{-1} region. Finally, the combined results are discussed in Part 4 in terms of a model of the isolated silanol distribution on aerosil and precipitated silica.

Experimental Section

The general experimental methods have been discussed in Chapter 2. With regard to spectra recorded at low temperature, the conducting gases used in the studies to be presented were H_2, He, or CO. At pressures between 0.5 and 2 Torr H_2 or He, the temperature near the sample surface was 82 ± 1 K. When CO was used as the conducting gas (and adsorbate) at pressures below 0.1 Torr, a slight increase in temperature was observed, as described in Chapter 2. We have verified (by subtracting the spectrum of silica recorded in He at 82 K from that at 87 K) that spectral artefacts in subtracted spectra, between 500 and 1000 cm^{-1} in the silica spectrum, are not produced at low pressures of CO. Room-temperature spectra were recorded at 295 K (22°C).

Part 1. 4000-5000 cm^{-1} Region

Introduction

The spectrum of silica in the region above 4000 cm^{-1} exhibits infrared absorption bands which have been assigned to overtones and combinations of the surface SiO–H stretching vibration with various low-frequency deformation modes. Tsyganenko has reported the transmission infrared spectrum of a thick (250 mg/cm^2) aerosil silica pellet which had been activated at 1200 K [52]. He reported an absorption band, having a frequency maximum at 4550 cm^{-1} in the room-temperature spectrum, which split into a doublet with maxima at 4515 and 4590 cm^{-1} when the sample was cooled in liquid nitrogen. These bands in the aerosil spectrum were assigned to combinations of the fundamental SiO–H stretching vibration at 3750 cm^{-1} with, an Si–O–H angle deformation mode at 840 cm^{-1}, and an Si–O

stretching mode at 765 cm^{-1}. The frequencies of the fundamental modes were calculated as the difference between the combination band frequencies and 3750 cm^{-1}.

Kustov *et al.* have studied silica gel by diffuse reflectance infrared spectroscopy in the near infrared region between 4000 and 9000 cm^{-1} [53]. In the room-temperature spectrum of silica gel, they observed a band with a maximum at 4550 cm^{-1}, and this band split into a doublet having maxima at 4520 and 4595 cm^{-1} when the sample was cooled to 82 K. These bands were assigned to combinations of the SiO—H stretch (3750 cm^{-1}) with two low-frequency fundamental modes. Another low-temperature doublet was observed which had maxima at 8110 and 8165 cm^{-1} and these were assigned to combinations of the first overtone of the stretching mode (7320 cm^{-1}) with the same low-frequency fundamental modes. When the silica gel was deuterated, the 4520, 4595 cm^{-1} bands were replaced by a single band at 3367 cm^{-1}, and the 8110, 8165 cm^{-1} bands were replaced by a single band at 6048 cm^{-1}. The authors calculated anharmonicity constants based on the frequencies of the combination bands and used this data to determine the frequencies of the fundamentals. They arrived at the following values: 765 and 870 cm^{-1} for the H-silica and 605 cm^{-1} for the D-silica. Based on the magnitude of the isotopic shift for H/D exchange, the 765, 605 cm^{-1} bands were assigned to Si—O—H and Si—O—D bending vibrations respectively, and the 870 cm^{-1} band to an Si—OH stretching vibration. Their assignments are contrary to the assignments proposed by Tsyganenko for aerosil silica.

In this study, we have compared the spectra of aerosil and precipitated silica in the 4000-5000 cm^{-1} region over a wide range of activation temperatures, and at low temperature. We have observed that the profile of the combination bands in the low-temperature spectra of both silicas varies with activation temperature, providing us with new insight into the spectroscopic assignment of these combination bands. A detailed comparison of the low-frequency region is presented in Part 3.

Results

Figure 4.1 shows the infrared spectra of A-800 and P-800, recorded at 82 K (Figure 4.1, A and A', respectively) and at room temperature (Figure 4.1, B and B', respectively) for samples containing 40 mg/cm^2 of silica. The sloping background in all of the spectra results from an increase in light scattering with frequency. For the precipitated silica, the problem of background light scattering is much more severe and this energy loss at the detector results in a poorer S/N for comparable observation times.

The room temperature-spectrum of either silica exhibits a broad, unresolved band with a maximum at 4550 cm^{-1}. At 82 K, and with 1 Torr H_2 added to provide a thermally conducting medium, this band splits into two components having maxima at 4510 and 4580 cm^{-1}. For 800°C activation, the relative intensities of the two component bands are about the same for both silicas. It is also apparent from Figure 4.1 that the frequencies of the two component bands separate when the temperature is lowered to 82 K; although the high-frequency and low-frequency components intensify and narrow upon cooling, the full width at half height (FWHH) of the overall band profile actually increases. This point will be discussed later with regard to the 3700-3800 cm^{-1} spectral region.

The low temperature-spectra for aerosil and precipitated silica, obtained under similar conditions, are shown in Figure 4.2 for samples which had been activated at 150, 450, 800, and 1000°C. Both series of spectra have been baseline-corrected between 4300 and 4700 cm^{-1} to remove the sloping background so that relative intensities of the two components are easier to visualize. Additionally, the spectra of precipitated silica have been smoothed in order to improve the presentation (the original spectrum of P-800 is shown in Figure 4.1 for comparison).

The low-temperature spectra of aerosil and precipitated silica in Figure 4.2 are noticeably different for samples activated below 800°C. The relative intensity of the two component bands, 4580/4510 cm^{-1}, is much greater for P-450 than for A-450, and decreases by a greater amount between 450 and 800°C activation for P-450. However, between 800

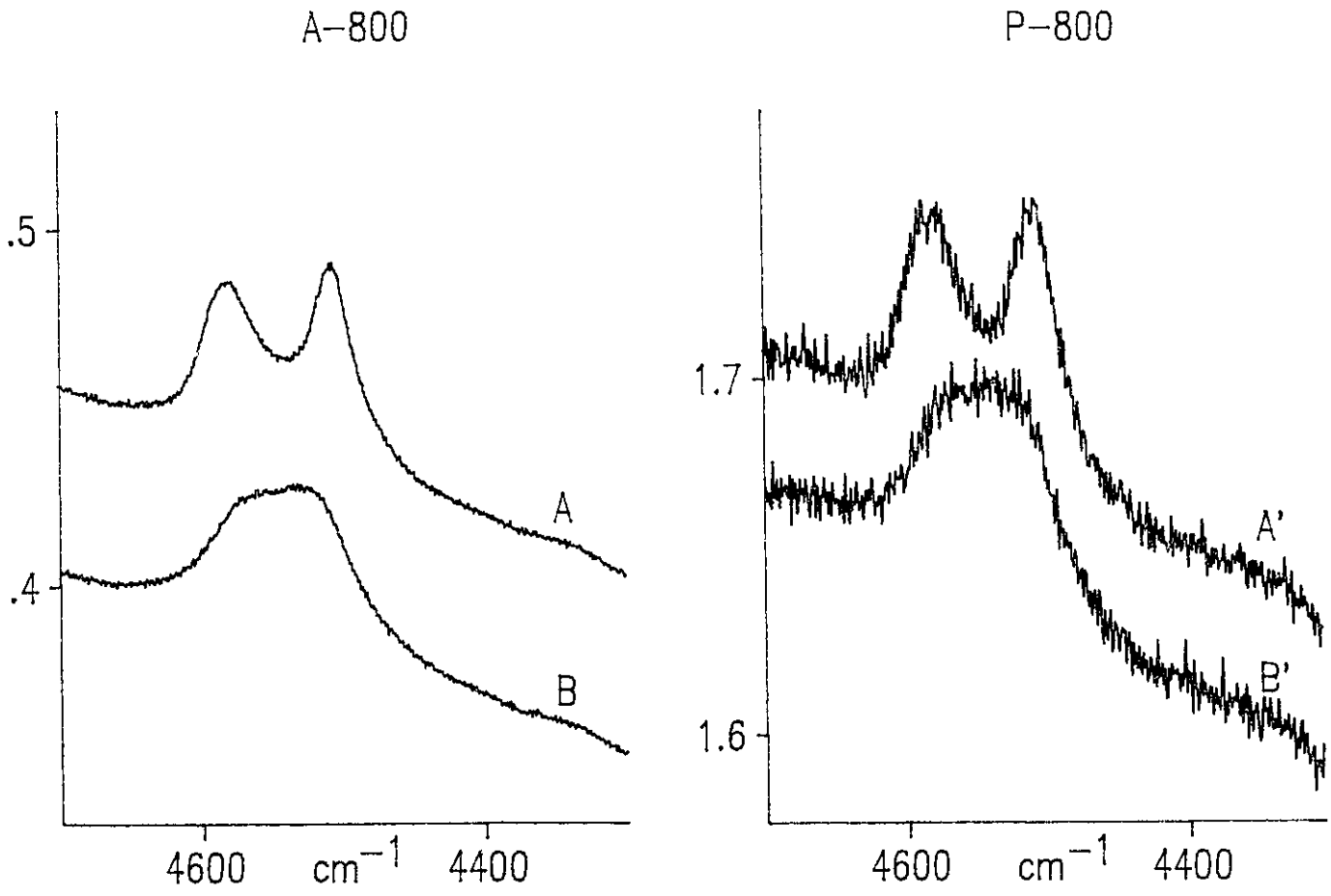

Figure 4.1. (A and A') Low-temperature infrared spectra of 40 mg/cm^2 A-800 and P-800 silicas, respectively, recorded with sample at 82 K. (B and B') Corresponding room-temperature spectra.

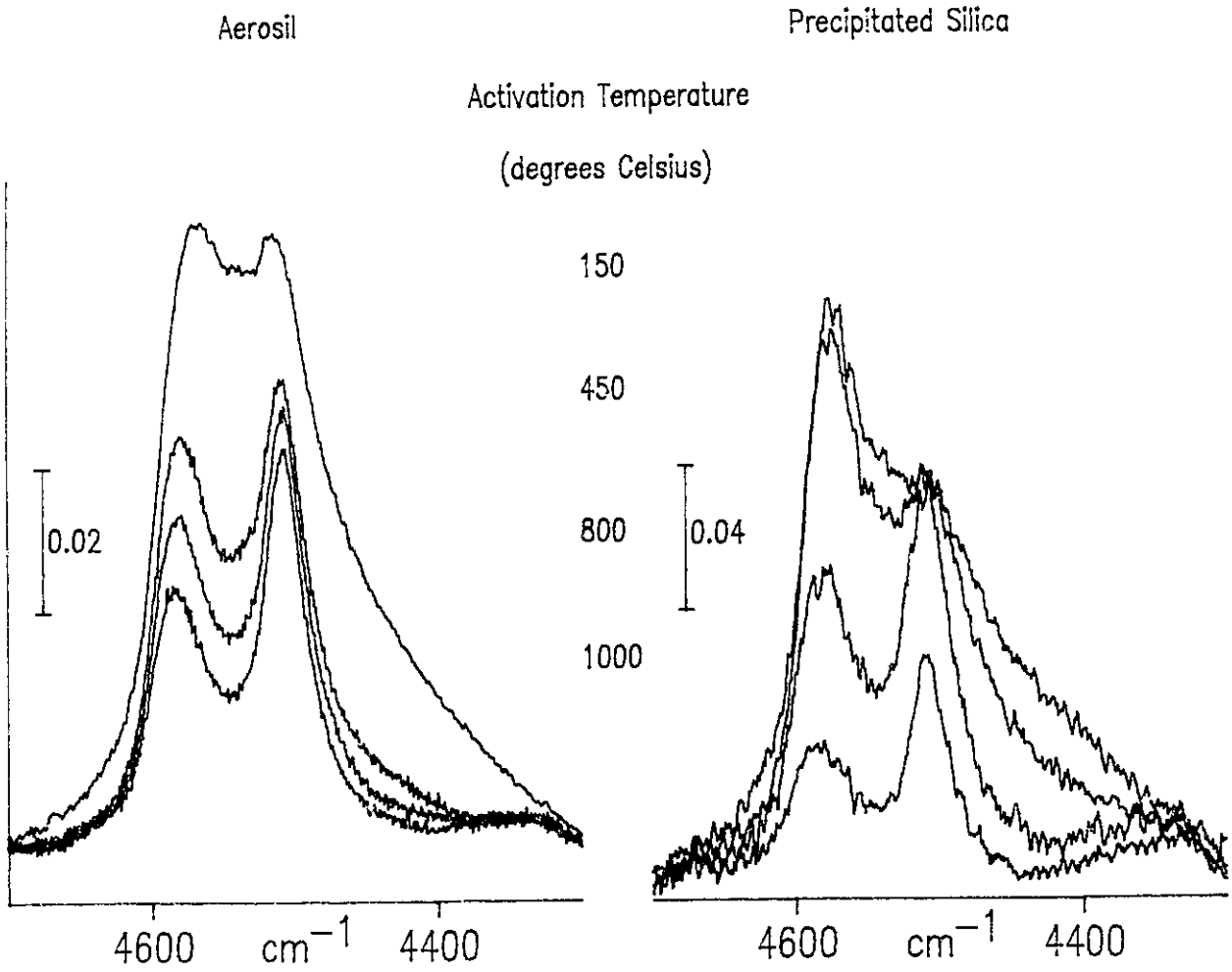

Figure 4.2. Baseline-corrected, low-temperature (82 K) spectra of aerosil and precipitated silica (40 mg/cm^2), activated in vacuum at the indicated temperatures.

and 1000°C, the spectra of the two silicas converge, *i.e.* they exhibit very similar combination band profiles. Finally, for 150°C activation, there appears to be a broad feature extending to about 4400 cm^{-1} which is superimposed on the 4510 cm^{-1} and 4580 cm^{-1} components of both silica spectra. This feature diminishes as the activation temperature is increased and, by 800°C, it is completely removed.

Deuteration of the silicas with D_2O or ND_3 completely removed the 4550 cm^{-1} band and a new feature appeared at 3370 cm^{-1}. Figure 4.3 shows the low-temperature spectra, before and after deuterium exchange, of 80 mg/cm^2 A-450 (A and B, respectively), and 40 mg/cm^2 P-450 (A' and B', respectively). A single band at 3370 cm^{-1} was also observed in the spectra of aerosil and precipitated silica activated at 150 or 800°C (not shown), and similar spectra have been observed by others [28,53].

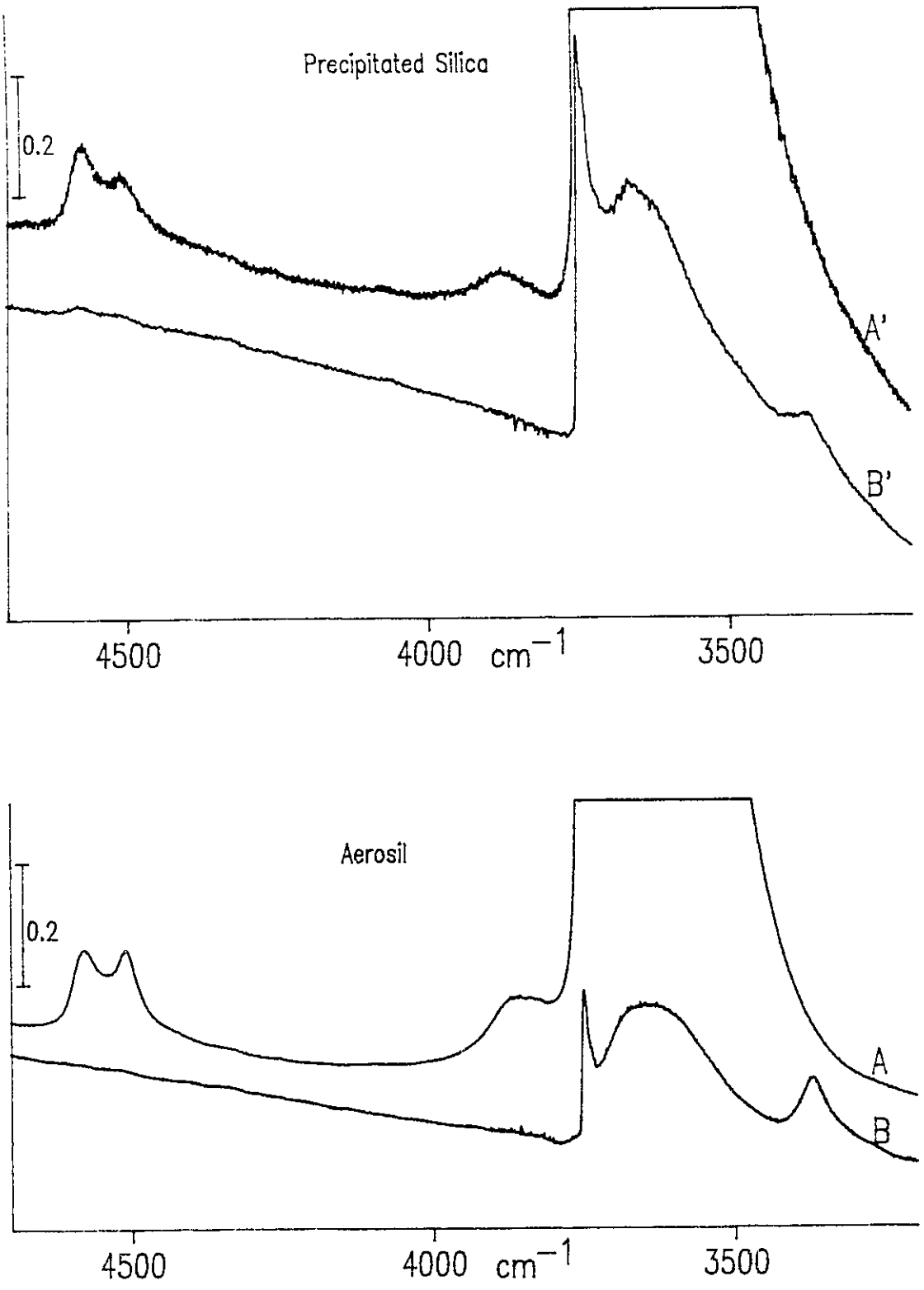

Figure 4.3. (A and A') Low-temperature spectra of 80 mg/cm^2 A-450, and 40 mg/cm^2 P-450, respectively. (B and B') Low-temperature spectra obtained after deuterium exchange of A and A', respectively.

Part 2. 3000-4000 cm^{-1} Region

Introduction

The spectral region between 3400 and 3800 cm^{-1} is one of the most informative regions in the infrared spectrum of silica. Since contributions to the spectrum from bulk silica modes are only observed below about 2000 cm^{-1}, the 3000-4000 cm^{-1} region exhibits the SiO—H stretching modes of the various surface silanol species on an otherwise featureless background.

The SiO—H stretching profile depends on the type of silica being studied (*i.e.* its origin) as well as the temperature at which the silica is activated during the vacuum pretreatment procedure. Both factors determine the distribution of surface silanol types which contribute to the silica spectrum. The infrared spectra of the SiO—H stretching profile in "as received" aerosil and precipitated silica, and assignments to various surface silanol types are discussed in Chapters 1 and 3. This section focuses on the spectrum of the isolated silanols on activated aerosil and precipitated silica.

One of the most significant features in the silica spectrum is the sharp 3748 cm^{-1} band assigned to isolated single or geminal silanols. This band dominates the spectrum for silicas activated at, or above about 350°C. However, there is an asymmetry to lower wavenumber which is quite noticeable after 350°C activation; this asymmetry gradually diminishes with increasing activation temperature, and is essentially gone after 800°C activation. Structural features have been observed in the 3748 cm^{-1} band, in the room-temperature spectrum [54], and in spectra recorded at elevated temperatures [55], and in these studies band-fitting methods were used to resolve a low-wavenumber component at around 3743 cm^{-1}. Similar studies by others could not reproduce the low-wavenumber feature, and it was suggested that the 3743 cm^{-1} band was probably an artefact caused by inadequate compensation for water vapour in the double beam instruments [56-58].

Direct, infrared spectroscopic evidence supporting the coexistence of isolated single and geminal SiOH on silica has not been reported to date. Theoretical calculations have

shown that the SiO–H stretching modes of single and geminal isolated silanols should differ in frequency by about 2 cm^{-1} [59]. However, as will be shown here, these cannot be resolved in the 3748 cm^{-1} profile at room temperature.

We have compared the band profiles of the surface SiO–H stretching modes (3700-3800 cm^{-1}) of aerosil and precipitated silica for temperatures of activation ranging between 150 and 800°C. High-resolution spectra have been recorded with the samples at room temperature and at 82 K, in order to take advantage of line-narrowing effects at low temperature while accurately sampling this narrow bandwidth. Under these conditions we have been able to closely examine the band at around 3748 cm^{-1}, and provide experimental proof of its composite nature for both the aerosil and precipitated silicas. We have also examined how the activation temperature dependence of the 3748 cm^{-1} profile is mirrored by the combination bands at 4580, 4510 cm^{-1}.

Results

Figure 4.4 shows the room-temperature spectra of the SiO-H stretching profiles for 10 mg/cm^2 samples of A-150 and P-150 (A and A', respectively), and A-450 and P-450 (B and B', respectively), recorded at 0.5 cm^{-1} resolution. Upon raising the temperature of activation from 150 to 450°C, most of the hydrogen-bonded silanols are removed and a single band remains. This band is asymmetric to lower wavenumber and has a maximum at 3746.9 cm^{-1} for A-450, and 3745.4 cm^{-1} for P-450 (Figure 4.4, B and B', respectively). The spectra of A-150 and P-150, and the changes which occur between 150 and 450°C activation for these silcias, have been discussed in Chapter 3. Similar spectra recorded at 2 cm^{-1} resolution are shown in Figure 3.1.

The room-temperature spectra, in the region of the isolated SiO–H stretching vibration, are shown on an expanded scale in Figure 4.5 for aerosil silica, and Figure 4.6 for precipitated silica, activated between 450 and 800°C. For 450°C activation, the spectrum of precipitated silica is much more asymmetric to lower wavenumber than that of aerosil silica,

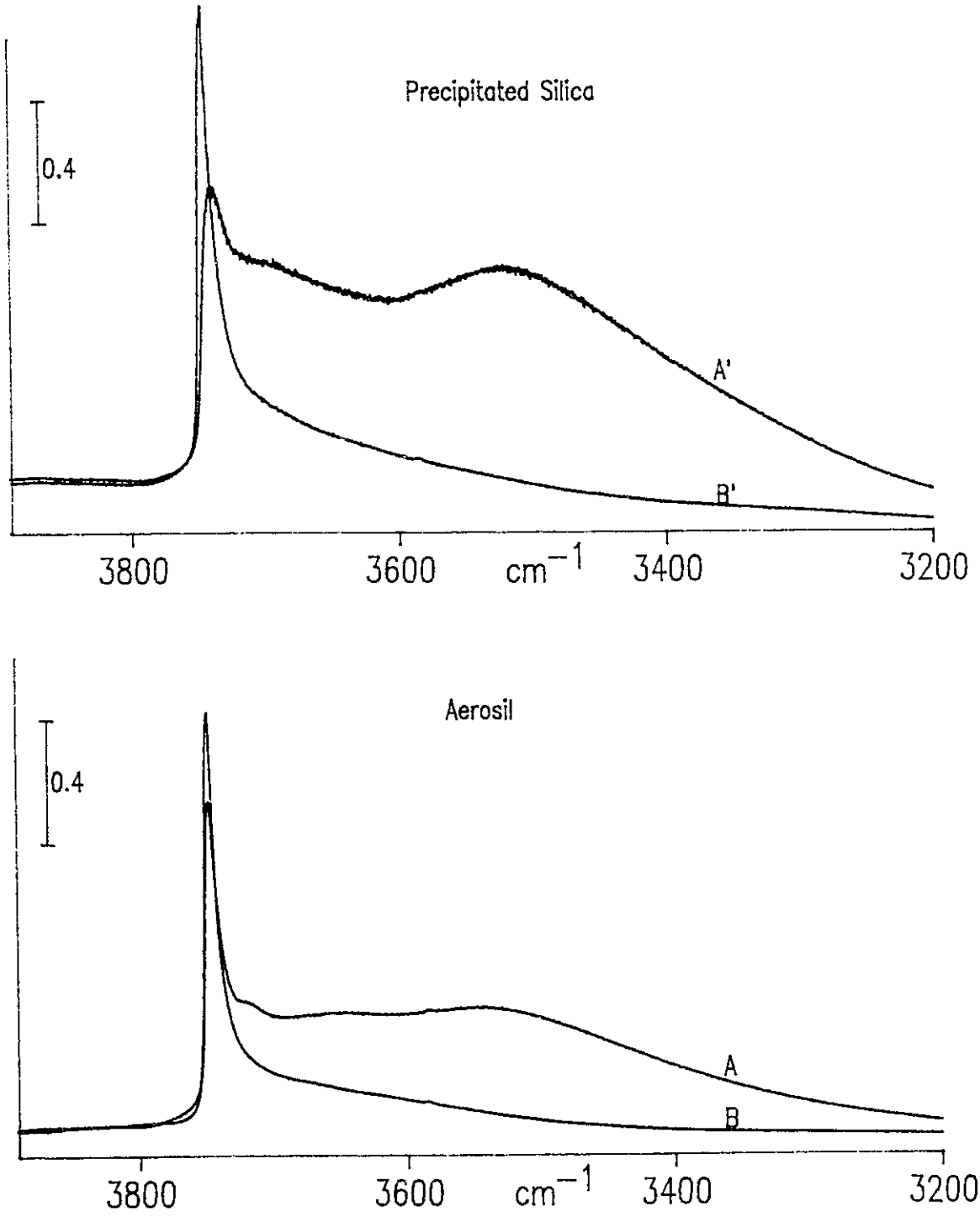

Figure 4.4. (A and A') 0.5 cm^{-1} resolution spectra of 10 mg/cm^2 A-150 and P-150 silica, respectively. (B and B') Spectra of A-450 and P-450, respectively.

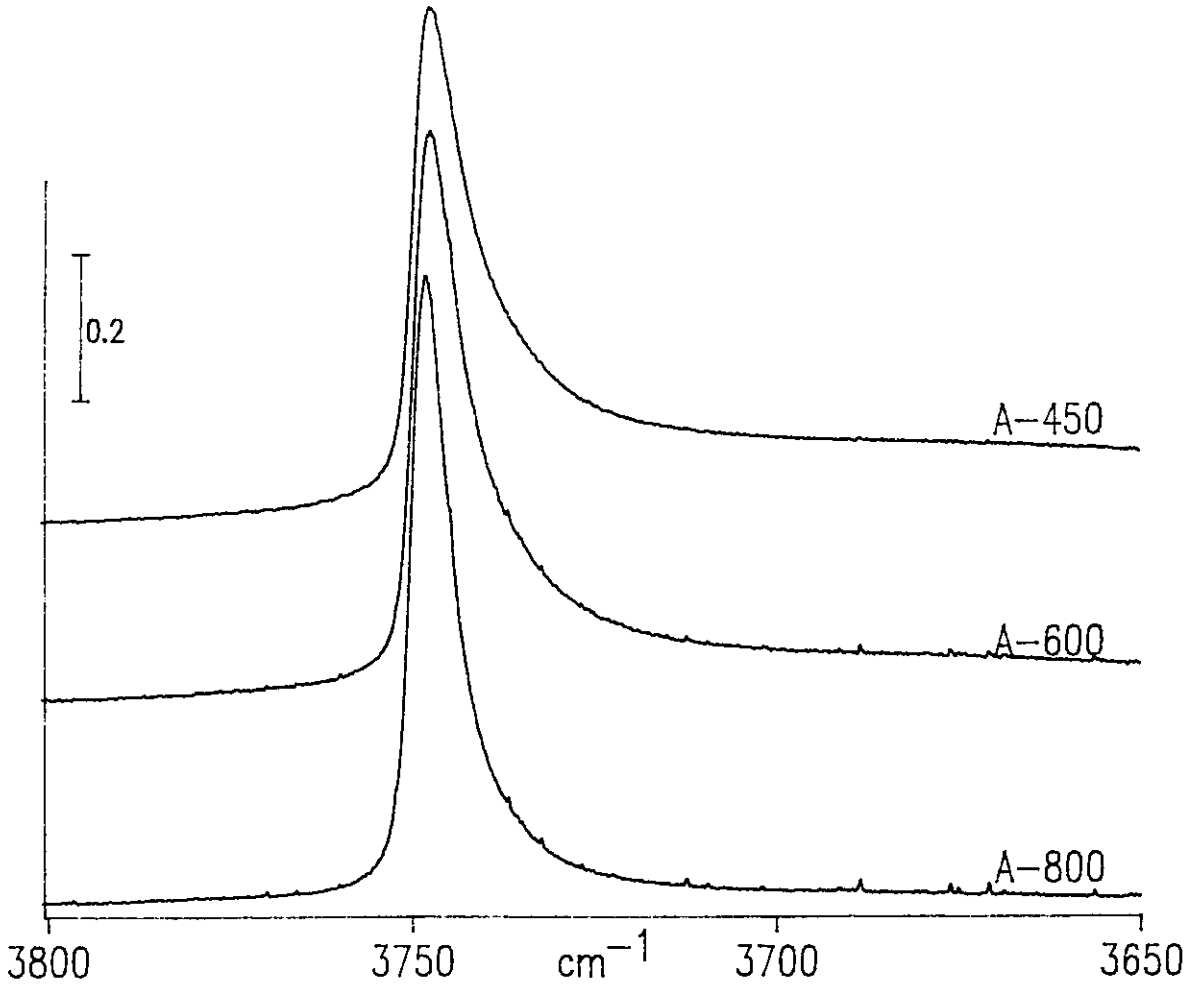

Figure 4.5. Room-temperature, high-resolution spectra of the isolated SiOH profile in aerosil silica.

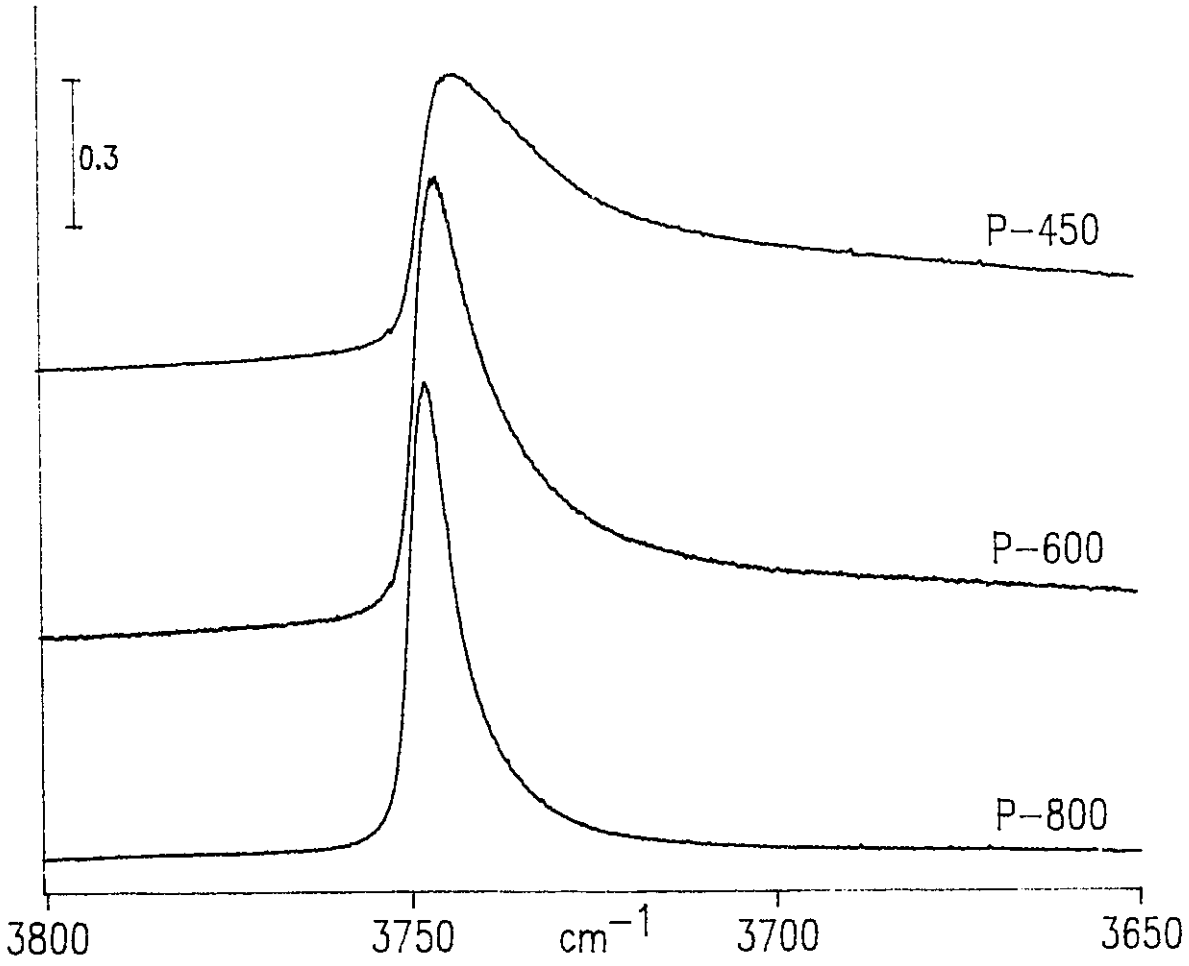

Figure 4.6. Room-temperature, high-resolution spectra of the isolated SiOH profile in precipitated silica.

but for 600°C activation, the profiles resemble one another more closely. When the activation temperature is increased further to 800°C, the asymmetry is almost completely removed for both silicas, and the isolated SiO–H profiles are no longer distinguishable.

The frequency at the intensity maxima and the FWHH of the isolated SiO–H band from the room-temperature spectra in Figures 4.5 and 4.6 are listed in Table 4.1. These data show that changes in the position of maximum intensity occur concurrently with changes in band shape between 450 and 800°C activation, *i.e.* the band maximum shifts to higher wavenumber as the band becomes more symmetric. The upwards shift in frequency with increasing activation temperature is much greater for precipitated silica than for aerosil silica. Similarly, the decrease in FWHH (due to a loss in intensity at lower wavenumber) is greater for the precipitated silica in going from 450 to 800°C activation. (The FWHH is so large for P-450 that it loses its significance and for this reason has been omitted in Table 1). For 800°C activation, both silicas have similar band maxima and half widths.

		Aerosil Silica		Precipitated Silica	
Activation Temp. °C	Sample Temp. °C	Max. cm^{-1}	FWHH[a] cm^{-1}	Max. cm^{-1}	FWHH[a] cm^{-1}
450	22	3747.2	9.4	3743.5	*
	-191[b]	3750.8	10.5	3746.5	*
600	22	3747.3	8.2	3746.2	11.1
	-191[b]	3751.1	9.1	3749.3	13.3
800	22	3748.0	6.2	3747.7	6.8
	-191[b]	3751.7	6.9	3751.2	8.3

Table 4.1. Frequency and Bandwidth Data for High-resolution spectra of Aerosil and Precipitated Silica.

(a) full width at half height (b) 82 Kelvin * see text.

The spectra in Figure 4.5 and 4.6 certainly suggest that the SiO—H band due to isolated silanols contains component bands due to different types of isolated silanols. Although they cannot be resolved at room temperature, they manifest themselves by imposing an asymmetry in the SiO—H profile and a shift in frequency at the band maximum, both of which are dependent upon the temperature of activation. Spectral deconvolution could be used to separate the component bands, but this method is subject to input parameters such as the number, the position, and FWHH of component bands. Alternatively, resolution enhancement can be achieved experimentally by recording the spectrum of the SiO—H stretching profile at low temperature (82 K). Figures 4.7 and 4.8 show the low-temperature spectra of aerosil and precipitated silica, respectively, for 450, 600 and 800°C activation. Each spectrum in Figures 4.7 and 4.8 was recorded *in situ* after cooling the silica sample whose room-temperature spectrum appears in Figures 4.5 and 4.6.

In all cases, when the silica samples were cooled to 82 K, the position of the band maximum shifted to higher frequency by about 4 cm^{-1}. This temperature dependence of the SiO—H vibrational frequency has been reported to be approximately linear over a wide range of temperatures [57,58], however, for the purpose of this study, it is the temperature dependence of the halfwidth of the SiO–H band which is most significant. The position at the intensity maximum and the FWHH for the low-temperature spectra are listed in Table 4.1 for comparison with the room-temperature data.

The isolated SiO—H band in the spectra of A-450 and P-450 develops a distinct low-wavenumber component at about 3738 cm^{-1} upon cooling to 82 K (shown with an arrow in Figures 4.7 and 4.8, respectively). The 3738 cm^{-1} band can still be seen as an inflection in the low-temperature spectra of A-600 and P-600, but is not evident for the 800°C activated silicas. However, the FWHH data in Table 4.1 show that the apparent width of the SiO—H band increases upon cooling either silica to 82 K, even after 800°C activation. This increase in FWHH undoubtedly results from a combination of line-narrowing and separation in frequency of the two component bands which are so clearly seen in the low-temperature

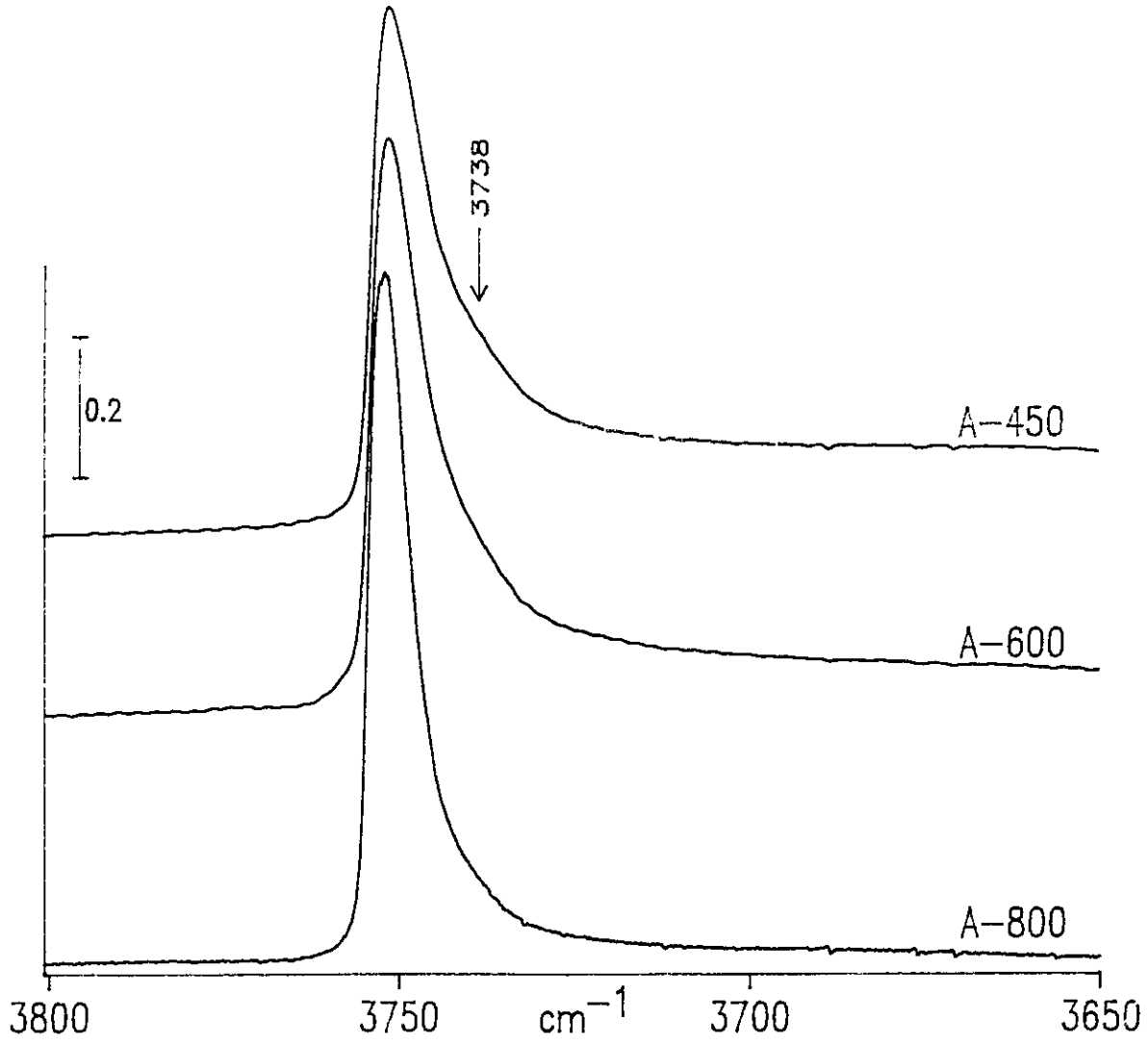

Figure 4.7. Low-temperature, high-resolution spectra of the isolated SiOH profile in aerosil silica. The room-temperature spectra are shown in Figure 4.5.

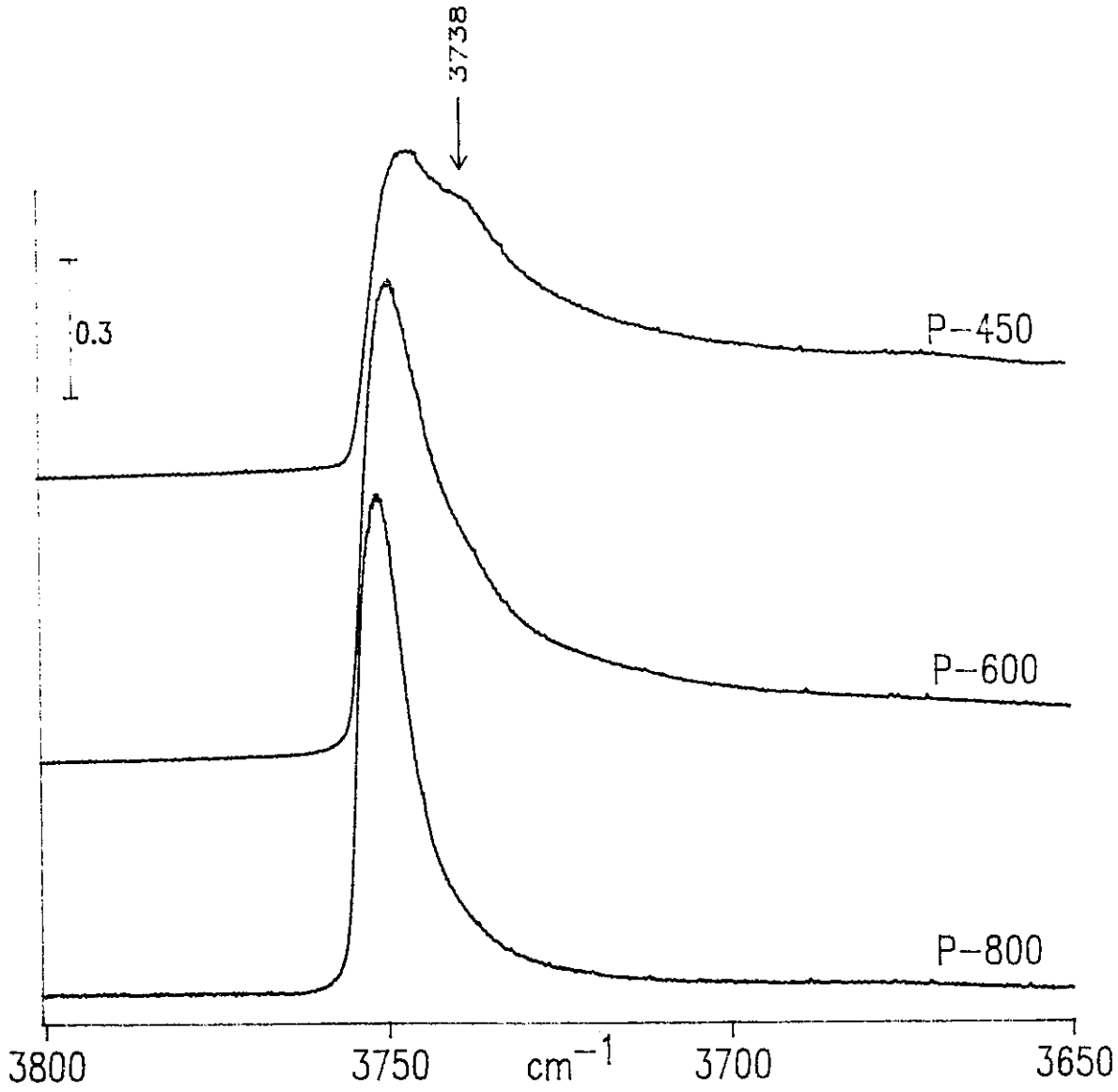

Figure 4.8. Low-temperature, high-resolution spectra of the isolated SiOH profile in precipitated silica. The room-temperature spectra are shown in Figure 4.6.

spectrum of P-450 (Figure 8).

The FWHH data in Table 4.1 is important as evidence of the 3738 cm^{-1} band, particularly in the case of aerosil silica because it has been the silica of choice in the majority of previous infrared studies. Ryason and Russell [58] studied the temperature dependence of the halfwidth of the 3750 cm^{-1} band in the spectrum of A-800 and found that FWHH increased between 100 and 800°C, but exhibited little change between and 100 and −150°C. They attributed the broadening of the SiO—H band at high temperature to increased rotational motion of the isolated silanols, and they suggested that surface heterogeneity and/or hot bands might account for the wider-than-expected FWHH and asymmetry observed at ambient, or below ambient temperatures. Our studies show that two distinct SiO—H bands, that differ in frequency by about 10 cm^{-1} at 82 K, are present in the spectra of aerosil and precipitated silicas activated between 450 and 800°C.

The high-resolution spectrum of P-450 silica in the 2400-2800 cm^{-1} spectral region, following H/D exchange with ND_3, is shown in Figure 4.9. The band at 2760 cm^{-1} in the room-temperature spectrum (Figure 4.9A) is due to the SiO—D stretching mode of the isolated silanols after deuterium exchange. Like the SiO—H band in the room-temperature spectrum P-450 (Figure 4.6), the SiO—D band in Figure 4.9A is also asymmetric to lower wavenumber even though, in this spectrum, there is no contribution from inaccessible silanols. As further evidence that the 3738 cm^{-1} feature in Figure 4.8 is due to an SiO—H stretching vibration, the low-temperature spectrum in Figure 4.9B shows a pronounced shoulder at 2756 cm^{-1} when the deuterated P-450 sample is cooled to 82 K. Thus, the 3738 cm^{-1} band experiences the same isotopic shift (ν_{OH}/ν_{OD} = 1.356) as the isolated SiOH band at 3746.5 cm^{-1} in Figure 4.8 (the 3746.5 cm^{-1} band shifts to 2762.7 cm^{-1}).

The ability to record high-resolution spectra of the SiO—H profile at low temperature has enabled us to clearly show its composite nature for both the aerosil and precipitated silicas. The component at about 3738 cm^{-1} is at least partly responsible for the asymmetry to low wavenumber, its intensity contribution is greater for low or moderate activation

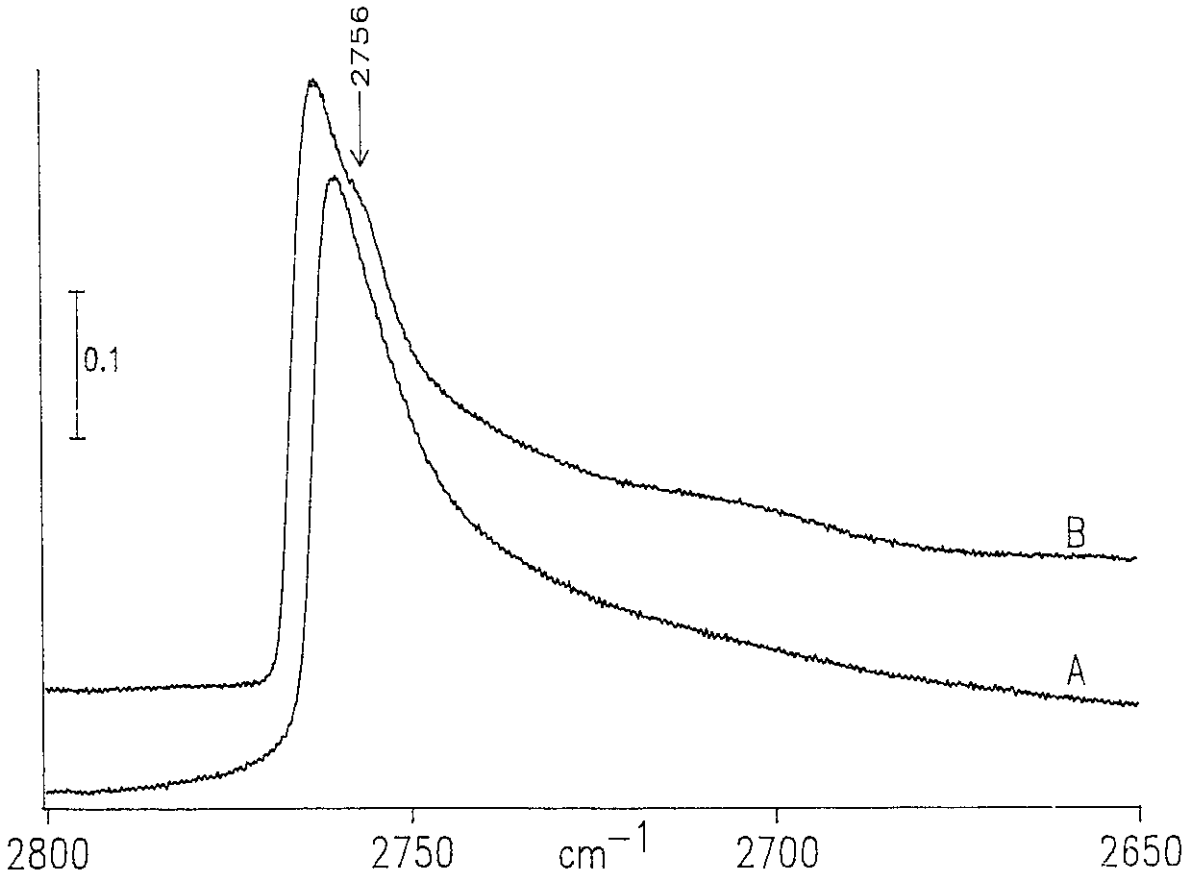

Figure 4.9. High-resolution spectra of the isolated SiOD profile of deuterium-exchanged P-450 silica at (A) room temperature and at (B) -191°C (82 K).

temperatures, and much more so for precipitated silica than for aerosil silica. For 800°C activation the contribution at 3738 cm^{-1} is quite small for either silica and, as a result, the SiO–H profiles more or less converge to a symmetrical band centred at 3748 cm^{-1}.

Thus, a parallel behaviour is observed in the SiO–H stretching profiles and the combination bands for both silicas. The low-temperature spectra show that the relative intensities of 4580/4510 cm^{-1} and 3740/3750 cm^{-1} are greater for 450°C activation than for 800°C activation, and they are significantly greater for P-450 than for A-450. For 800°C activation, the two silicas exhibit similar band profiles in both spectral regions.

Part 3. 500 - 1000 cm^{-1} Region

Introduction

The comparative study of aerosil and precipitated silica has been extended to the "window region" of the silica spectrum. The spectral region between 500 and 1000 cm^{-1} contains information related to the structure of surface silanols on silica because it is in this region where one can observe the Si–OH stretching vibrations and the Si–O–H bending vibrations of the various silanol types. The infrared spectrum of silica exhibits changes in this region when, (a) there is a change in the surface silanol distribution resulting from a particular activation pretreatment, (b) surface silanols are perturbed via interaction with physically adsorbed molecules on the silica surface, or (c) when surface silanols are replaced by new surface species in a chemical reaction. However, unlike other regions of the silica spectrum, surface vibrational modes are buried in the intense bulk silica modes and spectral subtraction must be used in order to observe the changes in the vibrational spectrum due to surface species.

Infrared bands at 870 and 950 cm^{-1} have been reported in the spectrum of silica gel, and have been assigned to Si–O–H bending and Si–OH stretching vibrations, respectively [60]. Boccuzzi *et al.* reported two bending vibrations of surface SiOH on aerosil, one at 760 cm^{-1}, and another ill-defined band between 760 and 900 cm^{-1} [61]. These bands were

assigned to free and hydrogen-bonded silanols respectively, based on results of dehydroxylation, deuteration, methoxylation, and pyridine adsorption experiments. Their experiments showed that deuterium exchange shifted the bending mode of the free silanols to 610 cm^{-1} while the exchanged H-bonded silanols absorbed between 610 and 750 cm^{-1}. They also found that, for activation temperatures above 600°C, only the free Si—O—H bending vibrations remained.

It is known that the interaction of CO at low temperature with surface silanols causes a downward shift in the SiO—H stretching vibration from around 3750 cm^{-1} to 3655 cm^{-1} [3,45,62]. However, the perturbation of the "free" Si—O—H bending vibrations between 750 and 875 cm^{-1} due to physically adsorbed CO is less clear [45]. In this study, we have used CO adsorption at low temperature to probe the low-frequency vibrations of surface silanols on aerosil and precipitated silica. Deuterium exchange of surface SiOH with ND_3, and chemical modification by reaction with BCl_3, have also been used to probe the bending vibrations of the surface silanols on both silicas. Unlike CO which reversibly adsorbs, ND_3 and BCl_3 alter the chemical structure of the surface silanols. These methods have been used to compare the low-frequency vibrational spectra of SiOH on aerosil and precipitated silicas activated between 450 and 800°C.

Results

Figure 4.10, A and B, show the low-temperature spectrum of A-450 silica, before and after CO adsorption at 82 K. Figure 4.10, A was recorded with an equilibrium pressure of 0.84 Torr H_2, and B was recorded following the evacuation of H_2 and subsequent addition of an equilibrium pressure of 2.0 Torr CO at 82 K. The series of difference spectra, Figure 4.10, C, D, E, F and G, show the progressive spectral changes as the equilibrium pressure of CO was varied between 0.03 and 2.0 Torr. Each difference spectrum in Figure 4.10 was obtained using spectrum A as the subtrahend spectrum. The negative feature at 980 cm^{-1} and the positive feature at about 995 cm^{-1}, which grow concomitantly in intensity with increasing CO

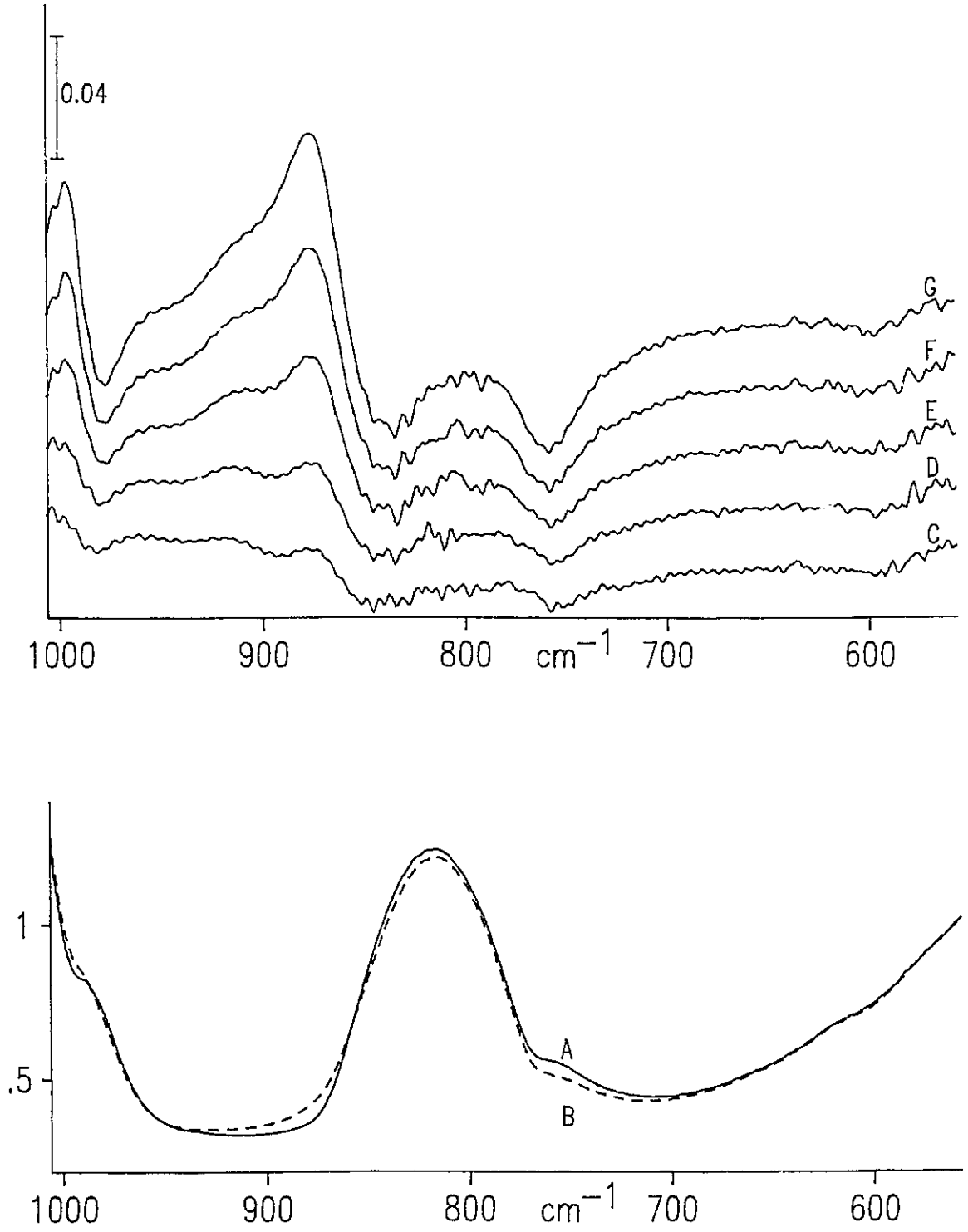

Figure 4.10 (A) 2.5 mg/cm^2 A-450 cooled to 82 K in 0.84 Torr H_2. (B) After evacuation of A, followed by addition of 2.03 torr CO at 82 K. (G) Difference spectrum, B minus A. The progressive difference spectra, C,D,E,F, were computed like G for equilibrium pressures of (C) 0.10, (D) 0.23, (E) 0.52, (F) 1.02 torr CO.

pressure, arise from the perturbation of the Si—OH stretching vibration causing it to shift to higher wavenumber. The stepwise adsorption of CO also produces negative features at 760 and 840 cm^{-1}, and a positive feature at 870 cm^{-1} with a shoulder at about 900 cm^{-1}.

A series of spectra in Figure 4.11, analogous to those in Figure 4.10 for A-450, show CO adsorption on P-450 at low temperature. The 980 cm^{-1} band assigned to the Si—OH stretching vibration of isolated silanols can be seen clearly the spectrum of P-450 (Figure 4.11A) whereas it appears only as a shoulder in the spectrum of A-450 (Figure 4.10A). The difference spectra for CO adsorbed on P-450 also reveal negative features at 760, and 840 cm^{-1}, and positive features at 870, 900 cm^{-1}(sh), which increase in intensity with increasing CO pressure, as was observed for A-450 in Figure 4.10. However, a closer comparison of Figures 4.10 and 4.11 reveals subtle differences between the two silicas with regard to CO adsorption. In the difference spectra of P-450 (Figure 4.11), the negative 840 cm^{-1} band is more intense than the negative 760 cm^{-1} band, whereas for A-450 (Figure 4.10), the relative intensities of the 840 and 760 cm^{-1} features are reversed.

Physical adsorption of CO on A-450 and P-450 reveals two distinct surface vibrational modes, at 760 and 840 cm^{-1}, in the spectral region where Si—O—H bending vibrations are expected to occur; the interaction of isolated SiOH with CO at 82 K apparently shifts these modes to higher wavenumber (870, 900(sh) cm^{-1}). Further, the relative intensities of the 840, 760 cm^{-1} features for A-450 and P-450 differ significantly (Figure 4.10, 4.11), just as the relative intensities at 4580, 4510 cm^{-1} differ in the low-temperature spectra of the combination bands (Figure 4.2). These results are most important in light of the evidence presented in Parts 1 and 2 of this comparative study. Consequently, other methods of probing the window region have been explored in order to confirm the findings of the CO adsorption studies, and these results are presented below.

The SiOH vibrational modes in the silica window region have been probed using H/D exchange. Substitution by deuterium does not alter the number or type of SiOH, provided that the same state of activation of the silica is maintained. Therefore, the difference

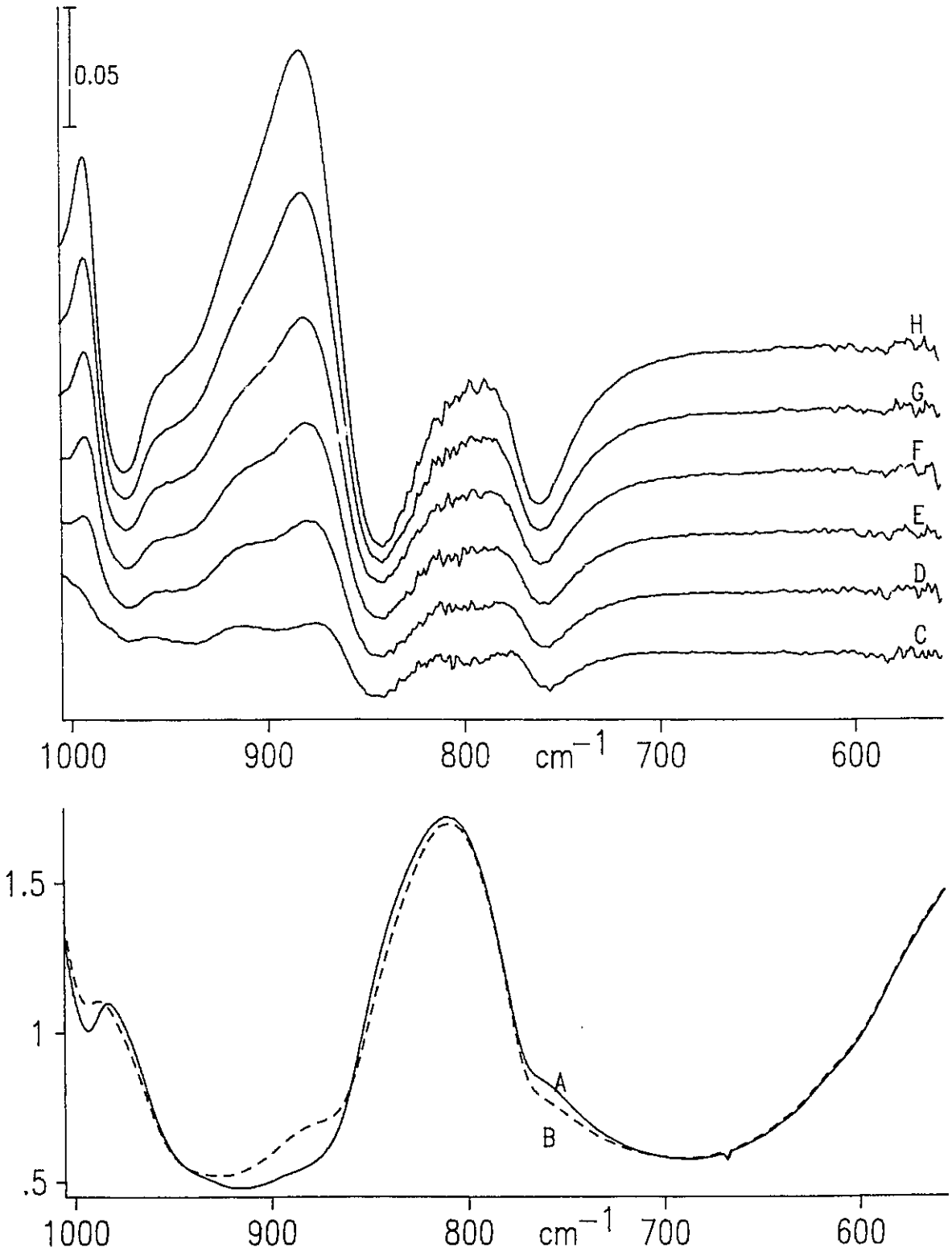

Figure 4.11. (A) 2.5 mg/cm^2 P-450 silica cooled to 82 K in 0.50 Torr He. (B) After evacuation of A, followed by the addition of 0.53 torr CO. (H) Difference spectrum, B minus A. The progressive difference spectra, C,D,E,F,G, were computed like H for equilibrium pressures of (C) 0.02, (D) 0.05, (E) 0.07, (F) 0.12, (G) 0.23 torr CO.

spectrum shows only the isotopic shifts of the surface vibrational modes due to SiOH which have exchanged. Figure 4.12, A and A' are the room-temperature difference spectra, D-silica minus H-silica for A-450 and P-450, respectively, following exchange with ND_3. Curves B and B' are the low-temperature difference spectra for the corresponding samples, recorded at 82 K and with a pressure of 0.50 Torr He. In the spectrum of either A-450 or P-450, negative features at 760 and 840 cm^{-1} are replaced by a single positive band at 610 cm^{-1}. Deuterium exchange also shifts the Si—OH stretching vibration to lower wavenumber, *i.e.* the negative 980 cm^{-1} band is replaced by a positive band at about 965 cm^{-1} for A-450, and 960 cm^{-1} for P-450. The room-temperature spectra (Figure 4.12, A and A') and low-temperature spectra (B and B') exhibit the same spectral features, although they are more intense and better resolved at low temperature.

In Figure 4.12, we observe that the negative 840 cm^{-1} band is slightly more intense than the negative 760 cm^{-1} band for A-450 (A or B), whereas it is significantly more intense than the negative 760 cm^{-1} band for P-450 (A' or B'). The same trend was observed for CO adsorbed on A-450 and P-450 (see Figures 4.10 and 4.11), and in the low-temperature spectra of the combination bands at 4580, 4510 cm^{-1} (Figure 4.2). The deuterium exchange results shown in Figure 4.12 are also consistent with the spectra shown previously in Figure 4.3, where thicker silica discs were used. That is, for both silicas, bands at 4580 and 4510 cm^{-1} are replaced by a single band at 3370 cm^{-1}, and bands at 840 and 760 cm^{-1} are replaced by a single band at 610 cm^{-1}. That a single band (albeit broad) appears at 610 cm^{-1} in the spectrum of either silica after H/D exchange is a peculiar result, so in order to support our findings in the window region, we investigated the adsorption of CO on deuterated A-450 and P-450.

The adsorption of CO on deuterated A-450 and P-450 was studied using the same method used for the H-silicas described previously. The spectra are shown in Figures 4.13 and 4.14, respectively. In both cases, spectrum A was recorded at 82 K in 0.5 Torr He, spectrum B was recorded with the indicated pressure of CO, and spectrum C is the difference

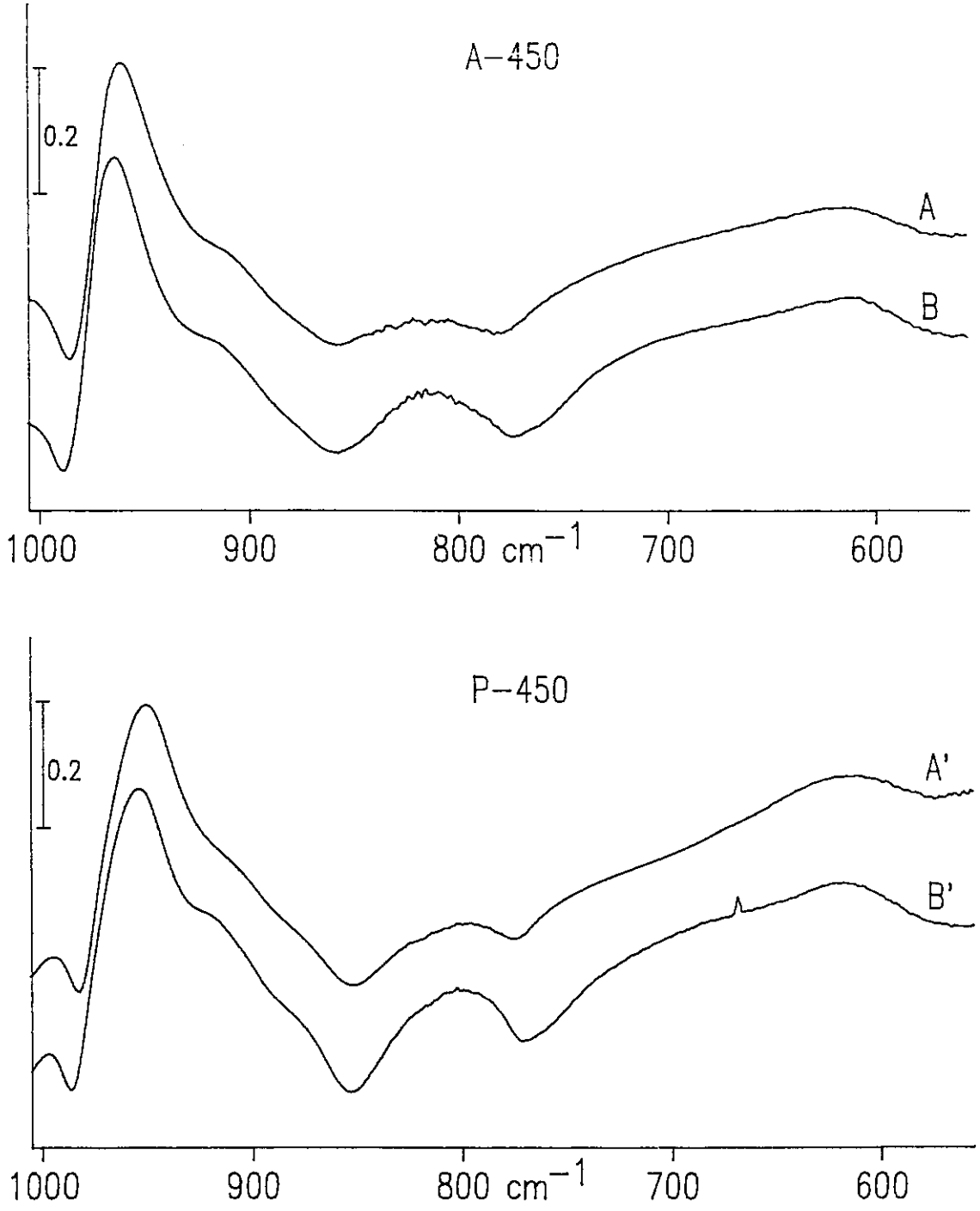

Figure 4.12. Difference spectra showing changes due to deuterium exchange of surface silanols. (A and A') Room-temperature difference spectra of D-silica minus H-silica for A-450 and P-450, respectively. (B and B') Corresponding low-temperature difference spectra.

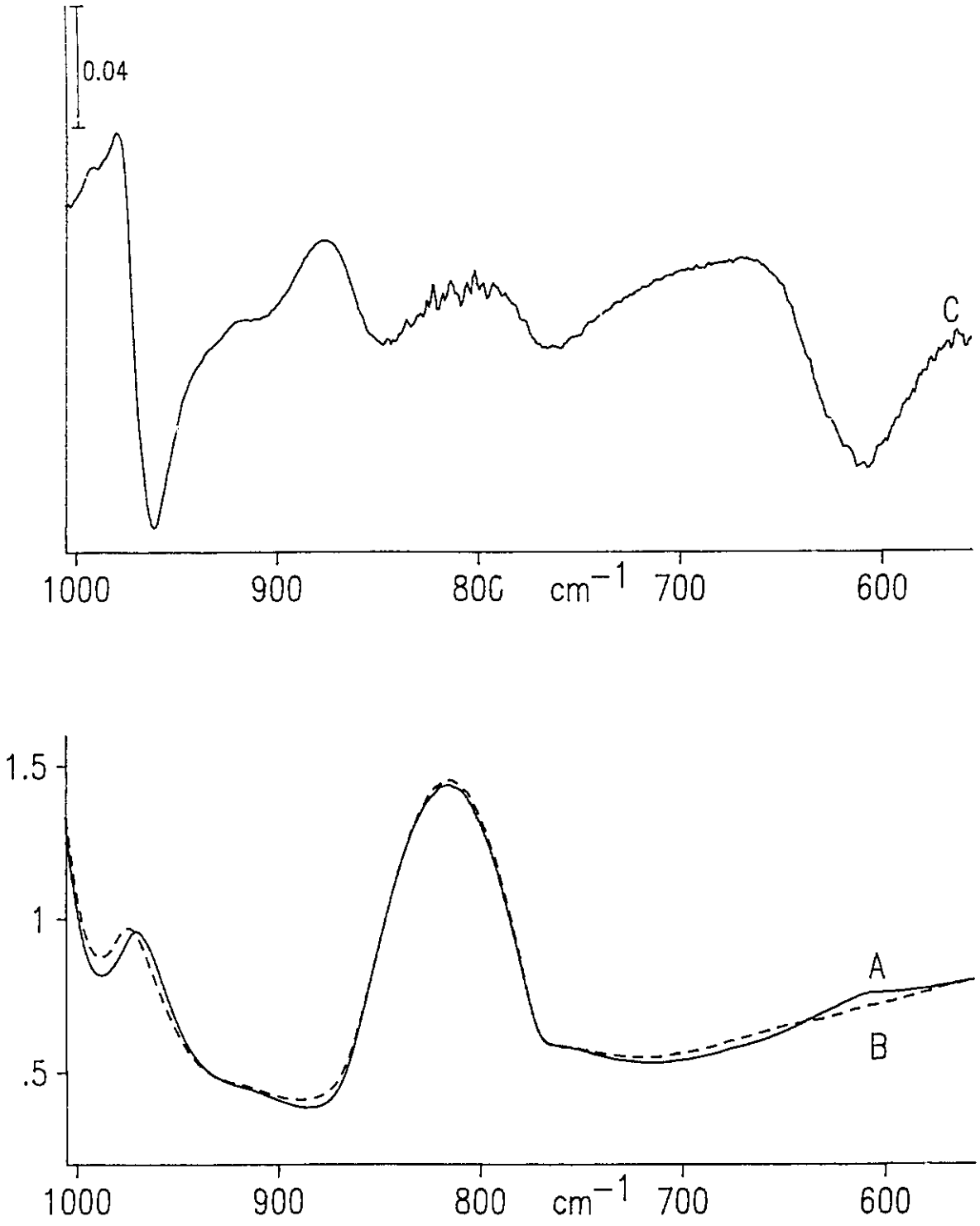

Figure 4.13. (A) Low-temperature spectrum of deuterated A-450 recorded at 82 K, 0.50 torr He. (B) After evacuation of A, followed by the addition of 2.1 torr CO at 82 K. (C) Difference spectrum, B minus A.

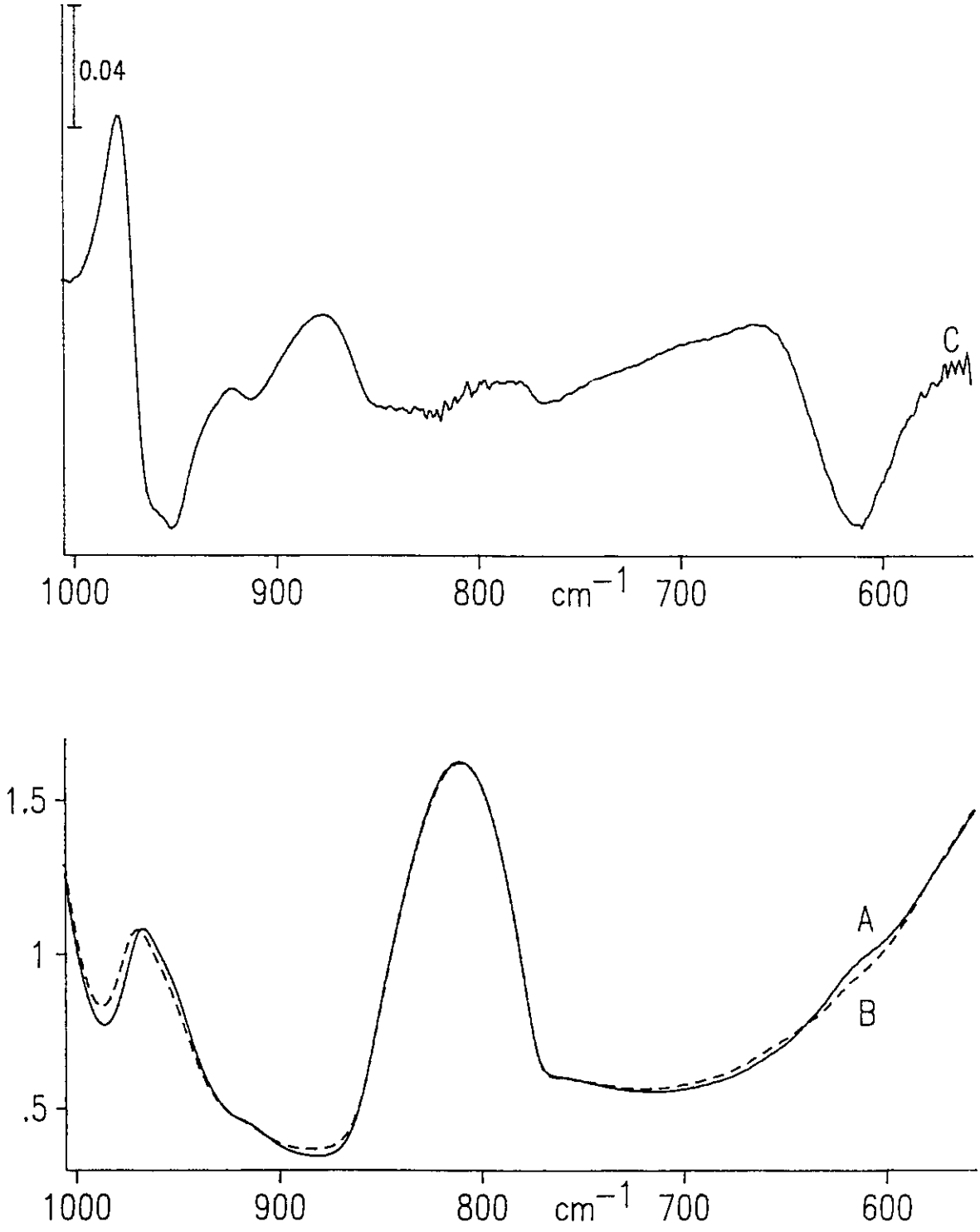

Figure 4.14. (A) Low-temperature spectrum of deuterated P-450 recorded at 82 K, 0.50 torr He. (B) After evacuation of A, followed by the addition of 1.0 torr CO at 82 K. (C) Difference spectrum, B minus A.

spectrum, B minus A. The difference spectra, curve C in Figures 4.13 and 4.14, clearly show a single negative band at 610 cm^{-1} and a broad positive band at about 670 cm^{-1}. The Si-OD stretching vibration is also shifted to higher wavenumber, as shown by the sharp negative feature at 965 cm^{-1} and positive feature at about 980 cm^{-1} in curve C of Figures 4.13 and 4.14. The weak negative 760, 840 cm^{-1} bands, and positive 870 cm^{-1} band are due to the interaction of CO with residual SiOH which were not exchanged.

The results obtained by studying CO adsorption and H/D exchange on A-450 and P-450 in the "window region" are consistent for both silicas, in either the H-silica or D-silica form. Furthermore, that the same results have been obtained by two different methods (physical adsorption at 82 K *vs.* isotopic exchange at room temperature) confirms the existence of two low-frequency surface vibrational modes, at 840 and 760 cm^{-1} for the H-silicas, and a single low-frequency mode at 610 cm^{-1} for D-silicas.

To this point, the comparative study in the silica window region (500-1000 cm^{-1}) has been purposely restricted to A-450 and P-450 silicas. Figure 4.2 shows that the two silicas are most distinguishable by their low-temperature spectra of the combination bands following activation at 450°C. At temperatures of activation above, or below about 450°C, the combination bands are less distinguishable. Therefore, <u>if</u> a correlation exists between the pairs of bands at 840 and 4580 cm^{-1}, and 760 and 4510 cm^{-1}, then 450°C activation would appear to be the optimum choice for distinguishing the two silicas by their low-frequency vibrations. Our results, thus far, indicate that A-450 and P-450 <u>can</u> be distinguished by the relative intensities at 840 and 760 cm^{-1}. We have yet to demonstrate, however, that the 840, 760 cm^{-1} bands exhibit similar changes in relative intensity to the 4580, 4510 cm^{-1} bands between 450 and 800°C activation. In order to explore this further, we have studied CO adsorption on A-800 and P-800. We have also studied the evolution of the 840, 760 cm^{-1} bands with increasing activation temperature for the reaction of BCl_3 with precipitated silica.

Figures 4.15 and 4.16 show the low-temperature spectra for CO adsorption on A-800 and P-800, respectively. The analogous spectra for A-450 and P-450 have already been

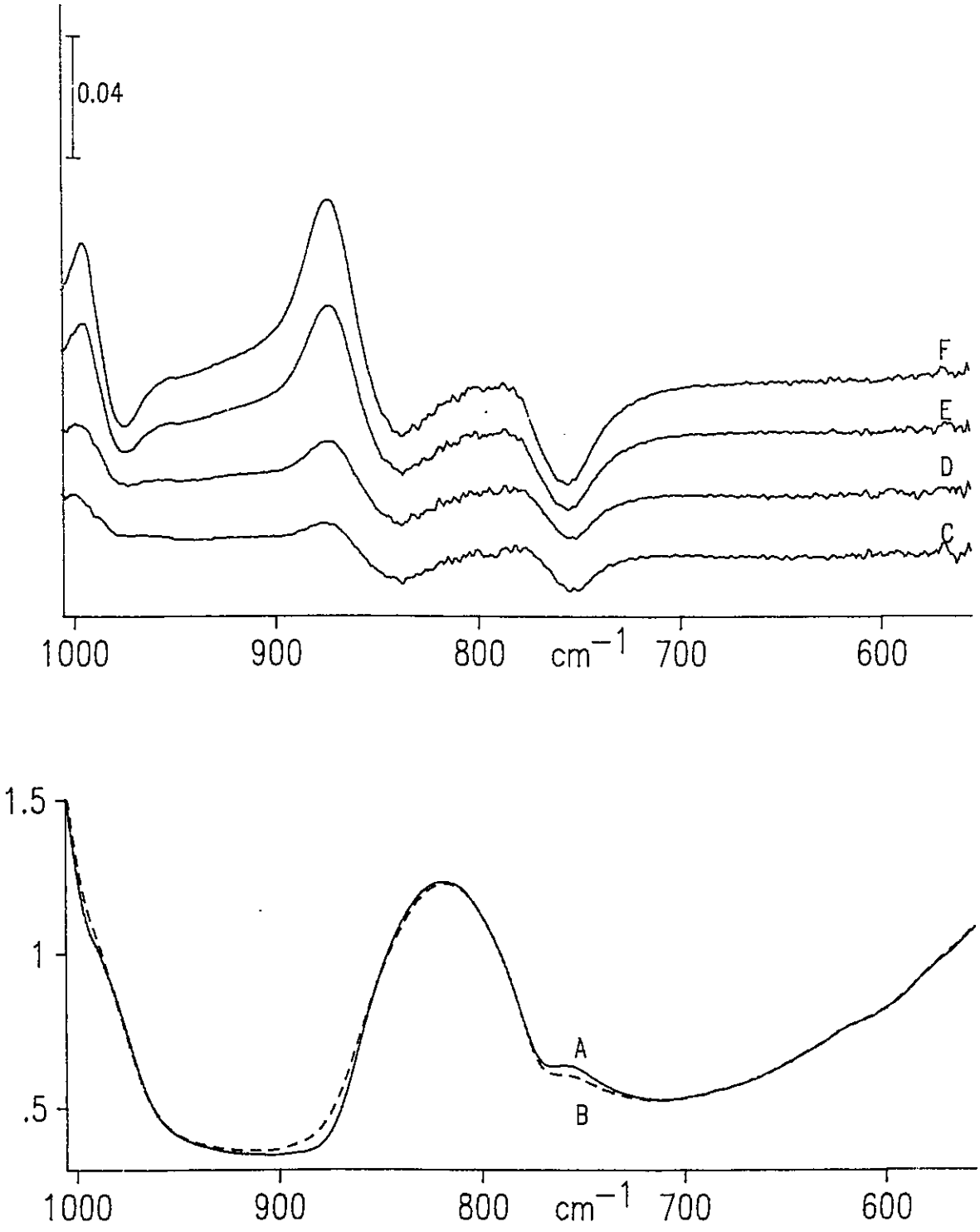

Figure 4.15. (A) Spectrum of A-800 recorded at 82 K, 0.50 torr He. (B) After evacuation of A, followed by the addition of 1.0 torr CO at 82 K. (F) B minus A. The difference spectra, C,D,E, were obtained like F for equilibrium pressures of, (C) 0.05, (D) 0.1, (E) 0.5 torr CO.

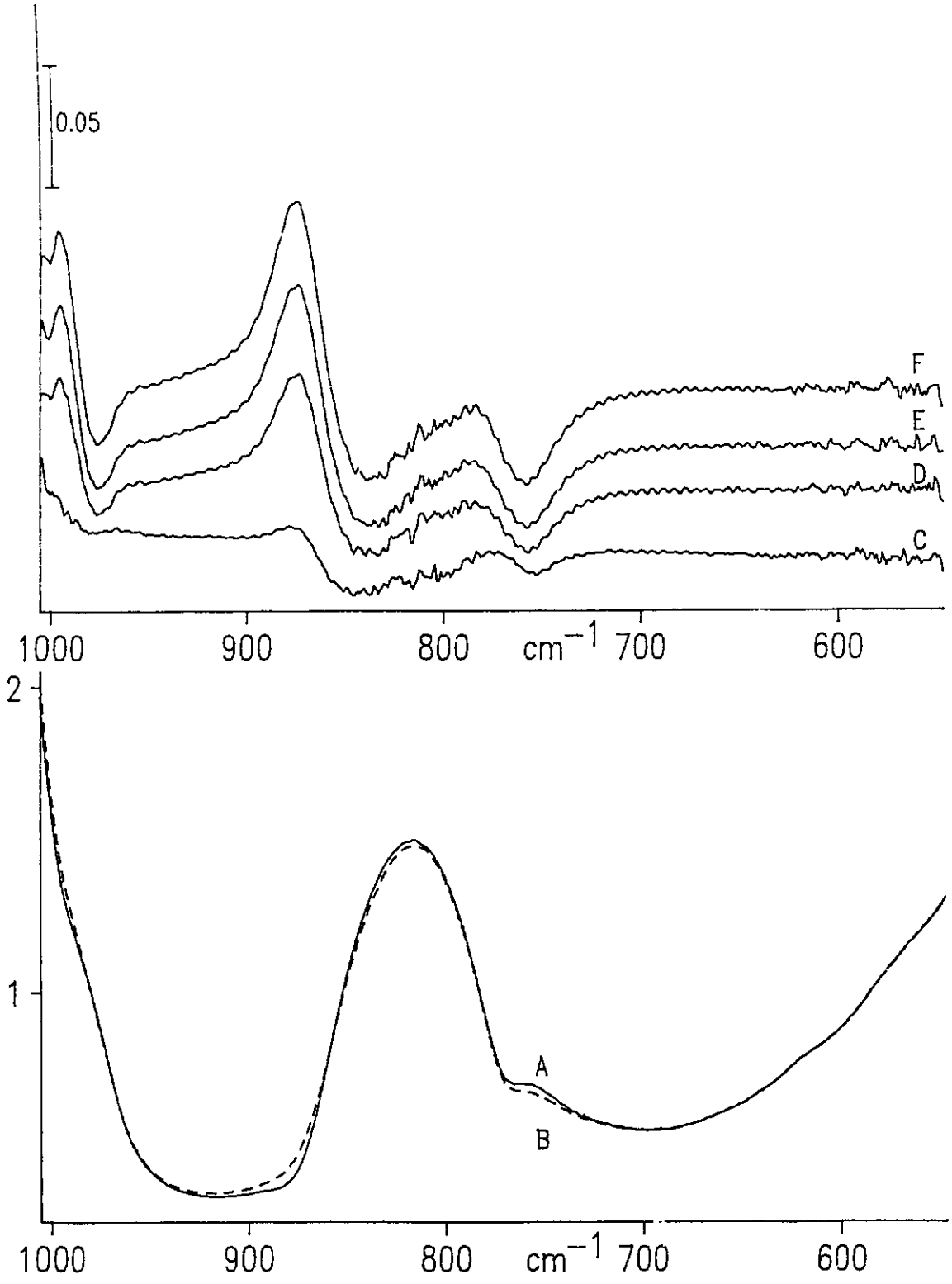

Figure 4.16. (A) Spectrum of P-800 recorded at 82 K, 0.50 torr He. (B) After evacuation of A, followed by the addition of 1.5 torr CO at 82 K. (F) B minus A. The difference spectra, C,D,E, were obtained like F for equilibrium pressures of, (C) 0.07, (D) 0.5, (E) 1.0 torr CO.

presented in Figures 4.10 and 4.11, respectively, and the assignment of the various spectral features has already been discussed. Comparing Figure 4.15F with 4.10G for aerosil, and Figure 4.16F with 4.11H for precipitated silica, we see that, upon going from 450 to 800°C activation, there is an apparent decrease in intensity of the 840 cm^{-1} band relative to that at 760 cm^{-1}, and this is especially noticeable for the precipitated silica. Thus, the relative intensities of the 840, 760 cm^{-1} pair of bands for A-800 and P-800 appear to resemble one another more closely than for A-450 and P-450, just as the low-temperature spectra of the combination bands for A-800 and P-800 resemble one another more closely. These experiments demonstrate qualitatively that the pair of bands at 840, 760 cm^{-1} mimic the behaviour of the pair of bands at 4580, 4510 cm^{-1} as the activation temperature is increased from 450 to 800°C, thereby providing further evidence that the 840, 760 cm^{-1} bands are the fundamentals belonging to the 4580, 4510 cm^{-1} combinations.

The reaction of BCl_3 with isolated SiOH on precipitated silica, activated between 450 and 1000°C, has been studied in order to observe the change in relative intensity of the 840, 760 cm^{-1} bands with activation temperature. Precipitated silica was chosen for this study because the spectra of the combination bands suggested that changes in relative intensity with increasing activation temperature might be more dramatic for precipitated silica than for aerosil. Further, BCl_3 was chosen as the probe molecule because (a) it completely reacts with isolated SiOH [63,64], and (b) infrared bands due to $SiOBCl_2$, the expected chemisorbed product of the reaction with isolated silanols, do not overlap the 840, 760 cm^{-1} bands due to SiOH [65].

The difference spectra for 2.5 mg/cm^2 samples of precipitated silica, activated at 450, 650, 800 and 1000°C, and subsequently reacted at room temperature with BCl_3 are shown in Figure 4.17. The intense positive features at about 920 cm^{-1} and 952 cm^{-1} are B—Cl stretching vibrations of surface $SiOBCl_2$ [64]. Additionally, broad negative features having maxima at around 850 and 770 cm^{-1} appear in the difference spectra, and these can be attributed to the disappearing surface SiOH modes. (When the same experiment was carried out using

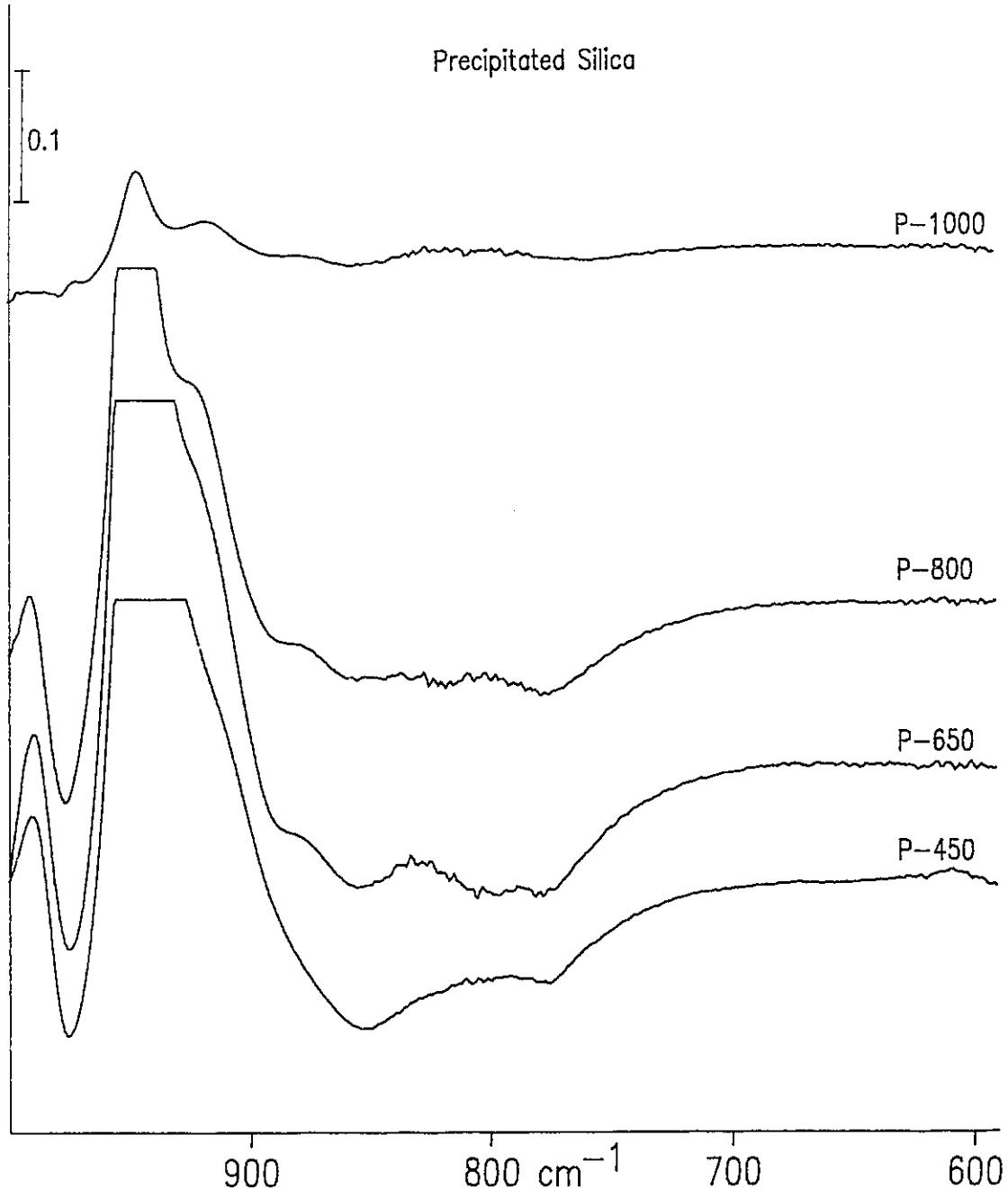

Figure 4.17. Room-temperature difference spectra showing spectral changes due to complete reaction of BCl_3 with 2.5 mg/cm^2 precipitated silica activated at the indicated temperature.

deuterated silica, these bands were not observed, but instead, a broad negative band appeared at around 620 cm^{-1}.) The difference spectra in Figure 4.17 show that, as the temperature of activation of the silica is increased from 450°C to 1000°C, the negative intensity at 850 cm^{-1} diminishes more, relative to 770 cm^{-1}. Given that the negative 850, 770 cm^{-1} bands are poorly resolved in Figure 4.17, we cannot speculate as to the nature of the apparent 10 cm^{-1} shift. However, these difference spectra exhibit qualitatively the same behaviour as the 4580, 4510 cm^{-1} bands for precipitated silica in Figure 4.2.

Part 4. General Discussion, Conclusions

Low-temperature adsorption of CO, and deuterium exchange have revealed 2 surface SiOH modes at 840 and 760 cm^{-1} on aerosil and precipitated silica. Both bands have been observed on aerosil and precipitated silica even after activation at 800°C. H/D exchange causes the disappearance of the 840, 760 cm^{-1} pair, and the appearance of a single band at 610 cm^{-1}. As shown by CO adsorption, the relative intensity of the 840, 760 cm^{-1} pair of bands is greater for P-450 than for A-450, and decreases upon going from 450 to 800°C activation. The same trend was observed for precipitated silica, activated between 450 and 1000°C, and chemically modified in a reaction with BCl_3.

A re-examination of the SiO—H stretching profile of aerosil and precipitated silica at high resolution and low temperature has enabled us to show the composite nature of the 3750 cm^{-1} band. The low-temperature spectra reveal a component band at around 3738 cm^{-1} which contributes to the asymmetry of the band profile; its contribution diminishes as the temperature of activation increases. For activation below 800°C, the 3738 cm^{-1} component contributes more to the precipitated silica spectrum than to the aerosil spectrum, resulting in more asymmetric profile and a lower band maximum in the room-temperature spectrum of the precipitated silica. We have also shown that two bands are resolved in the low-temperature spectrum of the SiO-D stretching region of P-450 silica. The 2760 cm^{-1} band has a low

wavenumber component at 2756 cm^{-1}.

A comparison of the two silicas in the region of the combination bands has shown that at low temperature, the relative intensity, 4580/4510 cm^{-1}, varies with activation temperature for both silicas. For activation at 450°C, 4580/4510 cm^{-1} is noticeably greater for the precipitated silica, however, as the activation temperature approaches 800°C, the relative intensities converge. This convergence in band shape at 4580, 4510 cm^{-1} is mirrored by the convergence in band shape and frequency maximum of the SiO–H stretching profile, and by the 840, 760 cm^{-1} bands. For both aerosil and precipitated silica, H/D exchange results in the disappearance of the 4580, 4510 cm^{-1} doublet, and the appearance of a single band at 3370 cm^{-1}.

Based on the results summarized above, we propose that the bands at 840, and 760 cm^{-1} are Si–O–H bending vibrations belonging to two different types, of isolated silanols, which we will refer to as **I** and **II**. The SiO–H stretching bands for these two silanol types occur at 3740, and 3750 cm^{-1}, respectively. (We will refer to the band at 3738 cm^{-1} as the 3740 cm^{-1} band in the discussion). Neither type **I** nor type **II** silanols are hydrogen bonded, since they are present on silicas activated above 800°C. The following combinations of fundamental vibrations can account for the observed frequencies of the combination bands:

$$840 + 3740 = 4580\ cm^{-1} \qquad \mathbf{I}$$

$$760 + 3750 = 4510\ cm^{-1} \qquad \mathbf{II}$$

Deuterium exchange of the type **II** silanols results in:

$$610 + 2760 = 3370\ cm^{-1}$$

The assignment of the 840 cm^{-1} and 760 cm^{-1} bands to vibrations belonging to the same surface species must be ruled out, because their relative intensity varies with activation

temperature. That the pairs of bands at, 4580 and 4510 cm^{-1}, 3740 and 3750 cm^{-1}, 840 and 760 cm^{-1}, exhibit similar changes in relative intensity with activation temperature is the most convincing evidence which supports the above band assignments to two unique surface species. These assignments are further supported by the nearly perfect additivity of the fundamental modes to give the observed frequencies of the combination bands.

In their earlier studies, band assignments by Kustov *et al.*, and Tsyganenko were based largely on the additivity of the fundamental vibrations to give the observed combination band frequencies, but our experimental evidence discredits the assignment of a band at 765 cm^{-1} [53], or a band at 840 cm^{-1} [52] to the Si—OH stretching vibration. Deuterium exchange experiments show that the 980 cm^{-1} band shifts to lower wavenumber by about 15 and 20 cm^{-1} for deuterated aerosil and precipitated silica, respectively, and the 980 cm^{-1} assignment to the Si—OH stretching vibration is now well established [2,41,66-68]. Our assignment of the 840 and 760 cm^{-1} bands to Si—O—H bending vibrations of type **I** and type **II** isolated silanols is plausible, based on the spectroscopic evidence presented here. Nevertheless, it remains to be explained why only one bending vibration is observed either as the fundamental or the combination band in the spectrum of deuterated silica. We propose the following explanation.

The frequency of the SiO—H stretching vibrations are far removed from the frequencies of other SiOH or SiO_2 vibrational modes, and thus are likely to exhibit pure SiO—H stretching character. Therefore, the absorbance at 3740 or 3750 cm^{-1} probably gives a reasonable measure of the relative number of type **I** or type **II** silanols, and we can conclude that there are many more type **II** silanols than type **I** on either silica. It follows that the relative number of type **I** silanols is greater on P-450 than on A-450, and decreases with increasing activation temperature on both silicas. One could postulate that, for the deuterated silicas, the relative intensities of the bending vibrations also reflect the relative numbers of type **I** and type **II** silanols. That is to say, the observed 610 cm^{-1} band is mainly due to type **II** silanols, but there could be a weak component due to type **I** silanols at about 630-640 cm^{-1} that it is not resolved in the rather broad 610 cm^{-1} feature.

For the H-silicas, a pure Si—O—H bending vibration would probably absorb at a frequency around 800 cm^{-1}. Recent studies involving molecular dynamics computer simulations of the vibrational spectrum of surface silanol groups on silica have predicted that the in-plane Si—O—H deformation mode would absorb at 780 cm^{-1} [69]. Bending vibrations of surface hydroxyl groups on ZnO have been observed at 840 cm^{-1} and 637 cm^{-1} for the ZnOH and ZnOD species, respectively [70]; these frequencies are close to the frequencies observed for the SiOH and SiOD species here. On the assumption that the 610 cm^{-1} band is a pure SiOD deformation mode which experiences an isotopic shift similar to ZnOD (840 / 637 = 1.32), we would expect to find the pure SiOH deformation mode at 805 cm^{-1} (610 x 1.32 = 805).

Tsyganenko explained the appearance of a doublet in the spectral region of the SiOH combination bands on the basis of a resonance interaction between the SiOH deformation mode and the previously assumed Si—OH stretching vibration around 800 cm^{-1}, giving rise to two low-frequency vibrations at 765 and 840 cm^{-1} [52]. Although his assignment of the Si—OH stretching mode was incorrect, we agree that the infrared bands observed at 840 and 760 cm^{-1} probably originate from mixing of the pure SiOH deformation modes with local SiO modes which also absorb at around 800 cm^{-1}. The infrared spectrum of silica has an intense band near 800 cm^{-1} due to bulk SiO vibrations, and bands at around 800 cm^{-1} have also been observed in the Raman spectrum [32]. Mixing or coupling of the pure deformation modes with nearly degenerate local SiO modes could give rise to the observed 840, 760 cm^{-1} bands whose frequency separation and extinction coefficients have been altered. The extent to which the SiOH and local SiO vibrations interact will depend on their near degeneracy [71], therefore, it is possible that the 840 cm^{-1} band has an extinction coefficient that is much larger than that observed at 760 cm^{-1} due to mixing. Upon deuteration, both bands are shifted away from the SiO modes, thereby removing the near degeneracy. Thus, as discussed above, in the spectra of the D-silicas these bands are no longer coupled with SiO modes and, having pure SiOD bending character, the extinction coefficient of the shifted 840 cm^{-1} band is diminished

to the extent that it is not resolved in the 610 cm^{-1} band.

It would be difficult, and perhaps unwarranted, to prove that either the 840 or 760 cm^{-1} band has significant mixed character, and in the absence of such a proof we recognize that our account of the disappearance of a band upon deuteration is somewhat speculative. In the spectra of both silicas, the relative intensity at 840/760 cm^{-1} is reflected in the relative intensity at 4580/4510 cm^{-1}, but **not** at 3740/3750 cm^{-1}. On the other hand, there is strong evidence supporting the assignment of the 840 and 3740 cm^{-1} bands to type **I** silanols. The above explanation accounts for the appearance of single bands at 610 **and** 3370 cm^{-1} in the spectra of the deuterated silicas. We have also been able to rationalize why the behaviour of the 840 cm^{-1} band mimics the behaviour of the 3740 cm^{-1} band, and why the ratio of 840/760 cm^{-1} gives the impression that there are more type **I** silanols than type **II** silanols when in reality the opposite is probably true.

In Chapter 1, the ^{29}Si NMR evidence supporting the coexistence of single and geminal isolated silanols on silica was discussed. Theoretical calculations predict the frequency separation between the symmetric and antisymmetric SiO–H stretching vibrations of a pair of isolated geminal silanols to be about 2 wavenumbers [59]. Although it is tempting to suggest that the type **I** silanols may be isolated geminal silanols, the solid state ^{29}Si NMR evidence indicates that both single and geminal silanols persist on aerosil silica activated at 800°C, and that the fraction of geminal silanols is more or less independent of the silica's origin (see Chapter 1). Our spectroscopic evidence indicates that the type **I** silanols are essentially eliminated after vacuum activation at 800°C and that, for a given temperature of activation, there are more type **I** silanols relative to type **II** silanols on the precipitated silica. Therefore, it is illogical to assign the 3738 cm^{-1} component of the isolated SiOH profile exclusively to isolated geminal silanols.

The 3750 cm^{-1} band in the silica spectrum is generally attributed to isolated single silanols (our type **II** silanols). The lower SiO–H stretching vibration, and higher Si–O–H bending vibration exhibited by the type **I** silanols might result from a weak interaction

between two vicinal silanols which are sufficiently far apart to prevent strong H-bonding interactions. On highly dehydroxylated silicas which have been rehydrated by adding micromolar quantities of water, a pair of vicinal isolated silanols are created when strained siloxane bridges are ruptured and these silanols absorb at 3742 cm^{-1} [23,72]. The silicas used here were not subjected to this dehydroxylation/rehydration treatment in order to create these sites and, furthermore, the type I silanols (3740 cm^{-1}) are more abundant on either silica when lower activation temperatures are used. However, the type I silanols may experience weak interactions similar to those responsible for the 3742 cm^{-1} band on highly activated, rehydrated silica. For example, isolated silanols projecting from internal surfaces may interact weakly with neighbouring sites due to their unique environment, thereby causing their SiOH stretching and bending vibrations to shift to lower, and higher frequencies, respectively. The spectroscopic evidence does not permit us to speculate further about the structure of the type I silanols.

An infrared band at 3737 cm^{-1} has been observed in the room-temperature difference spectrum of a hydrated silica gel which was evacuated at room temperature for 6 hrs [73]. Burneau *et al.* have also assigned a band at 3740-3750 cm^{-1} to outer silanols on silica gel which adsorb water more readily than the isolated silanols [19]. It would be interesting to extend our study to include a silica gel in order to determine if the type I silanols are more abundant on this material than on precipitated silica or aerosil silica. Similar studies of silicas that have been highly dehydroxylated, then rehydrated, could be carried out in order to probe the SiOH bending vibrations of the vicinal isolated silanols. These types of studies could be useful for understanding the structure of the type I silanols in relation to the origin of the silicas.

CHAPTER 5

Infrared Studies of the Adsorption of Carbon Monoxide, Nitrogen, and Methane on Aerosil Silica

Introduction

Studies of the interactions of probe molecules with surface sites provides a useful and important method for characterizing high-surface-area oxides using FTIR spectroscopy. The utility of probe molecules is derived from their chemical reactivity or their ability to coordinate to surface sites. Probe molecules have been used to characterize reactive sites on acidic oxides. For example, it is known that pyridine strongly coordinates to Lewis acid sites on alumina, and infrared bands in the spectrum of coordinated pyridine are a signature of these acidic sites [74]. In Chapter 3, surface modification using hydrogen-sequestering agents and H/D exchange probes enabled us to compare the surface silanol distribution on aerosil and precipitated silica, and in Chapter 4, physical adsorption of CO, exchange with ND_3 and D_2O, and chemical modification using BCl_3 were used to probe the low-frequency bending vibrations of isolated SiOH on the two silicas. In this chapter, we compare the infrared spectra of three weakly-interacting probe molecules, CO, N_2, and CH_4, adsorbed on aerosil silica. The extent to which these probes adsorb on silica at room temperature is negligible (an indication that the interactions are weak). However, at temperatures closer to their boiling points, adsorption is a facile process.

The probe molecules mentioned above cover a broad range of adsorbate-adsorbent interactions, and the nature of these interactions dictate the type of information which can be obtained from the infrared spectrum. As a general rule, the larger the probe molecule, the more complicated is its infrared spectrum. For simple molecules adsorbed on silica, the

infrared spectrum is not complicated by absorption bands due to the probe itself, either in the gas phase, or adsorbed. For example, the gas-phase spectrum of CO consists of a single fundamental stretching vibration, whereas N_2 is infrared inactive in the gas-phase. However, interactions between the probe molecule and an adsorption site can induce a dynamic dipole moment and (i) shift the frequency of allowed vibrations away from the gas-phase frequency, or (ii) cause inactive vibrational modes to become infrared active. Additionally, adsorbate-adsorbent interactions cause frequency shifts in the vibrational modes associated with surface sites (*e.g.* SiOH). Thus, information about the adsorption sites can be obtained from the spectra of the adsorbed probe.

In as early as 1956, McDonald studied the perturbation of the SiO–H stretching band caused by N_2 and CH_4 adsorption at 83 K on a 350°C activated aerosil silica [75]. He reported that adsorbed N_2 shifted the band at 3749 cm^{-1} due to free isolated SiOH to 3725 cm^{-1}, whereas adsorbed CH_4 shifted the isolated SiO–H stretching band to 3717 cm^{-1}. He also noted that complete removal (shift) of the 3749 cm^{-1} band occurred at a relative pressure of adsorbed N_2 which was several times lower than that predicted by the B.E.T. model for monolayer coverage, and he took this as evidence that N_2 preferentially adsorbs at surface silanol sites on silica.

The infrared spectrum of N_2 adsorbed on silica-supported platinum [76], alumina [77,78], zeolites [79,80] and other oxides [78] has been reported, but apart from the earlier work by McDonald, there have been relatively few infrared spectroscopic studies of N_2 adsorbed on silica [1,78]. This may be partly due to the fact that silica has few Lewis acid sites compared to other oxides and as a result, the relatively weak interactions with the silica surface cause the spectrum of adsorbed N_2 to be extremely weak. Nevertheless, considering the importance of N_2 adsorption for determining B.E.T. surface areas, this is somewhat surprising.

Sheppard and Yates have reported infrared spectra of methane ethylene, acetylene and hydrogen on porous silica glass [81]. They observed fundamental vibrational modes due to

adsorbed CH_4, C_2H_4 and H_2, which are forbidden in the gas-phase, and they were able to fit the observed infrared bands due to adsorbed CH_4 and H_2 to mathematical models which could account for possible rotational motion of the adsorbed species. Ghiotti *et al.* [45], and Beebe and Yates [62] have studied physical adsorption of CO on aerosil silica by infrared spectroscopy.

Ghiotti *et al.* observed two infrared bands in the spectrum of adsorbed CO on silica evacuated at room temperature, and these were assigned to CO adsorbed specifically at SiOH, and non-specifically on the dehydroxylated parts of the surface. On A-800 silica, they observed a third band which they also attributed to nonspecific adsorption on the dehydroxylated part of the surface. Both studies proposed that SiOH...CO rather than SiOH...OC is the surface species formed at silanol sites. The question of the relative stability of these two species has been addressed through the use of *ab initio* MO calculations of silanol (H_3SiOH) interacting with CO [82].

In this study, we report the complete vibrational spectra between 500 and 5000 cm^{-1} for the species SiOH...X (X = N_2, CH_4, CO) on 800°C activated aerosil silica, and the specific interaction of N_2, CH_4, and CO with surface SiOH is discussed.

Results

Figure 5.1 shows the progressive perturbation of the isolated SiO–H stretching band on A-800 for equilibrium pressures of adsorbed N_2 between 0.5 and 10 torr at 82 K. Weak interactions with N_2 caused a shift in frequency from 3752 to 3725 cm^{-1} but, under these conditions, a large fraction of the isolated silanols did not interact, as indicated by the residual intensity at 3752 cm^{-1}. The same experiment carried out with A-450 (not shown) resulted in a shifted band at 3713 cm^{-1}, and the 3752 cm^{-1} band diminished to about half of its initial intensity at an equilibrium pressure of 10 torr N_2. For both A-450 and A-800 the frequency of the band due to perturbed silanols did not vary with coverage in this range of pressures.

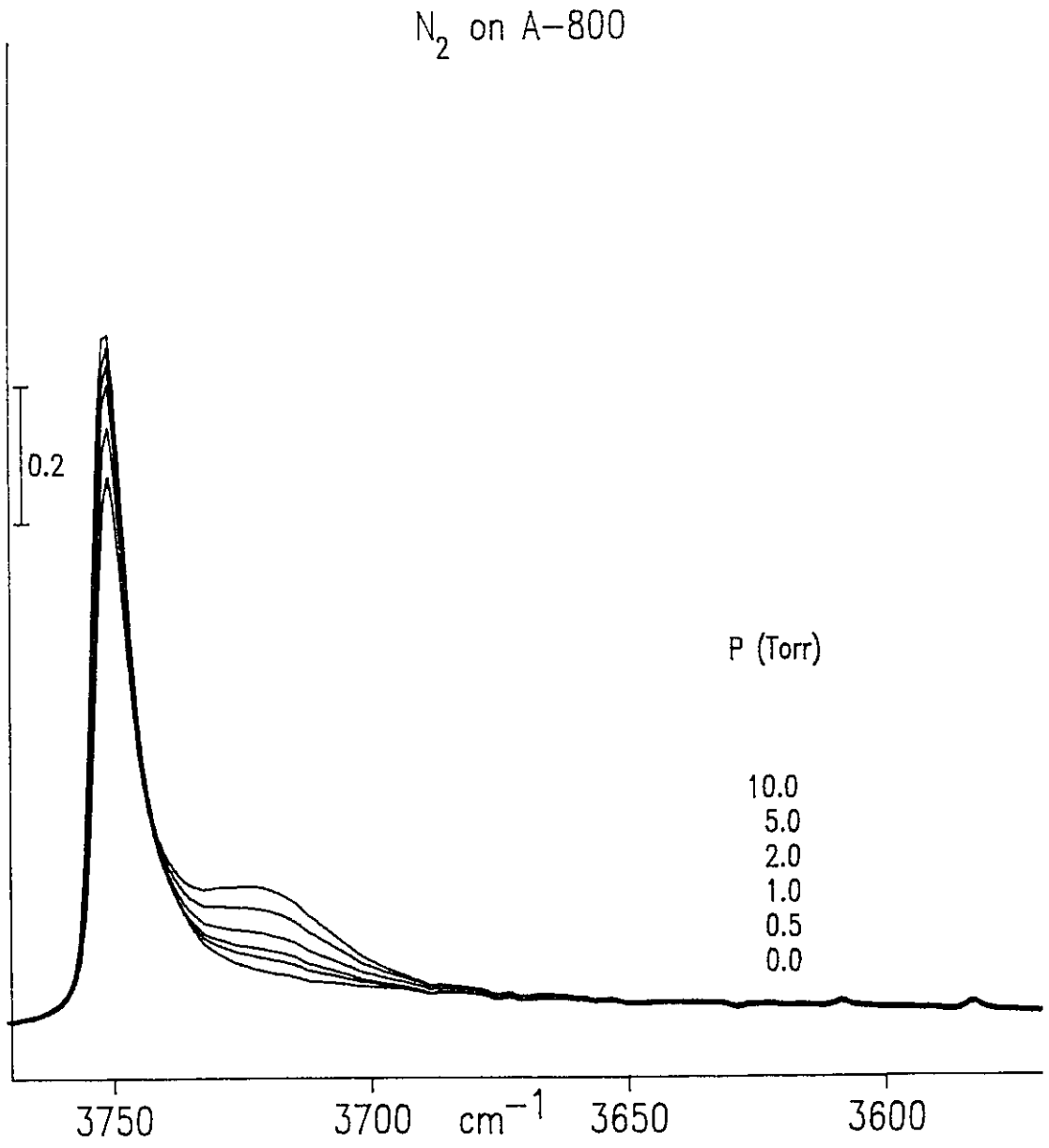

Figure 5.1. Infrared spectra showing the perturbation of the SiO–H stretching profile on A-800 silica due to adsorbed N_2 at the indicated equilibrium pressures at 82 K.

The spectra shown in Figures 5.2 and 5.3 were obtained when CH_4 and CO, respectively, were adsorbed on A-800 silica at the indicated equilibrium pressures. CH_4 adsorbed on A-800 silica shifted the isolated SiO—H band from 3752 to 3717 cm^{-1}, and a much larger shift (to 3665 cm^{-1}) was observed for adsorbed CO. As in the case of adsorbed N_2, we observed that the shift in frequency was about 10 cm^{-1} greater for CH_4 or CO adsorbed on A-450, the frequencies being 3708 and 3655 cm^{-1}, respectively.

In addition to studying the effects of these probe molecules on the SiO—H stretching vibration, we have also investigated their perturbation of the Si—O—H bending vibrations in the 750-900 cm^{-1} region. The difference spectra shown in Figure 5.4 were obtained by subtracting the reference spectrum (recorded in 0.50 torr He at 82 K) from the spectrum of the sample at equilibrium with the indicated pressure of CO, N_2 or CH_4 at 82 K.

The adsorption of CO on aerosil silica has already been discussed in detail in Chapter 4. For comparison's sake, the lower trace of Figure 5.4 shows the same series of difference spectra as in Figure 4.15 for CO on A-800, superimposed as a function of equilibrium CO pressure. The middle and upper traces show difference spectra, obtained in a similar manner, for N_2 and CH_4, respectively. For all three adsorbates, the intensity due to bending vibrations of isolated SiOH at 840 and 760 cm^{-1} decreases with increasing pressure, while a new feature appears at 850 cm^{-1} for CH_4, 860 cm^{-1} for N_2, and 875 cm^{-1} for CO. This progression is most obvious for the CO series, but the disappearance of the 840 cm^{-1} band is partly obscured in the case of N_2 by the overlapping 860 cm^{-1} feature. For CH_4 (upper trace), there is almost total overlap so that the positive 850 cm^{-1} feature only appears for pressures greater than about 0.5 torr CH_4.

The combination bands at 4510, 4580 cm^{-1} also exhibit changes in band shape when N_2, CH_4, or CO are adsorbed on very thick silica disks. Figure 5.5 shows the low-temperature spectra of A-800 silica (80 mg/cm^2) in the 4200-4800 cm^{-1} spectral region, recorded with 0.5 torr He (broken curves), and for varying pressures of N_2, CH_4, or CO adsorbed at 82 K (solid curves). Generally, there appears to be a shift in intensity from 4580,

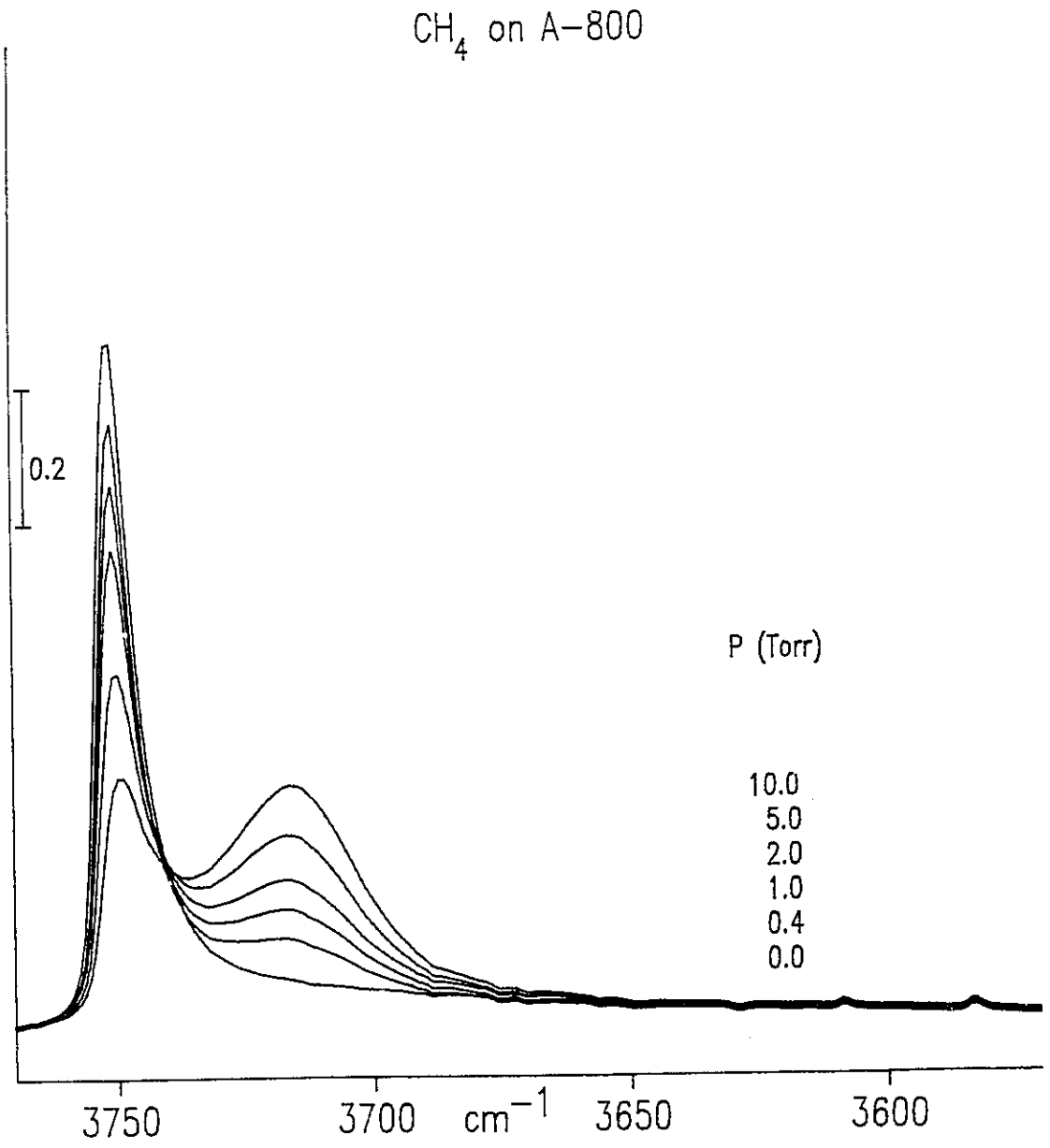

Figure 5.2. Infrared spectra showing the perturbation of the SiO—H stretching profile on A-800 silica due to adsorbed CH_4 at the indicated equilibrium pressures at 82 K.

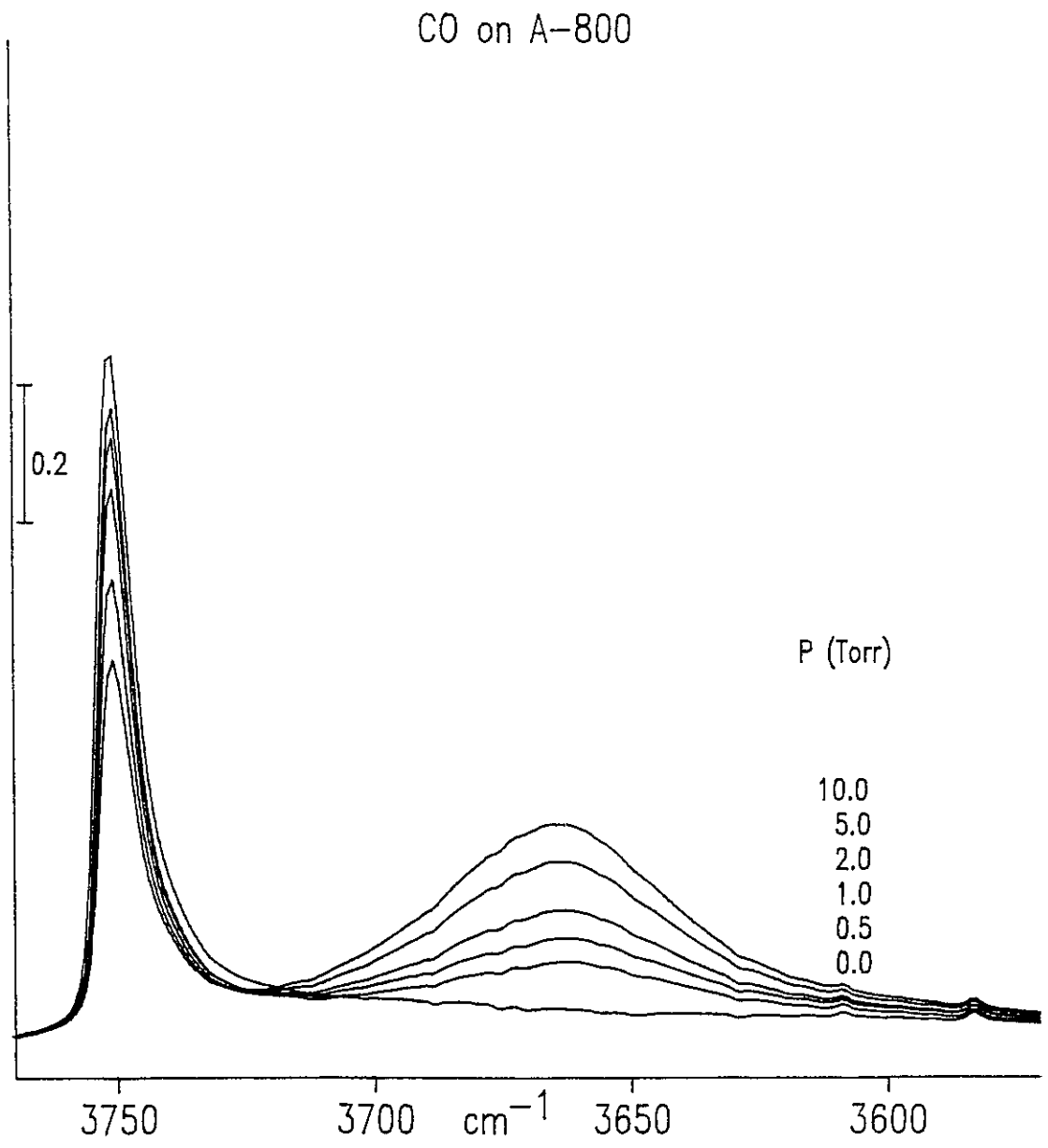

Figure 5.3. Infrared spectra showing the perturbation of the SiO—H stretching profile on A-800 silica due to adsorbed CO at the indicated equilibrium pressures at 82 K.

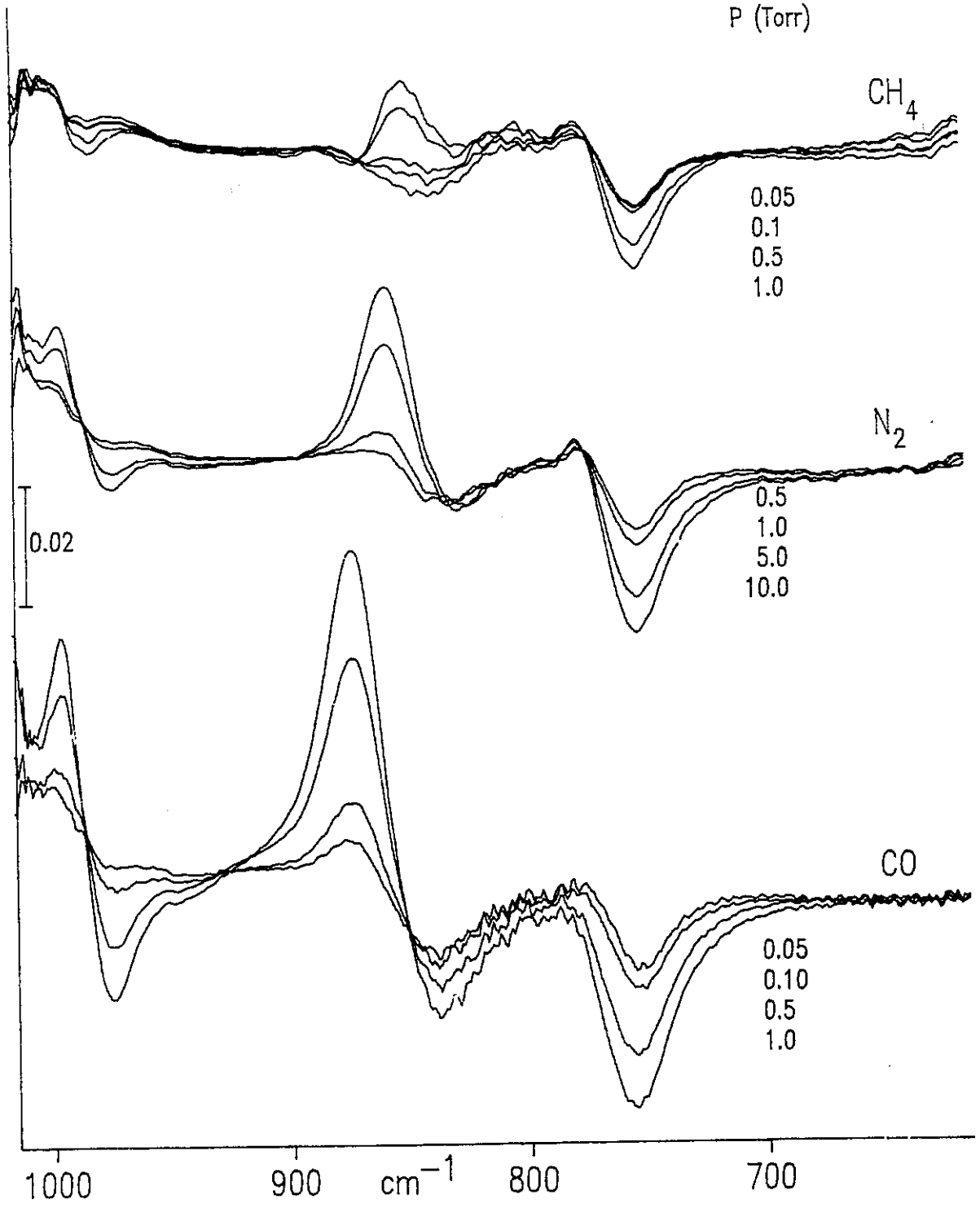

Figure 5.4. Difference spectra showing the perturbation of the fundamental bending vibrations due to adsorbed CH_4 (upper), N_2 (middle) and CO (lower) on A-800 silica. Each spectrum was obtained by subtracting the silica spectrum recorded in 1.0 torr He at 82 K from the spectrum recorded at the indicated equilibrium pressure of CH_4, N_2, or CO at 82 K.

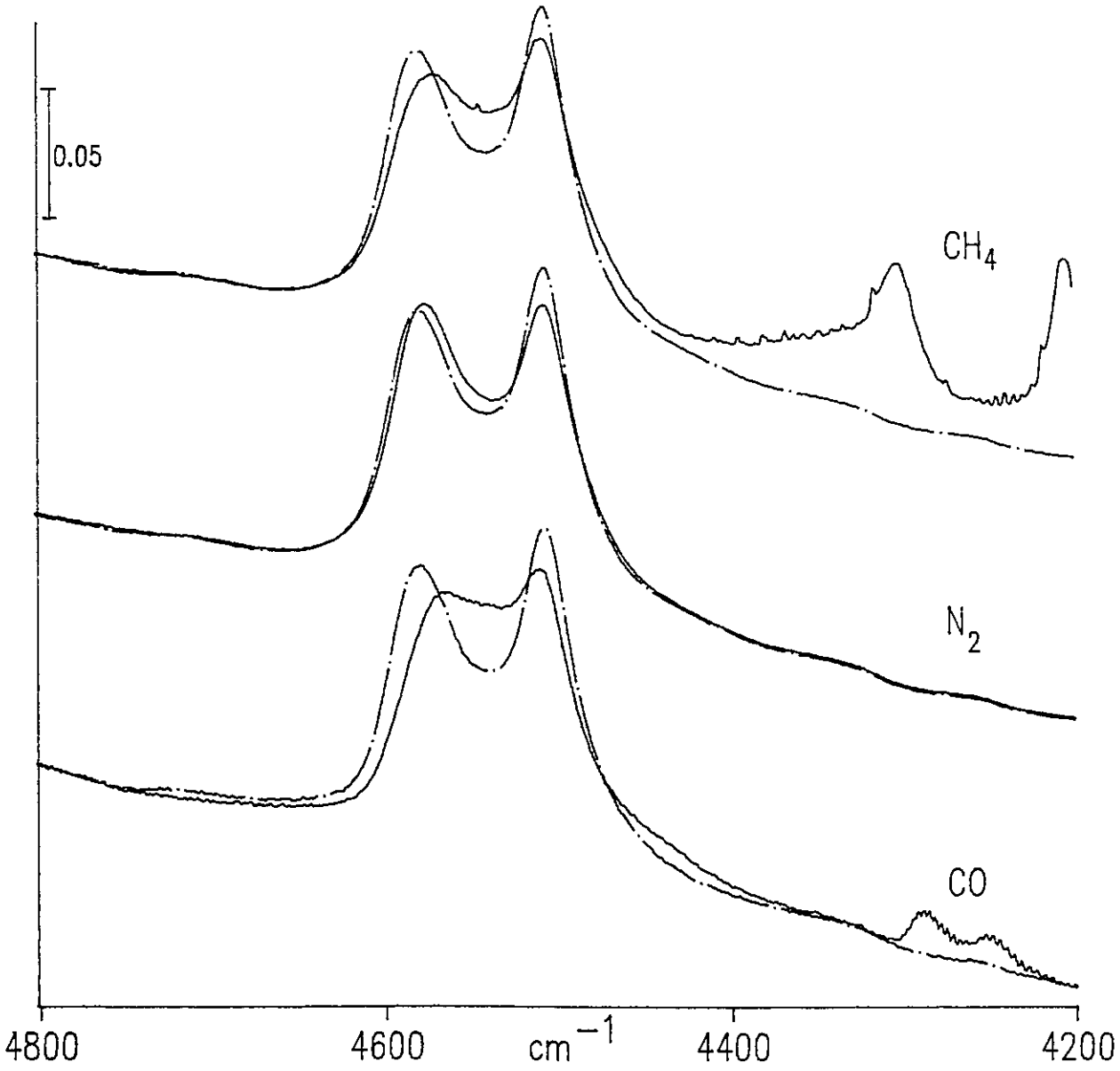

Figure 5.5. (Broken curves) Infrared spectra of 80 mg/cm^2 A-800 recorded in 0.50 Torr He at 82 K. (Solid curves) After evacuation of He and subsequent addition of, 1.00 Torr CH_4 (top), 10.0 Torr N_2 (middle), 1.00 Torr CO (bottom) at 82 K.

and 4510 cm^{-1} to a frequency somewhere in between, depending on the adsorbate used. This feature in the spectrum of SiOH...X may be attributed to a new component of the overall band profile which is the sum of the SiO–H stretching, and Si–O–H bending vibrations of the perturbed isolated silanols. Because a large fraction remain as free isolated silanols, these also contribute to the band shape at 4580, 4510 cm^{-1}. The calculated frequencies (*i.e.* the sum of the fundamental stretching and bending frequencies, neglecting anharmonicity) and observed positions of maximum intensity for the component due to SiOH...X are listed in Table 5.1. Unfortunately, because of the degree of band overlap, it is impossible to comment on the relative contributions to the overall band shape by the residual 4580 cm^{-1} and 4510 cm^{-1} bands.

cm^{-1}	SiOH	SiOH(CO)	SiOH(N_2)	SiOH(CH_4)
ν(SiO-H)	3750,3740	3665	3725	3715
δ(Si-O-H)	760,840	875,900[a]	860	850
$\nu + \delta$ (calc.)	4510,4580	4540	4585	4565
$\nu + \delta$ (obs.)	4510,4580	4540	4570	4550

Table 5.1. Frequency data for SiOH...X on A-800

(a) Refer to text.

To this point, we have only shown the changes in the infrared spectrum of the isolated SiOH brought about by the interaction with the adsorbed N_2, CH_4, and CO. However, the same interaction also causes changes to occur in the infrared spectrum of the probe molecules and these must be considered as well. The infrared spectra of N_2, CH_4, and CO adsorbed on aerosil silica are presented below.

Figure 5.6 shows the spectra of adsorbed methane on A-800 silica (80 mg/cm^2) after subtracting the gas-phase spectrum and the background silica spectrum. These spectra closely resemble the spectra obtained by Sheppard and Yates for methane adsorbed at low coverage on porous glass [81]. According to their assignments, the strongest band at 3006 cm^{-1} belongs to the antisymmetric C–H stretching mode of adsorbed CH_4, shifted to lower wavenumber from the gas-phase frequency of 3018 cm^{-1}. The much weaker feature at 2900 cm^{-1} belongs to the symmetric C–H stretching mode; this band is not allowed in the IR spectrum of the gas phase, but in the Raman spectrum a band appears at 2916 cm^{-1} which is assigned to this normal mode.

The spectrum of nitrogen adsorbed on A-800 silica (80mg/cm^2) at 82 K is shown in Figure 5.7. A single band is observed at 2329 cm^{-1} for equilibrium pressures of nitrogen less than 20 torr, in agreement with the frequency reported by Zeverev *et al.* [78]. In order to test whether the observed band at 2329 cm^{-1} is due to specific adsorption of N_2 at isolated SiOH sites we have done the following: in a different experiment which requires a much thinner sample (5 mg/cm^2, see Figure 5.1), changes in absorbance at 3752 cm^{-1} as a function of equilibrium pressure of N_2 were determined for the same pressures of N_2 as in Figure 5.7. A plot of A(3752) *vs.* A(2329) was found to be linear in this range of coverage. The relative absorbance of the band due to adsorbed N_2, A(2329)/A(3752), was determined from the slope of the plot and, taking into account the factor of 16 difference in the sample size, a value of 4.5×10^{-3} was calculated.

Figure 5.8 shows the spectrum of adsorbed CO on A-800 silica at 82 K for equilibrium pressures ranging between 0.10 and 2.0 Torr (corresponding to relative pressures, P/P_o, in the range 1.3×10^{-4} to 2.6×10^{-3} for P_o = 760 torr at 82 K). In each case, the contribution due to gas-phase CO at the same temperature and pressure has been subtracted from the original spectrum. Under these conditions, two bands are observed in the spectrum of CO adsorbed on A-800 silica, a stronger band at 2157 cm^{-1} and a weaker band at 2138 cm^{-1}. These spectra are virtually identical to those obtained using A-180 silica in [62].

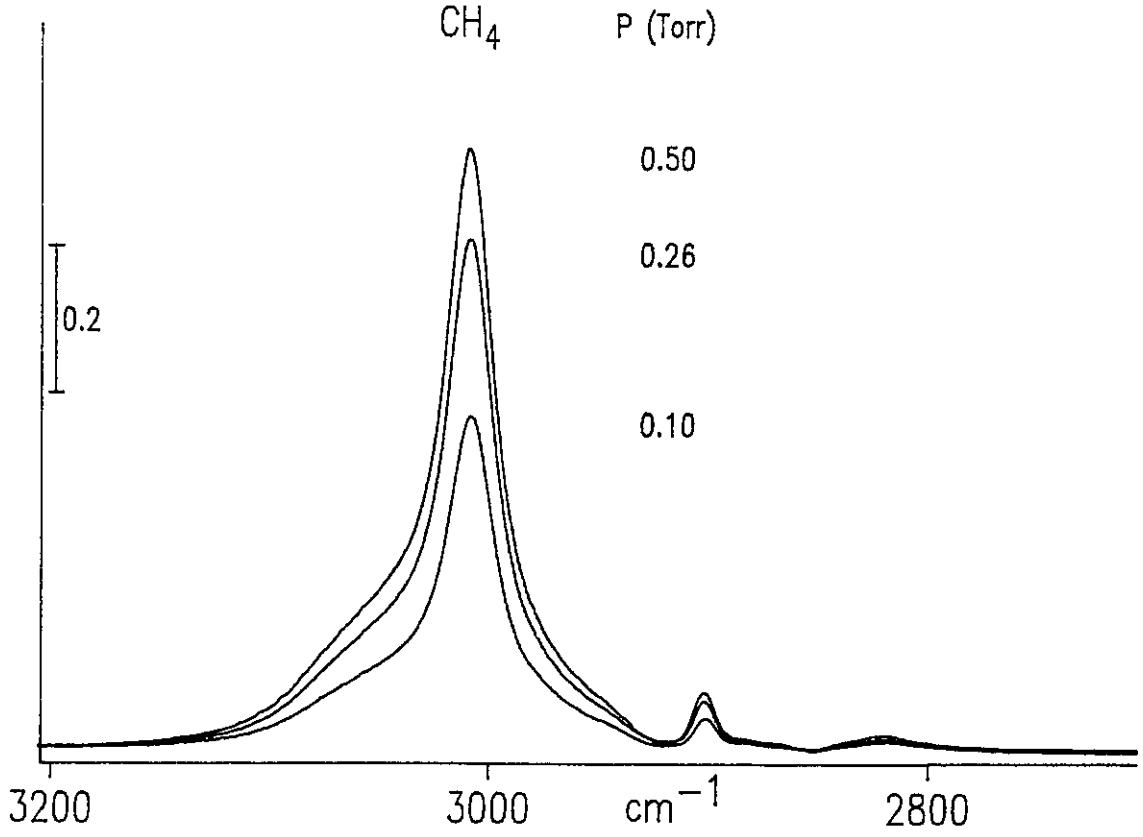

Figure 5.6. Infrared spectrum of adsorbed CH_4 on A-800 silica at the indicated equilibrium pressures at 82 K. The spectrum of gas-phase CH_4, and the silica background spectrum have been subtracted.

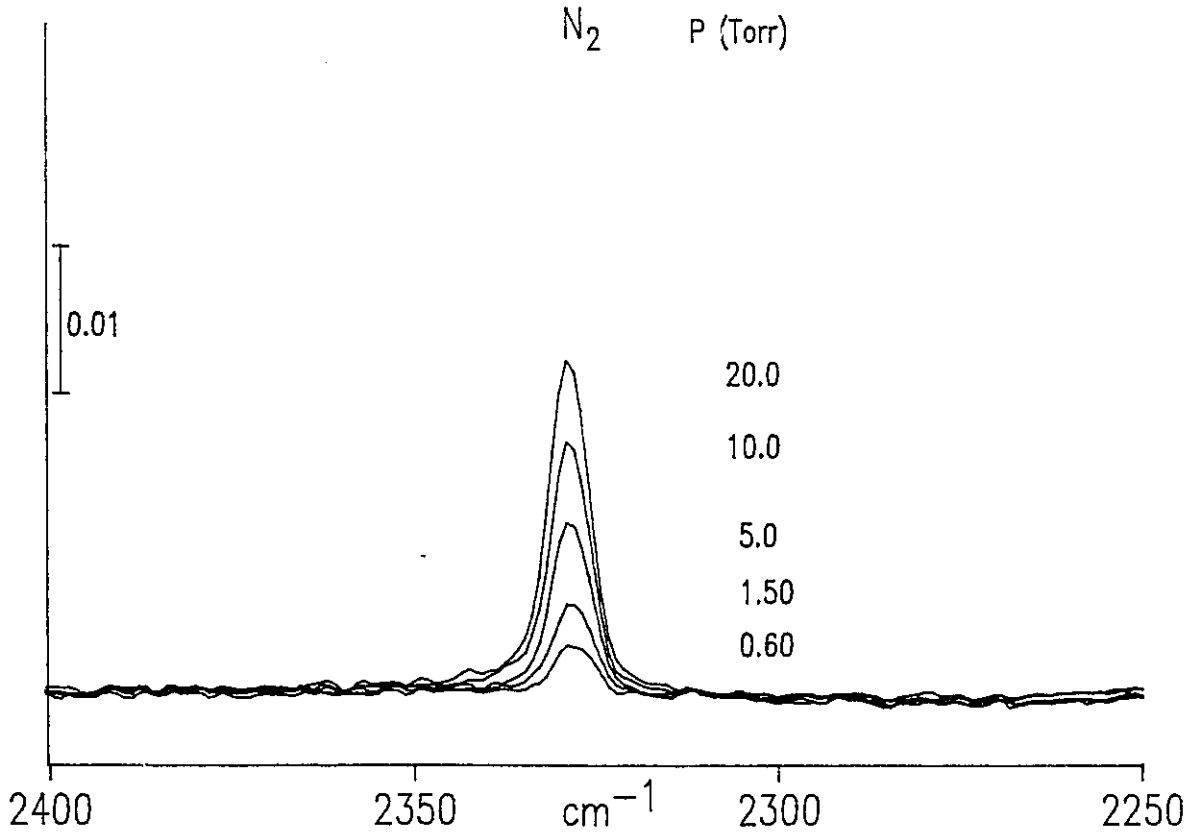

Figure 5.7. Infrared spectrum of adsorbed N_2 on A-800 silica at the indicated equilibrium pressures at 82 K. The spectrum of the silica background has been subtracted.

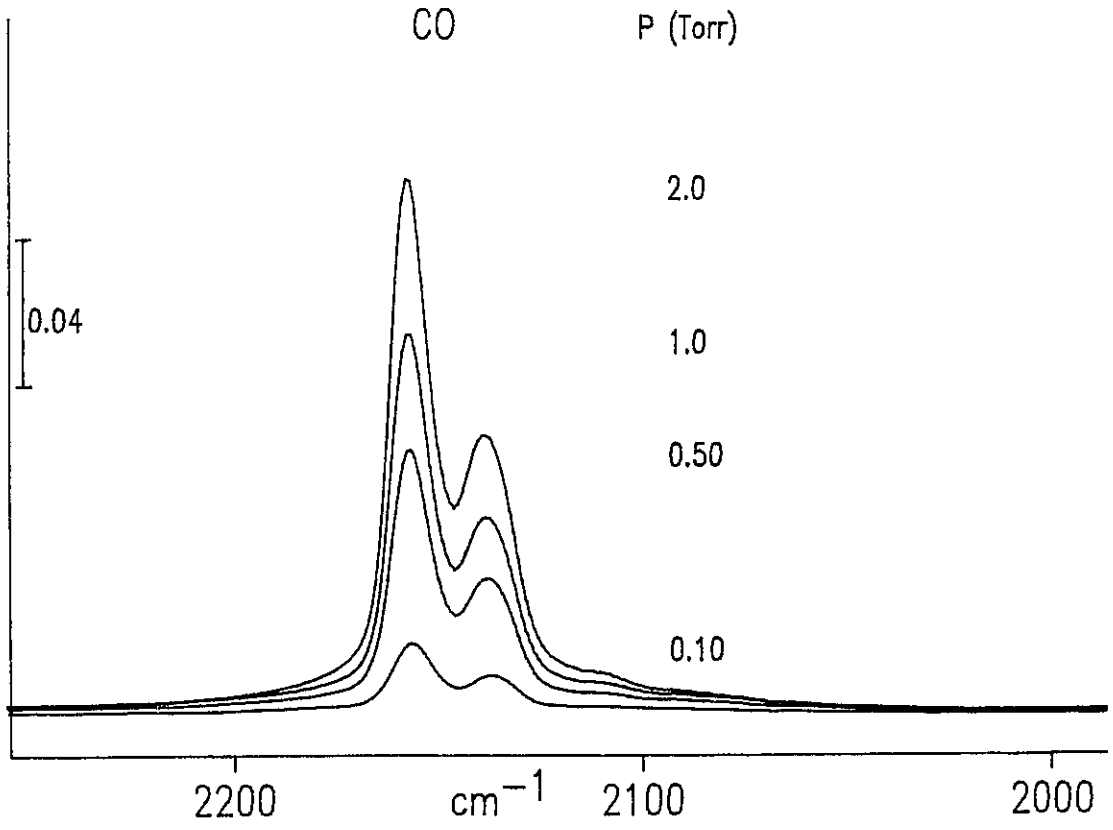

Figure 5.8. Infrared spectrum of adsorbed CO on A-800 silica at the indicated equilibrium pressures at 82 K. The spectrum of gas-phase CO, and the silica background spectrum have been subtracted.

Discussion

The infrared spectra in Figures 5.1 to 5.5 show how simple probe molecules (X = N_2, CH_4, CO) interact with isolated SiOH at 82 K. Specific adsorption at isolated SiOH sites on A-800 result in the formation of SiOH...X. The perturbation of the "free" SiOH vibrational modes by these molecules, *i.e.* the red-shifted SiO–H stretching vibration and the blue-shifted Si–O–H bending vibration, is similar to that due to weak hydrogen-bonding interactions [83]. Combination bands due to SiOH...X are also observed in the low-temperature spectrum. However, because the downward and upward shifts for the fundamental modes tend to cancel one another in the combination band, the SiOH...X combinations tend to overlap the residual 4510 and 4580 cm^{-1}, bands due to free SiOH. The observed vibrational frequencies of the free SiOH and perturbed SiOH...X species are summarized in Table 5.1.

Some of our first experiments, carried out using N_2, CH_4, and CO as low-temperature probe molecules, were directed at investigating the nature of the combination bands on silica. The initial experiments demonstrated that the band profile at 4580, 4510 cm^{-1} depended on many factors including, the type of silica used, the activation temperature employed, and the temperature at which spectra were recorded. How these factors affect the relative intensity of the 4580, 4510 cm^{-1} bands in the spectra of aerosil and precipitated silica has already been addressed in Chapter 4. We also observed subtle changes in the shape of the combination band shown in Figure 5.5, when N_2, CH_4, or CO adsorbed on silica at 82 K. Tsyganenko had observed similar changes in the spectrum following the adsorption of N_2 and CO, and first suggested that these were due to shifts in the fundamental SiOH stretching and bending vibrations [52]. These rather puzzling results prompted us to examine more closely the fundamental vibrational SiOH modes using a variety of low-temperature probes, including N_2, CH_4, and CO.

The most significant result of these studies is that physical adsorption of N_2, CH_4, and CO at low temperature can be used to probe the fundamental Si–O–H bending vibrations which are buried in the bulk silica modes (Figure 5.4). Arriving at the correct interpretation

of the difference spectra in Figure 5.4 required a comparison of experimental results using several different probe molecules, and various activation temperatures. The comparative studies (Chapter 4) of aerosil and precipitated silica using CO to probe the 500-1000 cm^{-1} spectral region followed the preliminary work presented here.

We have shown (in Figure 5.5, and Table 5.1) that the SiOH...X species contribute intensity to the combination band profile at a frequency near, or lower than the arithmetic sum of the fundamental stretching and bending frequencies, and further discussion of this effect is unwarranted. On the other hand, the perturbation of the fundamental SiOH vibrational modes varies significantly for N_2, CH_4, and CO, and the implications of this are discussed below.

For N_2 and CH_4 adsorbed on silica, the 3750 cm^{-1} band is replaced by a single infrared band to lower wavenumber (Figures 5.1 and 5.2), and the difference spectra in Figure 5.4 show that SiOH bending vibrations at 840 cm^{-1}, and 760 cm^{-1} are replaced by single positive features at 860 and 850 cm^{-1}, respectively. We have already pointed out that there is considerable overlap between the negative 840 cm^{-1} feature and the positive 860 cm^{-1} feature for adsorbed N_2; in the case of adsorbed CH_4, there is almost complete overlap. Thus, infrared bands due to perturbed type **I** and type **II** silanol species (described in Chapter 4) cannot be distinguished in the low-frequency region. The same problem arises in the 3700-3750 cm^{-1} region for A-450 or A-800 silica. In Figures 5.1 and 5.2, the 3725 cm^{-1} and 3715 cm^{-1} bands due to adsorbed N_2 and CH_4, respectively, overlap the free isolated SiOH profile, making it difficult to resolve the 3740 cm^{-1} component band.

In comparison, CO, which interacts more strongly and exhibits larger frequency shifts, does provide evidence for two SiOH...CO species having different bending vibrations. For A-800 silica, a band appears at 875 cm^{-1} and, although admittedly there is some overlap with the negative 840 cm^{-1} feature, there is also a certain degree of asymmetry towards 900 cm^{-1}. It has been shown previously that, for CO adsorption on A-450 and P-450 silica, a band appears at 870 cm^{-1} with a definite shoulder at about 900 cm^{-1} (compare Figures 4.15 and

4.10 for A-800 and A-450, respectively). The observed decrease in intensity at 900 cm^{-1} in going from 450°C to 800°C activation is consistent with a decrease in the number of type **I** silanols relative to type **II** silanols (refer to discussion of CO adsorption on A-450 and P-450, Chapter 4). Therefore, it is probable that the 900 cm^{-1} feature is the perturbed bending vibration corresponding to 840 cm^{-1} while the 875 cm^{-1} feature corresponds to the "free" SiOH bending vibration at 760 cm^{-1}. Finally, the spectra of CO adsorbed on A-450 and A-800 in the SiO—H stretching region show a decrease in intensity at 3740 and 3750 cm^{-1}, indicating that both types of isolated silanols interact to some extent. However, two stretching vibrations due to type **I** and type **II** SiO—H...CO cannot be resolved in the broad 3665 cm^{-1} band.

The spectra in Figures 5.1-5.3 show that not all of the "free" isolated SiOH are perturbed by N_2, CH_4, or CO at equilibrium pressures of less than 10 Torr, suggesting that less than a monolayer coverage is formed under these conditions. Further, the relative pressure due to 10 Torr N_2 at 82 K is $P/P_o = 8x10^{-3}$, whereas the B.E.T. monolayer coverage is expected to occur at $P/P_o \approx 0.1$ [75]. Finally, the SiO—H stretching frequencies of SiOH...X are independent of the coverage in this pressure range for either A-450 or A-800 silica, in agreement with previous studies [62,75]. We have noted that the SiO—H stretching frequency of SiOH...X is generally about 10 cm^{-1} lower for N_2, CH_4, or CO adsorbed on A-450 compared to A-800. One could postulate that, because there are more isolated SiOH/nm^2 on A-450 than on A-800, a greater surface density of SiOH...X is formed on A-450, and resultant lateral interactions cause the SiO—H frequencies to appear at a lower frequency than for the same molecule adsorbed on A-800. However, at relative pressures well below that for a monolayer coverage, lateral interactions are probably minimal. An alternative explanation might be that interactions occur with type **I** and type **II** silanols (the 3740 cm^{-1} and 3750 cm^{-1} bands, respectively), and because the type **I** silanols are more abundant on A-450 than A-800, interactions with these silanols shifts the maximum of the perturbed SiO—H band to lower wavenumber. In the absence of other experimental data,

further comment on the nature of the shift would be purely speculative.

There is no evidence in the spectrum of adsorbed CH_4 (Figure 5.6) to suggest that this molecule adsorbs at sites other than isolated SiOH on A-800. The single band at 2900 cm^{-1} suggests that specific adsorption occurs at one type of site only (SiOH), and broad wings which appear in the spectrum of the 3006 cm^{-1} bands have been attributed to rotational motion of the adsorbed molecule [81]. Similarly, the single symmetric band at 2329 cm^{-1} in the spectrum of adsorbed nitrogen on A-800 silica (Figure 5.7) is indicative of specific interaction with surface sites that are energetically equivalent. The frequency of the band (related to the strength of the interaction [78]), and evidence for H-bonding of isolated SiOH strongly suggest that adsorption occurs at SiOH sites on A-800 silica. Further, the linear plot of A(3752) *vs.* A(2329), and the invariance of the frequency of the 2329 cm^{-1} band with increasing coverage, further support specific interaction with isolated SiOH, as opposed to nonspecific adsorption which causes perturbation of surface SiOH via lateral interactions.

Ghiotti *et al.* have reported that a low coverage of adsorbed CO on hydroxylated aerosil at 123 K produce two bands in the infrared spectrum, at 2157 and 2137 cm^{-1} [45]. They assigned the stronger band at 2157 cm^{-1} to CO which specifically adsorbs at surface silanol sites, and the weaker 2137 cm^{-1} band to CO which interacts to a lesser extent with other surface sites. For activation at temperatures greater than 650 K, they observed a shoulder on the 2137 cm^{-1} band at about 2130 cm^{-1}, and an increase in intensity at 2137 cm^{-1} relative to 2157 cm^{-1} with increasing activation temperature. Their spectrum of adsorbed CO on A-800 shows a feature at about 2137 cm^{-1} having a definite shoulder at about 2130 cm^{-1}, and which is almost double in intensity with respect to the 2157 cm^{-1} band, even at low coverage.

Our spectra in Figure 5.8 of adsorbed CO on A-800 silica resemble those obtained by Beebe and Yates at 83 K using A-180 silica [62] more than they resemble the spectra obtained by Ghiotti *et al.* at 123 K using A-800 silica [45]. In Figure 5.8, the 2157 cm^{-1} band has almost double the intensity of the 2138 cm^{-1} band and the spectra do not show a definite

shoulder at around 2130 cm^{-1}, as was reported in [45]. Given the much lower temperature used in our studies compared to those of Ghiotti *et al.* (82 K here *vs.* 123 K in [45]), the spectral differences may not be meaningful if the adsorption equilibria for the different sites are temperature dependent. Further, the close agreement between our spectra and those obtained by Beebe and Yates at 83 K, also suggests that the temperature at which CO adsorption occurs may have a greater effect on the infrared spectrum than the activation temperature of the silica. Nevertheless, Figure 5.8 shows that, under the experimental conditions used in the present study, a single band appears at 2157 cm^{-1} which may be ascribed to the CO stretching vibration of type **I** or type **II** SiOH...CO.

Conclusions

The adsorption of N_2, CH_4, and CO at 82 K provides a useful means of probing the vibrational modes of surface silanol groups on silica. With the aid of spectral subtraction, it is possible to observe the fundamental SiOH bending vibrations of the type **I** and type **II** silanols which are masked by the strong absorption of the bulk SiO_2 modes. This study has permitted the assignment of the vibrational frequencies of the adsorbed species, SiOH...X (X = N_2, CH_4, CO), in the 500 to 5000 cm^{-1} spectral region.

For a given probe, infrared bands due to adsorbed N_2, CH_4, and CO cannot distinguish SiOH...X species resulting from interactions with type **I** or type **II** silanols. The isolated SiO—H stretching band shifts to lower wavenumber for all three probe molecules, and for a given probe, the position of the shifted band maximum is about 10 cm^{-1} lower for 450°C activation than for 800°C activation. This may be due to interactions between type **I** and type **II** silanols. There is little information to be gained concerning specific interactions with type **I** or type **II** SiOH from the profile of the combination bands of SiOH...X, due to the fact that these bands overlap the combination bands of "free" isolated SiOH. Nevertheless, there is direct evidence which shows that all three probes interact with SiOH bending vibrations of type **I** and type **II** silanols, at 840 and 760 cm^{-1}, respectively.

CO produces the largest frequency shifts, and this may be an advantage in so far as bands which appear do not overlap those which disappear in the adsorption process. It may be possible, in a future study of precipitated silica, to study the disappearance of the 3740 and 3750 cm^{-1} SiO–H stretching bands in order to determine if type **I** or type **II** silanols preferentially interact with this probe.

CHAPTER 6

Trimethyl Phosphite Adsorbed on Silica: An NMR and Infrared Study

Introduction

The interaction of phosphorus compounds with oxides has been of considerable recent interest for several reasons. One is related to the enhanced acidity of phosphate impregnated oxide catalysts [84-89]. Another is concerned with the fate of organophosphorus compounds used as pesticides or nerve gases when they come into contact with soil [89-96]. Although there have been several studies of the adsorption of the nerve gas simulant, dimethyl methylphosphonate (DMMP), on various metal oxides [89-93], the surface chemistry of the isomeric compound, trimethyl phosphite (TMP) has received less attention.

In this study we have used ^{31}P magic angle spinning (MAS) NMR spectroscopy and infrared (IR) spectroscopy to examine the interaction of gaseous trimethyl phosphite ($P(OCH_3)_3$, or TMP) on silica, over a range of temperatures from 20 to 400°C. Silica was chosen for this initial study because Lewis acid/base sites are absent for temperatures of activation below about 450°C, so that coordination with the phosphorus lone pair electrons is avoided [18,72]. Therefore, chemisorption or isomerization to DMMP is expected to arise solely from an interaction between TMP and the surface silanol (SiOH) groups.

^{31}P, having magnetic spin 1/2 and a receptivity of 0.0665 relative to ^{1}H [97], is an ideal probe nucleus for studying the surface chemistry of TMP using solid state NMR spectroscopy. As will be discussed later, the combined ^{31}P NMR-IR technique provides a powerful method in surface chemistry by virtue of the species-selective and quantitative aspects (one signal per ^{31}P nucleus, for each type of ^{31}P nucleus) of NMR spectroscopy, and

the qualitative and bonding-specific aspects (group frequencies, and the ability to observe H-bonding, physical or chemical adsorption) of infrared spectroscopy.

This was a collaborative project: while the infrared work is part of the original research in this thesis, the NMR work was contributed by, and is gratefully credited to Professor Ian Gay at Simon Fraser University. Our conclusions could only be reached based on both sets of spectroscopic evidence, and for this reason, the combined results are presented here.

Experimental Section

The infrared and NMR experiments were carried out using aerosil silica, Cab-O-Sil HS-5, which was vacuum activated at 350°C for 1 h, either in the infrared cell or NMR tube. When other conditions were used, these will be described in the text. Room-temperature (23 ± 2 °C) experiments were carried out in the 300-mL volume conventional IR cell, while experiments at elevated temperatures were carried out in the 80-mL volume variable-temperature cell. The infrared cells and other details of the infrared experiments are discussed in Chapter 2. Details of the NMR experimental methods are presented below.

^{31}P NMR measurements were carried out on a 1.4 T instrument, giving a resonance frequency of 24.3 MHz for ^{31}P. Two types of excitation were used; for studying weakly bound species, excitation was by 90-deg pulses, using the pulse sequence of Duncan *et al.* to suppress artefacts [98]. For more rigid species, single-contact Hartmann-Hahn cross polarization, with spin temperature alternation was used [99].

In both types of experiment a proton decoupling field of 55 kHz strength was used. This is sufficient to decouple direct bonded P-H dipolar interactions. In principle, 90-deg pulses give uniform excitation of all ^{31}P resonances. In practice, since spectra are signal averaged at a fixed time interval, resonances whose T_1 relaxation times are longer than this interval are attenuated. For most of the spectra in this work a repetition interval of 1 s was used. Cross polarization, on the other hand, specifically excites ^{31}P with a significant dipolar

coupling to ^{1}H and hence is biased in favour of immobile species with short P-H distances. Signal enhancement by a factor of 2.5, and repeatability on the ^{1}H relaxation time scale, make cross polarization much more sensitive for the detection of small quantities of such species.

For the detection of direct P-H bonding, two methods were used. With mobile species, it was sufficient to turn off the decoupler and observe the large single-bond coupling. For rigid species, cross polarization with a 70-μs decoupler delay was used [100]. This completely eliminated signals from P-H bonded species, but only partially attenuated signals from ^{31}P with more distant ^{1}H.

Samples for NMR study were prepared on a vacuum line, in 5-mm NMR tubes, which were sealed after sample preparation. For samples involving high-temperature reaction with TMP, the NMR tube was sealed to a larger tube having a volume of 120 mL. Reaction occurred with the silica spread in a thin layer on the bottom of the larger tube and the silica was poured under vacuum into the NMR tube, which was then sealed. For studies involving time evolution of species, TMP was condensed into a liquid nitrogen cooled NMR tube containing the silica sample. The time of reaction in these studies was taken as the interval between removal of the sample from the dewar and the midpoint of the corresponding NMR measurements. For these studies, the NMR data accumulation took 4.5 min. The sealed tubes were spun at the magic angle, using a spinner previously described [101]. Spinning rates between 2 and 3 kHz were used in the present investigation. NMR measurements were carried out at 23 ± 2°C.

Trimethyl phosphite was purchased from Aldrich and had a stated purity of >99%. The ^{31}P NMR spectrum of liquid TMP indicated that there was less than 0.1% P-containing species as impurities.

Results

(a) Adsorption at 23°C, NMR Spectra

The aerosil silica used in this work has about 1.6 ± 0.1 accessible SiOH groups/nm^2 after activation in vacuum at 350°C (as measured gravimetrically from SiOH/SiOD exchange with ND_3) and a small number of "inaccessible" silanols that are perturbed due to interparticle contact [18]. Therefore, the number of accessible silanols is about 0.86 mmol/g of silica.

1.58 mmol/g of TMP was condensed into a sample of A-350 silica and, ten minutes after warming the sample, the ^{31}P NMR spectrum shown as curve A in Figure 6.1 was recorded. A strong peak is observed at 142 ppm and a weak one at 12 ppm in Figure 6.1A. The 12 ppm peak has a P-H coupling of 720 ± 20 Hz. Liquid TMP has a chemical shift of 140 ppm; dimethyl phosphite (DMP) has a shift of 11 ppm, and a P-H coupling of 700 Hz. Thus it is clear that the observed peaks are due to unreacted TMP, together with some DMP. Further, both resonances remain narrow in the absence of proton decoupling, and no spinning side bands are seen, indicating that both species must be moving with considerable freedom on the surface.

TMP might be expected to react with SiOH through one of the following routes:

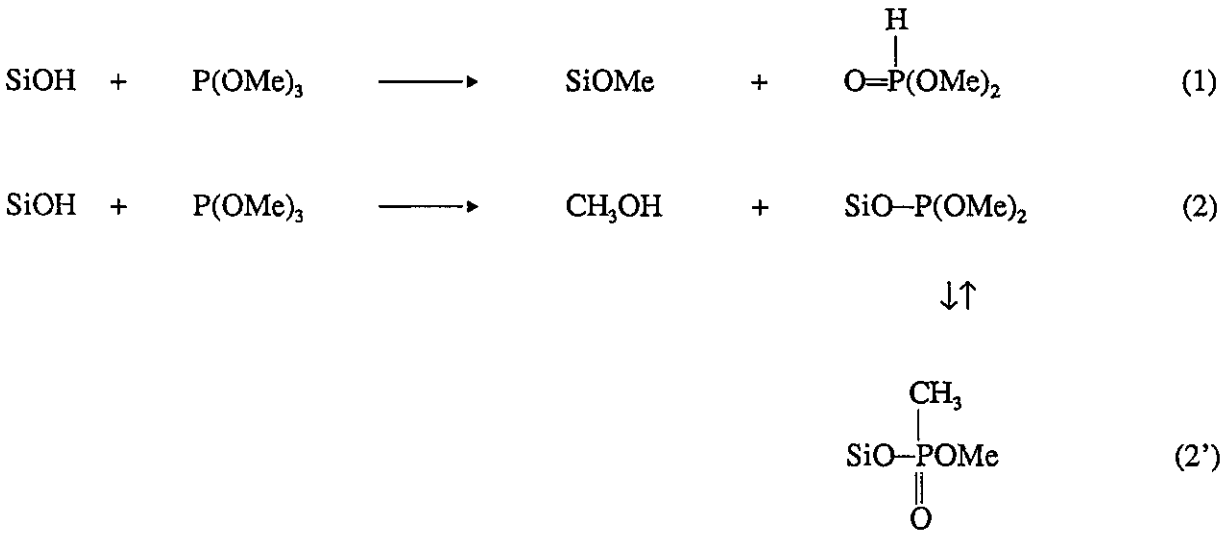

Figure 6.1. Room-temperature ^{31}P NMR spectra for A-350 silica with 1.58 mmol of TMP per g of SiO_2. (A) 10 min after warming sample to room temperature. (B) After 235 min. (C) After 1360 min. The chemical shifts (X axis) are with respect to H_3PO_4.

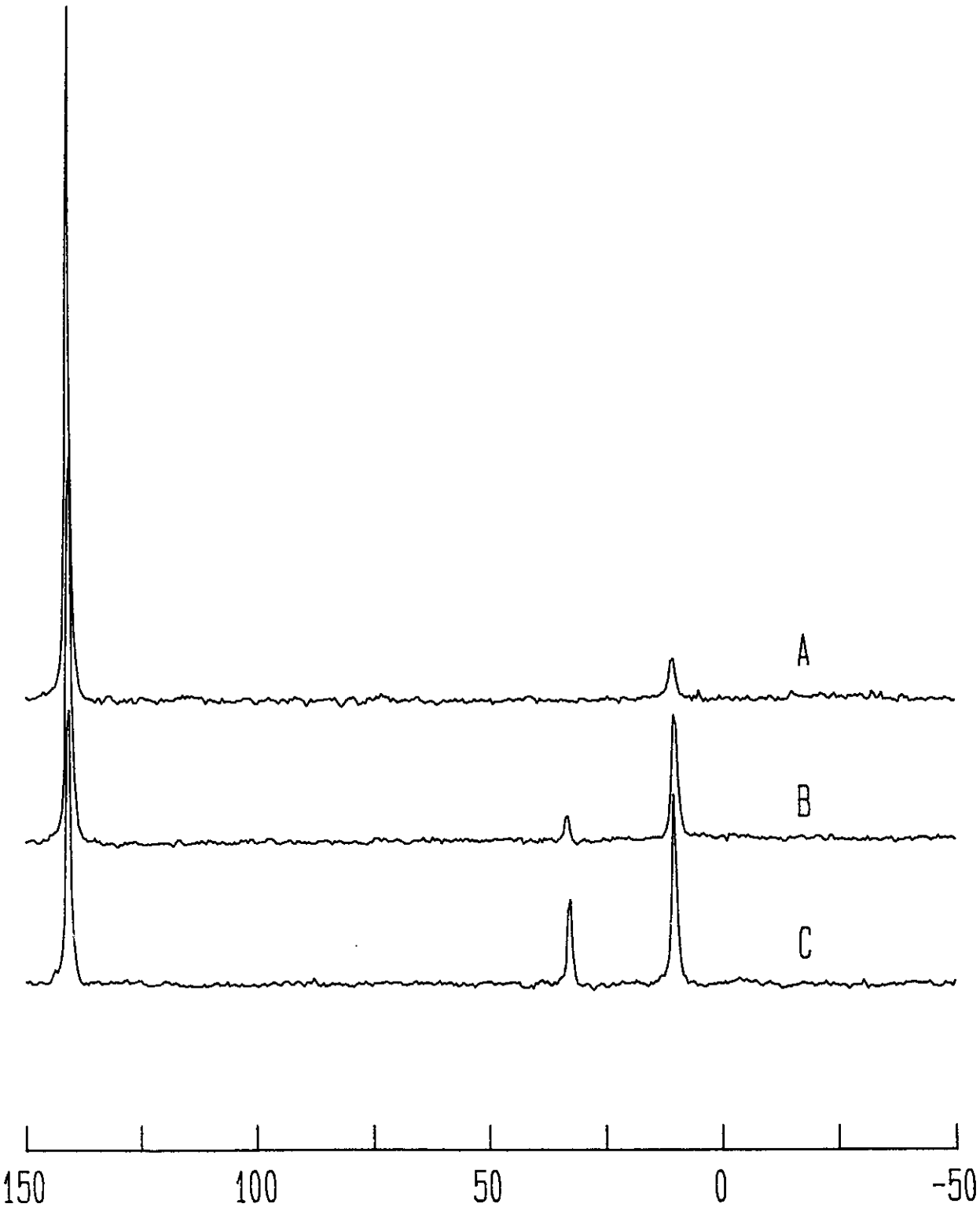
A
B
C
150
100
50
0
-50

The observed spectrum for short reaction times suggests that only (1) is occurring. Further evidence, to be presented below, shows that (1) is indeed the initial reaction, and there is no evidence for products of (2) or (2') at 23°C, even after long reaction times.

During the next 50 min the TMP signal rapidly decreased while that due to DMP increased and, after a total reaction time of 60 min, a new weak signal was detected at 36 ppm. This signal slowly increased over the next 1500 min while the TMP and DMP signals continued to decrease. Figures 6.1, B and C, show the spectra after 235 and 1360 min, respectively, and Figure 6.2A shows a plot of the integrated intensities of these three signals over 1500 min, and the sum of the integrated intensities of these three signals. The 36 ppm resonance is close to that for liquid DMMP at 32 ppm and, therefore, we assume that the isomerization of TMP to DMMP, catalyzed by silica, occurs via reaction 3.

$$P(OMe)_3 \longrightarrow CH_3 - \overset{\overset{O}{\|}}{P}(OMe)_2 \qquad (3)$$

As will be discussed further below, the products DMP and DMMP were also identified by infrared and mass spectrometry. Therefore, we conclude that at 23°C the reaction between aerosil silica and TMP primarily yields DMP via reaction 1, accompanied by a small quantity of DMMP via reaction 3. The near constancy of the total phosphorus signal in Figure 6.2A indicates that these are the only major reactions, and the relatively constant value of the DMP signal after about 800 min indicates that reaction 1 had essentially ceased.

When 87 μmol TMP were added to the silica initially, the quantity of DMMP produced after 1500 min reaction (Figure 6.2A) was 21 μmol. When 45 μmol of TMP were added (nearly equal to the number of SiOH groups), a similar curve to Figure 6.2A was observed (not shown) except that less DMMP was produced with time (5.7 μmol after 1500 min). With 22 μmol of TMP, no DMMP was detected until 1200 min and 1.1 μmol was present after 1500 min. For both the 45 and 22 μmol TMP experiments, the tendency of DMP to reach a constant plateau was less evident, particularly with the smaller initial dose.

Figure 6.2. Time evolution of the integrated intensities of the ^{31}P signal of TMP (■), DMP (□), and DMMP (♦). The sum of the integrated areas of these three signals is indicated by (+). In each case 1.58 mmol/g of TMP was added to 55 mg samples of (A) A-350, (B) A-650, and (C) A-900.

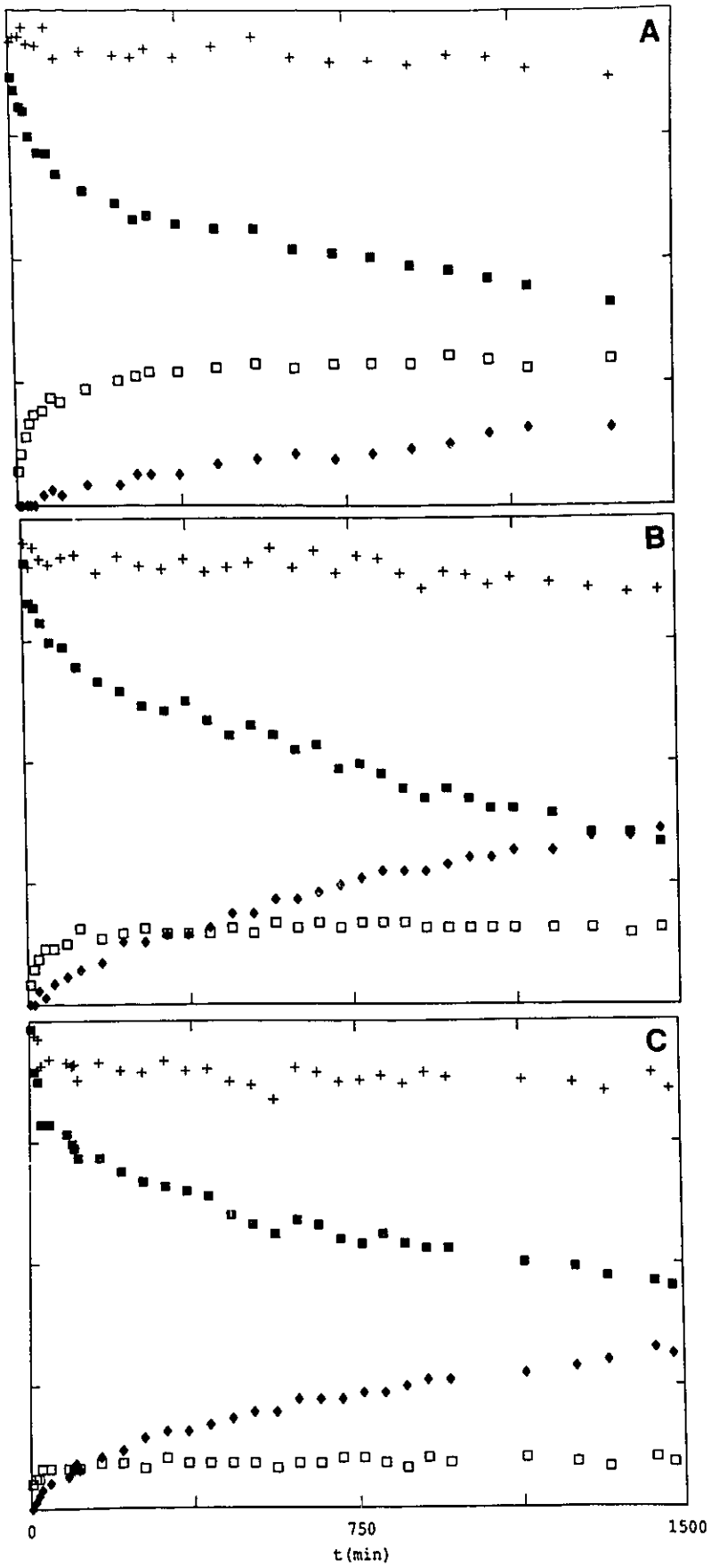
A
B
C
0
750
1500
t(min)

The initial rates of formation of DMP also decreased with decreasing TMP dose. After 100 min reaction the quantities produced were 20, 12, and 6.5 μmol, respectively. These and other results for the three reaction conditions are summarized below in Table 6.1 and will be discussed further later.

1. TMP added, mmol/g	1.58	0.82	0.40
2. TMP added,[a] μmol	87	45	22
3. ratio TMP/SiOH [b]	1.9	1.0	0.5
4. μmol TMP (1500 min)	37	17	3.9
5. μmol DMMP (1500 min)	21	5.7	1.1
6. μmol DMP (1500 min)	29	22	17
7. μmol DMP (100 min)	20	12	6.5

Table 6.1. TMP adsorption Data for Reaction with A-350 Silica

(a) Calculated for 55 mg silica.

(b) The accessible silanol density is 1.6 SiOH/nm^2 or 47 μmol SiOH for a 55 mg sample.

Two additional experiments were carried out in order to determine how the concentration of SiOH groups would influence the course of the reaction. The same quantity of TMP/g of silica as was used to obtain the data shown in Figure 6.2A (1.58 mmol/g) was added to samples of A-650 (1.0 ± 0.1 SiOH/nm^2) and A-900 (0.5 ± 0.1 SiOH/nm^2) silica. The results are plotted in Figure 6.2, B and C, for 650 and 900°C activation, respectively. Qualitatively, less DMP and more DMMP were produced relative to that for curve 6.2A, and in both cases, the production of DMP reached an almost constant plateau after a relatively short period into the reaction. The three curves (Figure 6.2, A, B and C) show that the DMMP/DMP ratio apparently increases with the temperature of activation of the silica.

(b) Adsorption at 23°C, Infrared Spectra

The infrared spectrum of 10 mg/cm^2 A-350 is shown in Figure 6.3A. Twenty hours following the admission of about 1.0 mmol/g of TMP to the above sample the spectrum in Figure 6.3B was observed. The strong bands from 3000 to 2800 cm^{-1} are mainly due to the CH_3 stretching modes of gas phase TMP, the weak band near 2450 cm^{-1} is the P—H stretching mode of DMP, and very weak absorptions near 900 cm^{-1} in the window region of the silica spectrum are due to DMMP. The basis of these assignments and spectra expanded in the 2450 and 900 cm^{-1} spectral regions will be discussed in more detail below. Figures 6.3, C and D, show the spectra of gas-phase TMP and DMP, respectively. Using established group frequencies [102] and published data [103-105], the vibrational assignments for TMP, DMP, and DMMP are listed in Table 6.2.

Figure 6.4 shows details of the spectral changes between 3800 and 2400 cm^{-1} which occurred over a 20 h period following the addition of TMP to 10 mg/cm^2 A-350 (in this experiment, 2.0 mmol/g of TMP was added). The sharp 3747 cm^{-1} band was immediately replaced by a broad band at 3390 cm^{-1}, characteristic of a hydrogen-bonding interaction between SiOH and TMP. The 3390 cm^{-1} band shifted with time to 3250 cm^{-1}, a shoulder grew to higher wavenumber of the sharp 2840 cm^{-1} peak, and a new weak asymmetric band appeared having a maximum at 2457 cm^{-1} and a shoulder at 2440 cm^{-1}. A band in the 2400-2470 cm^{-1} spectral region is indicative of the presence of PH-containing species [102,104] and Figure 6.5A shows the evolution of this band on an expanded wavenumber scale. An infrared and mass spectroscopic analysis of the species which could be frozen in a liquid nitrogen trap following evacuation after about 30 min reaction showed that TMP and DMP were present. Finally, adsorption of TMP on a fully deuterated sample of A-350 silica (SiO—D at 2760 cm^{-1}) resulted in identical spectral features except that the 3400-3200 cm^{-1} features shifted to 2300-2200 cm^{-1} and the 2457 cm^{-1} band appeared at 1792 cm^{-1}. The downward shift by a factor of 1.38 is expected for H/D stretching modes [102,106].

Figure 6.3. (A) Room-temperature infrared spectrum of 10 mg/cm^2 A-350 silica. (B) 20 h after addition of 1.0 mmol/g of TMP. (C and D) Infrared spectra of 2.0 Torr of gaseous TMP and DMP, respectively, in a 10 cm gas cell. (E and F) Infrared spectra as for curve B after 5 min and 20 h evacuation, respectively. The bar at the top left represents an absorbance of 1.0 for A, B, E, and F; 0.75 for C; and 0.25 for D.

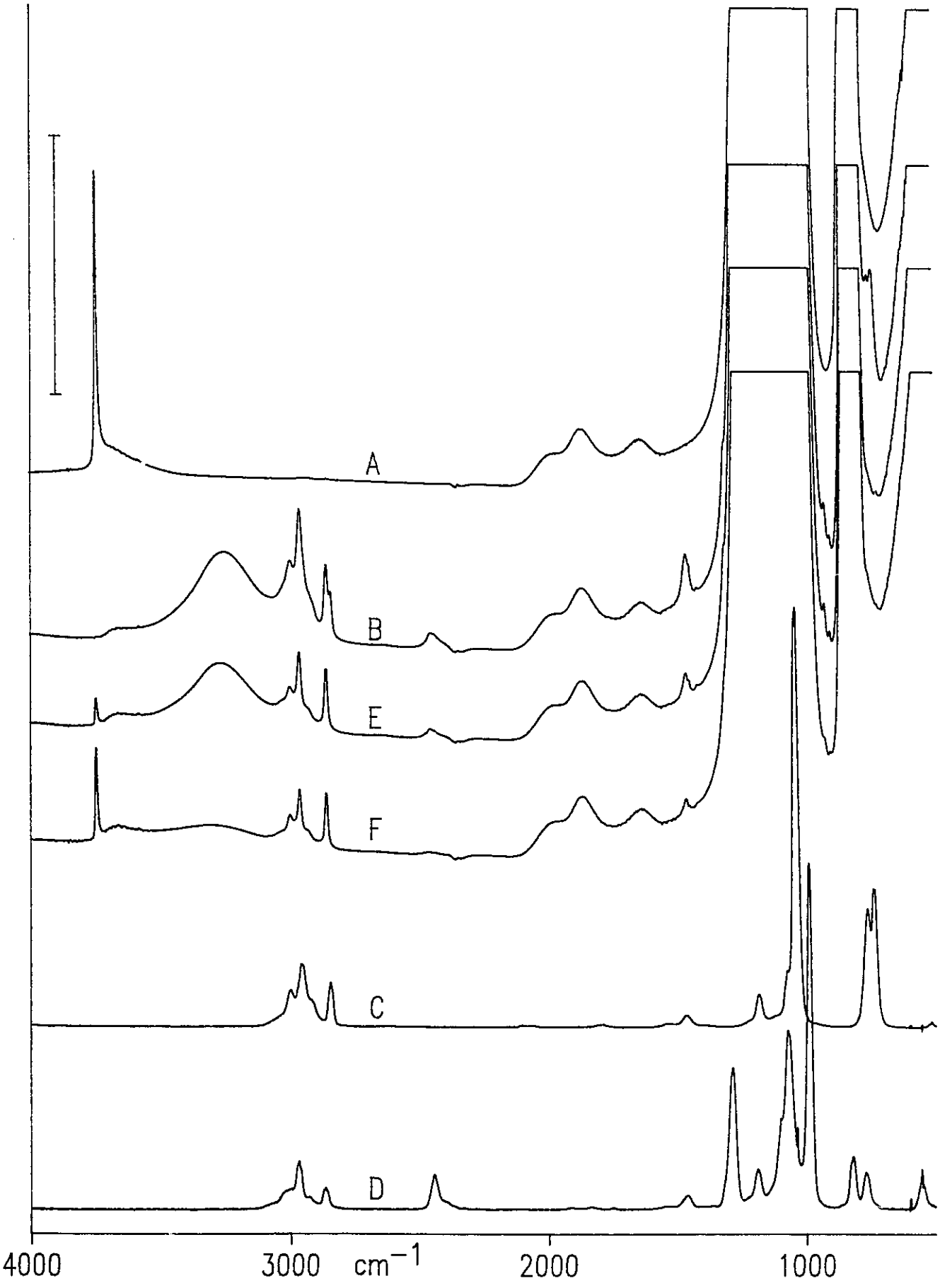
A
B
E
F
C
D
4000
3000
cm⁻¹
2000
1000

Vibration	$POCH_3$	PCH_3
(CH_3)	3005–2995 (w) 2960–2950 (s) 2860–2840 (s)	3005–2995 (w) 2930–2920 (w)
(CH_3)	1475–1460 (m) 1250–1230 (w)	1425–1415 (vw) 1325–1315 (m)
(CH_3)	1190–1170 (m)	920–890 (s)
O–C	1050–980 (vs)	
O–P	830–740 (s)	
P–C		730–680 (w)
	Miscellaneous	
P=O	1300–1240[b] 1240 (DMMP liquid) 1286 (DMMP gas) 1265 (DMP liquid)	
P–H	2443 (DMP gas) 2430 (DMP liquid)	

Table 6.2. Group Frequencies (cm^{-1}) for Various P–X Functional Groups[a]

(a) from references 7, 10, 20-23
(b) General range for a noninteracting P=O bond

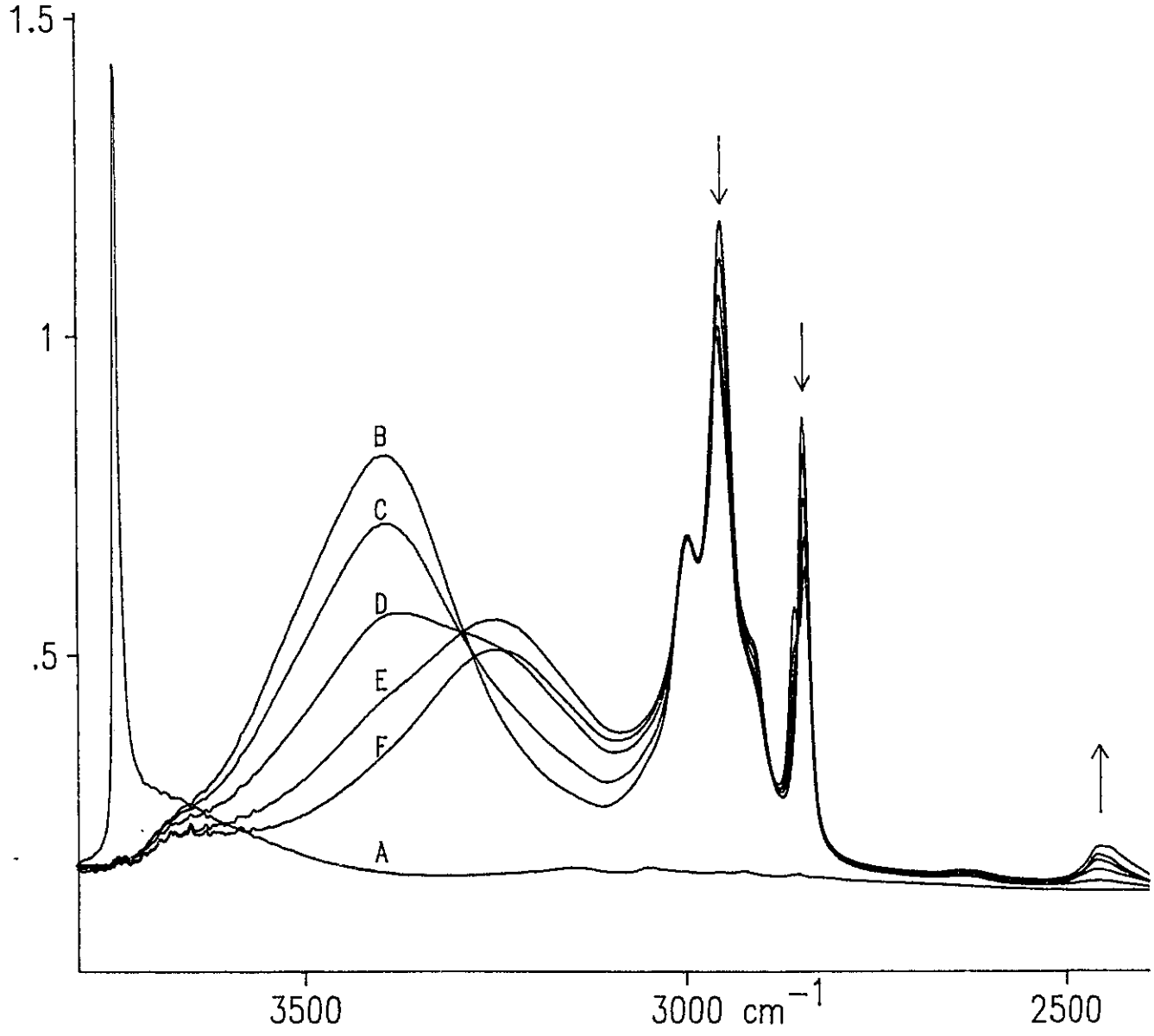

Figure 6.4. (A) Room-temperature infrared spectrum of 10 mg/cm^2 A-350 silica. (B) 1 min after addition of 2.0 mmol/g of TMP. Subsequent spectra show the time evolution of the reaction after: (C) 30 min, (D) 2 h, (E) 6 h, (F) 20 h.

Figure 6.5.
(A) Time evolution in the P—H stretching spectral region for the experiment described in Figure 6.4. The band is growing in intensity and the spectra shown were recorded after 1 min, 30 min, 1 h, 2 h, 4 h, 6 h and 20 h following the addition of TMP to the sample.

(B) Adsorption at 23°C of DMP on A-350 silica (top curve) and evolution of the spectra (decreasing intensity) after evacuation for 1 min, 5 min, 15 min, 45 min, 105 min and 240 min (see text).

(C) Infrared spectrum of DMP adsorbed on a methoxylated silica after conversion of the SiOH groups to $SiOCH_3$.

(D) Adsorption at 23°C of 1.7 mmol/g of TMP on A-1000 silica (bottom curve) and evolution of the spectra (increasing intensity) after 30 min, 1 h, 3 h, 7 h, 11 h and 20 h reaction.

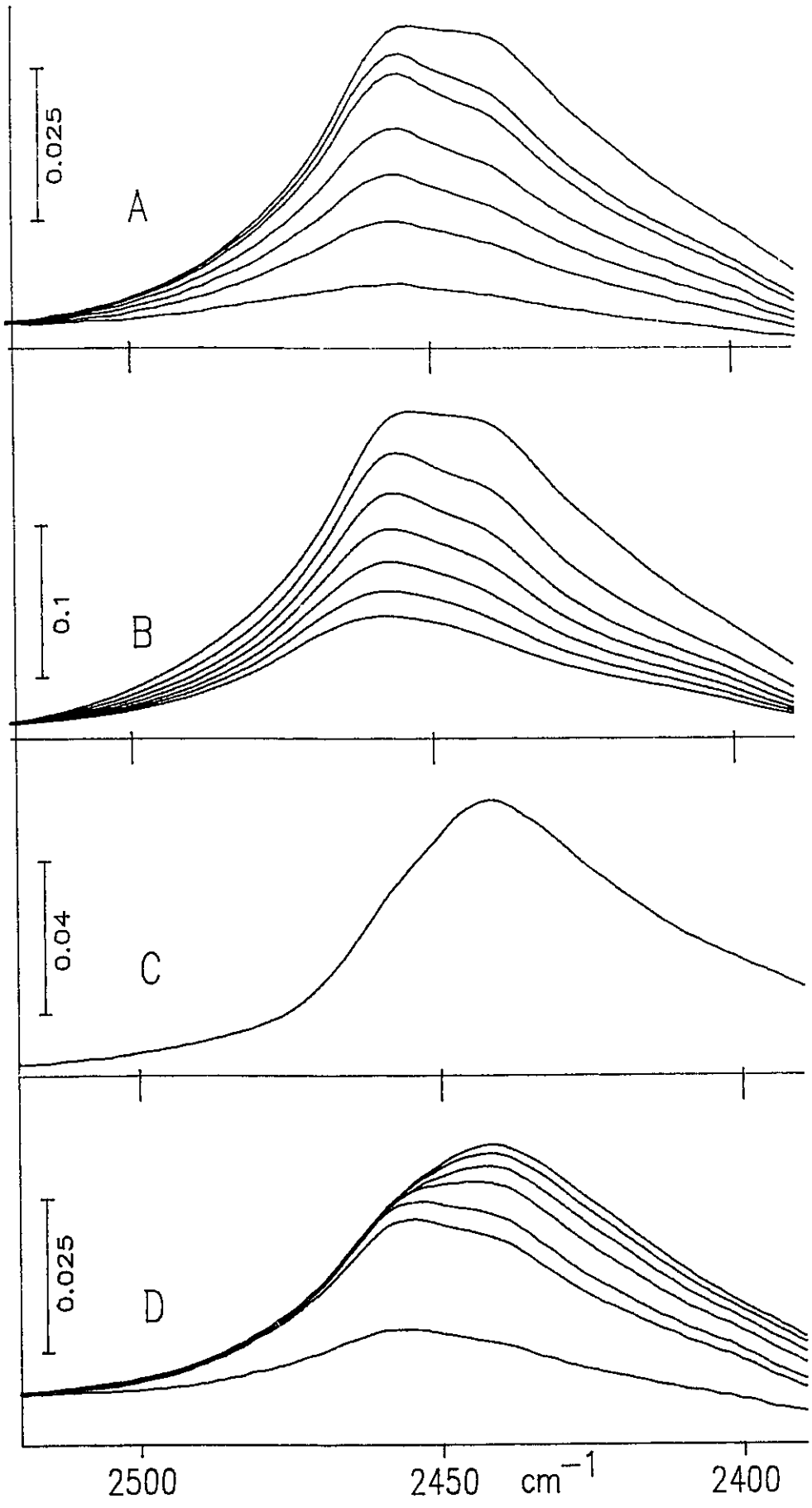
0.025
A
0.1
B
0.04
C
0.025
D
2500
2450
cm^{-1}
2400

For greater than about 1 h reaction, new weak bands appeared at 1421, 1315, 920, and 900 cm^{-1}, and steadily grew in intensity with time. (Spectra showing the evolution of the these bands for a reaction with A-800 silica are shown in Figure 6.6). Evacuation through a liquid nitrogen cooled trap, and subsequent IR and mass spectroscopic analysis showed that a third product, DMMP, was present. Phosphorus compounds containing a PCH_3 functional group have unique PCH_3 deformation and rocking modes at the above frequencies which are not found for $POCH_3$ functional groups (see Table 6.2), further confirming the presence of DMMP.

Figure 6.3, E and F, show the spectral changes upon evacuation after 20 h reaction. Evacuation for 5 min (Figure 6.3E) resulted in partial restoration of the 3747 cm^{-1} peak and a reduction in the intensity of the CH_3 stretching and deformation bands (3000 and 1470 cm^{-1}). After 20 h evacuation the 3747 cm^{-1} band had regained 35% of its initial intensity, although there was still some residual H-bonded SiOH intensity, and the peaks in the 2450 and 900 cm^{-1} spectral regions due to DMP and DMMP, respectively, had not completely disappeared, showing how tenaciously both species adsorb. Evacuation or mild heating so as to remove the last traces of DMP and DMMP left a spectrum from 3000 to 1300 cm^{-1} which was essentially identical to that shown in Figure 6.3F, having bands at 3000, 2958, 2858 and 1470 cm^{-1}, characteristic of $SiOCH_3$ groups on silica [106]. This species was stable up to 400°C evacuation, confirming that the only chemisorbed surface species was indeed $SiOCH_3$. Therefore, in accord with the NMR results, reaction 1 appears to be the only dissociative process occurring at 23°C, accompanied by the slower isomerization (reaction 3) to produce DMMP. Note also that, even after 20 hours, not all of the SiOH groups react at 23°C.

A-350 silica contains some surface silanols which are inaccessible to larger molecules whereas A-800 silica has no inaccessible silanols and exhibits a relatively symmetrical SiOH peak (see Chapters 3 and 4). The adsorption of TMP on A-800 silica showed similar features in the 3800-2400 cm^{-1} spectral region as reported above, and both DMP and DMMP were produced. The quantity of DMP, as judged by the intensity in the P–H spectral region, was

about 0.60 of that generated for a 350°C activated sample, but the quantity of DMMP (1315 cm^{-1} band) was about 2.2 times greater. Figure 6.6 shows the evolution of the 1315/1421 and 920/901 cm^{-1} peaks due to DMMP as a function of time up to 20 h reaction. Subsequent evacuation for 48 h restored the SiOH intensity to about 40% of its original value and only the spectrum of $SiOCH_3$ was observed. This result is comparable to that found using NMR with a 900°C activated sample.

(c) High Temperature Reactions

Following adsorption of TMP for 20 h at 23°C on A-350 silica, the sample was subsequently heated to various temperatures between 100 and 400°C and, after cooling to 23°C, the infrared spectra were recorded. The spectral changes were somewhat complex, suggestive of the formation of various new PH-, $POCH_3$-, and PCH_3-containing species, the group frequencies of which all lie in relatively narrow frequency domains [102]. The ^{31}P NMR spectra under the same reaction conditions for each of the three samples previously described showed that up to seven new resonances were detected having chemical shifts in the range −17 to +22 ppm, a range usually associated with the formation of phosphate and polyphosphate-like species [107]. It is not possible to identify the nature of these species nor is this fruitful, given the complexity of the reacting system where any or all of TMP, DMP, and DMMP might further chemisorb on silica, or react with each other, or react with chemisorbed products.

Although TMP is a relatively volatile species at 23°C having a vapour pressure of about 40 Torr, those of DMP and DMMP are about 2 Torr and it is difficult to ascertain whether even a prolonged evacuation removes all traces of physically adsorbed DMP or DMMP from the surface of silica. Therefore, we have studied the adsorption of TMP on silica at 100°C or above where facile desorption of DMP and DMMP would be expected during evacuation. In the IR experiments to be described below, all spectra were recorded with the sample at 100°C.

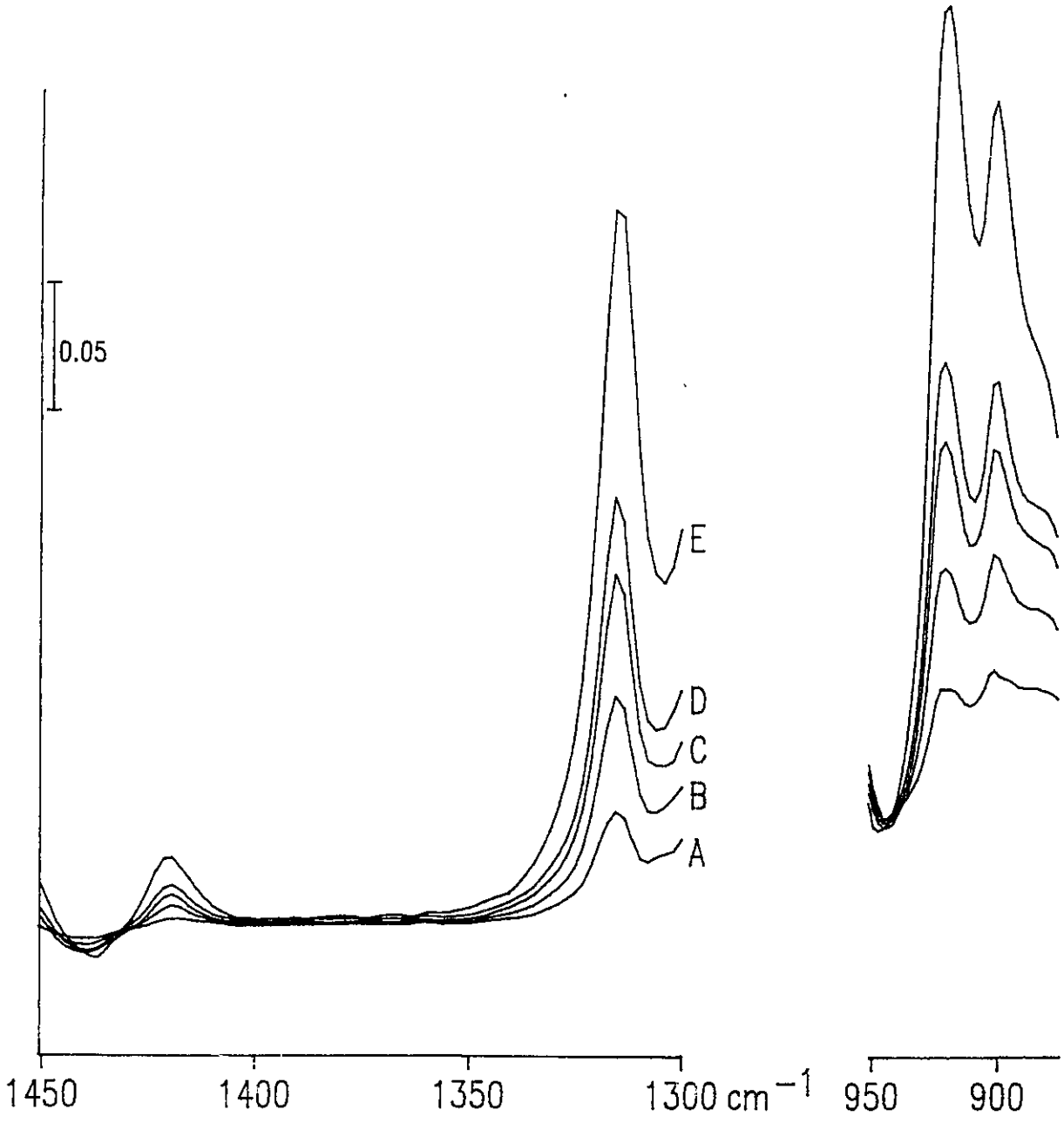

Figure 6.6. Difference spectra showing the growth of the DMMP bands on A-800 silica after addition of 1.6 mmol/g of TMP at 23°C. The difference spectra were obtained by subtracting the spectrum observed immediately after addition of TMP from those obtained after, (A) 20 min, (B) 1 h, (C) 2 h, (D) 3 h, (E) 20 h reaction.

Infrared spectra in the 3800-2400 cm^{-1} spectral region following the addition of 1.0 mmol/g of TMP to A-350 silica at 100°C are shown in Figure 6.7. Initially, a broad band appeared initially at about 3390 cm^{-1} along with the P—H band near 2450 cm^{-1}; the isolated SiOH peak did not immediately disappear, but its intensity slowly decreased during a period of about 4 h along with that of the 3390 cm^{-1} band. (Figure 6.7 shows the residual 3747 cm^{-1} intensity after 3.5 h; this band disappeared after 4 h.) The P—H band did not increase in intensity with time, but rather, the band shape changed as the 2457 cm^{-1} band decreased in intensity leaving the 2440 cm^{-1} band. Although the bottom spectrum shown in Figure 6.7 was recorded after 20 h reaction, it was qualitatively similar to that observed after 4 h reaction except that the broad band at 3390 cm^{-1} was slightly more intense after 4 h. Therefore, after 4 h or 20 h reaction most of the SiOH groups had reacted. Brief evacuation of the gas phase after 20 h reaction removed all gas-phase species and left a weak residual peak at 2460 cm^{-1}. Analysis of the trapped evacuation products showed that only TMP and DMP were present and that, even after long reaction times, no DMMP was produced. These results show that reaction 1 goes to completion under these conditions and that isomerization to DMMP does not occur. The absence of DMMP at 100°C was also verified in an NMR experiment.

Prolonged evacuation at 100°C or even evacuation at 200°C did not decrease the intensity of the 2460 cm^{-1} peak discussed above, suggesting that a chemisorbed species was present. The boiling point of DMP is 175°C and one would expect that evacuation under the above conditions would desorb all DMP. No other IR bands were detected using a 10 mg/cm^2 disk, but any P=O bands present would be hidden in the bulk SiO_2 absorption between 1250-1300 cm^{-1}. Therefore, we carried out an experiment with a 2.5 mg/cm^2 disk which is transparent to about 1250 cm^{-1}. After the 350°C activation 2.4 mmol/g of TMP was allowed to react with the sample for 1 h at 100°C. Figure 6.8 shows a series of difference spectra after subtraction of the silica background. Figure 6.8A was recorded with TMP present and infrared bands at 1465, 790, and 740 cm^{-1} are due to adsorbed or gas-phase TMP. There are also weak bands at 2457 and 2440 cm^{-1} (not shown) due to DMP; this species

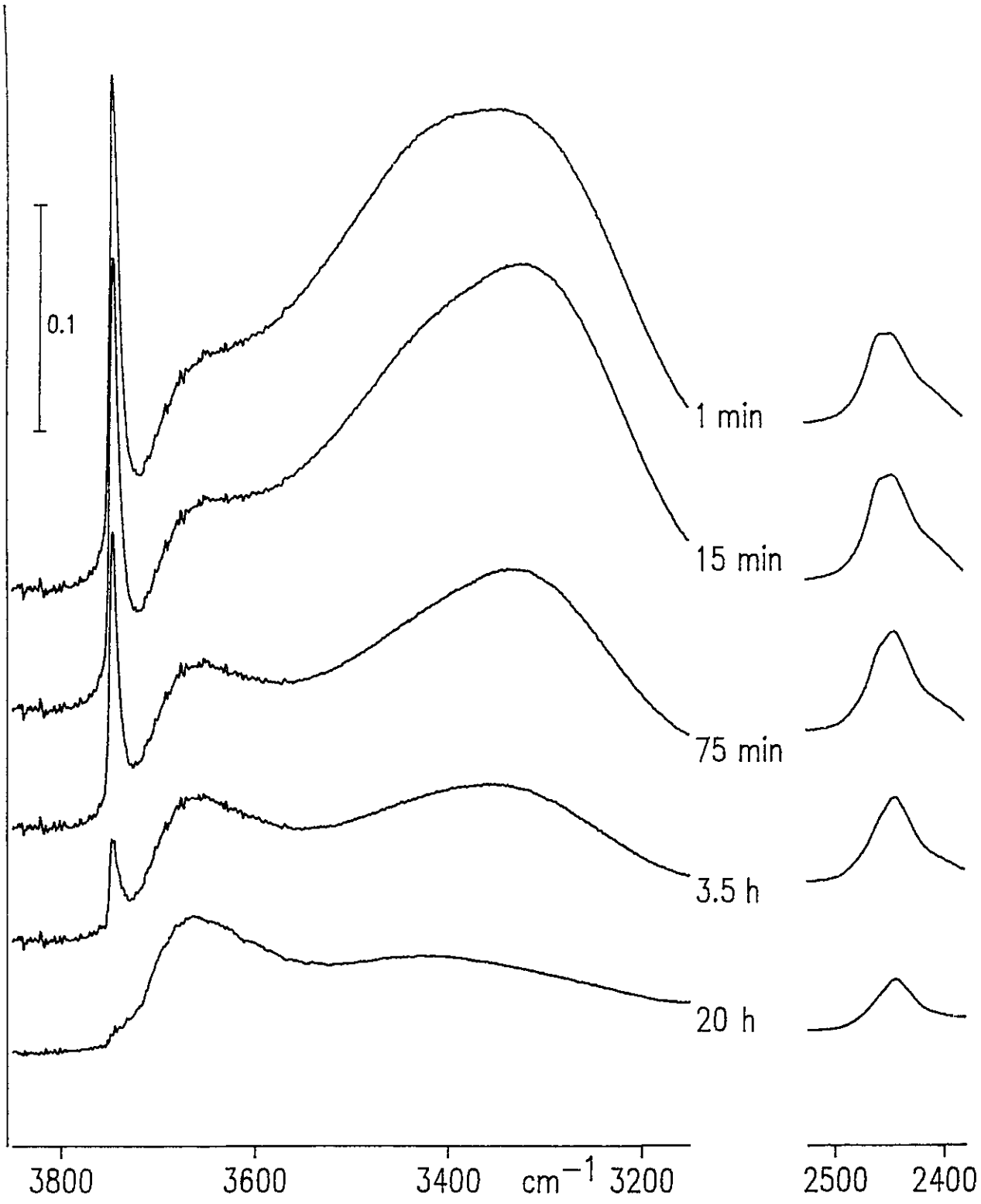

Figure 6.7. Infrared spectra observed following addition of 1.0 mmol/g of TMP to A-350 silica at 100°C (all spectra recorded with the sample at 100°C) after the indicated reaction times.

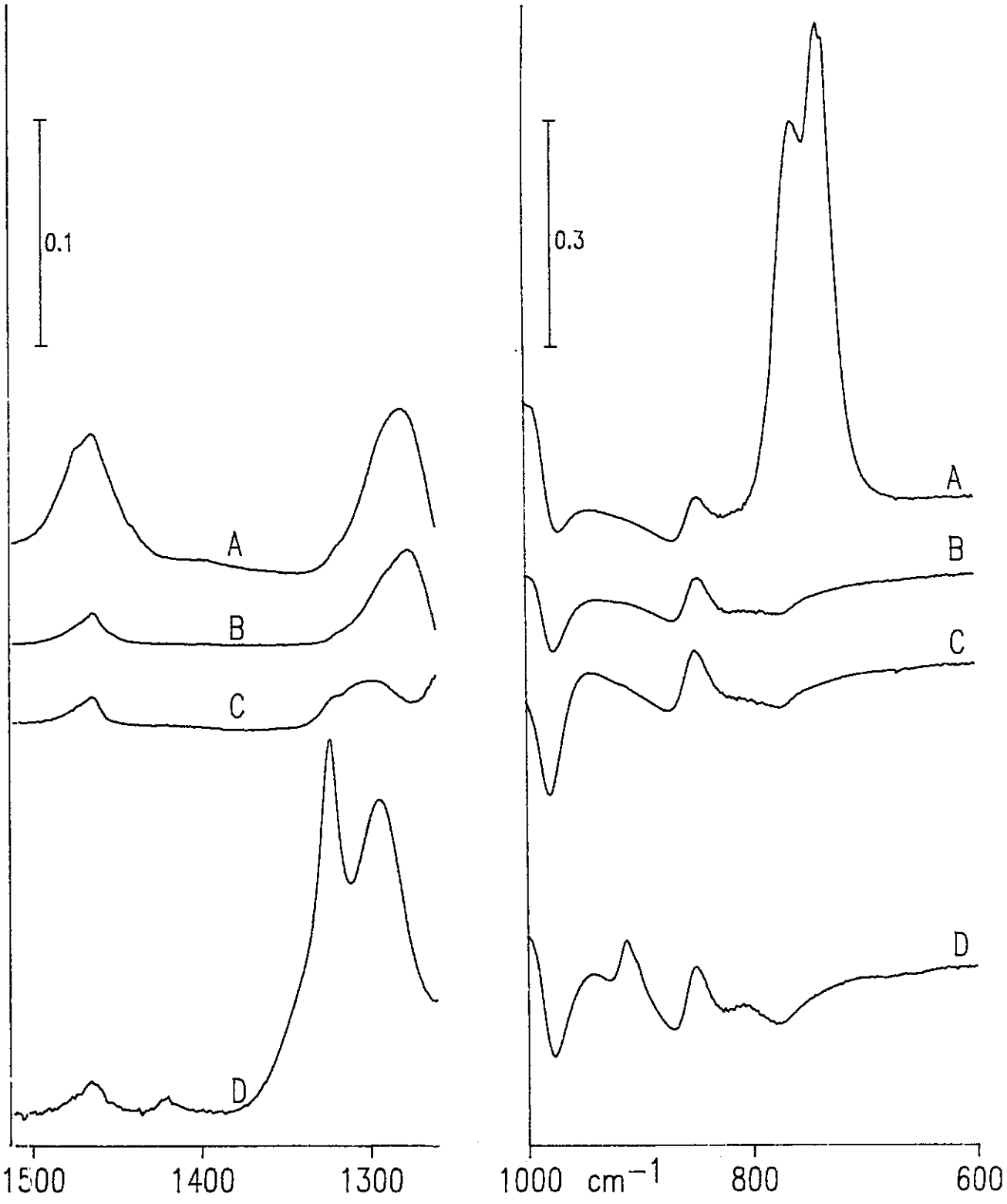

Figure 6.8. (A) Difference spectra observed after addition of 2.4 mmol/g of TMP to 2.5 mg/cm^2 A-350 silica at 100°C. The spectrum of the A-350 SiO_2 was subtracted in each case. (A) After 1 hr reaction (B) Evacuation of A for 15 min. (C) Heating B in vacuum to 400°C for 30 min and cooling to 100°C. (D) Re-addition of 1.0 mmol/g of TMP to C at 100°C, heating for 1h to 350°C, evacuation for 30 min at 350°C and cooling to 100°C.

would also be expected to have modes at 1465 cm^{-1} and in the 800-750 cm^{-1} regions (see Table 6.2 and Figure 6.3D) but these would be masked by those of the excess unreacted TMP. In addition there is a band at 1280 cm^{-1} in the spectral region of unassociated P=O stretching vibrations (Table 6.2) and a weak peak at 850 cm^{-1} which is a known mode of $SiOCH_3$ [108]. Finally, the "negative" dip at 980 cm^{-1} is due to the disappearance of the Si–OH stretching mode (see Chapter 4) of surface SiOH groups which were converted to $SiOCH_3$ as the reaction proceeded.

Evacuation for 15 min (Figure 6.8B) removed the TMP (and DMP) leaving a band at 1280 cm^{-1} and weak bands at 850, 1470 (and 2460 cm^{-1}). Upon heating this sample at 400°C under vacuum (Figure 6.8C), the intensity of the 1280 cm^{-1} band decreased (there was a similar decrease in the intensity of the 2460 cm^{-1} band), its peak maximum shifted to 1295 cm^{-1}, and a shoulder appeared at 1320 cm^{-1}. There were no further spectral changes with longer evacuation times.

This experiment shows that a strongly chemisorbed species is created during reaction at 100°C which contains a P–H mode and a P=O mode. The bands in the 800-740 cm^{-1} spectral region are associated with the O–P vibration of $POCH_3$ groups, and their absence after evacuation indicates that the surface species does not contain this functional group (these are normally strong bands, see Figure 6.3, C and D). The simplest structure which would account for these spectroscopic observations is the bridged species, **I**:

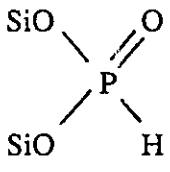

(I)

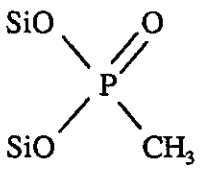

(II)

The appearance of a very weak band near 1320 cm^{-1}, suggestive of a PCH_3-containing species, might indicate that a small number of species **II** is also present.

After the 1 h reaction above, only about 80% of the SiOH groups had reacted. A second 1.0 mmol/g dose of TMP was added to the sample at 100°C, the sample was heated to 350°C for 1 h, and then evacuated at 350°C for 30 min. The spectrum in Figure 6.8D was observed, having strong bands at 1323 and 1295 cm^{-1}, accompanied by weaker bands at 1421, 913, and 902 cm^{-1}. These are the characteristic modes of a PCH_3 species. As a result of this last treatment the P—H mode at 2460 cm^{-1} disappeared and we assume that species **I** was converted to species **II**.

In a different experiment, 0.40 mmol/g of TMP was added to 10 mg/cm^2 A-350 at 23°C and the temperature was raised to 400°C, held there for 30 min, and then evacuated for 30 min. The IR spectra before and after reaction (1500-800 cm^{-1}) are shown in Figure 6.9. In addition to $SiOCH_3$ as a product, the new spectral features at 1421, 1323, 913, and 902 cm^{-1} are the characteristic bands of a PCH_3-containing species, most probably species **II**. Therefore, the infrared evidence suggests that a chemisorbed species having structure **I** is formed during reaction at 100°C whereas, upon subsequently heating this in the presence of TMP to 350°C, or by simply heating TMP/SiO_2 from 23°C to 400°C, species **II** is favoured.

NMR experiments were carried out in order to test whether the above hypotheses were plausible. A sample was activated at 350°C, and cooled to 100°C. 1.2 mmol/g of TMP was added and allowed to react for 1 h, and then the sample was evacuated for 1 h at 100°C. The ^{31}P NMR spectrum (Figure 6.10A) observed by cross polarization contained a single peak at -5 ppm. Delayed decoupling (Figure 6.10B) showed this to be an immobile species with a direct P—H bond. The long proton relaxation time, approximately 10 s, confirmed the absence of motion in this species. Observation of the spectrum at slow spinning speeds produced substantial spinning side bands and the chemical shift anisotropy was estimated, by the method of Herzfeld and Berger [109] to be 172 ± 5 ppm. Both the shift and its anisotropy are consistent with a phosphite species such as **I**.

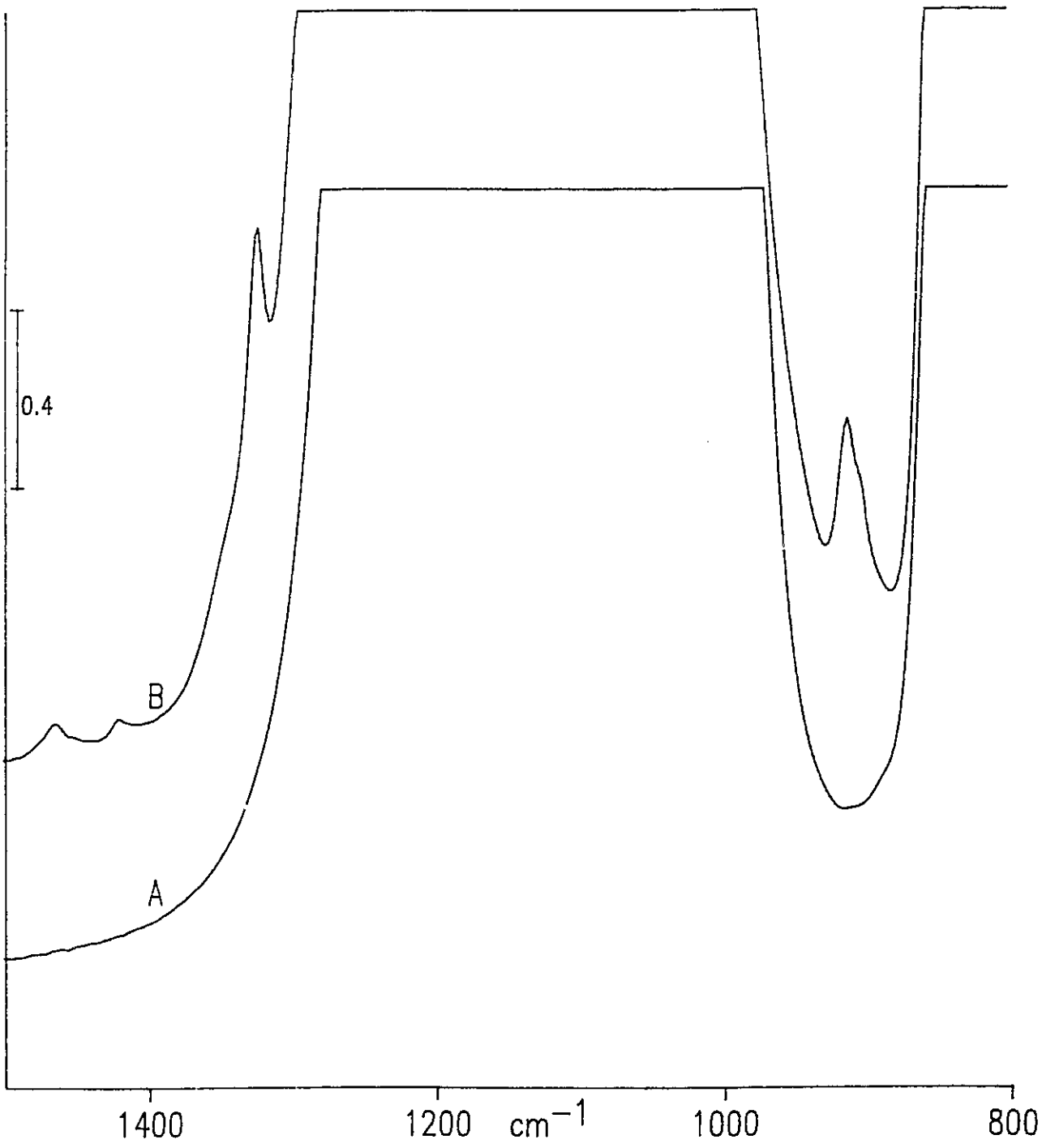

Figure 6.9. (A) Infrared spectrum of 10mg/cm^2 A-350 at 23°C. (B) After adding 0.4 mmol/g of TMP to A at 23°C, raising the temperature to 400°C for 30 min, evacuating at 400°C for 30 min, and cooling to 23°C.

Figure 6.10. Room-temperature ^{31}P NMR spectra recorded after reaction of 1.2 mmol/g of TMP for 1 h with A-350 silica at 100°C. (A) Normal CP/MAS spectrum. (B) As for A but with 70 μs decoupler delay (see text). The chemical shifts (x-axis) are with respect to H_3PO_4.

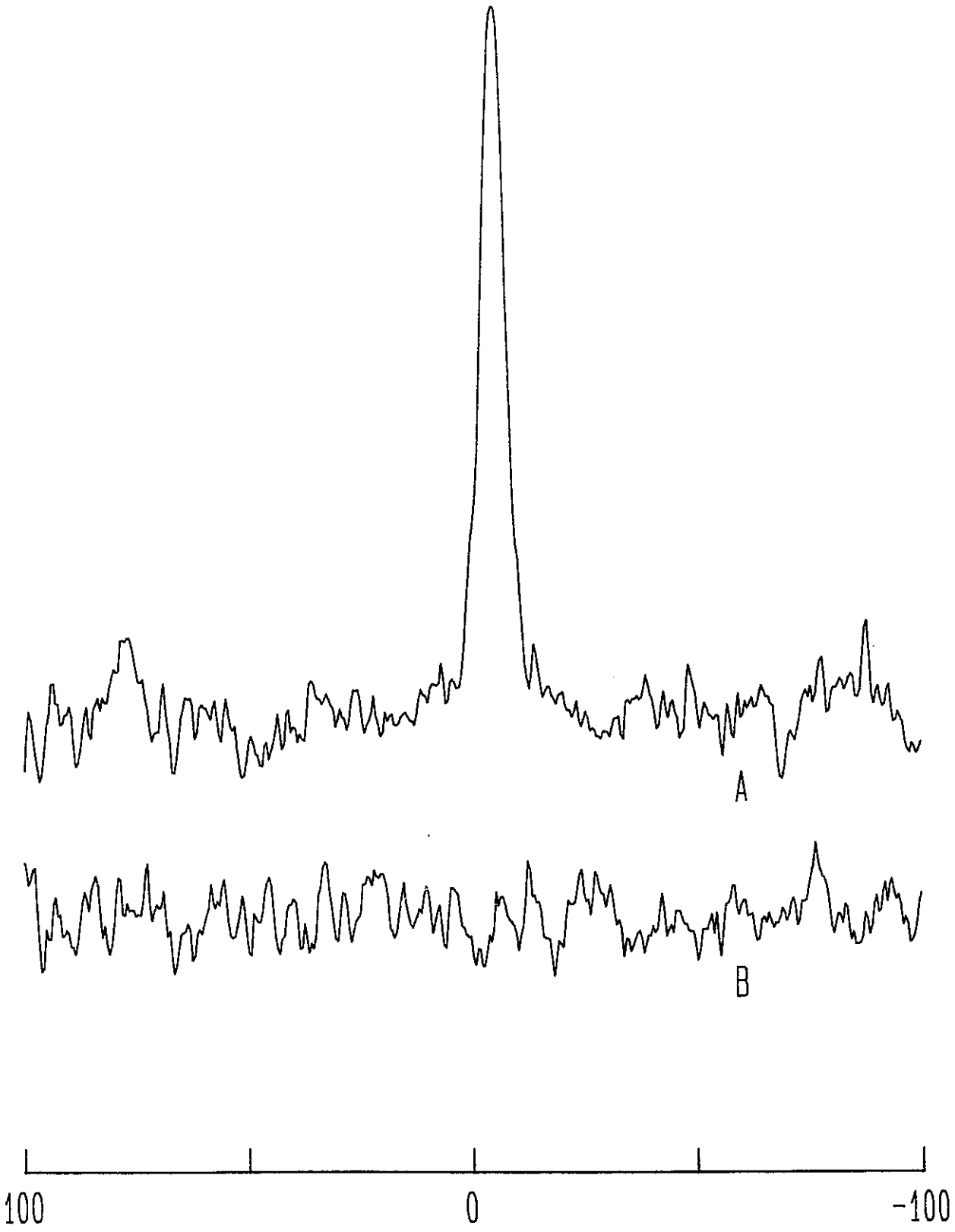
A
B
100
0
-100

In a separate experiment 1.4 mmol/g of TMP was added to A-350 silica at about 40°C; it was heated to 400°C and held for 1 h, evacuated at 400°C for 30 min, and cooled to 23°C. A strong resonance at +9 ppm having a shoulder at +20 ppm was detected and neither species contained a P—H bond. Further heating of this sample at 400°C for an additional 90 min resulted in no change in the signal. The same spectra were also observed if TMP was added directly to a sample at 400°C. These experiments are not inconsistent with structure **II** but additionally suggest that a second less abundant species might be present.

Discussion

(a) Reaction Rates

The results show that the major initial species produced from TMP adsorption on silica at 23°C are physically adsorbed DMP and chemisorbed $SiOCH_3$. The isomerization of TMP to DMMP, although less favourable than reaction 1 initially at 23°C, also occurs via reaction 3.

The numbers in the first column of Table 6.1 for 1.58 mmol/g of TMP were mainly taken from the data that are plotted in Figure 6.2A. Plots for 0.82 and 0.40 mmol/g of TMP are not shown but data for these reactions are also given in Table 6.1. The initial formation of DMP on all of the 350°C activated samples occurs rapidly and qualitatively the initial rate is higher for a greater TMP/SiOH ratio (compare rows 3 and 7). The quantities of DMMP produced after long reaction times (1500 min, row 5) indicate a decrease in the extent of isomerization with decreasing dose of TMP. This is almost certainly related to the greater decrease in the amount of TMP when the TMP/SiOH ratio decreases. For example, after 1500 min, the quantity of TMP left unreacted for the largest and smallest initial dose of TMP (37 *vs* 3.9 μmol, respectively, row 4) differs by a factor of 9.5 whereas the initial amounts (row 2) only differed by a factor of 4.0.

For the reaction with A-350 where the initial TMP concentration was greater than the SiOH concentration, the production of DMP apparently reached a plateau after about 800 min (Figure 6.2A). This plateau was reached much earlier for the A-650 and A-900 samples for the same initial dose of TMP (Figure 6.2, B and C). The very rapid initial rise in the DMP concentration followed by a plateau suggests that the production of DMP was rapidly inhibited early in the reaction. Some data pertaining to the reactions described in Figure 6.2 are given in Table 6.3. Note that the quantities of DMP produced at the plateaux are in the ratios of about 1:2:3.4 for 900, 650, and 350°C activation, respectively. This ratio is nearly equal to the ratio of the silanol densities for aerosil silica activated at these temperatures (1:2:3.1). However, more important is the observation that the plateaux occur when the amount of DMP formed is about equal to one half of the initial number of SiOH groups. Therefore, the reaction becomes strongly inhibited when half of the SiOH groups have reacted to yield DMP. A possible cause for this is discussed below.

Curve (Figure no.)	2A	2B	2C
Activation Temp., °C	350	650	900
(1) μmol DMP formed at plateau	27	16	8
(2) μmol TMP added	87	87	87
(3) μmol SiOH initially[a]	47	30	15
(4) μmol SiOH at plateau	20	14	7

Table 6.3. TMP Adsorption Data for Silicas Having Differing Initial Silanol Densities
(a) for a 55 mg sample

(b) The Mechanism of the DMP Reaction

The mechanism of the reaction to give DMP probably involves a variation of the Michaelis-Arbuzov rearrangement [110] as follows:

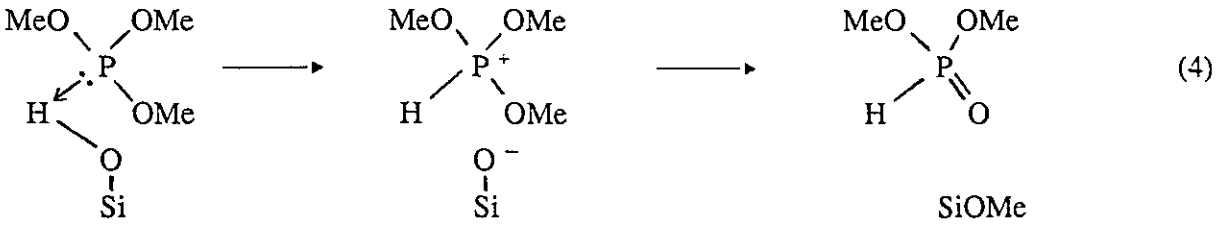

(4)

This mechanism explicitly involves an interaction of the lone pair electrons on phosphorus with the proton of an SiOH group. Although we cannot be specific as to the exact nature of the transition state, we know that the reaction apparently ceases when about half of the SiOH groups have been consumed. As will be discussed further below, DMP strongly H bonds with unreacted SiOH groups. Therefore, if DMP can migrate to an adjacent unreacted SiOH then, after 50% of the SiOH groups will have reacted, the remaining 50% will be H bonded to DMP and we assume that these sites do not permit formation of the necessary transition state for reaction 4 to occur. This might explain why the reaction effectively ceases when half of the SiOH groups are consumed. As will be discussed below, this does not prevent the isomerization to DMMP.

(c) The Mechanism of the DMMP Reaction

The isomerization reaction at 23°C with a 350°C activated silica is a minor side reaction but is relatively more important for a silica activated at 650-1000°C. The IR and NMR data have shown that more DMMP relative to DMP is produced when (a) the silica has been activated at higher temperatures, and (b) when TMP is in excess relative to the number of silanol groups for activation at 350°C. This suggests that there may be sites on silica which play a catalytic role in the isomerization process.

A silica which has been activated at temperatures above 450°C has reactive sites (characterized by IR bands at 908 and 888 cm^{-1}) which exhibit Lewis acidity [72,111,112] and we considered that the greater extent of production of DMMP relative to DMP on the highly activated samples might be due to the presence of these sites. To test this, a silica was activated at about 1000°C and sufficient methanol was added so as to just consume these sites [111]. TMP was added and, as with the previous 650-900°C activated samples, a similarly large quantity of DMMP relative to DMP was produced. Therefore, we conclude that the Lewis sites created as a result of the activation are not responsible for the isomerization.

The reaction leading to DMP consumes SiOH and generates $SiOCH_3$ according to (4). Therefore, on a surface that has undergone partial reaction with TMP, both SiOH and $SiOCH_3$ are present and it is conceivable that either of these could catalyze the isomerization of TMP to DMMP.

In order to test whether $SiOCH_3$ alone are implicated in the isomerization reaction, we studied the reactivity of TMP on a highly methoxylated silica which had been activated at 350°C and subsequently methoxylated at 400°C with CH_3OH such that about 95% of SiOH was converted to $SiOCH_3$ (it is very difficult to achieve greater than about 95% conversion via this method). After addition of TMP, DMMP was again formed after 24 h, in quantities which were about 50-75% of that formed on a non-methoxylated silica.

This ambiguous result did not totally alleviate our suspicions that $SiOCH_3$ generated via (4) might catalyze the isomerization to DMMP. That is, with CH_3 replacing H in (4) one might have a mechanism for a catalyzed process which gives DMMP as the product. However, in a similar experiment using a 350°C activated sample which was methoxylated with CD_3OD to give about 95% $SiOCD_3$, the same quantity of PCH_3-containing DMMP was produced as in the experiment with non-deuterated methanol. Therefore, although reaction (4) probably describes the mechanism of formation of DMP, it cannot (with H replaced by CH_3) describe the mechanism of isomerization of TMP to DMMP.

As a second approach to producing a methoxylated surface which contained no SiOH, a silica was activated at 1000°C so that all inaccessible silanols would be removed and the sample was methoxylated at 400°C via repeated exchange with MeOH over a 24 hour period. Because water is a product of the methoxylation a very small number of H-bonded silanols re-formed, as was evident from the appearance of an extremely weak broad band at about 3600 cm^{-1}. These silanols were then reacted with hexamethyldisilazane, HMDS, resulting in their conversion to $SiOSiMe_3$. We estimate from infrared intensities of the resultant SiOMe and $SiOSiMe_3$ species that >95% of the silanols on the A-1000 sample were replaced by the former and the rest by the latter. Following addition of 1.5 mmol/g of TMP to this sample for 24 h, no DMMP (or other product) was detected.

The above result indicates that silanol groups rather than methoxyl groups are implicated in the isomerization. A plausible mechanism involving a SiOH group as a catalyst exists whereby the oxygen of a methoxyl group (rather than phosphorus) is protonated by SiOH as follows:

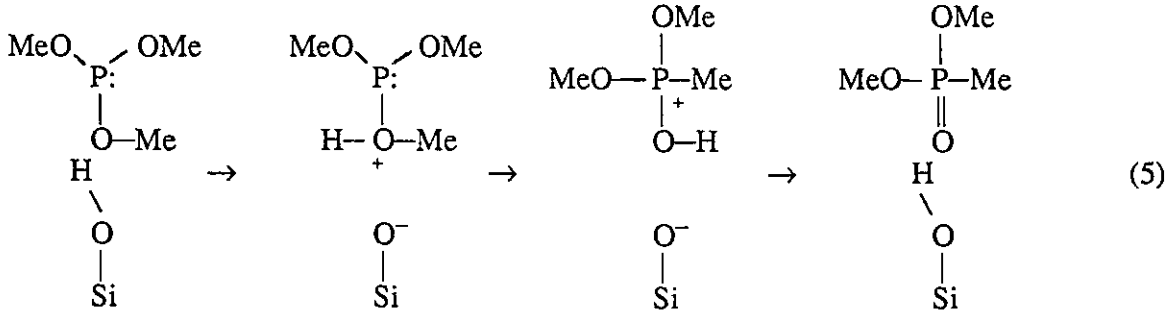

(5)

As long as SiOH groups remain accessible to the reactant, however many are present, isomerization would be possible. Note that the restrictions on forming the necessary transition state in (5) might be less severe than for reaction 4 because there are three equivalent methoxyl groups in TMP which are more distant from the central P atom. Therefore, even in the presence of adsorbed DMP, isomerization may still be a facile process.

(d) The P—H Band at 2460-2440 cm^{-1} and the Role of Hydrogen Bonding

Figure 6.5A shows the evolution of the P—H band of DMP during reaction on A-350 silica. In Figure 6.5B we show spectra of DMP alone adsorbed on a similarly activated silica, as a function of the time of evacuation. The most intense spectrum was observed following adsorption of sufficient DMP such that the isolated SiOH peak at 3747 cm^{-1} had disappeared giving rise to an intense broad band at 3200 cm^{-1} due to H bonding with DMP (we have verified that DMP does not chemisorb on silica). The subsequent spectra were recorded following evacuation at the indicated times and the intensity variation and changes in band shape as DMP desorbed were very similar to those shown in Figure 6.5A for the TMP reaction itself. Note that the low-wavenumber component at 2440 cm^{-1} disappeared first following evacuation. In a separate experiment DMP was added to a silica in which all SiOH groups had been reacted with TMP. The P—H peak which was observed is shown in Figure 6.5C and has its peak maximum at the lower wavenumber with no apparent shoulder at 2460 cm^{-1}. Gaseous DMP has a symmetrical P—H peak at 2443 cm^{-1} and in liquid DMP it is at 2435 cm^{-1}. Therefore, we conclude that the 2460 cm^{-1} peak is due to DMP which is hydrogen bonded to SiOH and that the 2440 cm^{-1} peak is due to physically adsorbed DMP.

Figure 6.5D shows the time evolution of the spectra in the P—H spectral region during the reaction of TMP on the 1000°C activated sample discussed above. Note that after about 1 h reaction the formation of DMP clearly slowed down, and virtually ceased after 3 h or 180 min. This is consistent with the previous IR and NMR results for 800 and 900°C activation. The integrated intensity of this band after 3 h was 87% of that after 20 h reaction, clearly showing that a sort of "plateau" had been reached in the production of DMP. Beyond 3 h reaction, difference spectra (not shown) revealed that all of the "new" intensity was at 2440 cm^{-1}. Therefore, after about 3 h reaction, additional DMP became physically adsorbed on the surface, even though silanol groups were still available. (The 87% figure for relative band areas quoted above is not to be considered a meaningful quantitative result for the proportions of H-bonded and physisorbed DMP, nor for the fraction of total DMP produced after 3 *vs*

20 h reaction, because we do not know the integrated absorption coefficients of these two species.)

The infrared results discussed above clearly support the results obtained from the NMR experiments, but also show that H-bonding and diffusional effects can also influence the course of this complex reaction. We will discuss this in the next section.

(e) Steric and Diffusional Effects

To complete the discussion of the room temperature reaction we want to account for the observation that the SiOH-catalyzed isomerization of TMP yields a greater quantity of DMMP on the more highly activated silicas where the surface density of SiOH is lower initially. Until the plateau is reached, DMP and $SiOCH_3$ are forming as SiOH is consumed. Beyond the plateau, the quantities of DMP, SiOH, and $SiOCH_3$ are almost constant. Most of the DMMP is generated after the plateaux are reached, particularly for the 650 and 900°C activated samples and, although not shown in Figure 6.2, DMMP growth continues for at least 100 h. Therefore, during this stage, isomerization is the major process occurring.

The data given in row 1 of Table 6.3 show that, for the three samples studied, there is more DMP at the plateau for a lower activation temperature. It follows that there is also proportionally less "free space" on these samples. That is, for the highest SiOH surface density initially, a greater proportion of the surface is occupied by DMP and $SiOCH_3$ at the plateau. It is not possible to determine whether it is the reduction in this "free space" or the greater amount of DMP that inhibits the rate of formation of DMMP. However, given that isomerization is still a relatively facile process on a methoxylated surface which contains a small number of SiOH and almost no DMP, we suggest that the greater quantity of DMP produced on the more highly hydroxylated silica is probably the major contributing factor. More DMP combined with less "free space" probably severely inhibits diffusion of reactants and products on the surface, making it more difficult to achieve the necessary transition state for isomerization. Further speculation is unwarranted.

(f) Reactions at Higher Temperatures

The reaction between TMP and silica at 100°C generated DMP rapidly and the reaction went to completion in about 4 h. That the intensity in the P—H spectral region (Figure 6.7) did not increase with time after the initial introduction of TMP is presumably related to the desorption of H-bonded DMP as SiOH were consumed. During the course of the reaction the H-bonded peak at 2457 cm^{-1} decreased, whereas that due to physically adsorbed DMP at 2440 cm^{-1} remained relatively constant up to 3.5 h reaction and then decreased for 20 h reaction. This evolution is consistent with the SiO—H spectral region which also shows, by virtue of the decrease in intensity of the isolated and H-bonded silanol bands, that SiOH is consumed more rapidly at this temperature.

As opposed to the reaction at 23°C, a phosphorus-containing chemisorbed species was produced and, most strikingly, no DMMP was generated. The latter result was unexpected and will be discussed first. Recall that this reaction was only studied for a 350°C activated silica.

The vapour pressures of TMP and DMP (and DMMP) are considerable at 100°C and we assume that physical adsorption would be less favourable than at 23°C. The chemisorption reaction which yields DMP is favoured initially over isomerization even at 23°C and this appears to be much more the case at 100°C. Therefore, either the silanols are consumed too rapidly to permit significant isomerization or the residence time which is required to give rise to the necessary transition state for the isomerization of TMP is insufficient at 100°C. Because we cannot measure the activation energies and preexponential factors for either reaction at 23°C, further comment is unwarranted.

The nature of the chemisorbed species formed at 100 or 400°C needs little additional discussion. Species **I** is a relatively minor chemisorbed product during reaction at 100°C and this is relatively stable up to 400°C evacuation. Species **II** containing a PCH_3 functional group is created when the reaction with TMP is carried out at 400°C, or if excess TMP is added at a lower temperature and the sample is subsequently heated to 400°C.

The nature of the reaction at 400°C is obscure because we have found that, if TMP is heated to about 350°C in the absence of silica, some isomerization occurs in the quartz IR cell whereas none occurs below 325°C. Therefore, it is difficult to say whether **II** forms from TMP and silica or from DMMP and silica. Templeton and Weinberg [90] suggested that the reaction of DMMP with Al_2O_3 at 400°C gave a species $(AlO)_3PCH_3$. In spite of having a four-coordinated P atom, their spectrum indicated that a P=O bond was absent. Species **II** definitely has a P=O bond and the assignment is justified based on the limited data available.

Conclusions

The conclusions concerning the reaction of TMP with aerosil silica can be summarized as follows:

(1) At 23°C TMP reacts rapidly initially with SiOH groups on silica to give chemisorbed $SiOCH_3$ and H-bonded DMP. The product DMP inhibits the reaction causing it to virtually cease after about half of the SiOH have been consumed. The inhibition arises because of the very strong H-bonded interaction between DMP and the unreacted SiOH groups.

(2) SiOH catalyzes the isomerization of TMP to DMMP at 23°C and the quantity of DMMP produced increases as the number of SiOH groups decreases. This is related to the decrease in the amount of DMP produced and the blocking effect of DMP on the isomerization. DMMP is also strongly H bonded to residual SiOH groups.

(3) A mechanism for the formation of DMP and DMMP has been suggested and the role of diffusion and steric inhibition has been discussed.

(4) At 100°C the reaction of TMP to give DMP is so strongly favoured that all accessible SiOH are consumed and isomerization of TMP to DMMP does not occur. In addition to DMP, a small quantity of a chemisorbed species having the proposed structure $(SiO)_2P(O)H$ is produced. This species is stable up to 400°C.

(5) When TMP/SiO_2 is heated from 23°C to 400°C, in addition to $SiOCH_3$, a new strongly chemisorbed species having the proposed structure, $(SiO)_2P(O)CH_3$, is produced along with a smaller quantity of an as yet unidentified species. The nature of this reaction is obscure because TMP isomerizes to DMMP in the gas phase at about 350°C, even in the absence of silica.

Finally, this study illustrates the power of a combined IR/NMR approach for studying a problem of this nature. The details provided above could not have been deduced by using either technique alone. We summarize these advantages below.

NMR spectroscopy clearly showed which species were mobile or immobile (physically and H-bonded species as opposed to chemisorbed species) and provided essential quantitative data relative to the proportions of various P-containing species during reaction at 23°C. Such information is difficult to obtain by IR spectroscopy alone.

IR spectroscopy showed details of the fine structure of the adsorption and chemisorption processes, *e.g.* H bonding, changes in H bonding during reaction, and the distinction between H-bonded and physically adsorbed DMP. Infrared experiments quickly demonstrated that $SiOCH_3$ was not a catalyst in the isomerization of TMP to DMMP, and also showed that a chemisorbed species which contained a single $POCH_3$ group could not have been created after reaction at 100°C or 400°C.

CHAPTER 7

Dimethylzinc Adsorbed on Silica

Introduction

Metal alkyl compounds play an important role in the chemical modification of silica and in the characterization of the texture and reactivity of the silica surface. These compounds are generally known to be efficient hydrogen-sequestering (HS) agents, *i.e.* a reaction with surface silanols at room temperature on silica involves the substitution of hydrogen by a metal alkyl derivative. The general form of the reaction between a methyl metal (M = B, Al, Ga, Zn, Cd, Hg, Me = CH_3) and a single surface silanol site on silica may be written as:

$$\text{SiO–H} + \text{Me}_n\text{M} \longrightarrow \text{SiO–M(Me)}_{n-1} + \text{CH}_4 \qquad (1)$$

For the very reactive $AlMe_3$ molecule, however, it has been suggested that other reaction pathways also exist [63,113-118]. In addition to (1) a reaction with vicinal pairs of silanols would result in the formation of a bridged $(SiO)_2AlMe$ species as in reaction 2, and surface siloxane sites would react according to (3).

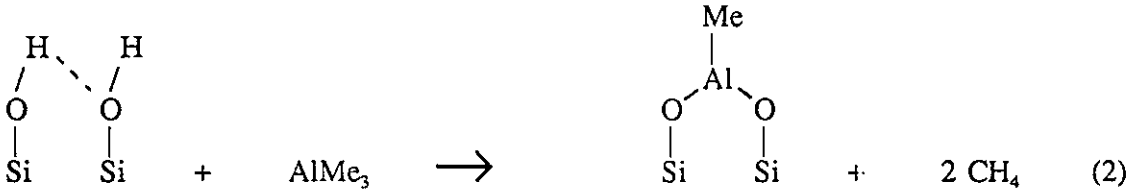

(2)

(3)

Infrared and Raman spectroscopic studies of the chemisorption of $GaMe_3$ on silica [49] have concluded that $GaMe_3$ predominantly reacts according to (1) above, producing surface $SiOGaMe_2$, and that this reaction occurs with single and vicinal pairs of silanols. The extent to which surface siloxane sites react with $GaMe_3$ is very small for silicas activated at temperatures up to 500°C. However, for 1000°C activation, a reaction like (3) occurs with a small number of reactive siloxane sites on the silica surface.

An HS agent possessing a small cross sectional area and which reacts rapidly and monofunctionally at room temperature with surface silanols might be considered to be an ideal probe molecule for characterizing the silica surface. In Chapter 3, we compared several probe molecules and discussed why the best probe would ideally meet all of the above requirements. $AlMe_3$, for example, reacts via (1) and (3) above to produce $SiOAlMe_2$ but only reaction 1 involves surface SiOH, therefore, gravimetric experiments cannot be used to directly relate the mass change of a silica sample reacted with $AlMe_3$ to the number of surface silanol sites. Similarly, CH_4 is a product of reactions 1 and 2 but not reaction 3, therefore, chromatographic determinations of the CH_4 generated in a reaction between $AlMe_3$ and silica can be used to determine the total number of silanols reacting, but cannot be used to determine the coverage of $SiOAlMe_2$ on the surface, or to distinguish between various silanol types which react.

In most cases, a combination of analytical techniques is required in order to overcome problems of the type discussed above for $AlMe_3$. For example, FTIR spectroscopy may be used to aid in surface structure determination, while quantitative data may be obtained from gravimetric and/or chromatographic studies. Alternatively, a great improvement might also be realized using a better probe molecule.

The present investigation has been directed at studying the chemisorption of dimethylzinc ($ZnMe_2$) on aerosil silica in order to assess its utility as a surface probe molecule. $ZnMe_2$ is slightly smaller than $AlMe_3$ (B.E.T. area = 0.257 nm^2 for $ZnMe_2$ compared to 0.321 nm^2 for $AlMe_3$), and is the most accessible of the HS agents studied by

our group (see Chapter 3). Furthermore, because $ZnMe_2$ contains only two methyl groups bonded linearly to zinc, one might expect a single reaction with surface silanol groups on silica, *i.e.*

$$SiO\text{—}H \quad + \quad ZnMe_2 \quad \longrightarrow \quad SiO\text{—}Zn\text{—}Me \quad + \quad CH_4 \qquad (4)$$

$ZnMe_2$ has been used to determine the surface silanol density on silica by quantitatively measuring the methane generated according to reaction 4 in a gas-chromatographic apparatus [119]. However, to our knowledge, no infrared spectroscopic studies of the reaction between $ZnMe_2$ and aerosil silica have been reported to date.

In the present investigation, the chemisorption of $ZnMe_2$ on aerosil silica has been studied by using FTIR spectroscopy (500 to 4000 cm^{-1}) for silica samples activated at 150, 450, and 800°C. The results indicate that the reaction of $ZnMe_2$ with silica is more complicated than expected and cannot be accounted for by reaction 4 alone. Thin film experiments have been carried out in order to uncover low-frequency vibrational modes which might aid in the interpretation of the unusually complex C—H stretching profiles. Possible structures of the chemisorbed products, and factors which may contribute to dimethylzinc's unexpected HS reactivity are discussed.

Results

1. $ZnMe_2$ on 150°C Activated Silica

A reaction between dimethylzinc and A-150 silica at room temperature produced methane in the gas phase and caused significant changes to occur in the infrared spectrum of silica between 2500 cm^{-1} and 4000 cm^{-1}. Figure 7.1A shows the infrared spectrum of A-150 silica (10 mg/cm^2) and Figure 7.1B is the spectrum recorded after complete reaction with excess $ZnMe_2$ at 23°C followed by evacuation at 23°C. The 3747 cm^{-1} band due to isolated

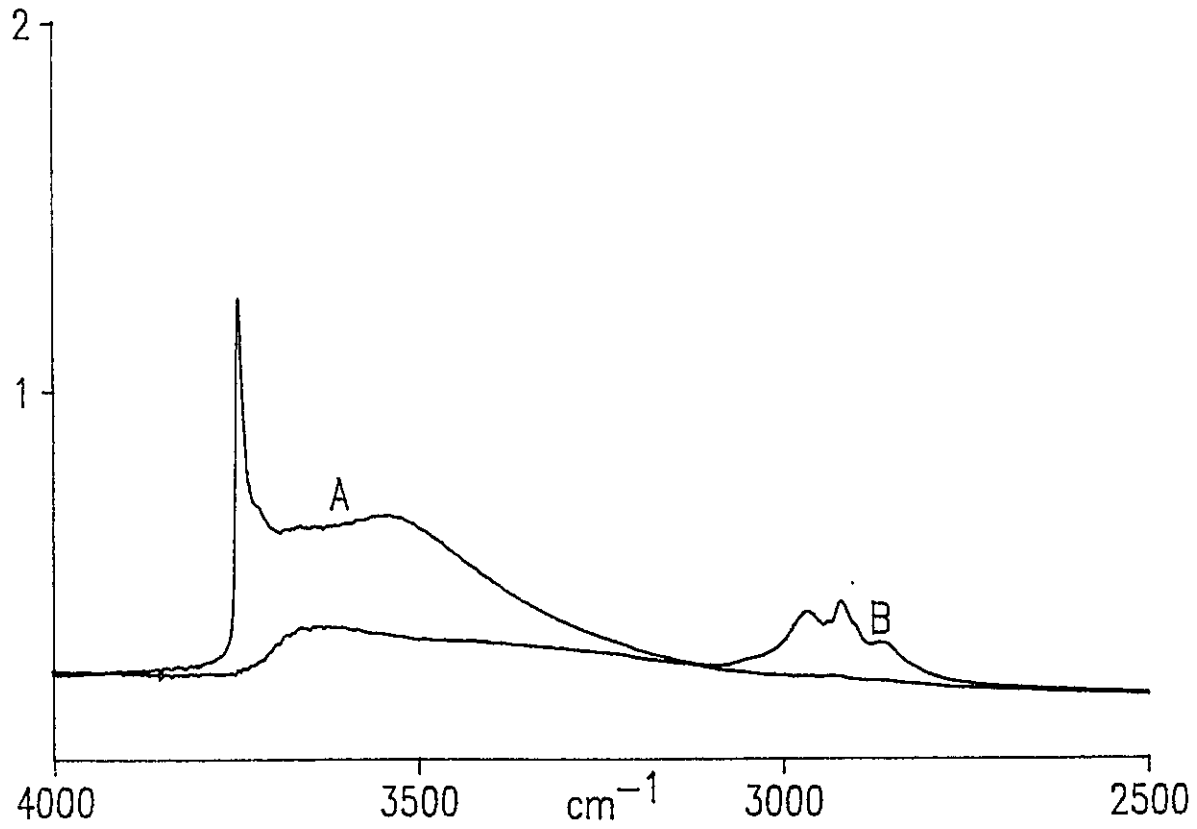

Figure 7.1. Infrared spectrum of 10 mg/cm^2 A-150 silica, (A) before, and (B) after complete reaction with dimethylzinc at 23°C, followed be evacuation at 23°C.

silanols disappeared, along with the terminal SiOH (3720 cm^{-1}) and most of the H-bonded silanols (3520 cm^{-1}). The broad weak band (Figure 7.1B) at about 3660 cm^{-1} which persists after complete reaction is due to silanols which are inaccessible to $ZnMe_2$ (see Chapter 3). The same spectrum also shows new bands appearing at 2964, 2920, and 2860 cm^{-1} with a much weaker band at 2937 cm^{-1} and a shoulder at 2900 cm^{-1}. These bands all appear in the expected frequency range for methyl C–H stretching modes belonging to chemisorbed products of the $ZnMe_2$/silica reaction.

Figure 7.2 shows a similar set of "before and after" spectra for the partial reaction of $ZnMe_2$ with A-150 silica. In this experiment, a 20 mg/cm^2 sample was used, and the reaction was not allowed to go to completion, *i.e.* any unreacted $ZnMe_2$ and gas-phase CH_4 produced in the reaction were evacuated before the 3747 cm^{-1} band had completely disappeared.

Figure 7.3A shows the difference spectra for the partially reacted sample (Figure 7.2, A minus B) and the totally reacted sample (Figure 7.1, A minus B). The inset of Figure 7.3 is an expanded plot of the 2800 to 3100 cm^{-1} region. Bands having positive intensity in Figure 7.3 are due to spectral features which have been removed and those having negative intensity are due to features which have been produced.

For the partially reacted 20 mg/cm^2 sample, new bands appeared at 2964, 2920, and 2860 cm^{-1} (Figure 7.3A), however, the 2937 cm^{-1} band and the shoulder at 2900 cm^{-1} were not observed, contrary to the spectrum after complete reaction (Figure 7.3B). The difference spectra in Figure 7.3 also show that, in the case of partial reaction with $ZnMe_2$, more H-bonded and terminally H-bonded silanols react relative to isolated silanols; in Figure 7.3A the broad band at about 3550 cm^{-1} and the shoulder at 3720 cm^{-1} are more intense relative to the 3747 cm^{-1} band when compared to Figure 7.3B.

In another experiment, the reaction of $ZnMe_2$ with deuterated A-150 silica was followed by recording spectra at various stages of the reaction. At successive intervals the deuterated sample was exposed to 5 Torr $ZnMe_2$ in the infrared cell for a period of time sufficiently long to cause a noticeable change in the infrared spectrum. Following this, the

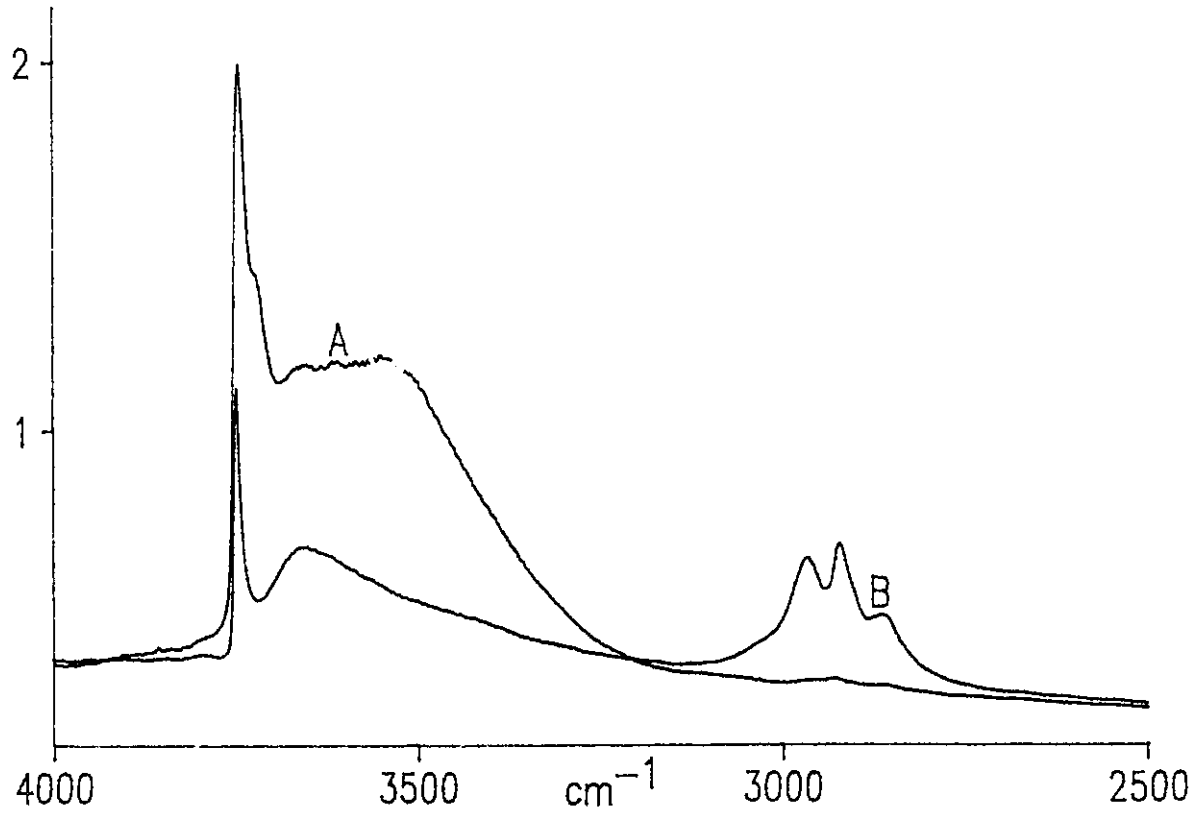

Figure 7.2. Infrared spectrum of 20 mg/cm^2 A-150 silica, (A) before, and (B) after partial reaction with dimethylzinc at 23°C, followed by evacuation at 23°C.

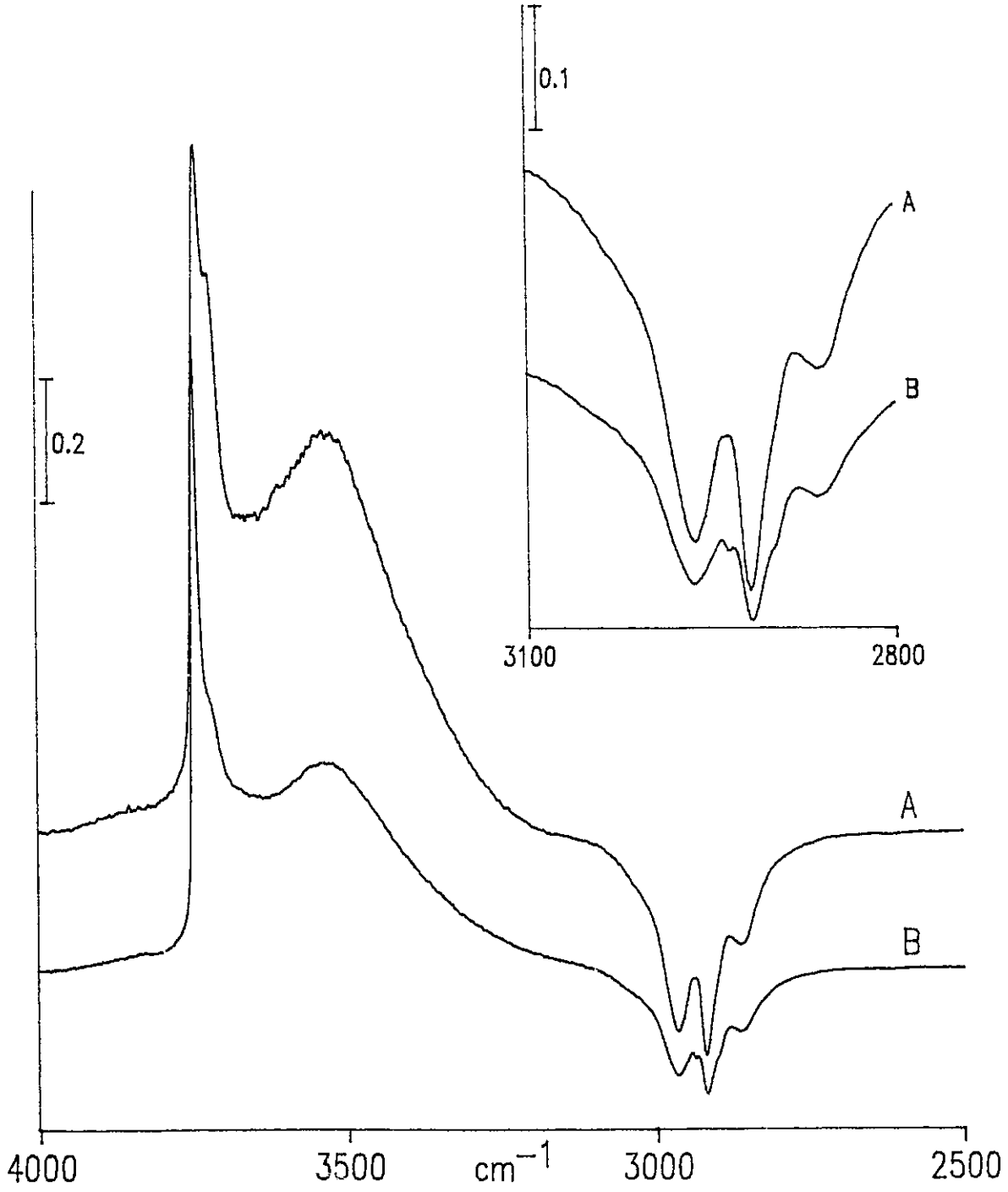

Figure 7.3. Difference spectra showing, (A) partial reaction (Figure 7.2, A minus B), and (B) total reaction (Figure 7.1, A minus B). The inset spectra are expansions of the methyl C–H stretching region.

sample was evacuated at room temperature for 1 minute prior to recording the spectrum in order to remove any residual physisorbed or gas-phase $ZnMe_2$ and gas-phase CH_3D that had been produced during that interval. This brief evacuation was a necessary step because the spectrum of the chemisorbed species on the surface can only be obtained in the absence of both the gas-phase spectrum of $ZnMe_2$ and physically adsorbed $ZnMe_2$. It should also be mentioned that, as the reaction proceeded, longer exposure times were required to produce similar quantities of surface species at each stage of the reaction. Such a procedure could thus be regarded as a spectroscopic titration of the silica surface with $ZnMe_2$, that permits the relative numbers of surface species to be monitored throughout the reaction.

Deuteration of the surface SiOH via D_2O exchange was performed prior to reacting with $ZnMe_2$ so that, in the same experiment, a comparison could be made between $ZnMe_2$ and D_2O regarding their accessibility towards SiOH. D_2O exchange provides a useful means of probing the maximum number of accessible surface silanols without altering the chemical reactivity of the silica surface towards hydrogen-sequestering reagents like $ZnMe_2$. This subject has been addressed in more detail in Chapter 3.

The series of spectra plotted in Figure 7.4 shows the evolution of the reaction of $ZnMe_2$ with deuterated A-150, described above. In the spectrum of the deuterated sample before reaction, Figure 7.4A, the SiO—D stretching mode of the isolated surface silanol was shifted from 3747 cm^{-1} to 2760 cm^{-1} while the hydrogen-bonded and terminal SiO—D stretching vibrations of vicinal H-bonded silanols appeared at 2620 cm^{-1} and 2740 cm^{-1}, respectively. As the reaction proceeded, the SiO—D stretching modes disappeared and were gradually replaced by the C—H stretching modes at 2964, 2920 and 2860 cm^{-1}. This progression is indicated by arrows in Figure 7.4. The weaker bands at 2937 and 2900 cm^{-1} were observed only in the later stages of the reaction (Figure 7.4, E and F) in agreement with the experiments previously discussed for the non deuterated samples.

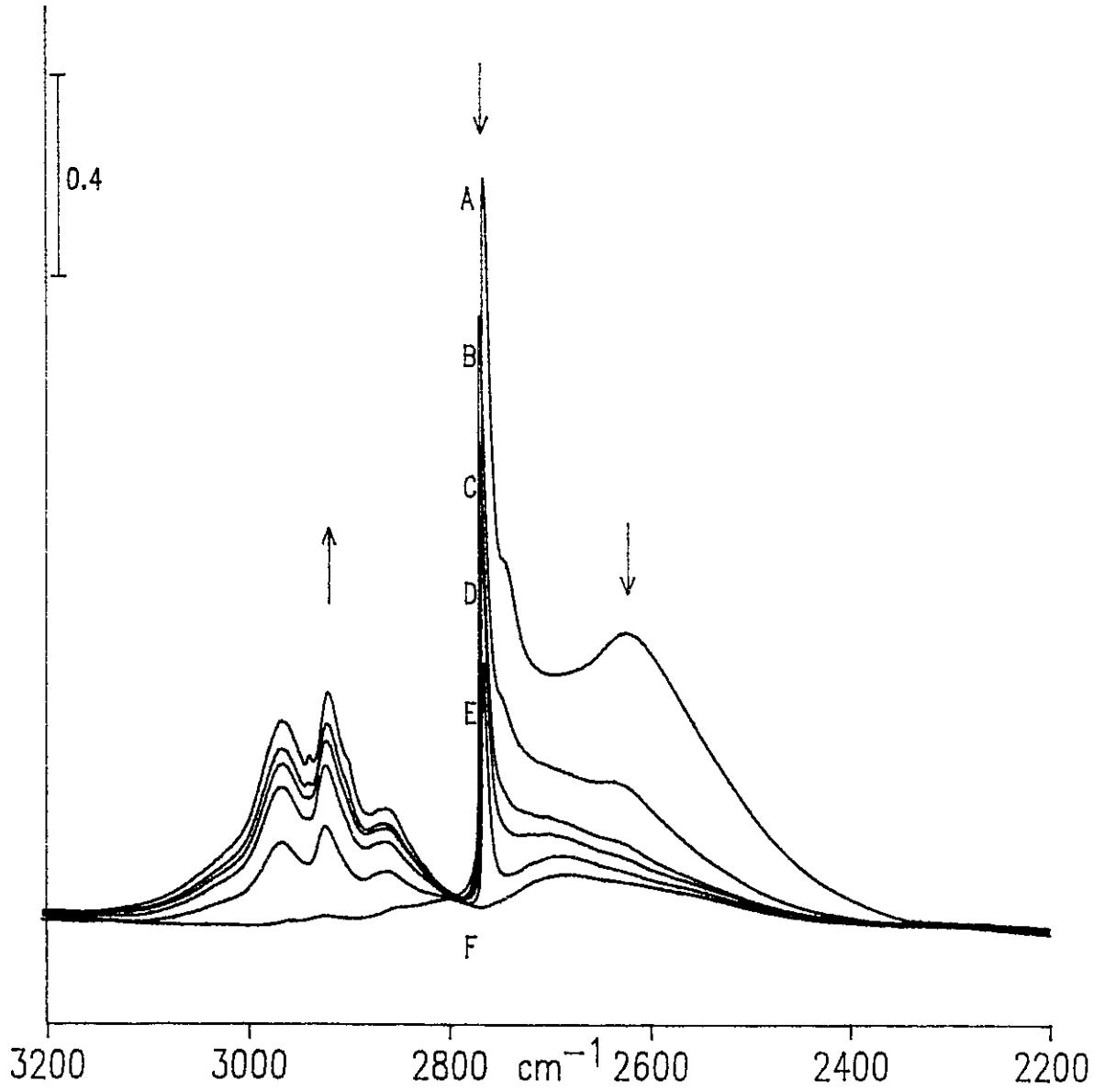

Figure 7.4. (A) Infrared spectrum of deuterated A-150 silica. (B) After exposure of A to 5 Torr dimethylzinc for 1 min followed by evacuation for 1 min at 23°C. (C) After second exposure to 5 Torr $ZnMe_2$ as in (B). (D) After third exposure as in (B). (E) After 3 additional exposures, to 5 Torr $ZnMe_2$ for 2 min followed by 1 min evacuation each at 23°C. (F) After complete reaction with dimethylzinc at 23°C followed by evacuation at 23°C.

In order to show what had reacted or formed during a given interval, difference spectra were computed as follows: the first interval corresponds to Figure 7.4, A minus B, the second interval corresponds to B minus C, *etc.* The difference spectra for the first and last intervals are plotted between 2200 and 3200 cm^{-1} in Figure 7.5 to show the changes in the profiles of both the SiO–D stretching region and the methyl C–H stretching region as the reaction evolved. These difference spectra were also computed such that positive intensity indicates spectral features that disappeared while negative intensity indicates spectral features that formed during a particular interval. Figure 7.5A shows clearly that during the first interval many more H-bonded silanols reacted relative to isolated silanols, whereas during the last interval (Figure 7.5B) reaction occurred almost exclusively with isolated silanols.

Dramatic changes in the profiles of the methyl C–H stretching region were also observed for the series of computed difference spectra. The complete series is shown on an expanded scale in Figure 7.6. The relatively strong bands at 2964, 2920, and 2860 cm^{-1} bands were the only bands observed in Figure 7.6A during the early stages of reaction, although it is possible that very weak 2937 and 2900 cm^{-1} bands could not be resolved in the presence of the much stronger trio. On the other hand, the 2937 and 2900 cm^{-1} bands were clearly seen in the final stages of the reaction (Figure 7.6E), and by this time the intensity of the 2964, 2920, and 2860 cm^{-1} bands had diminished significantly.

The results presented above provide convincing evidence which supports the existence of at least two distinct, chemisorbed species which are products of the reaction between $ZnMe_2$ and a 150°C activated aerosil silica surface. It is apparent that a reaction with isolated or hydrogen-bonded silanols on A-150 produces two different CH_3-containing species, which have characteristic methyl C–H stretching modes in the 2800 to 3000 cm^{-1} region. At this point, the two surface species may be identified as **A** and **B**, respectively, and their C–H stretching frequencies are summarized in Table 7.1. Further comment on the structure of these surface species is reserved for the discussion.

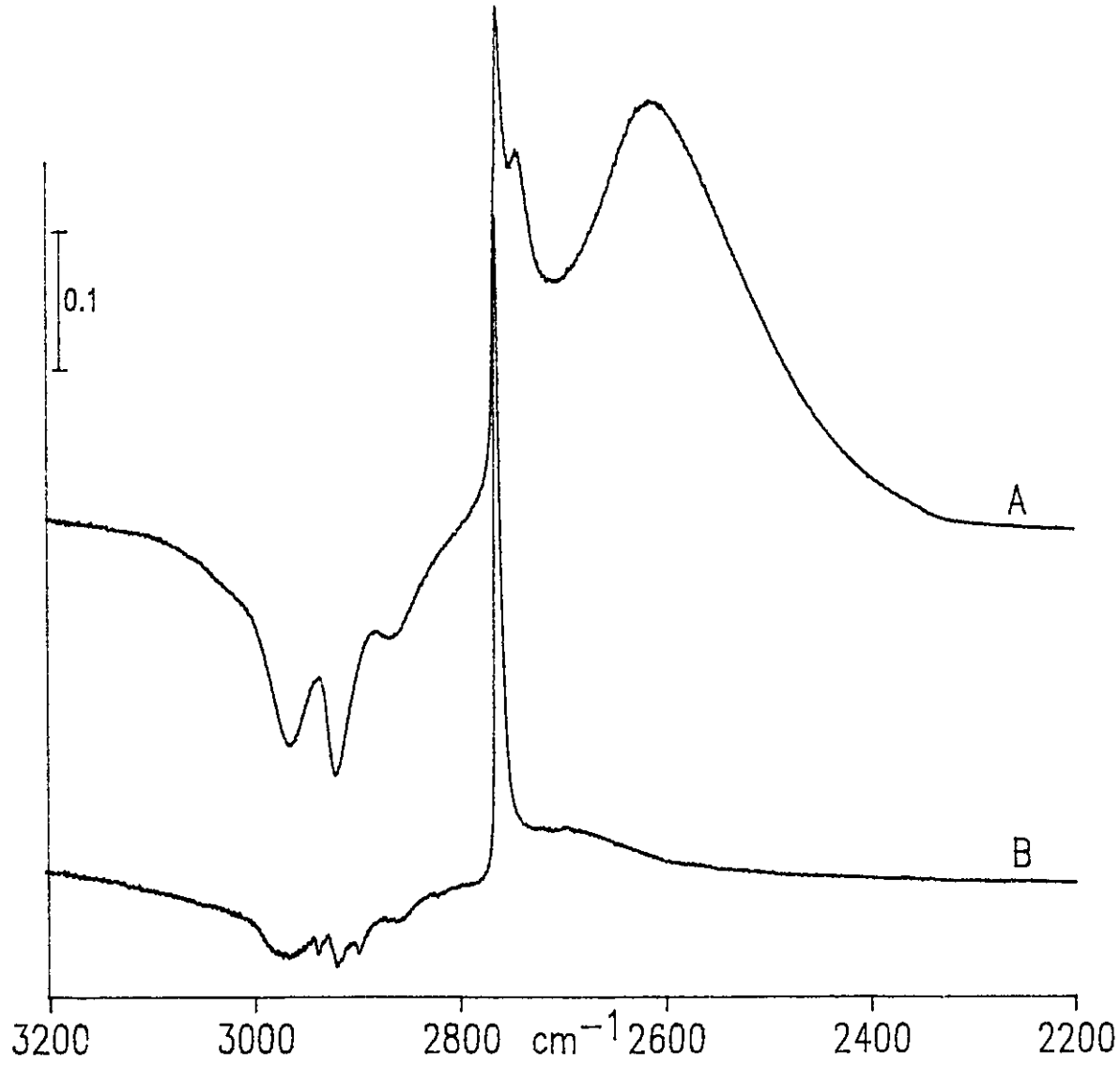

Figure 7.5. Difference spectra for the sample in Figure 7.4 showing what had reacted (A) during the first interval of reaction (Figure 7.4, A minus B), and (B) during the last interval of reaction (Figure 7.4, E minus F).

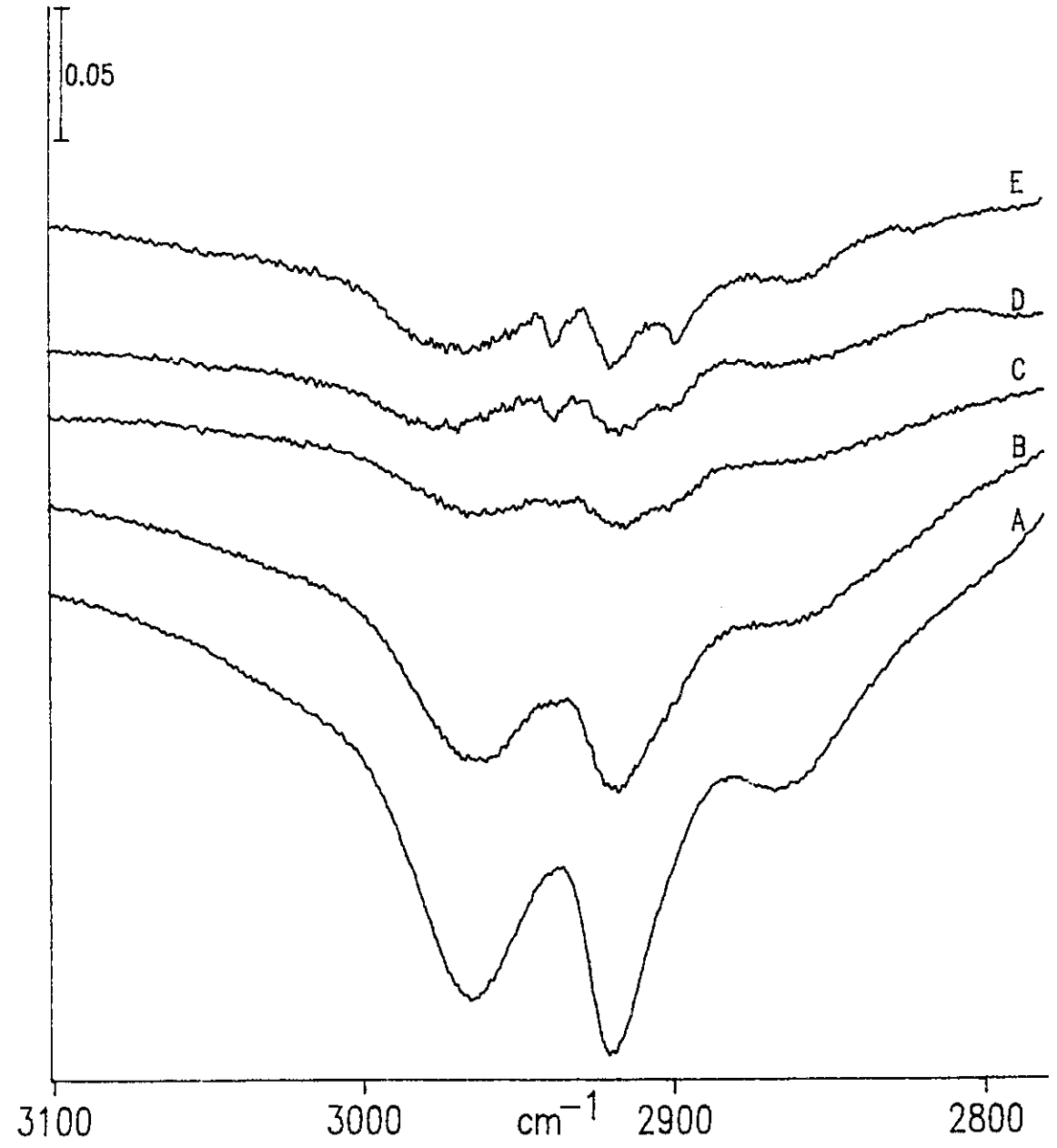

Figure 7.6. Difference spectra showing what was formed (negative intensity) in the methyl C–H stretching region during each stage of reaction for the sample in Figure 7.4, (A) A-B, (B) B-C, (C) C-D, (D) D-E, (E) E-F.

Species A	Species B
2937	2964
2898	2920
2820	2860

Table 7.1. Methyl C–H stretching frequencies (cm^{-1}) for chemisorbed species **A** and **B** on $ZnMe_2$-treated aerosil silica.

2. $ZnMe_2$ on 450°C and 800°C Activated Silica

When aerosil silica is activated at temperatures beyond about 200°C, significant changes in the infrared spectrum occur in the region of the surface SiO–H stretching modes. Between 150°C and 450°C activation the majority of the H-bonded and inaccessible silanols condense to form surface siloxane sites and water is eliminated from the surface. This is accompanied by a slight increase in the number of isolated silanols, from about 1.1 to 1.4 $SiOH/nm^2$, although the total number of accessible silanols decreases (see Chapter 3). Only isolated silanols remain on A-800 silica, but a small number of reactive siloxane sites (about 0.1 sites/nm^2 determined gravimetrically from reaction of A-800 with NH_3) are also created between 450 and 800°C [111,112].

The spectra of 10 mg/cm^2 A-450 and A-800 silica are shown in Figure 7.7A and 7.8A, respectively, and these have been discussed in detail in Chapters 3 and 4. Figures 7.7B and 7.8B are the corresponding spectra recorded after complete reaction of A-450 and A-800 with excess $ZnMe_2$ at room temperature followed by evacuation for 15 min.

The difference spectra showing changes in the silica spectrum for $ZnMe_2$-treated A-450, A-800, and the spectrum for complete reaction with A-150 silica (see Figure 7.3B) are compared in Figure 7.9. For these difference spectra it is possible to make relative comparisons of band intensities and certain trends are clearly seen when absolute intensities

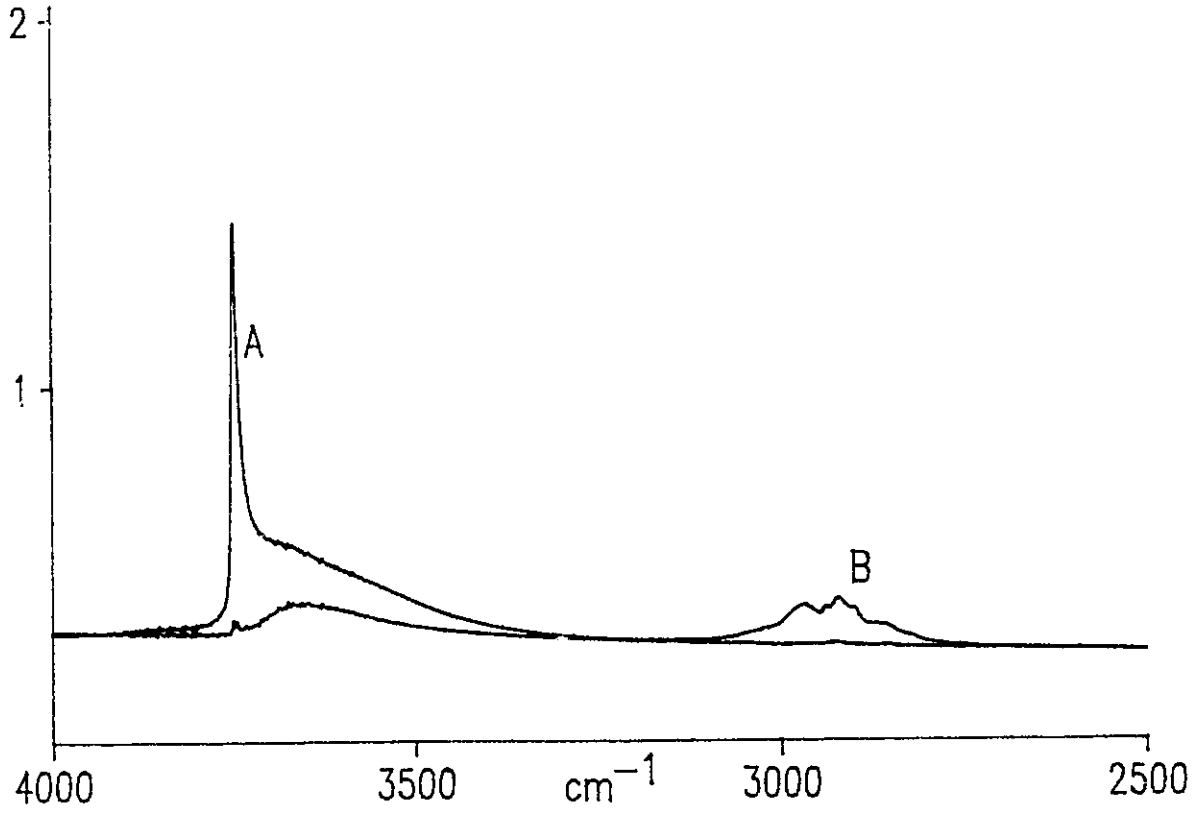

Figure 7.7. Infrared spectrum of 10 mg/cm^2 A-450 silica, (A) before, and (B) after complete reaction with dimethylzinc at 23°C, followed by evacuation at 23°C.

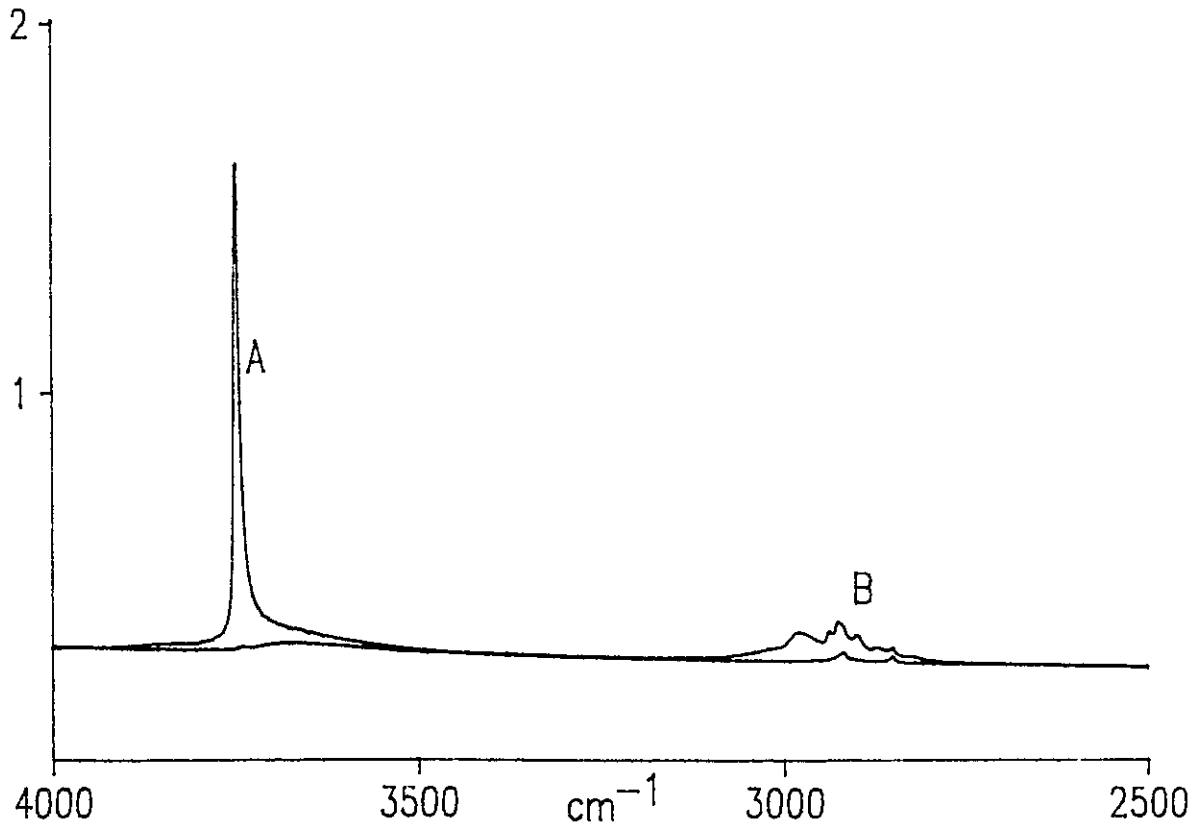

Figure 7.8. Infrared spectrum of 10 mg/cm^2 A-800 silica, (A) before, and (B) after complete reaction with dimethylzinc at 23°C, followed by evacuation at 23°C.

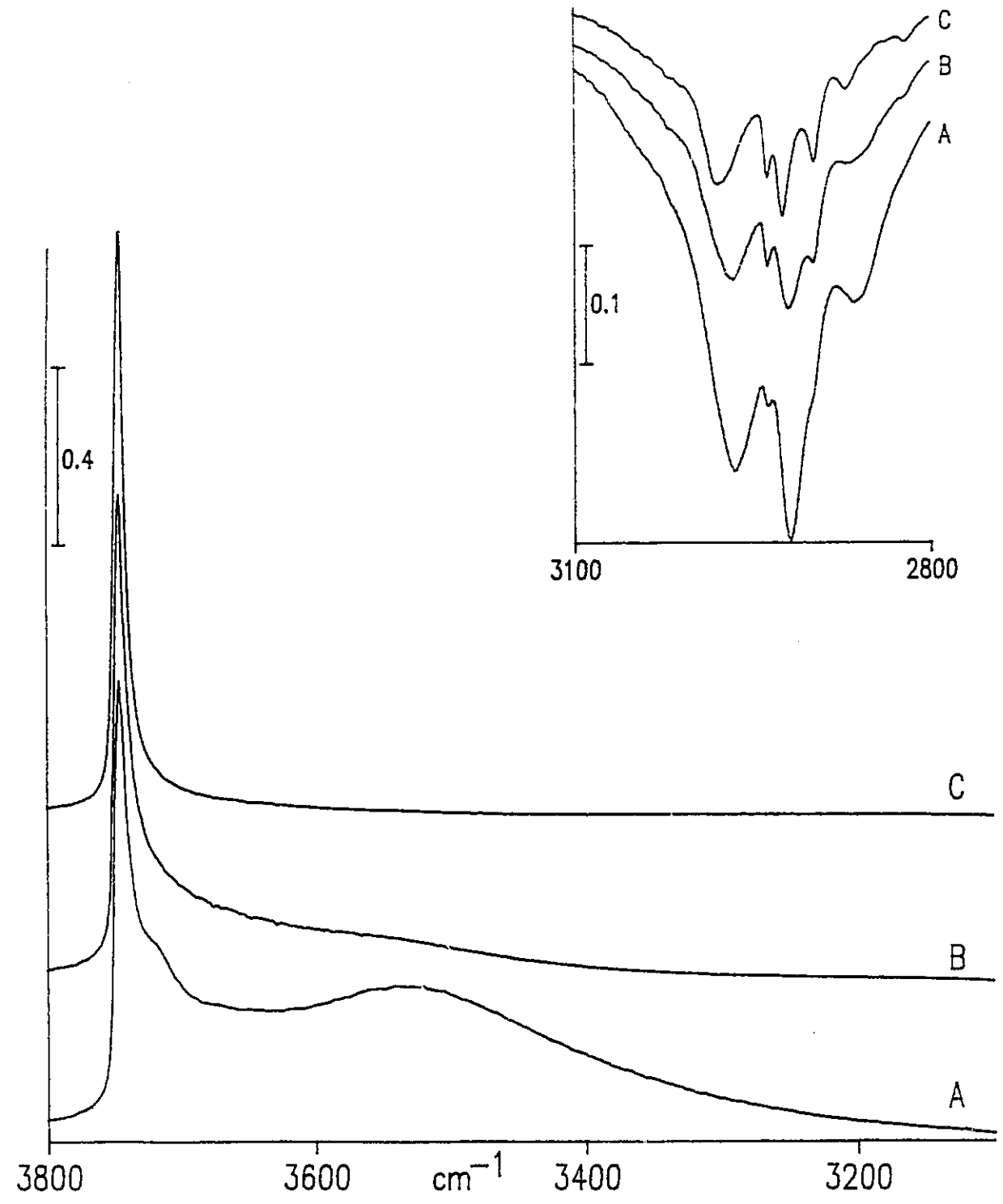

Figure 7.9. Difference spectra showing what had reacted (positive intensity) in the SiO–H stretching profile for complete reaction of dimethylzinc with, (A) A-150, (B) A-450, and (C) A-800 silica. The inset spectra show what was produced (negative intensity) in the methyl C-H stretching region.

are compared (for example, the change in the SiO—H region with increasing activation temperature). However, no attempt has been made to quantify the numbers of surface species which reacted or formed because the spectra were obtained from separate experiments involving different activation temperatures without using a normalization procedure.

The lower traces of Figure 7.9 show the changes which occurred in the SiO—H stretching region during the reaction between $ZnMe_2$ and A-150, A-450, and A-800 silica. Figure 7.9A shows that all of the isolated and most of the H-bonded silanols reacted with A-150. In Figure 7.9B, the sharp band due to isolated silanols (3748-3738 cm^{-1}) is the dominant feature, however, there is a slight tail to lower wavenumber indicating that a small number of residual perturbed silanols (3550-3720 cm^{-1}) also reacted. Figure 7.9C shows that (as expected) only isolated SiOH reacted on A-800.

The upper traces of Figure 7.9 show the same series of spectra in the C—H stretching region using an expanded scale. The difference spectrum for $ZnMe_2$-treated A-450 silica (Figure 7.9B) has two well-resolved bands at 2937 and 2898 cm^{-1}, and a very weak feature at 2820 cm^{-1} in addition to the 2964, 2920, and 2860 cm^{-1} bands. When compared to Figure 7.9A, it is apparent that the 2964, 2920, 2860 cm^{-1} trio in Figure 7.9B diminished relative to the 2937 and 2898 cm^{-1} bands upon increasing the activation temperature from 150°C to 450°C. Additionally, the band maxima in Figure 7.9B shifted from 2964 to 2968 cm^{-1} and from 2860 to 2865 cm^{-1}. The trend con.inues for an 800°C activated sample as shown in Figure 7.9C. The band which appeared at 2968 cm^{-1} is even weaker and has a maximum at 2980 cm^{-1}. The 2920 cm^{-1} band has shifted to 2924 cm^{-1}, and a very weak band appears at 2870 cm^{-1}. The 2937, 2898 and 2820 cm^{-1} bands do not appear to have changed appreciably between 450°C and 800°C activation.

3. Reaction of $ZnMe_2$ with Silica Thin Films

The results presented above have dealt mainly with the 2000 to 4000 cm^{-1} spectral region of silica, where changes in the SiO—H and C—H stretching profiles are easily accessed

using samples containing 10 mg/cm^2 silica. Other vibrational modes associated with $ZnMe_2$-treated silica are buried in the bulk silica modes below 1300 cm^{-1}, and a thin film technique, employing a supported silica film on an inert transparent material must be used to access these surface modes. This technique has been described in Chapter 2 and elsewhere [22].

In an attempt to observe the skeletal modes of the various surface CH_3-containing species produced in the reaction between $ZnMe_2$ and A-150 or A-450, the reaction has been studied using thin silica films supported on either a transparent KBr window or a metal screen (200 mesh Ni or 40 mesh stainless steel). The thin film technique permits access to the total spectral region of silica below 1300 cm^{-1} using transmission infrared spectroscopy; the lower limit of about 400 cm^{-1} is dictated by the interferometer's KBr optics.

The spectrum of A-150 aerosil silica (~0.1 mg/cm^2) before and after complete reaction with $ZnMe_2$ at 23°C is shown in Figure 7.10, A and B, respectively. Figure 7.10, C and D, show the spectrum of the supporting KBr window that was heated under vacuum at 150°C (Figure 7.10C) and was subsequently exposed to 2.3 Torr $ZnMe_2$ at 23°C (Figure 7.10D) in a "blank" experiment. The very weak features at 1306, and 1186 cm^{-1}, and the much stronger bands at 706 and 613 cm^{-1} in Figure 7.10D are due to gas-phase $ZnMe_2$ (see Table 7.1 below) and these bands were completely removed upon evacuation following Figure 7.10D. Thus, the blank experiment confirmed that no reaction occurs with the KBr supporting window which could contribute to the difference spectrum in the thin film experiment.

The difference spectra showing changes which occurred in the silica spectrum as a result of a reaction with $ZnMe_2$ are shown in Figure 7.11. Figure 7.11B is the difference spectrum for reaction with A-150, *i.e.* Figure 7.10, B minus A. Figure 7.11, A and C show the spectral changes for the reaction with A-25 and A-450 silica, respectively. Bands which were created during the reaction appear as positive features in Figure 7.11 while those which were removed appear as negative features. Finally, the spectra in Figure 7.11 have been normalized to the intensity of the bulk silica mode at 475 cm^{-1} so that the intensities in the

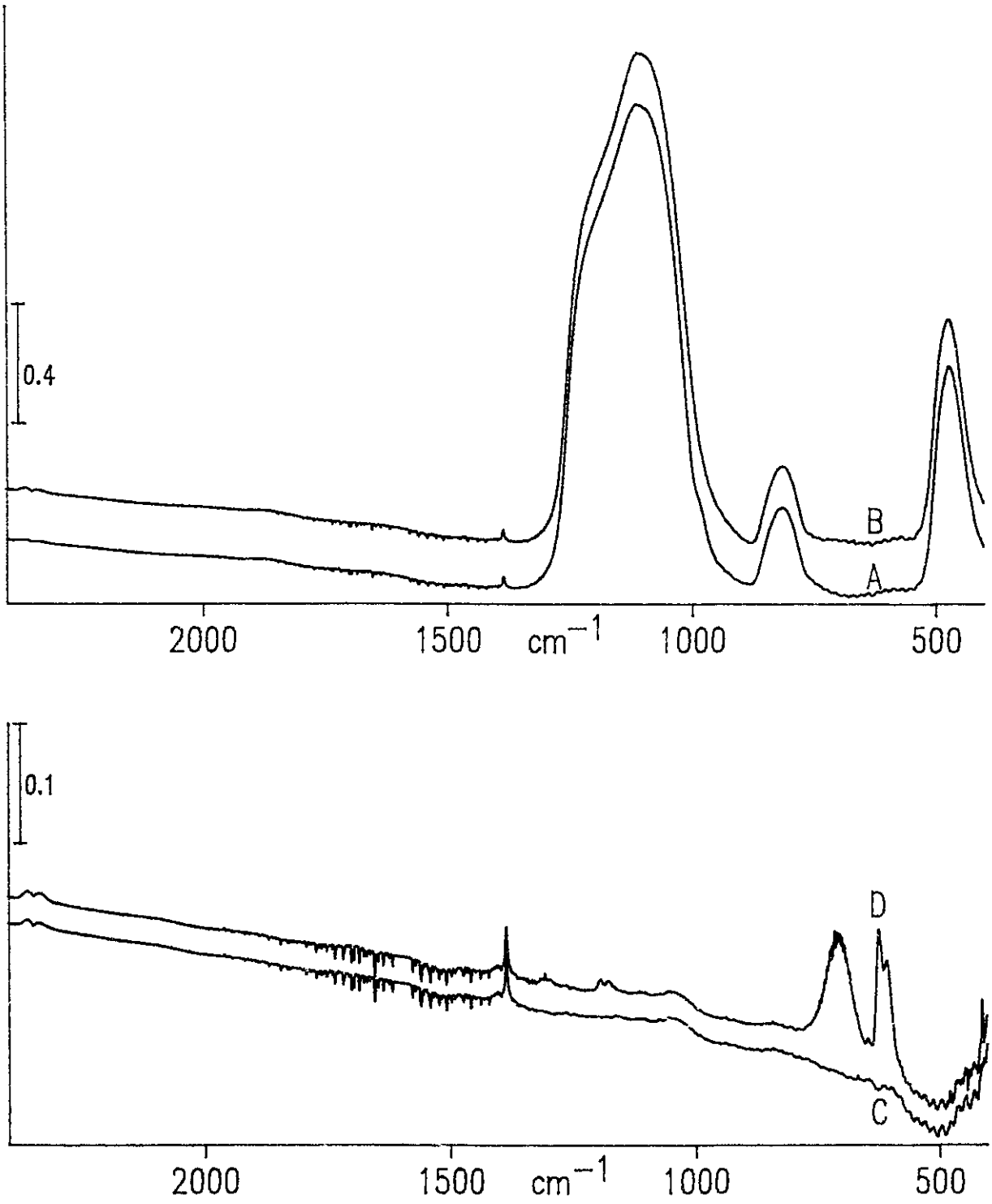

Figure 7.10. Infrared spectrum of A-150 silica thin film (0.2 mg/cm^2), (A) before, and (B) after complete reaction with dimethylzinc at 23°C, followed by evacuation at 23°C.
(C) Infrared spectrum of supporting KBr window after vacuum activation at 150°C.
(D) Infrared spectrum of supporting KBr window and 2 Torr dimethylzinc in a 10 cm gas cell.

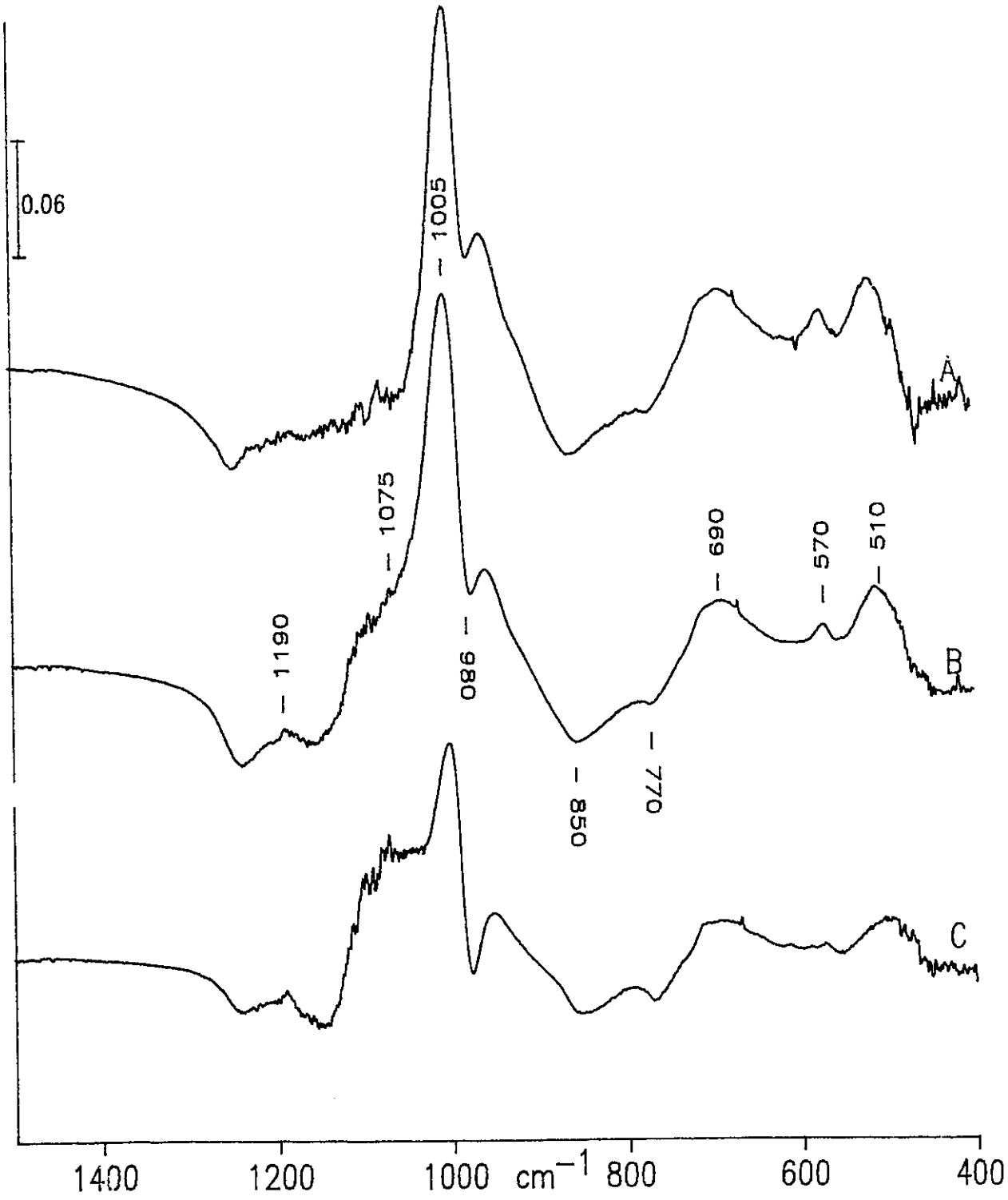

Figure 7.11. Normalized difference spectra (see text) showing spectral changes which occurred during a complete reaction of dimethylzinc with silica thin films activated at (A) 23°C, (B) 150°C, and (C) 450°C. Positive features have been created during the reaction.

difference spectra roughly correspond to thin films containing the same quantity of silica. The peak maxima of the features to be discussed below are labelled in Figure 7.11B.

The reaction between $ZnMe_2$ and surface SiOH on A-25, A-150 and A-450 silica produced a negative band at 980 cm^{-1} due to the Si—OH stretching mode of isolated SiOH, and negative bands at 850 and 770 cm^{-1} due to the SiOH bending modes (Chapter 4). These spectral features were replaced by an intense new band at about 1005 cm^{-1}, which is almost certainly the antisymmetric Si—O—$ZnCH_3$ stretching vibration; a band at 1002 cm^{-1} has been assigned to the antisymmetric Si—O—$GaMe_2$ stretching mode of $GaMe_3$-treated silica [49], and on $AlMe_3$-treated silica this band appears at 1000 cm^{-1} [120]. The intensity of the 1005 cm^{-1} band did not change upon going from 23°C to 150°C activation, but decreased by about a factor of 2 for 450°C activation. We have shown in Chapter 3 that the surface density of accessible SiOH also decreases by a similar amount between 150 and 450°C activation.

Several other band assignments are proposed for $SiOZnCH_3$ based primarily on the gas-phase spectrum of $ZnMe_2$. Table 7.2 summarizes the infrared spectroscopic data in the low-frequency region for gas-phase $ZnMe_2$ [121] and for $ZnMe_2$ adsorbed on silica.

Gas-phase $ZnMe_2$		$SiOZnCH_3$	
$\delta_a(CH_3)$	1301 m		
$\delta_s(CH_3)$	1183 m	$\delta_s(CH_3)$	1190
CH_3 rock	704 vs, br	CH_3 rock	690
$\nu_a(Zn—C)$	613 vs	$\nu(Zn—C)$	570
$\nu_s(Zn—C)$	511 R		
		$\nu_a(Si—O—Zn)$	1075, 1005
		$\nu_s(Si—O—Zn)$	510

Table 7.2. Infrared frequencies (cm^{-1}) of gas-phase $ZnMe_2$ and $ZnMe_2$-treated silica. (vs) very strong. (m) medium. (br) broad. (R) Raman active

Three new bands were observed to lower frequency at 690, 570 and 510 cm^{-1}. The 690 cm^{-1} band is most likely a CH_3 rocking mode; in gas-phase $ZnMe_2$ this mode appears at 704 cm^{-1} and is very intense. The band at 570 cm^{-1} could be assigned to the Zn—C stretching vibration of $SiOZnCH_3$ because this band is expected to lie about midway between the asymmetric and symmetric Zn—C stretching modes of gas-phase $ZnMe_2$ (those frequencies are 613 cm^{-1} and 511 cm^{-1}, respectively). The 510 cm^{-1} band in the spectrum of adsorbed $ZnMe_2$ could possibly be the symmetric Si—O—Zn stretching vibration. Bands at about 490 cm^{-1} have been attributed to ν_s(Si—O—M) in the Raman spectrum of adsorbed $TiCl_4$, HMDS, and $GeClMe_3$ [115], and the ν_s(Si—O—Ga) mode of surface $SiOGaMe_2$ has been assigned to a band at 440 cm^{-1} observed in the Raman spectrum of adsorbed $GaMe_3$ [47,48]. A very weak band appeared at 1190 cm^{-1}, close to the frequency of the symmetric CH_3 deformation mode at 1183 cm^{-1} in gas-phase $ZnMe_2$. This band is most likely the symmetric CH_3 deformation mode of a surface $SiOZnCH_3$ species.

Based on the spectra of the methyl C—H stretching and SiO—H stretching regions presented earlier we have tentatively assigned bands to two different chemisorbed species, **A** and **B**, on $ZnMe_2$-treated silica which are the products of a reaction with isolated and H-bonded silanols, respectively (see Table 7.1). Unfortunately, the spectra in Figure 7.11 do not provide any direct evidence for more than one surface species and, accordingly, we have assigned the low-frequency vibrations to the most likely product, *i.e.* $SiOZnCH_3$ from reaction 4. It is possible that the low-frequency vibrational modes of species **A** and **B** are not well-resolved in Figure 7.11, or that the infrared bands belonging to either species are so weak (due to the small quantity of silica being sampled) that their intensities are approaching the limit of detection. In all likelihood, both of these factors probably contribute to the above problem.

The difference spectra in Figure 7.11 show that, for $ZnMe_2$ reacting with A-150 and A-450, a broad band develops at about 1075 cm^{-1}. (This band is absent in Figure 7.11A, appears as a shoulder in 7.11B, and is even more intense in 7.11C.) The apparent evolution

of the 1075 cm^{-1} band with increasing activation temperature might be associated with the production of more than one type of chemisorbed surface species. Therefore, we have carried out some additional experiments to determine the effects of activation temperature and deuterium exchange of the surface silanols on the spectra in the 1000 to 1300 cm^{-1} region, in an effort to understand the nature of the 1075 cm^{-1} band. These results are presented below.

A series of difference spectra showing the changes in the silica spectrum with increasing activation temperature is shown in Figure 7.12. In each case, the spectrum of A-23 silica was subtracted from the thin-film spectrum of silica which had been activated between 150 and 450°C. In the region below 1000 cm^{-1}, negative features in the spectra can be attributed mainly to the elimination of surface silanols with increasing activation temperature, resulting in the disappearance of the Si—O—H bending vibrations of isolated and H-bonded silanols. The progressive difference spectra also show that Si—O—Si stretching modes centred at 1160 and 1080 cm^{-1} disappear while a strong band is created at about 1005 cm^{-1} and a weak band is created near 1260 cm^{-1}.

It is likely that the spectral changes between 1000 and 1300 cm^{-1} shown in Figure 7.12 are the Si—O—Si stretching vibrations associated with the elimination of vicinal H-bonded surface silanols (and a small number of inaccessible silanols), producing surface siloxane sites. It would be difficult experimentally, by using transmission infrared spectroscopy alone, to determine the exact origin of these SiOSi modes, owing to the large number of possible configurations (some more strained than others) in an amorphous silica. However, as we will show here, these modes are <u>not</u> affected greatly by H/D exchange for A-450 silica and, therefore, are more likely associated with vicinal or H-bonded silanols than isolated silanols.

Figure 7.13, A and B, are the difference spectra obtained after A-450 silica (~0.1 mg/cm^2) was exchanged with ND_3 and subsequently evacuated at 23°C (Figure 7.13A) and at 450°C (Figure 7.13B). Spectral features at around 980, 840, and 760 cm^{-1} are known to be associated with isolated SiOH and have been discussed in detail in Chapter 4, however, that there are few features in the spectrum above 1000 cm^{-1} indicates that this region does not

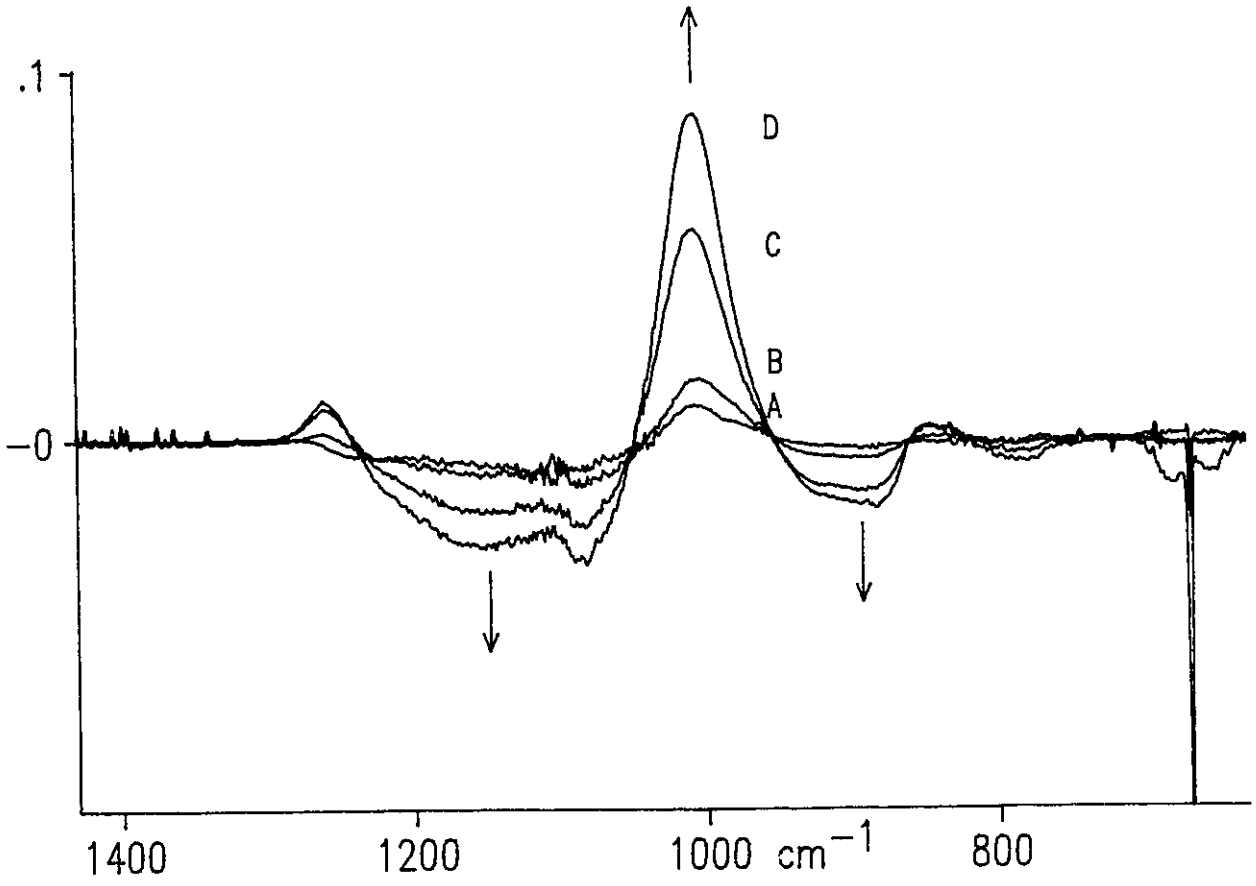

Figure 7.12. Difference spectra showing spectral changes for a silica thin film activated between 23 and 450°C. (A) A-150 minus A-23, (B) A-250 minus A-23, (C) A-350 minus A-23, (D) A-450 minus A-23. Arrows pointing downwards indicate features which are removed with increasing activation temperature.

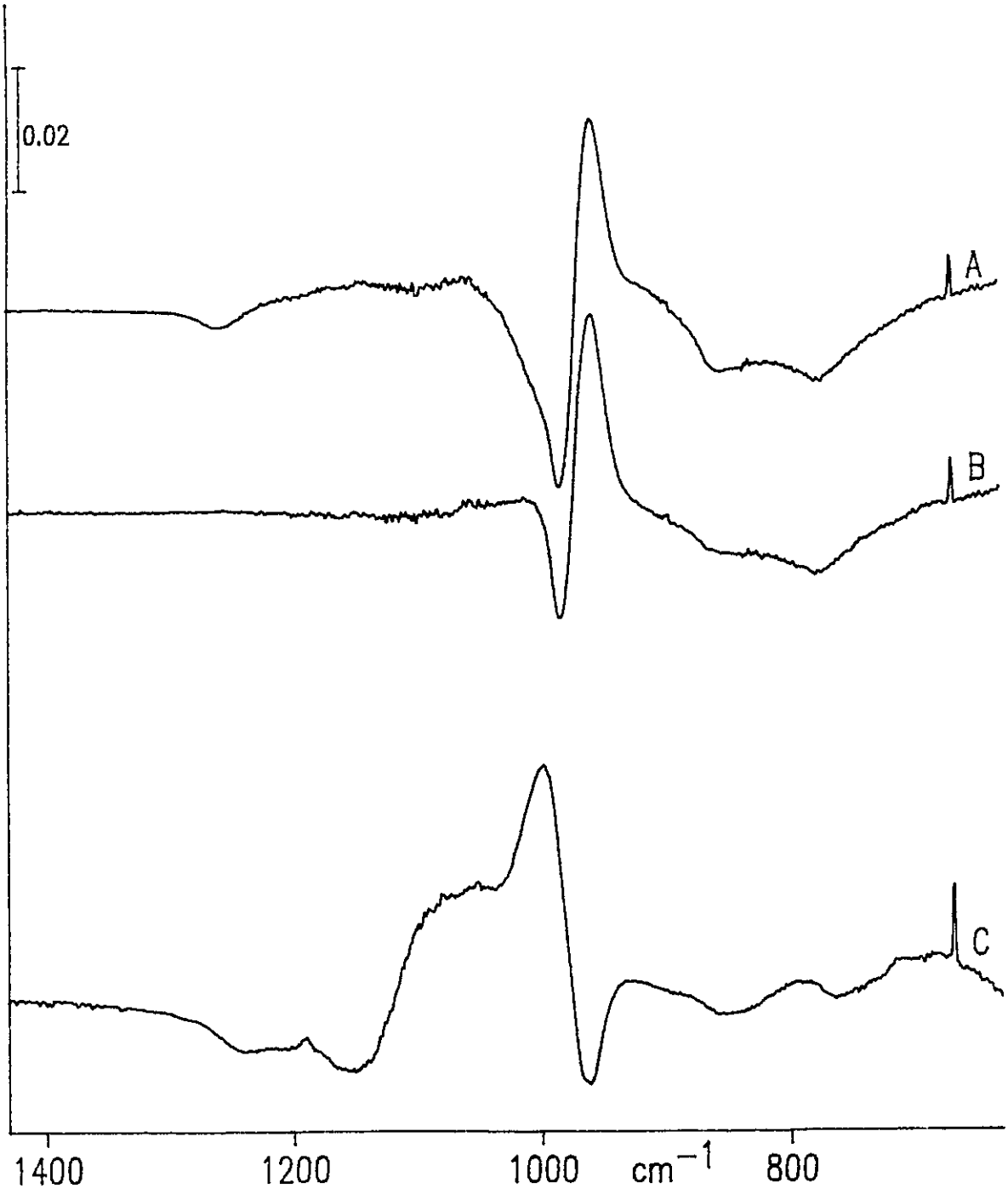

Figure 7.13. (A) Difference spectrum showing spectral changes during H/D exchange of A-450 silica thin film at 23°C followed by evacuation at 23°C. (B) Difference spectrum obtained as in A but followed by evacuation at 450°C. (C) Difference spectrum showing spectral changes for complete reaction of deuterated A-450 silica thin film with dimethylzinc at 23°C followed by evacuation at 23°C.

contain Si—O modes ascribable to isolated SiOH. The weak negative feature at 1260 cm^{-1} in Figure 7.13A may be due to a reaction of a small number of siloxane sites with ND_3 at 23°C; Figure 7.13B shows that reactivating the silica at 450°C after deuterium exchange produces no feature at 1260 cm^{-1}.

Figure 7.13C is the difference spectrum obtained after the deuterated thin film of A-450 silica had been reacted with $ZnMe_2$ at 23°C and evacuated at 23°C (the analogous spectrum for non deuterated A-450 is shown in Figure 7.11C). There are several features here which are typical of a deuterated sample: the negative band due to the Si—OH stretching vibration of isolated SiOD has shifted from 980 cm^{-1} (Figure 7.11C) to 965 cm^{-1}, and weak bands due to residual isolated Si—O—H bending modes appear as negative features at 840 and 760 cm^{-1}. In the 1000 to 1300 cm^{-1} region, Figure 7.13C is almost identical to Figure 7.11C, thereby confirming that the surface modes found in this spectral region are <u>not</u> affected significantly by H/D exchange of isolated SiOH.

<u>Discussion</u>

The results obtained for the reaction of $ZnMe_2$ with A-150 silica have been described in terms of two chemisorbed species, **A** and **B**. The spectroscopic evidence strongly suggests that species **A** is the product of the reaction between $ZnMe_2$ and isolated silanols, whereas species **B** is produced when H-bonded silanols react. Furthermore, it is known that, for a 150°C activated silica surface, there are very few reactive siloxane sites [72,111,112], and in the absence of any experimental evidence to the contrary (discussed further below), we propose that Si-O-Si do not play a significant role in the reaction of $ZnMe_2$ with A-150 silica.

The reaction between isolated silanols on A-150 silica and $ZnMe_2$ could produce species **A** according to reaction 5:

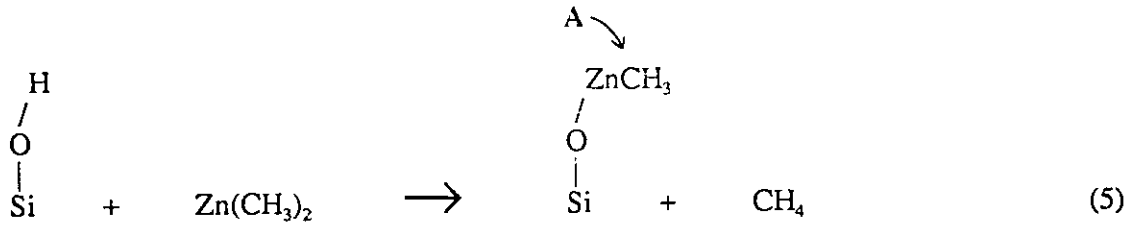

(5)

Because the isolated silanols occupy sites which are sufficiently far apart so that H-bonding interactions with other surface silanols does not occur, one would expect that species **A** also occupies relatively unhindered sites on the chemically modified silica surface. Moreover, bonding of species **A** to the silica surface presumably occurs through a linear O—Zn—C bond where the coordination number of Zn is 2, as in gas-phase $ZnMe_2$.

Dimethylzinc and methylzinc halides are known to form stable complexes with electron-donor ligands such as pyridine, bipyridine, Et_2O or THF so that the zinc centre is tetracoordinated. Infrared and Raman data for the skeletal vibrations of these complexes in the liquid and solid state indicate that complexation with donor ligands tends to lower the Zn—C symmetric and antisymmetric stretching frequencies; the extent to which this occurs is an indication of the ligand's donor ability [122].

Two other interesting alkylzinc complexes involving tetracoordinated zinc are methylmethoxyzinc tetramer, $(MeZn(OMe))_4$, and methyl(trimethylsiloxy)zinc tetramer, $(MeZn(OSiMe_3))_4$. These complexes have a structure whereby Zn is coordinated to 3 oxygen atoms and one methyl group. In an infrared spectroscopic study of the latter compound, bands at 541 and 437 cm^{-1} were assigned to the Zn—C stretch and the Zn—O stretching vibrations, respectively [123].

It is apparent that steric factors may play an important role in determining whether species **A** or **B** is formed on the silica surface. If a vicinal pair of H-bonded silanols reacted according to the scheme shown above for isolated silanols, it is not unreasonable to suggest that steric interactions between the neighbouring methyl groups might cause a shift in the methyl C—H stretching frequencies. An alternative explanation for the formation of species **B**

takes into account dimethylzinc's tendency to form stable complexes with electron donor ligands. Whereas a single Zn—O bond is formed in the reaction with isolated silanols, the proximity of vicinal silanols could result in the formation of a methylzinc species coordinated by two vicinal surface oxygens, *i.e.*

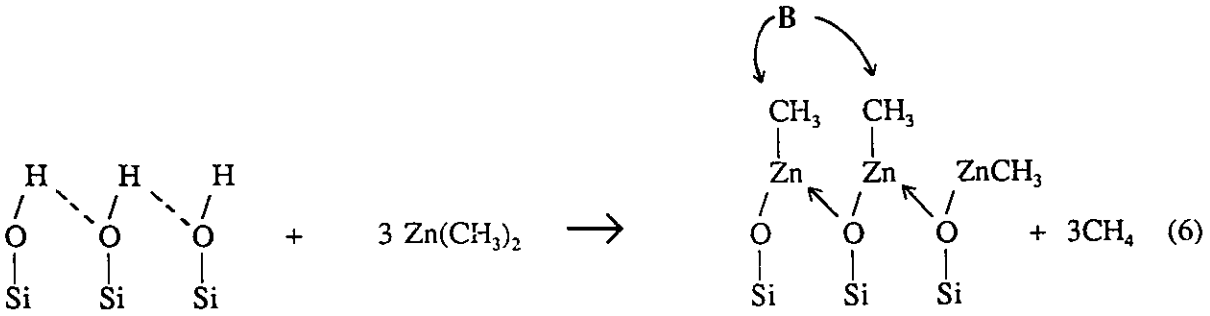

(6)

A change in electron density on the coordinated metal for the bidentate species **B** could alter the methyl C—H bond strength slightly, thereby causing the asymmetric and symmetric C—H stretching frequencies to shift from those observed for species **A**.

The characteristic product of the reaction between surface siloxane sites and $M(CH_3)_n$ is surface $SiCH_3$ (see reaction 3 for $AlMe_3$), and the antisymmetric and symmetric methyl C—H stretching frequencies for this surface species should be close to those observed in compounds having methyl groups attached to Si. For example, in the Raman spectrum of trichloromethylsilane adsorbed on silica, bands have been observed at 2983 and 2915 cm^{-1}, and these have been assigned to the antisymmetric and symmetric C—H stretching modes, respectively, of $SiOSi(CH_3)Cl_2$ [115]. Infrared bands at 2983 and 2925 cm^{-1} have been assigned to $SiCH_3$ produced in the reaction of siloxane sites on A-500 silica with trimethylgallium [49], and a band at 2980 cm^{-1} has been similarly assigned in the spectrum of dissociatively chemisorbed methane on reactive silica [124].

It is often difficult to observe the C—H stretching modes of surface $SiCH_3$ in the presence of much stronger $SiOM(CH_3)_n$ C—H stretching bands. Subsequent hydrolysis or reaction with HCl at room temperature is expected to remove the latter species preferentially leaving only $SiCH_3$ on the surface [47,49,63]. Therefore, we carried out the following

experiments in order to determine if $SiCH_3$ is produced in a reaction between $ZnMe_2$ and surface siloxane sites on silica.

A sample of A-150 silica that had been completely reacted with $ZnMe_2$ and evacuated at 23°C (Figure 7.1) was subsequently reacted with water at 23°C and evacuated at 23 and 150°C. This virtually eliminated bands in the C–H stretching region and the isolated SiOH band was partially restored (along with a broad feature due to H-bonded species). Gas-phase CH_4 was also detected as a product of the hydrolysis reaction which presumably yields surface SiOH and additionally, SiOZnOH and/or ZnO. We concluded that $SiCH_3$ was not produced on $ZnMe_2$-treated A-150.

When 20 mg/cm^2 of $ZnMe_2$-treated A-800 silica (see Figure 7.9C for similar spectrum of C–H stretching region) was subsequently reacted with excess HCl for 10 min at 23°C and evacuated for 2 min at 23°C, a pair of weak bands remained at 2983 and 2925 cm^{-1}, the SiOH band at 3748 cm^{-1} was restored to about 90% of its initial intensity, and a very broad band typical of hydrogen bonding extended from about 3400 to 2800 cm^{-1}. A band at 3016 cm^{-1} with the gas-phase present in the infrared cell indicated that CH_4 had been produced in the reaction with HCl. Given that the isolated SiOH band was almost completely restored, we expect that the other product of the reaction was $ZnCl_2$ adsorbed on the silica surface, *i.e.*

$$SiOZnCH_3 + 2\,HCl \longrightarrow SiOH + CH_4 + ZnCl_2 \qquad (7)$$

For the A-800 sample, the intensity of the relatively sharp 2983 cm^{-1} band was less than 0.02 absorbance for a 20 mg/cm^2 sample, indicating that although some $SiCH_3$ was present, this surface species probably cannot account for all of the intensity at about 2980 cm^{-1} in the rather complex C–H stretching profile shown in Figure 7.9C. In addition to **A**, **B**, and $SiCH_3$ on the surface of $ZnMe_2$-treated A-800, other species may also exist, however, our present data do not allow us to speculate further about their possible structure.

It was hoped that the thin film experiments with A-150 and A-450 (Figure 7.11, B and C) would provide spectroscopic evidence for the two chemisorbed surface species, **A**, and **B**. The frequency of the symmetric methyl deformation band in methyl aluminum compounds is generally sensitive to the electron-donating ability of the ligands on the metal. For example, $\delta_s(Al—CH_3)$ is observed at, 1173 cm^{-1} in $[MeAlCl_3]^-$ [125], 1185 cm^{-1} in $Me_3Al{\leftarrow}OMe_2$ and 1194 cm^{-1} in $Me_2(Cl)Al{\leftarrow}OMe_2$ [126], 1192 cm^{-1} in $(Me_2AlOSiMe_3)_2$ [127], 1208 cm^{-1} in $(Me_2AlOMe)_3$ [128], and 1208 cm^{-1} in Al_2Me_6 [129]. We anticipated that the group frequencies of the chemisorbed $SiOZnCH_3$ species might exhibit a similar trend. Similarly, evidence for two Zn—C stretching vibrations might have been used to distinguish **A** and **B** on the surface, however, only one methyl deformation band and one Zn—C stretching band were observed and these were both very weak (this is partly due to the small quantity of silica being sampled). Furthermore, only one methyl rocking mode ($690cm^{-1}$) was observed although this band was broad and poorly resolved. To summarize, there is no evidence for methyl vibrations below 1300 cm^{-1} which would confirm that several chemisorbed species are present, however, other bands may exist which cannot be detected here.

The combined spectra shown in Figures 7.11-7.13 suggest that the two features at about 1075 cm^{-1}, and 1000 cm^{-1} are associated with surface Si—O—ZnMe stretching modes. It is apparent from this work that the disappearance of H-bonded silanols during the reaction with A-25 or A-150 may explain, in part, why the 1075 cm^{-1} feature appears to increase in intensity with increasing activation temperature (Figure 7.11). From the spectra in Figure 7.12 (showing changes in the spectrum of silica associated with the condensation of vicinal silanols), we expect that during a reaction with $ZnMe_2$ on A-25 or A-150 the simultaneous disappearance of bands at 1160 and 1080 cm^{-1}, and the formation of a band at 1075 cm^{-1}, would produce a spectral artefact in this region. The present infrared data do not permit a more conclusive assignment to the 1075 cm^{-1} band.

It is fortuitous that dimethylzinc reacts more slowly with surface silanols than other HS agents. We have shown in Figure 7.4 that a complete reaction with 10 mg/cm^2 A-150

silica occurs in about 15 min at 23°C. By comparison, $AlMe_3$ and $TiCl_4$ completely react away the surface silanols in about 12 s, and 1 min, respectively, at 23°C (see Chapter 3). Time-resolved FTIR studies of the SiO—H stretching profile during the $AlMe_3$ reaction indicate that the ratio of the number of isolated silanols to the number of H-bonded silanols which react in a given time interval does not change appreciably as the reaction proceeds, although for such a fast reaction, diffusion of the reactant to the surface sites may be a limiting factor. Because the time intervals required to produce Figure 7.4 were 1 min or greater, it was possible to halt the dimethylzinc reaction by evacuating excess reactant at each interval, in order to obtain a signal-averaged spectrum. Finally, that the isolated silanols were the last to react with $ZnMe_2$ on A-150 silica suggests that an interaction with neighbouring silanols may facilitate the reaction, however, there is insufficient data to permit further speculation about possible reaction mechanisms.

Conclusions

This study has shown that the chemisorption of dimethylzinc on aerosil results in the formation of at least three different surface species, depending on the activation temperature employed. On aerosil silica activated at 150°C, dimethylzinc reacts with isolated and hydrogen-bonded silanols producing two chemisorbed species, **A** and **B**, and we have suggested that these coordinate to the surface by one and two Zn—O bonds, respectively. For 450°C activation, the reaction with isolated silanols predominates, however, a small number of H-bonded silanols which do not condense between 150 and 450°C also react. A small number of reactive siloxane sites react with dimethylzinc on aerosil activated at temperatures greater than about 450°C, producing surface $SiCH_3$. On $ZnMe_2$-treated A-800 silica, products of a reaction with isolated silanols and siloxane sites are the major chemisorbed species observed.

Thin film experiments for the purpose of aiding in the characterization of the various

chemisorbed products, were successful to an extent: although several low-frequency modes associated with surface $SiOZnCH_3$ were observed, poor sensitivity and possibly band overlap prevented the detection of infrared bands ascribable to individual species. Other techniques such as Raman or IR-PAS might be more effective for identifying these bands.

The present study has shown that the chemisorbed products in the reaction between dimethylzinc and isolated or H-bonded silanols are different. Ironically, the molecule least likely to react bifunctionally with vicinal silanols has produced the most convincing evidence in favour of such a reaction. The implication here is that, if dimethylzinc can coordinate through 2 surface oxygens, then other more reactive HS agents of similar steric dimensions ($AlMe_3$, $GaMe_3$, BCl_3) probably also react bifunctionally.

Is $ZnMe_2$ the perfect probe molecule? Perhaps not. On the other hand, dimethylzinc's ability to manifest its reactivity toward isolated and H-bonded silanols in the methyl C-H stretching profile is a remarkable feature which has not been observed in reactions of other HS agents with silica. This unexpected reactivity may prove to be valuable for understanding the reactivity of other HS agents on silica, and for this reason, we intend to carry out FTIR studies of the reaction of dimethylcadmium ($CdMe_2$) with silica in order to determine if similar results are obtained with the cadmium analogue as were obtained with $ZnMe_2$. In principle, the $CdMe_2$ reactions could also be studied by using solid state Cd NMR, and the combined NMR-IR technique could eventually lead to conclusive evidence regarding the structure and surface densities of the various methyl-containing surface species that are produced.

REFERENCES

1. R. K. Iler " The Chemistry of Silica ", John Wiley & Sons, New York, N.Y. (1979).

2. A. P. Legrand, H. Hommel, A. Tuel, A. Vidal, H. Balard, E. Papirer, P. Levitz, M. Czernichowski, R. Erre, H. Van Damme, J. P. Gallas, J. F. Hemidy, J. C. Lavalley, O. Barrès, A. Burneau, Y. Grillet *Adv. Colloid Interface Sci.* **33**, 91-330 (1990).

3. M. Hair " Infrared Spectroscopy in Surface Chemistry ", Marcel Dekker, New York, N. Y. (1967).

4. A. V. Kislev, V. I. Lygin " Infrared Spectra of Surface Compounds ", John Wiley & Sons, New York, N.Y. (1975).

5. S. J. Gregg, K. S. W. Sing " Adsorption, Surface Area and Porosity ", Academic Press Inc. (London) Ltd. (1982).

6. Cabot Corporation, Technical Bulletin (1986).

7. R. K. Harris, C. T. Knight, D. N. Smith *J. Chem. Soc. Chem. Commun.*, 726 (1980).

8. R. K. Harris, C. T. Knight *J. Chem. Soc. Faraday Trans. 2* **79**, 1525 (1983).

9. P. C. Hiemenz " Principles of Colloid and Surface Chemistry ", Marcel Dekker Inc., New York, N.Y. (1977).

10. S. Brunauer, P. H. Emmett, E. Teller *J. Am. Chem. Soc.* **60**, 309 (1938). See also, A. L. McClellan, H. F. Harnsberger *J. Colloid Interface Sci.* **23**, 577 (1967).

11. B. B. Mandelbrot " The Fractal Geometry of Nature ", W. H. Freeman, New York, N.Y. (1982).

12. D. Avnir, P. Pfeifer *J. Chem. Phys.* **79**, 3558 (1983).

13. D. Avnir, D. Farin, P. Pfeifer *J. Chem. Phys.* **79**, 3566 (1983).

14. D. Avnir, D. Farin, P. Pfeifer *Nature* **308**, 261 (1984).

15. A. J. Hurd, D. W. Schaefer, J. E. Martin *Phys. Rev. A* **35**, 2361 (1987).

16. A. J. Hurd, D. W. Schaefer, D. M. Smith, S. B. Ross *Langmuir* **4**, 977 (1988).

17. J. Mathias, G. Wannemacher *J. Colloid Interface Sci.* **125**(1), 61 (1988).

18. B. A. Morrow, A. J. McFarlan *J. Non-Cryst. Solids* **120**, 61 (1990).

19. A. Burneau, O. Barrès, J. P. Gallas, J. C. Lavalley *Langmuir* **6**, 1364 (1990).

20. L. T. Zhuravlev *Langmuir* **3**, 316 (1987).

21. P. R. Griffiths, J. A. de Haseth " Fourier Transform Infrared Spectrometry ", (Chemical Analysis; Vol. 83) John Wiley & Sons, New York, N.Y. (1987).

22. B. A. Morrow, C. P. Tripp, R. A. McFarlane *J. Chem. Soc. Chem. Commun.*, 1282 (1984).

23. P. Hoffmann, E. Knözinger *Surface Sci.* **188**, 181 (1987).

24. P. Van der Voort, I. Gillis-D'Hammers, E. F. Vansant *J. Chem. Soc. Faraday Trans.* **86**(22), 3751 (1990).

25. F. H. Hambleton, J. A. Hockey, J. A. G. Taylor *Nature* **208**, 138 (1965).

26. F. H. Hambleton, J. A. Hockey, J. A. G. Taylor *Trans. Faraday Soc.* **62**, 801 (1966).

27. M. Zaborski, A. Vidal, G. Ligner, H. Balard, E. Papirer, A. Burneau, *Langmuir* **5**, 447 (1989).

28. A. Burneau, O. Barrès, J. P. Gallas, J. C. Lavalley *Langmuir* **7**, 1235 (1991).

29. B. A. Morrow, I. D. Gay *J. Phys. Chem.* **92**, 5569 (1988).

30. G. E. Maciel, D. W. Sindorf *J. Am. Chem. Soc.* **102**, 7607 (1980).

31. G. E. Maciel, D. W. Sindorf *J. Am. Chem. Soc.* **105**, 1487 (1983).

32. C. J. Brinker, R. J. Kirkpatrick, D. R. Tallant, B. C. Bunker, B. Montez *J. Non-Cryst. Solids* **99**, 418 (1988).

33. A. Tuel, H. Hommel, A. P. Legrand, Y. Chevallier, J. C. Morawski *Colloids and Surfaces* **45**, 413 (1990).

34. B. A. Morrow, P. Ramamurthy *J. Phys. Chem.* **77**, 3052 (1973).

35. N. K. Hota, C. J. Willis *J. Organometal. Chem.* **9**, 169 (1967).

36. J. F. Hanlan, J. D. McCowan *Can. J. Chem.* **50**, 747 (1972).

37. R. O. Carter III *Appl. Spectrosc.* **40**(2), 272 (1986).

38. P. Hoffman, E. Knözinger *Appl. Spectrosc.* **41**, 1303 (1987).

39. D. B. Chase *Appl. Spectrosc.* **38**(4), 491 (1984).

40. K. Tanabe, M. Misono, Y. Ono, H. Hattori *Stud. Surface Sci. Catal.* **51**, 92 (1989).

41. B. A. Morrow *Stud. Surface Sci. Catal.* **57A**, A161 (1990).

42. J. Chmielowiec, B. A. Morrow *J. Colloid Interface Sci.* **94**, 319 (1983).

43. C. G. Armistead, A. J. Tyler, F. H. Hambleton, S. A. Mitchell, J. A. Hockey *J. Phys. Chem.* **73**, 3947 (1969).

44. A. J. Tyler, F. H. Hambleton, J. A. Hockey *J. Catal.* **13**, 35 (1969).

45. G. Ghiotti, E. Garrone, E. Morterra, F. Boccuzzi *J. Phys. Chem.* **83**, 2863 (1979).

46. M. S. Paterson *Bull. Minéral.* **105**, 20 (1982).

47. R. A. McFarlane Ph. D. Thesis, University of Ottawa (1986).

48. B. A. Morrow, R. A. McFarlane *Langmuir* **2**, 315 (1986).

49. B. A. Morrow, R. A. McFarlane *J. Phys. Chem.* **90**, 3192 (1986).

50 D. W. Sindorf, G. E. Maciel *J. Phys. Chem.* **86**, 5208 (1982).

51. L. R. Snyder, J. W. Ward *J. Phys. Chem.* **70**, 3941 (1966).

52. A. A. Tsyganenko *Russ. J. Phys. Chem.* (Eng. Trans.) **56**(9), 1428 (1982).

53. L. M. Kustov, V. Yu. Borovkov, V. B. Kazanskii *Russ. J. Phys. Chem.* (Eng. Trans.) **59**, 2213 (1985).

54. M. L. Hair, W. Hertl *J. Phys. Chem.* **73**, 2372 (1969).

55. F. H. Van Cauwelaert, P. A. Jacobs, J. B. Uytterhoeven *J. Phys. Chem.* **76**, 1434 (1972).

56. J. A. Hockey *J. Phys. Chem.* **74**, 2570 (1970).

57. B. A. Morrow, I. A. Cody *J. Phys. Chem.* **77**, 1465 (1973).

58. P. R. Ryason, B. G. Russell *J. Phys. Chem.* **79**, 1276 (1975).

59. J. Sauer, K. P. Schröder *Z. Phys. Chemie, Leipzig* **266**, 379 (1985).

60. M. Hino, T. Sato *Bull. Chem. Soc. Jpn.* **44**, 33 (1970).

61. F. Boccuzzi, S. Coluccia, G. Ghiotti, C. Morterra, A. Zecchina *J. Phys. Chem.* **82**, 1298 (1978).

62. T. P. Beebe, P. Gelin, J. T. Yates, Jr. *Surface Sci.* **148**, 526 (1984).

63. R. J. Peglar, F. H. Hambleton, J. A. Hockey *J. Catal.* **20**, 309 (1971).

64. V. M. Bermudez *J. Phys. Chem.* **75**, 3249 (1971).

65. K. Nakamoto " Infrared Spectra of Inorganic and Coordination Compounds ", John Wiley, New York, N.Y. (1970).

66. C. A. Murray, T. J. Greytak *Phys. Rev.* **B20**, 3368 (1979).

67. E. J. Heilweil, M. P. Casassa, R. R. Cavanaugh, J. C. Stephenson *J. Chem. Phys.* **82**, 5216 (1985).

68. A. Burneau, O. Barrès, J. P. Gallas, J. C. Lavalley *Proc. Int. Workshop FTIR Spectroscopy*, Ed. E. F. Vansant, Antwerp, 108 (1990).

69. K. S. Smirnov, E. P. Smirnov, A. A. Tsyganenko *J. Electron Spectrosc.* **54/55**, 815 (1990).

70. A. A. Tsyganenko, J. Lamotte, J. Saussey, J. C. Lavalley *J. Chem. Soc. Faraday Trans. 1* **85**(8), 2397 (1989).

71. G. Herzberg " Infrared and Raman Spectra ", Van Nostrand, New York, N.Y. (1959).

72. B. A. Morrow, I. A. Cody *J. Phys. Chem.* **79**, 761 (1975).

73. S. P. Zhdanov, L. S. Kosheleva, T. I. Titova *Langmuir* **3**, 960 (1987).

74. E. P. Parry *J. Catal.* **2**, 371 (1963).

75. R. S. McDonald *J. Am. Chem. Soc.* **79**, 850 (1957).

76. T. A. Egerton, N. Sheppard *J. Chem. Soc. Faraday Trans. 1* **70**, 1357 (1974).

77. S. A. Zubkov, V. Yu. Borovkov, S. G. Gagarin, V. B. Kazansky *Chem. Phys. Lett.* **107**(3), 337 (1984).

78. S. M. Zeverev, K. S. Smirnov, A. A. Tsyganenko *Kinet. Catal.* **29**(6), 1251 (1988).

79. H. Forster, M. Schuldt *J. Chem. Phys.* **66**(11), 5237 (1977).

80. H. Forster, M. Schuldt *J. Mol. Struct.* **47**, 339 (1978).

81. N. Sheppard, D. J. C. Yates *Proc. Roy. Soc. London* **A238**, 69 (1956).

82. P. Ugliengo, V. R. Saunders, E. Garrone *J. Phys. Chem.* **93**, 5210 (1989).

83. G. C. Pimentel, A. L. McClellan " The Hydrogen Bond ", W. H. Freeman & Co., San Francisco, Ca. (1960).

84. G. Busca, G. Ramis, V. Lorenzelli, P. R. Rossi, A. L. Genestra, P. Patrono *Langmuir* **5**, 911 (1989).

85. K. I. Hadjiivanov, D. G. Klissurski, A. D. Davydov *J. Catal.* **116**, 498 (1989).

86. A. Munnour, C. Ecolivet, D. Cornet, J. F. Hemmidey, J. C. Lavalley *Mat. Chem. Phys.* **19**, 301 (1988).

87. I. L. Mudrakovskii, V. M. Mastikhin, N. S. Kotsarenko, V. P. Mastikhin *Kin. i Katal.* **29**, 165 (1988).

88. R. D. Ramsier, P. N. Henriksen, A. N. Gent *Surface Sci.* **203**, 72 (1988).

89. J. G. Ekerdt, K. J. Kalabunde, J. R. Shaplely, J. M. White, J. T. Yates, Jr. *J. Phys. Chem.* **92**, 6182 (1988).

90. M. K. Templeton, W. H. Weinberg *J. Amer. Chem. Soc.* **107**, 97 (1985).

91. M. A. Henderson, T. Jin, J. M. White *J. Phys. Chem.* **90**, 4607 (1986).

92. V. S. Smentkowski, P. Hagans, J. T. Yates, Jr. *J. Phys. Chem.* **92**, 6351 (1988).

93. B. Aurian-Blajeni, M. M. Boucher *Langmuir* **5**, 170 (1989).

94. M. K. Templelton, W. H. Weinberg *J. Amer. Chem. Soc.* **107**, 774 (1985).

95. S. T. Lin, K. J. Kalabunde *Langmuir* **1**, 600 (1985).

96. M. P. Nadler, R. A. Nissan, R. A. Hollins *Appl. Spectrosc.* **42**, 634 (1988).

97. R. K. Harris " Nuclear Magnetic Resonance Spectroscopy ", Pitman Publishing Inc., Marshfield, Mass. (1983).

98. T. M. Duncan, J. T. Yates, Jr., R. W. Vaughan *J. Chem. Phys.* **73**, 975 (1980).

99. E. O. Stejakal, J. Schaefer *J. Magn. Reson.* **560**, 18 (1975).

100. S. J. Opella, M. H. Frey *J. Amer. Chem. Soc.* **101**, 5854 (1979).

101. I. D. Gay *J. Magn. Reson.* **58**, 413 (1984).

102. N. S. Colthup, L. H. Daly, S. E. Wiberley " Introduction to Infrared and Raman Spectroscopy ", Academic Press Inc., New York, N.Y. (1964).

103. R. A. Nyquist *Spectrochim. Acta* **22**, 1315 (1966).

104. R. A. Nyquist *Spectrochim. Acta* **25A**, 47 (1969).

105. B. J. Van der Veken, M. A. Herman *J. Mol. Struct.* **96**, 233 (1983).

106. B. A. Morrow *J. Chem. Soc. Faraday Trans. 1* **70**, 1527 (1974).

107. I. L. Mudrakovskii, V. P. Shmachkova, N. S. Kotsarenko, V. M. Mastikhin *J. Chem. Phys. Solids* **47**, 335 (1986).

108. J. B. Benziger, S. J. McGovern, B. S. H. Royce *A.C.S. Symposium Series* **288**, 463 (1985).

109. J. Herzfeld, A. E. Berger *J. Chem. Phys.* **73**, 6021 (1980).

110. A. K. Bhattacharya, G. Thyagarajan *Chem. Rev.* **81**, 415 (1981).

111. B. A. Morrow, I. A. Cody *J. Phys. Chem.* **80** 1995 (1976).

112. B. A. Morrow, I. A. Cody *J. Phys. Chem.* **80** 1998 (1976).

113. D. J. C. Yates, G. W. Dembinski, W. R. Kroll, J. J. Elliott *J. Phys. Chem.* **73**, 911 (1969).

114. J. Kunawicz, P. Jones, J. A. Hockey *Trans. Faraday Soc.* **67**, 848 (1971).

115. B. A. Morrow, A. H. Hardin *J. Phys. Chem.* **83**, 3135 (1979).

116. M. J. D. Low, A. G. Severdia, J. Chan *J. Catal.* **69**, 384 (1981).

117. J. B. Kinney, R. H. Staley *J. Phys. Chem.* **87**, 3735 (1983).

118. M. E. Bartram, T. A. Michalske, J. W. Rogers *J. Phys. Chem.* **95**, 4453 (1991).

119. A. A. Galinski, P. N. Galich *React. Kinet. Catal. Lett.* **38**(2), 281 (1989).

120. A. J. McFarlan B. Sc. Thesis, University of Ottawa (1986).

121. I. S. Butler, M. L. Newbury *Spectrochim. Acta* **33**, 669 (1977).

122. D. F. Evans, I. Wharf *J. Chem. Soc.* A, 783 (1968).

123. F. Schindler *Angew. Chem. Int. Ed. Eng.* **4**, 876 (1965).

124. C. Morterra, M. J. D. Low *Annal. N.Y. Acad. Sci.* **220**, 135 (1973).

125. K. Kawai, I. Kanesaka, F. Ichimura *Spectrochim. Acta* **26**, 593 (1970).

126. S. Takeda, R Tarao *Bull. Chem. Soc. Jpn.* **38**, 1567 (1965).

127. H. Schmidbaur *J. Organometal. Chem.* **1**, 29 (1963).

128. Von G. Mann, A Haaland, J. Weidlein *Z. Anorg. Allg. Chem.* **398**, 231 (1973).

129. J. P. Gray *Can. J. Chem.* **41**, 1511 (1963).